RINA

WATERJET PROPULSION 5

11 - 12 December 2008

THE ROYAL INSTITUTION OF NAVAL ARCHITECTS
10 Upper Belgrave Street
London SW1X 8BQ

Telephone: 020 7235 4622
Fax: 020 7259 5912

ISBN No: 978-1-905040-50-6

CONTENTS

Waterjet Applications in Vessels that Operate in Multiple Modes

D Borrett and P Rae, Hamilton Jet, New Zealand

Off-Design Behaviour of Waterjets

N Bulten and R Verbeek, Wärtsilä Propulsion Netherlands BV, The Netherlands

Research on the Optimum Blades Number of Mixed Flow Pump Based on CFD

Qiongfang Yang, Yongsheng Wang, Zhihong Zhang, and Mingmin Zhang, Naval University of Engineering, China

A Multi-Objective Automatic Optomisation Stratergy for Design of Waterjet Pumps

M Zangeneh, University College London, UK

Waterjet Pump Development for High Performance and Higher Power Density

R Aartojärvi and M Heder, Rolls-Royce AB, Sweden

Research on Hydrodynamic Performance of Hybrid Propulsion System

C Sun, Y Wang and Z Li, University of Naval Engineering, China

Testing Air-Augmented Waterjet Propulsion

A Gany, A Shemer, A Gofer and D Har-Lev, Faculty of Aerospace Engineering, Technion – Israel Institute of Technology, Haifa, Israel

Simulation of Dynamic Characteristics of Waterjet and its Application on Troubleshooting

Yongsheng Wang and Jiangming Ding, University of Naval Engineering, China; Zhirong Liu and Wenshan Xu, Guangzhou Marine Engineering Corp., China

Numerical Simulation and Analysis of Cavitation Performance of Waterjet

Chengjiang Liu, Yongsheng Wang and Zhihong Zhang, Naval University of Engineering, China

Overview of Recent Developments in Testing of Waterjets at NSWCCD

M Donnelly and S Gowing, Naval Surface Warfare Center, Carderock Division, W.Bethesda, MD, USA

Active Rudder Control

Nils Morén, MJP Marine Jet Power AB, Sweden
Stanislav Pavlov, MTD Company, Ltd., Russia

Scaling of Waterjet Propulsor Inlet Wakes

M B Wilson, Naval Surface Warfare Center, Carderock Division (NSWCCD), USA

Calculation and Analysis for Vortex-Induced Vibration of Waterjet Grid

Shuping Chang, Yongsheng Wang and Zhiyang Pang, Naval University of Engineering, China
Wenshan Xu, Guangzhou Marine Engineering Corporation

Authors' Contact Details

WATERJET APPLICATIONS IN VESSELS THAT OPERATE IN MULTIPLE MODES

D Borrett and **P Rae**, Hamilton Jet, New Zealand

SUMMARY

Commercial waterjet installations emerged predominantly in high-speed vessels such as passenger ferries that operate over a relatively narrow displacement and speed range. The design goals have therefore focused mainly on high-speed propulsive efficiency. However, waterjets are increasingly employed in vessels that have significant duty-cycles over a wide range of speeds and loading conditions, together with demanding manoeuvring requirements, Understanding the design characteristics that enable waterjets to achieve both high-speed efficiency and high manoeuvrability is critical to meeting the requirements of emerging waterjet markets.

A waterjet's ability to absorb high power without breakaway cavitation is governed by the nozzle-to-inlet diameter ratio, pump configuration and intake geometry. Steering nozzles and reverse deflectors can be designed to allow the waterjet to effectively emulate an azimuth thruster. With minimal dead band, low actuation loads and dedicated electro-hydraulic controls, rapid, accurate and efficient thrust vectoring is possible.

An offshore crew boat equipped with a dynamic positioning system is used to illustrate the requirements and capabilities of waterjets in “multi-mode” applications. Waterjets for this type of vessel must perform over the wide range of transit speeds resulting from variations in cargo loading, and deliver the high manoeuvrability needed for accurate station keeping. In addition to the waterjet propulsive efficiency at speed, key factors in achieving these goals are the steering efficiency, cavitation margins under high loading conditions, high available static thrust, and the speed and accuracy of thrust vectoring.

With careful design optimisation, waterjets can offer efficient performance across a wide range of vessel operating modes, providing an effective and versatile propulsion solution.

1. INTRODUCTION

Commercial waterjet installations emerged predominantly in high-speed vessels such as passenger ferries that operate over a relatively narrow displacement and speed range. The design goals have therefore focused mainly on high-speed propulsive efficiency. However, waterjets are increasingly employed in vessels that have to perform well in several different operating modes, covering a wide range of speeds and loading conditions, together with demanding manoeuvring and station keeping in offshore conditions.

This paper introduces some typical multi-mode vessel applications, examines the design characteristics that enable waterjet propulsion systems to achieve high performance levels over these wide ranging types of vessel operations, and looks in more detail at the propulsion solution for an offshore crew boat.

2. MULTIPLE MODE VESSEL APPLICATIONS

The following section outlines the special requirements of three different vessel types that operate for significant periods in distinct, multiple modes.

2.1 PILOT BOATS

Pilot boats typically have twin or triple waterjets giving a transit speed in the 30 to 35 knot range. They have special manoeuvring requirements for transferring pilots to and from large vessels that are making way at around 8-10 knots. The transfer process is a potentially dangerous operation due to interaction between the two moving vessels, and requires a high degree of skill on the boat operator’s part. High thrust levels with very rapid response are needed. A common technique while manoeuvring alongside a moving vessel is to run the engines at a fixed high RPM and 'trim' the waterjet reverse buckets to control the forward speed. The jet thrust response is therefore dependent only on the reverse and steering hydraulics and not the engine response. Combined with small travel on the helm wheel, this allows very precise control during the critical pilot transfer stage with the ability to quickly pull away from the moving vessel when required.

For pilot boats the key waterjet requirements are to provide high thrust without cavitation at relatively low forward speeds, together with rapid response of the reverse bucket and steering nozzle. These characteristics are simply not available with other types of propulsor.

2.2 PATROL BOATS

Patrol boats typically have three distinct modes - a low speed 'loitering' mode, a patrolling/cruise mode (at perhaps 70-80% power) and a high-speed chase/attack mode. They have to manoeuvre close to other vessels for boarding and may also perform rescue duties. Their particular type of high-speed operation requires the ability to manoeuvre aggressively and to accelerate and decelerate rapidly.

Many different propulsion configurations are used including propellers, waterjets, surface drives and combinations of these systems. Waterjets are well suited for this application due to their good manoeuvring characteristics for both low and high speed operations, rapid acceleration for chase/attack, 'crash stop' capability and high efficiency at transit speeds. Triple waterjet installations are common, with the centre unit often being of a smaller size to provide efficient loitering capability. The centre jet may also be employed to provide high-speed boost as well as loitering and therefore must operate over a very wide speed range.

The key waterjet requirements are the ability to provide efficient loitering and transiting, rapid acceleration without cavitating, and responsive manoeuvring at both high and low speeds.

2.3 CREW BOATS

Crew boats are used to transfer personnel and cargo to and from offshore platforms. In recent years these vessels have increased in size to the point where they now carry out many of the tasks previously done by offshore supply vessels, such as transferring cargo, fuel and other liquids.

The cargo-carrying role of these vessels means that they operate at greatly different displacements between lightship and full load. One reason for the success of waterjets in these vessels is that, compared to an equivalent propeller driven boat, waterjets make use of full engine power irrespective of the state of loading and transit speed. Propellers have to be 'pitched' to meet the required speed at the maximum loading condition and cannot propel the boat significantly faster when it is light. Waterjets, however, allow the full engine power to be used at all conditions: this translates into significantly higher speeds when a vessel is light or partially loaded.

The second requirement of these vessels is for accurate station keeping while at an offshore platform. Increasingly, and predominately for safety reasons, this is being done under automatic control via a dedicated dynamic positioning (DP) system. The waterjets are required to deliver high thrust without cavitation at 'bollard pull' conditions for this mode of operation, as well as fast and accurate response of the control surfaces.

2.4 HYDRODYNAMIC DESIGN ASPECTS OF WATERJETS FOR MULTIPLE MODES

For a given waterjet nozzle size, power input and vessel speed, the efficiency of the waterjet system (quasi-propulsive coefficient or QPC) is determined mainly by the uniformity of the flow field entering the pump, the efficiency of the pump and discharge nozzle, and the minimisation of losses from other necessary features such as intake screens. Other variables affecting the overall propulsive coefficient (OPC) such as the wake fraction and thrust deduction values are hull and speed dependent and are not included in this discussion.

2.4 (a) Intake Flow Uniformity

An ideal intake would present a uniform flow field to the pump rotor under all operating conditions. Achieving this would necessitate a variable geometry intake which is generally deemed too complex and costly. The challenge for the waterjet designer therefore is to achieve good performance across the required range of operating conditions within the fixed-geometry constraints. In the type of vessels being discussed, the duty cycle can involve significant periods of operation anywhere from zero up to 50 knots..

A long shallow intake is the obvious solution to achieving good flow uniformity at the impeller plane under high-speed conditions. Such long intakes generally have a less than desirable shape for good low speed and static thrust performance, where a steeper ramp and intake floor plus larger radii around the sides and rear of the intake are desirable. Long intakes also increase the entrained water mass, lengthen the drive shaft and increase the inboard structural intrusion. Waterjet performance tests at Hamilton Jet have shown that a number of intake designs intended for optimal high speed performance could, in fact be reduced in length by 20% with no reduction in the high-speed performance of the waterjet.

An important feature of the waterjet intake is the cutwater, or ’lip' at the rear of the intake opening. For high-speed it is generally best to employ a small lip radius, no ramp underneath the lip and a shallow intake floor. However, this is virtually the opposite of the geometry required for good low speed performance, which profoundly affects bollard pull and manoeuvring thrust. A larger lip radius can be employed on an intake otherwise optimised for higher speeds, in order to improve the static thrust performance.

For a given nozzle size, power input, vessel speed and therefore flow rate, a waterjet design with a smaller inlet diameter (larger Nozzle-to-Inlet Ratio or NIR) has higher inlet velocities, an improved Inlet Velocity Ratio (IVR) and greater impeller plane flow uniformity at high speed. Increasing the waterjet NIR has a much greater influence over the QPC at higher speeds than changes to the intake geometry. The downside of a higher NIR waterjet design is reduced cavitation performance and static thrust for a given pump configuration, unless a large impeller blade area is employed - with consequential loss of pump efficiency.

2.4 (b) Pump Performance

The waterjet NIR is the principal design parameter that determines the pump configuration to be employed. A larger NIR pump will generally be selected for high speed as noted above. However, larger NIR pumps can exhibit poor low speed or static thrust performance and significant pump taper (radius change) is required to achieve even a minimum acceptable level of cavitation performance.

Figure 1 shows the relationship between NIR and maximum static thrust (bollard pull) for a family of similar waterjet pumps operating on the same intake, showing the reduction in static thrust with increased NIR.

The ability of a particular waterjet design to be successful in a wide range of vessel applications is critically dependent on the choice of NIR. It is fair to say that in hydrodynamic design, reducing the trade-offs between good low and high speed performance is a significant area of research for most major waterjet manufacturers.

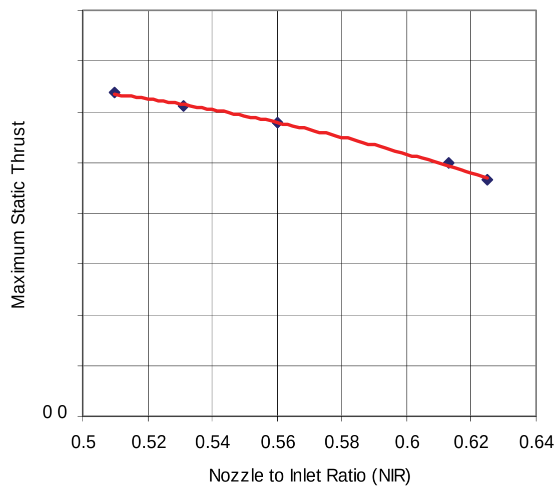

Figure 1 - Reduction in Static Thrust with NIR

Another focus of recent waterjet development has been the reduction in waterjet envelope size. It is a relatively straightforward task to design a highly efficient waterjet pump within a large envelope (higher radial flow component) but somewhat more challenging to design a highly efficient, compact pump with very good cavitation resistance.

Under uniform flow conditions the achievable efficiency of axial flow waterjet pump designs can however, be very close to that of mixed flow types.

Most mixed flow pumps employed in waterjets today have a maximum pump diameter around 40% larger than the inlet, resulting in a less than compact installation package – typically 20% larger in diameter than the equivalent nozzle size axial flow pump.

Comparing two commercially available waterjets from different manufacturers, one axial flow and the other mixed flow, both of the same nozzle size and operating at the same power input and rpm, the axial flow waterjet has a 5-6 knot lower speed limit for continuous cavitation-free operation, and over 20% higher maximum static thrust, which greatly increases its versatility in multi-mode applications.

2.4 (c) Steering Efficiency

A further design consideration that has a particular bearing on the vessel OPC is the performance of the waterjet steering system.

When a vessel is operating in a seaway with significant wind and wave conditions, the steering demands are often high in order to maintain a set course. Experience with well-designed nozzle type steering systems has shown that transit times can be reduced by up to 5% on longer runs, when compared to external deflector type systems, translating directly into an improvement in overall propulsive efficiency of the same order. This ’course-keeping’ efficiency has less benefit on shorter runs in calm waters, but these conditions are generally much less common.

On the passenger ferry ’Ocean Flyte’, a 31m, 30 knot monohull operating in Singapore waters, a 1.5 knot higher average speed over a one-hour run was measured following an upgrade from an external spherical deflector type steering to a high efficiency ‘JT’ type steering nozzle system. The latter also provides greater manoeuvring thrust as the design is not affected by the ’flooding’ of the steering system when the vessel is stationary.

2.4 (d) Design Parameters

Table 1 summarises the relevant design parameters for various waterjet operating modes. Achieving the widest effective operational range possible is of course a significant development goal for waterjet designers.

Operating Mode	**High Speed**	**Laden Cruise**	**Low Speed, High Power**	**Static Thrust**
Speed Range (kts)	35 - 50	20 - 30	8 - 12	-2 - +2
Example	Passenger ferry	Crew boat - laden	Pilot transfers, towing	Station keeping
Intake	Long/low ramp angle	Medium	Medium	Short/ steep
Intake Lip Radius	Small	Medium	Medium	Large

NIR	High	Medium	Medium/ low	Low
Pump optimised for	Efficiency	Efficiency with cavitation margins for unlimited operation	Breakaway cavitation resistance	Breakaway cavitation resistance
Steering Nozzle	High course keeping efficiency	High course keeping efficiency	Fast response, high accuracy	Fast response most important
Reverse Duct	N/A	N/A	Fast response, high accuracy	Fast response

Table 1 - Summary of Design Parameters for Different Operating Modes

2.5 STATIC THRUST CHARACTERISTICS

The power level that can be used with a particular waterjet under bollard-pull or static thrust conditions is determined by the waterjets' resistance to cavitation; a potential problem in all types of propulsor. It occurs when the propulsor blades become very highly loaded, creating sufficiently low pressure in the water to cause a rupture and form a cavity. The subsequent collapse of the cavity due to the pressure of the surrounding fluid, releases a significant amount of energy in the form of an acoustic shock-wave. This energy can be sufficient to cause erosion of the metal parts in the vicinity of the cavitation, resulting in serious damage if allowed to continue. Thrust levels from a waterjet can reduce dramatically during cavitation, and permanent damage to components causes gradual degradation of propulsive efficiency.

For vessels that must achieve the best possible static thrust and manoeuvring performance, waterjets are often selected in a larger sizing than for other vessel types. This is one way of improving cavitation margins, as well as contributing to better propulsive efficiency.

Figure 2 illustrates the relationship between static thrust and engine power for a Hamilton HM811 waterjet matched with a 1340kW engine – a common combination on many crew boats. At a power level around 1000 kW, the pump efficiency is starting to reduce - indicating the initial onset of cavitation. Further gains in static thrust can be achieved beyond this point as more power is applied, but at the expense of increasing cavitation levels. At a power level of approximately 1350 kW the thrust level peaks, and attempting to apply more power only results in increased cavitation and reduced thrust. With the engine matching shown, high levels of cavitation are avoided, with maximum thrust being achieved at the full engine power. For station keeping, thrust at this maximum power level would normally only occur for short periods, and practical experience with crew boats over many years has shown that cavitation related damage is therefore avoided.

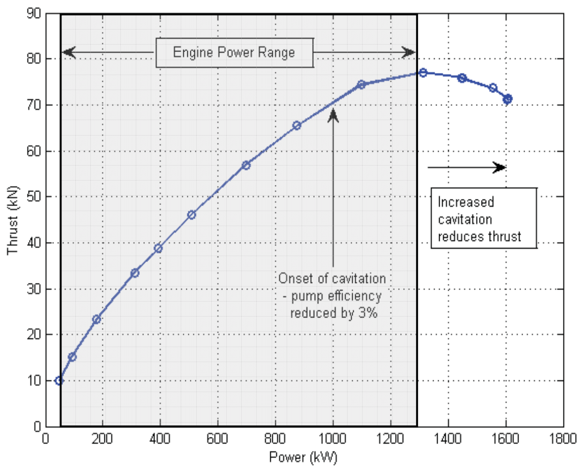

Figure 2 – HM811 Static Thrust vs Engine Power

If more powerful engines are used with the same waterjets, measures need to be taken to ensure that the power is limited, to avoid sustained operation in the cavitation region. In crew boats, this limit is controlled by the dynamic positioning system. When the vessel changes to transit mode, the cavitation margin increases with forward speed, allowing higher power to be applied.

2.6 CONTROL OF THRUST FOR MANOEUVRING

Apart from the availability of high static thrust, the key to good manoeuvrability lies in the design of the control surfaces that direct the thrust. Manoeuvring thrust is produced in a waterjet by splitting the jet stream into different components and varying the ratio of flow between these components. There are two different design approaches in common use for achieving this.

The first method, seen in many larger waterjets, uses a box shaped steering deflector with a reverse deflector 'flap' mounted on it so that the whole assembly swivels when the steering is actuated. When the reverse deflector is deployed the flow is split into two components that are opposed by 180 degrees at all steering angles. When the reverse deflector is set so as to balance the ahead and astern components of flow (zero speed), no side thrust vector can be generated since the flow components remain opposed by 180 degrees at all steering angles. Figure 3(a) shows the approximate thrust envelope for this type of steering/reverse mechanism. Waterjets using this design are more limited in manoeuvring capability and are not well suited to DP operations.

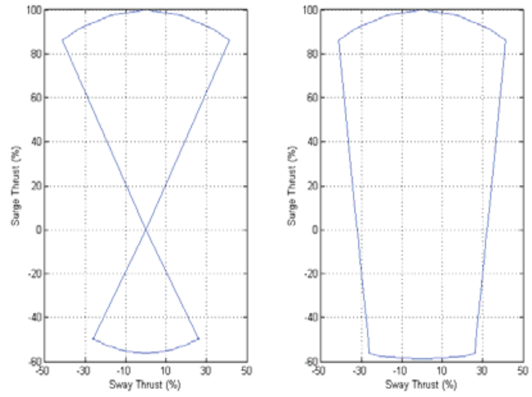

Figure 3 - Thrust Envelopes for (a) Steering-Mounted and (b) Split Duct Reverse

In the second design approach, the reverse duct is attached to the waterjet housing. It can be raised and lowered independently and does not rotate with the steering nozzle. The jet stream first passes through the steering nozzle before being intercepted by the reverse duct which then turns part or all of the flow back under the hull to produce reverse thrust. This type of reverse duct has split passages, which allow either two or three flow components to be generated. It produces a thrust envelope as shown in Figure 3(b), allowing a thrust vector to be obtained at any azimuth. The method of achieving this is described below.

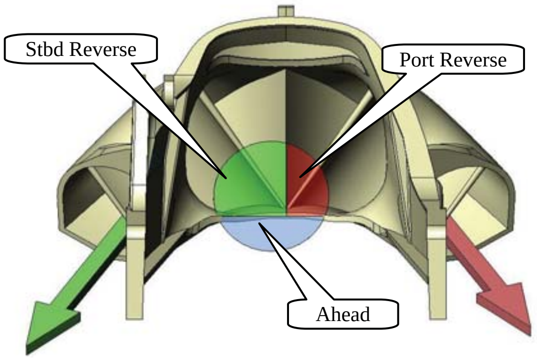

Figure 4 - View into Reverse Duct along Jet Stream

Figure 4 shows a view looking aft along the jet axis into the reverse duct, which is partly lowered into the jet stream. In this view the steering nozzle is angled slightly to starboard. The jet stream is split into three components as follows:

- The 'Ahead' component which goes underneath the reverse duct.
- The 'Port' component which goes into the port side of the reverse duct.
- The 'Starboard' component which goes into the starboard side of the reverse duct.

The 'Ahead' component is only acted on by the steering nozzle. The volume of flow in this component is dependent on how far the reverse duct is lowered. The remaining flow goes into the reverse duct where it is further split into port and starboard components with the ratio determined by the steering nozzle position.

When the reverse duct is fully raised all the flow goes astern, providing maximum ahead thrust. This is the normal under-way condition. By moving the steering nozzle, this flow (shown right in plan view) can be diverted to provide steering forces.

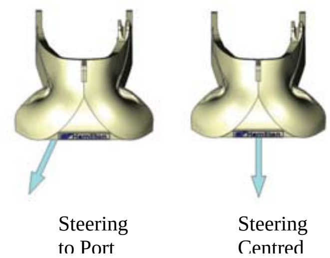

When the reverse duct is partially lowered, the jet stream is split into two or three components. The flow below the duct goes straight astern as before and can be directed to port or starboard by the steering nozzle. The upper flow component that enters the reverse duct is further split into port and starboard components. The reverse duct turns these flow components round and ejects them from the port and/or starboard outlets in a forward direction underneath the hull, producing astern thrust. By altering the steering nozzle angle, the ratio of flow entering the port and starboard sides of the reverse duct can be varied.

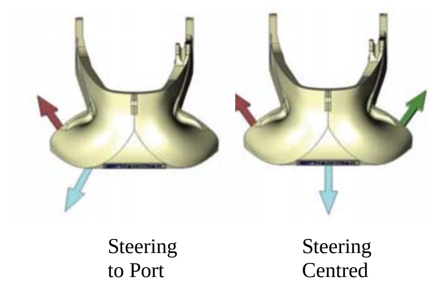

When the thrust from the ahead and astern components is in equilibrium, the jet is said to be at the 'zero speed' position. The key feature of the split passage reverse duct is that in this condition, even though there is no net ahead/astern thrust, by moving the steering nozzle, side thrust is generated, allowing the vessel to 'steer' even when stationary. In the case of DP operations, this side thrust can be directly used with thrust from a bow thruster to hold the vessel against cross winds and currents.

When the reverse duct is fully lowered, it captures all the flow and maximum astern thrust is produced. By moving the steering nozzle, the ratio of flow entering the port and starboard passages can be varied, thus providing steering forces in the astern direction.

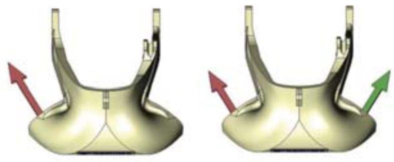

When the jet stream is deflected by the steering nozzle and reverse duct, some energy is lost. With an efficient steering nozzle design this loss may be no more than 5% at maximum steering deflection.

Losses in the reverse duct are higher due to the greater angles through which the water is deflected and the fact that the flow astern is directed down and to the sides to avoid hitting the vessel's transom, resulting in a non-ideal vector. The astern thrust achieved with the split duct reverse bucket is thus approximately 60% of the ahead thrust.

2.7 THRUST RESPONSE

Vessels that use waterjet propulsion are comparatively light in weight and therefore respond quickly when acted on by wind, wave and current forces. For manoeuvring and dynamic positioning the waterjet thrust response must be fast enough to counter these disturbances before the vessel moves too far from the desired position and heading. The thrust can be directed rapidly and precisely on a waterjet by moving the reverse duct and steering nozzle to new positions and adjusting the engine RPM.

A simple analysis demonstrates the relationship between thrust response and position keeping ability for a 7m test vessel. Figure 5 shows simulation results of the surge position error following an input disturbance of 300 N. The reverse hydraulic system is modelled by a first order lag with the time constant τ_r varying between 0 and 1 second. It can be seen that the position error following the disturbance is only 0.15m when $\tau_r = 0$, increasing to 0.64m when $\tau_r = 1$.

In each case the vessel controller has been optimised to match the different values of τ_r so that the position control loop does not become unstable. As τ_r increases, the position control loop gain has to be reduced to maintain stability and it is this gain reduction that results in a greater position error.

It can be seen that for this example, a value of $\tau_r = 0.25$ seconds would be acceptable. Not much improvement is possible if this lag is eliminated completely ($\tau_r = 0$), but above a value of $\tau_r = 0.25$, position errors increase exponentially.

In addition, with a slower hydraulic response, since the vessel moves further off position, the correcting thrust has to be applied for longer, possibly involving a higher engine speed and resulting in more energy being used. Applying a correcting thrust rapidly and early is more fuel efficient.

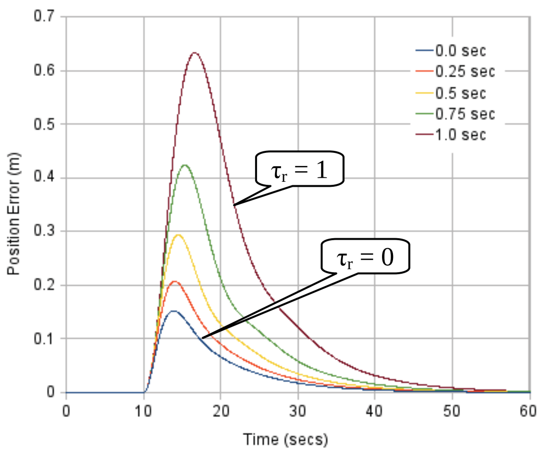

Figure 5 - Position Errors for Different Reverse Hydraulic Response Times

Obviously, as vessel size increases, so its response becomes slower, and longer time constants in the hydraulic system can be tolerated. However, as the above analysis demonstrates, it is important to match the waterjet control response to the expected vessel response; otherwise position keeping accuracy will be compromised, particularly where this is automated.

The JT type steering nozzle and the split duct reverse bucket are both designed for minimum actuation loads. This helps to reduce the size, weight and power requirements of the hydraulic system, while achieving rapid response rates.

As well as the characteristics of the hydraulics, thrust response is also dependent on how quickly the engine can change speed. This varies with engine size and type, but is invariably slower than the steering and reverse actuators. To reduce dependency on the engine response while manoeuvring, the RPM can be held at a higher setting so that greater thrust levels are produced immediately the jet hydraulics move.

In Figure 6 the innermost area shows a thrust envelope with an engine at low idle. Thrust direction and magnitude are controlled within this area by positioning the reverse duct and steering nozzle. Raising the engine speed above low idle increases the size of the inner envelope as indicated. This allows a greater proportion of the thrust to be controlled only by the reverse and steering positions, giving a faster response that is not limited by the engine response. This mode of operation is commonly used on pilot boats and it is also applicable to station-keeping.

2.8 THRUST RESOLUTION

Waterjets provide virtually infinite thrust resolution during manoeuvring. At lower thrust levels this is dependent on the accuracy with which the reverse duct and steering nozzle can be positioned. Using electronic closed loop control, positioning accuracy of a hydraulic cylinder to better than 1% is readily achievable and this equates to a resolution of about 0.2% of the maximum thrust. At higher thrust levels, the resolution is dependent on how accurately the engine speed can be controlled. Given engine speed control to within 10 RPM for example, about 0.7% thrust resolution would be obtained for an HM811 waterjet.

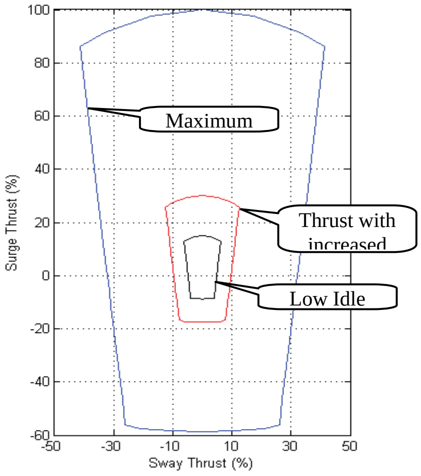

Figure 6 - Jet Thrust Envelopes with Varying Engine Speed

Conventional main drive propeller systems cannot achieve such accuracy over the direction and magnitude of thrust for manoeuvring. It is the combination of high thrust levels, rapid response and fine resolution that make waterjets excel in high performance manoeuvring applications.

2.9 MANOUEVRING THRUST EFFICIENCY

Using main drive propulsion (propellers or waterjets) for manoeuvring of high speed craft represents a compromise that cannot match the efficiency of dedicated manoeuvring thrusters. However, to fit vessels such as crew boats with a full set of separate thrusters for station keeping is not considered a viable option due to the added weight, cost and complexity.
Typical thrust/power figures for a propeller azimuth thruster are quoted as 150N/kW[1]. By comparison, main drive waterjets achieve approximately 72N/kW. This reduced efficiency is compensated by the fact that high power levels are available from the main engines. With four waterjets, an excess of thrust is available at the stern of the vessel for manoeuvring and the maximum athwartships thrust is limited by the bow thruster capability not by the waterjets. Selecting waterjets as the main propulsion provides powerful manoeuvring thrusters ‘for free’.

3. CASE STUDY – OFFSHORE CREW BOAT

This section examines in more detail the application of waterjet propulsion to a recent offshore crew boat, the ‘Joyce McCall’.

3.1 MARKET DRIVERS

Over the last 8 years waterjets have taken significant market share from conventional propeller systems in crew boats built in the USA. This is quite surprising since most crew boats are designed for speeds somewhat below the typical waterjet domain, and therefore cannot compete with propellers on grounds of propulsive efficiency alone. The primary drivers cited for selecting waterjets for these vessels are as follows:-

- The ability to achieve higher speeds in light to mid range cargo load conditions.
- Improved manoeuvrability under manual and automatic control with high bollard pull and 'azimuth thruster' characteristics.
- Reduced vessel draft which allows shallow water operations.
- Reduced vessel dry-dockings, waterjets being largely immune to damage from debris and underwater obstacles.
- Less maintenance and improved life for propulsion machinery since waterjets do not overload engines and gearboxes remain permanently engaged when manoeuvring.
- Jet driven steering and reverse hydraulics do not require AC power - no loss of steering control in a 'deadship' situation.
- Integrated engine, steering and reverse control system provides ease of installation for the builder.
- Simple interface with DP systems and rapid set up.

3.2 PROPULSION REQUIREMENTS

At 54 metres in length with a loaded displacement of 500 tonnes, this vessel is near the top of the current size range for crew boats. Waterjet selection was based on the required speeds at light and loaded displacements and the need to maintain adequate cavitation margins under full load cruise and while manoeuvring. Four waterjets were specified, this being the most common arrangement, although some vessels using six jets are now under construction in the USA.

The selected HM811 waterjets have the following characteristics:-

Max. Continuous Power (cruise)	2800 skW
Max. Continuous Power (DP)	1000 skW
Max. Thrust (DP)	70 kN

In order to meet the requirements for dynamic positioning, this vessel is fitted with a retractable azimuth thruster at the bow. A separate tunnel thruster uses the same power source for docking purposes. The particulars for the 'Joyce McCall', are summarised in Table 2.

Length overall	53.8 m
Length BP	48.01 m
Beam	9.14 m
Depth	4.11 m
Light Displacement	205 MT
Loaded Displacement	508 MT
Main engines	4 x Cummins KTA50 M2
Power	4 x 1340 kW @ 1900 RPM
Waterjets	4 x Hamilton HM811
Bow thrusters	1 x 150 kW Tunnel 1 x 150 kW azimuth
Speed at 450 LT displacement	18.5 kts
Speed at 210 LT displacement	31 kts

Table 2 - Joyce McCall Particulars

3.3 TRANSIT PERFORMANCE

In a vessel of this type, the hull resistance increases by a factor of approximately three times between the light and fully loaded conditions. If this vessel was to be driven by fixed-pitch propellers (as the majority of crew boats are), these would be selected for the required speed of the vessel *at the fully laden condition*, otherwise engine overloading would occur. When the same (prop driven) vessel is at light displacement, its top speed is only slightly higher than the fully laden speed because this becomes limited by how fast the propeller can rotate. In the light condition the engine RPM becomes limited by the governor but the engine is only lightly loaded, unable to make use of the full power available[2]. This is rather like being stuck in too low a gear.

In contrast, the waterjet absorbs power more consistently across the whole operating speed range of the vessel. It cannot overload the engine, even when the vessel is fully laden. When the vessel is running light, the waterjet can convert the available engine power into a much higher transit speed. Figure 7 shows the jet thrust and resistance curves for the 'Joyce McCall' at the different loading conditions.

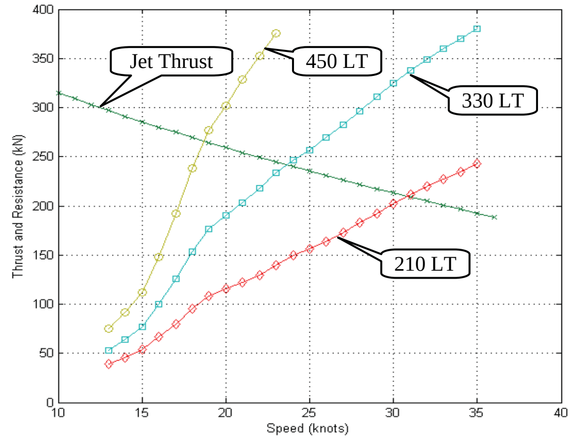

Figure 7 - Waterjet Crew Boat Speed at Different Loading Conditions

Under fully loaded operating conditions, a propeller driven vessel will be somewhat more efficient than an equivalent waterjet vessel. However, when considering the overall duty cycle, much of which is with light or medium loads, waterjets achieve significantly faster round trips and/or a greater operating range.

3.4 STATION KEEPING PERFORMANCE

Dynamic positioning systems operate by actively controlling the vessel in three degrees of freedom – surge, sway and yaw, based on one or more high accuracy positioning systems and heading sensors. The ability of a vessel to hold position under the influence of current, wind and wave forces is defined by the ‘DP capability plot’. This plot provides a measure of the combined forces that the vessels thrusters are capable of. A crew boat uses the main drive waterjets in combination with one or more bow thrusters to create the desired forces and moments for station keeping.

The DP capability plot for the 'Joyce McCall' is shown in Figure 8. The plot clearly illustrates that high thrust levels are available in the surge direction, but limited thrust is available in sway. In the latter case, this vessel is able to hold station when side on to a 1.5 knot current and approximately 10 knots of wind, but beyond that, insufficient thrust is available. In fact this limitation is purely due to the bow thruster which has to approximately match the side thrust from the waterjets, of which there are four with significantly higher power available. This is not really a problem, since these vessels would normally hold station bow or stern-on to the wind and waves

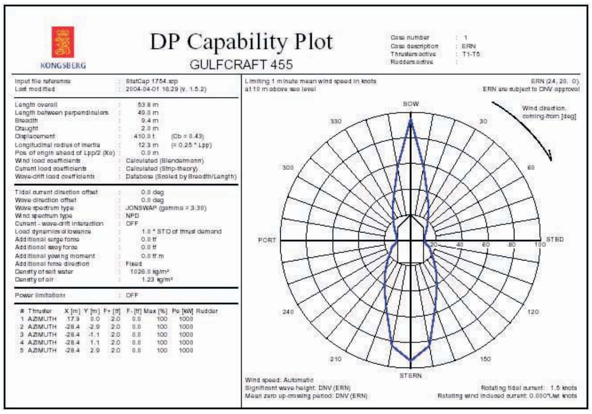

Figure 8 - DP Capability Plot

3.5 CONTROL SYSTEM DESIGN

Larger Hamilton waterjets currently use the Modular Electronic Control System (MECS) which provides steering, reverse, engine speed and gearbox control. An additional Dynamic Positioning Interface Module (DPIM) provides the link between the jet controls and a DP system.

The DP system computes desired thrust vectors for each waterjet and the bow thrusters(s), as required to hold the vessel in position. To simplify the interface with the waterjet controls, the DPIM incorporates a real-time jet thrust model that computes the waterjet steering and reverse and engine speed demands, in response to the DP demanded thrust vectors. From the DP systems perspective, the waterjet therefore has similar characteristics to an azimuth thrusters. This greatly simplifies system installation and commissioning.

3.6 THRUST ALLOCATION FOR DYNAMIC POSITIONING

With four waterjets plus a bow thruster available for station keeping, there are many ways in which to combine the thrust forces for maintaining position. The methods, referred to as ‘thruster allocation’ are developed against various optimisation measures, such as minimising thruster power or minimising the effects on the vessel of thruster failure. Different allocation schemes may be employed depending on the weather conditions or the type of operation being carried out. The method for generating sway thrust for the Joyce McCall is illustrated in Figure 9(a).

As shown, the jet and bow thruster vectors are directed athwartships together to generate sway thrust while balancing the rotational moment; the jet side thrust being allocated equally to all waterjets.

Assuming that the current and wave drift forces act at the vessel mid point (centre of rotation) while the wind forces act 3 metres ahead of this point in the same direction, each waterjet need only produce about 15% of it's available side thrust in order to balance the bow thruster and 10 knot wind moments. Thus the main propulsion would operate at quite low power levels to hold station against these side forces, resulting in good fuel efficiency.

The jet thrust envelope is limited to a circular area having a radius equal to the minimum thrust level, as shown in Figure 10, to more closely emulate an azimuth thruster and simplify the DP calculations. Compensation for the different thrust efficiencies that vary with the azimuth demand, is automatically carried out in the DPIM by adjustments to the engine RPM. The imposed restriction in ahead/astern thrust using the circular envelope is not a limitation in practice but does restrict the derived DP capability plot in the ahead/astern directions.

Apart from low power usage, a further advantage of this method is that all waterjets can thrust in the same direction and the thruster re-allocation in the event of a failure becomes straightforward. The loss of one or two waterjets out of four would be unlikely to have a great effect on sway controllability under DP as excess side thrust is available from the remaining jets.

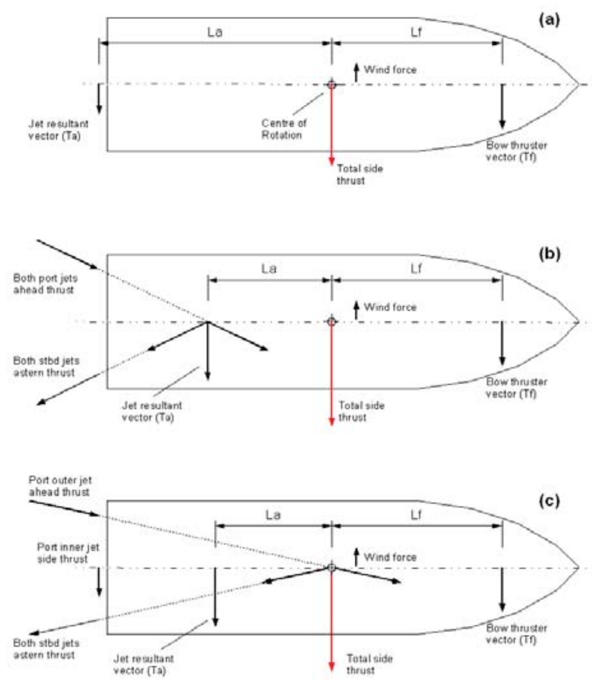

Figure 9 - Allocation Methods for Side Thrust

Figure Figure 9(b) and (c) illustrate two alternative methods for producing side thrust using four waterjets. Both methods make use of the excess jet thrust that is available in the longitudinal direction to produce additional side thrust by a ‘push-pull’ technique (used in propeller crew boats[3]), achieving an increase of approximately 35% over method (a). However, considerably higher power levels are required from the waterjets in order to obtain this increase.

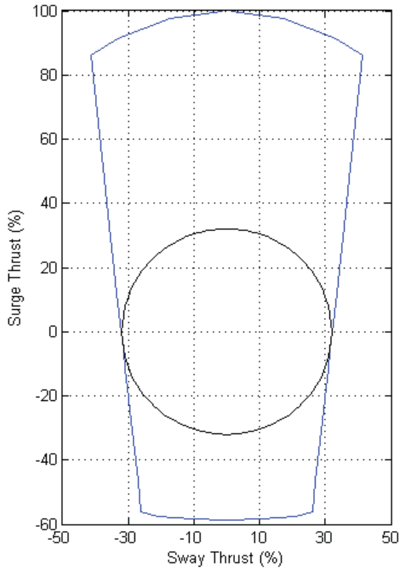

Figure 10 - Circular Thrust Envelope for Dynamic Positioning

4. CONCLUSIONS

Waterjet propulsion provides an excellent solution for vessels that operating in multiple modes. Through appropriate design optimisation it is possible to achieve efficient high-speed propulsion in different operational regimes, as well as high levels of static thrust. Together with fast and accurate control of thrust through optimised steering nozzle and reverse duct designs, the demanding needs for manoeuvring and automated station keeping can be readily met. The ability of the waterjet to emulate an azimuth thrusters also provides ease of interfacing with dynamic positioning systems.

The problem of cavitation under high loading can be managed through careful hydrodynamic design, appropriate selection of jet size, correct matching to engine power, and where necessary, controlled limiting of the applied power levels.

The demand for multiple mode vessels continues to provide challenges, a recent example being a catamaran crew boat design having a top speed of over 40 knots, together with more stringent, higher redundancy station keeping capabilities[4]. Waterjets are ideally suited to fulfilling these new propulsion requirements.

5. REFERENCES

1. 2. Bekker, Joe, R. Is a Drop-Down Better Than a Tunnel Thruster? http://www.thrustmastertexas.com/applications/dropDownBetterThanTunnelThruster.html

3. Alexander, K. (1995). Waterjet versus Propeller Matching Characteristics. *Naval Engineers Journal*, May 1995, 129-139.

Moen, Lars, K. (2004). Crew Boat Station Keeping – Challenges and Solutions. *Dynamic Positioning Conference Workboats/OSVs,* September 2004. http://seacormarine.com/crewzer/index html

Our thanks to Gulf Craft,Inc. and Kongsberg Maritime for the information that they contributed towards this paper.

6. AUTHORS BIOGRAPHIES

Dick Borrett is a Senior Development Engineer at Hamilton Jet, New Zealand. He worked in the field of hydrodynamics and control of underwater vehicles for British Aerospace and Dowty Maritime in the UK before moving to New Zealand in 1992. There he joined Hamilton Jet to establish an in-house capability in electronic control system design and manufacturing.

Since that time he has been involved in new product development for subsequent generations of control system. As well as leading the design of the current Modular Electronic Control System (MECS), he was also responsible for analysis and software development on the DP Interface Module that provides Hamilton waterjets with 'azimuth thruster' capabilities.

Dick is currently researching new ideas for waterjet manoeuvring and control and has a number of New Zealand and USA patents granted and pending.

Philip Rae has managed the research, product development and product support functions at Hamilton Jet for nearly 10 years. A mechanical engineer by training, he worked principally in application engineering and business development prior to completing a business degree and moving into technical management.

He has extensive experience with a wide range of waterjet applications and is directing new product development programs for both waterjets and electronic control systems.

OFF-DESIGN BEHAVIOUR OF WATERJETS

N Bulten and **R Verbeek**, Wärtsilä Propulsion Netherlands BV, The Netherlands

SUMMARY

Waterjets and waterjet inlets are usually designed for a limited number of operational conditions. During a turn and in manoeuvring conditions the flow in the inlet will deviate quite considerably from the flow in normal sailing conditions. This will have an effect on the required shaft torque and the available pressure just upstream of the pump, expressed in available NPSH. A third typical off-design condition, besides low speed manoeuvring and high speed steering is three jet operation for a vessel with four waterjets installed. Simulations of the effects in off-design conditions are carried out with aid of a commercial CFD code. The paper gives an overview of the different phenomena occurring at the various off-design conditions and how this will affect overall performance. The effects on the performance are also reviewed in light of the improved cavitation behaviour of the new axial flow pump types LJX and WLD.

NOMENCLATURE

D	Diameter	[m]
NPSH	Net positive suction head	[m]
n	Shaft revolution rate	[s^{-1}]
p	pressure	[Pa]
v_{ship}	ship speed	[$m\ s^{-1}$]
w	Wake fraction	[-]
α	Drift angle	[degrees]
ε	Inlet loss coefficient	[-]
κ	Pump specific NPSH	[-]
ρ	Density	[$kg\ m^{-3}$]

1. INTRODUCTION

Evaluation of the performance of a waterjet installation is mainly based on the design operating condition. When the performance of various installations at the design point is more or less identical, additional operating conditions can be included in the evaluation. In this paper the performance at some typical off-design conditions will be addressed. Examples of these conditions are: (i) low speed manoeuvring, (ii) high speed steering and (iii) 3 jet operation at a vessel with 4 installations. Differences in performance can be related to the propulsive efficiency, power absorption of the pump or the available margins against cavitation. Large variations in power absorption can lead either to overloading of the engine, resulting in black smoke in the exhaust gases or in over-speeding of the impeller. Reduction of the cavitation margins will result in more cavitation and in extreme cases even to thrust break-down due to severe cavitation.

The research described in this paper is based on numerical analyses of the flow through a complete waterjet installation of the Lips-Jets E-type pump. The background of the Computational Fluid Dynamics (CFD) method is described in the following section.

Section 3 deals with the descriptions of the analysed conditions. The calculated performance for the various conditions will be presented in section 4. In section 5, the benefits of the new axial flow LJX/WLD pumps with improved cavitations margins will be evaluated. The conclusions of the research will be presented in section 6.

2. BACKGROUND OF NUMERICAL ANALYSES

The numerical analyses are based on the Reynolds-Averaged Navier Stokes (RANS) equations. For the calculations a mesh has been built, which includes the waterjet inlet duct, the E-type impeller, stator bowl and the nozzle. The CFD method and the generation of the mesh are described in detail in the PhD-thesis of Bulten [1].

Figure 1 shows a picture of the complete mesh as used in the CFD analyses. The numerical domain is meshed with hexahedral cells, based on a multi-block approach. This method ensures good control over the quality of the cells near the walls, in which the effects of the boundary layer development are modelled. The complete mesh of the pump unit consists of about 1.35 M cells.

Effects of turbulent flow are captured with the standard k-ε turbulence model. This model is utilised at the authors' company for many years. Implementation of the body forces due to rotation of the impeller is based on the quasi-steady Multiple-Frame-of-Reference method. In this way the impeller is frozen at a certain fixed angular position.

The inflow is prescribed at the front plane and depending on the drift angle on one of the side planes. The remainder of the sides of the numerical domain are treated as constant-pressure planes. The flow rate through the pump is governed by the prescribed RPM of the impeller.

It has been found that the results of calculations of the waterjet installation operating at free sailing operating conditions were in good agreement with the full scale performance of the installation [2].

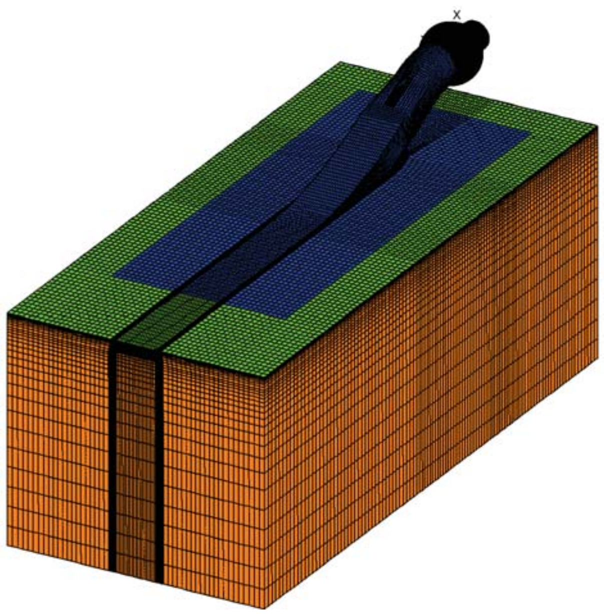

Figure 1: mesh of complete waterjet installation as used in CFD analyses

3. ANALYSED CONDITIONS

Three typical conditions have been identified as typical off-design conditions: low speed manoeuvring, high speed steering and 3-jet operation. It should be clear that off-design does not mean not-used-in-operation for these conditions. Evaluation of the performance in these conditions can thus be important, when the overall performance is reviewed.

3.1 LOW SPEED MANOEUVRING

The CFD calculations for the low speed manoeuvring conditions are carried out for 2 ship speeds, i.e. 3 and 6 knots. The revolutions of the pump are set to a realistic value corresponding to about 30% power. This condition is marked in figure 2 (6 knots, 31% power). The drift angles have been varied between -60 and +60 degrees. Both negative and positive angles have been analysed because of the non-symmetrical nature of the problem. This asymmetry is created by the rotation of the impeller. It is therefore expected that the torque of the impeller might show differences in behaviour when operating in positive and negative drift angles.

3.2 HIGH SPEED STEERING

The calculations for the high speed steering are performed for 30 and 35 knots. Though this is a few knots below the design speed, it is expected to represent a realistic condition, since the vessel will always lose some speed during a steering manoeuvre [3]. The revolutions of the pump are selected to simulate 100% power. The drift angles have been varied between -30 and +30 degrees. Under normal circumstances the drift angles will be much lower than 30 degrees.

3.3 THREE-JET OPERATION

In case of failure of an installation, the active number of waterjet installations on a vessel will be reduced. So in case of a vessel with four waterjets installed and one in failure mode, only three jets are left for propulsion. This can have a significant influence on the margins against cavitation, as shown in the two figures below. These figures show that the ship speed will drop from 44 knots in four-jet operation to about 33 knots in three-jet operation. Moreover, the margin against cavitation of about 11 knots at four-jet operation vanishes almost completely at three-jet operation.

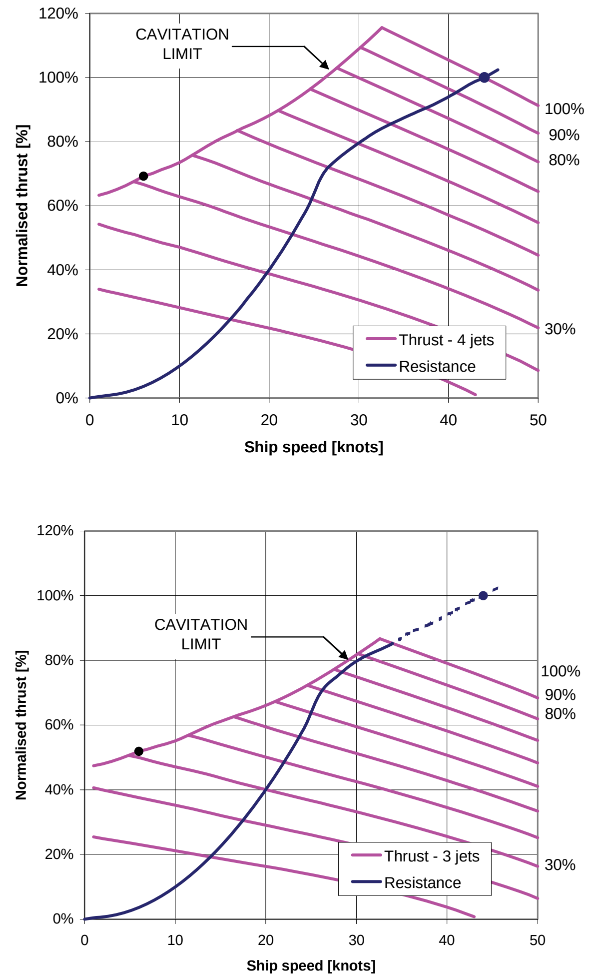

Figure 2: E-type thrust diagram for 4 jets (top) and 3 jets for given resistance line

4. PERFORMANCE EVALUATION AT OFF-DESIGN CONDITIONS

The performance analysis of the waterjet installation is based on the impeller torque and the available total pressure just upstream of the impeller among others.

Evaluation of the torque of the impeller can give an indication of the risk of overloading the engine. In case of increased shaft torque the engine temperatures might increase too much and black smoke can be produced. This should be avoided as much as possible.

The total pressure can be expressed as the available Net Positive Suction Head (NPSH):

$$NPSH_A = \frac{p_{tot}}{\rho g} \qquad [1]$$

with the density of the water.
For normal free sailing conditions the available NPSH can be estimated based on:

$$NPSH_A = \frac{p_\infty - p_v}{\rho g} + \frac{v_{ship}^2}{2g}(1-\varepsilon)(1-w)^2 \qquad [2]$$

where p_v is the vapour pressure, v_{ship} the ship speed, a coefficient representing losses in the inlet ducting and w the wake fraction.

In order to evaluate the performance of the pump the available NPSH is compared to the required NPSH of the pump. This required NPSH is related to each pump design, and it is related to the operational point of the pump according to:

$$NPSH_R = \frac{\kappa}{g} \cdot n^2 D^2 \qquad [3]$$

The specific NPSH is represented by . The pump operation is given by the pump speed n and diameter D.
As long as the available NPSH exceeds the required NPSH of the pump, the margins against cavitation are sufficient. A significant drop of the available NPSH, for example during manoeuvring, might lead to increased cavitation of the pump. In such condition, the benefits of the improved cavitation margins of the LJX/WLD pumps can be exploited.

4.1 LOW SPEED MANOEUVRING

The evaluation of the performance during manoeuvring is based on calculations for two different ship speeds. All calculations are carried out at a fixed rate of revolutions of the pump. The impeller torque at zero drift angle has been used to normalise the results of all other drift angles. Figure 3 shows the normalised torque for the two ship speeds for various drift angles between -60 and + 60 degrees.

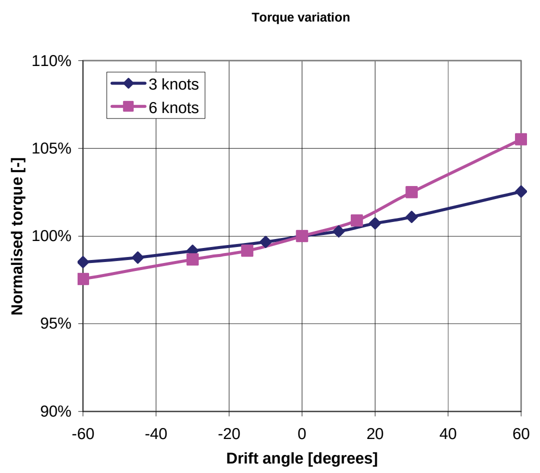

Figure 3: normalised torque variation at low speed manoeuvring for 3 and 6 knots

It can be seen that the effect of the drift angle is asymmetrical on the impeller torque. For the largest drift angle analysed, an increase of torque of about 5% is observed, moreover the effect of the ship speed seems to be linear. Extrapolation of the results towards larger drift angles and larger ship speeds may give torque increases in order of 10%.

Analysis of the flow field just upstream of the impeller revealed the presence of a swirl-component in the flow, which is related to the drift angle. This swirl of the flow can be regarded as a small variation of the impeller rotational speed. Thus with a swirl in the direction of the impeller rotation a small reduction of the RPM is felt, whereas a counter rotating swirl results in a small increase of RPM.

The effect of manoeuvring on the available NPSH is shown in figure 4. The values are normalised with the NPSH at zero drift angle for both ship speeds. It can be seen that the variation in NPSH is more or less symmetrical, which is in accordance with the expectations. Since the reduction in NPSH can be regarded as additional frictional loss in the inlet ducting (thus upstream of the impeller), it is expected that the behaviour would be similar for positive and negative drift angles.

For the largest drift angles a reduction in NPSH of about 8% is observed. This reduction will decrease the margins against cavitation. Since it was shown in figure 2 that the manoeuvring point is located near the cavitation limit, it is likely that the reduction in NPSH due to manoeuvring will result in increased cavitation.

For identical cavitation behaviour during manoeuvring the RPM of the pump should to be reduced with about 4%, based on eqn. [3], which is equivalent with about 12% power.

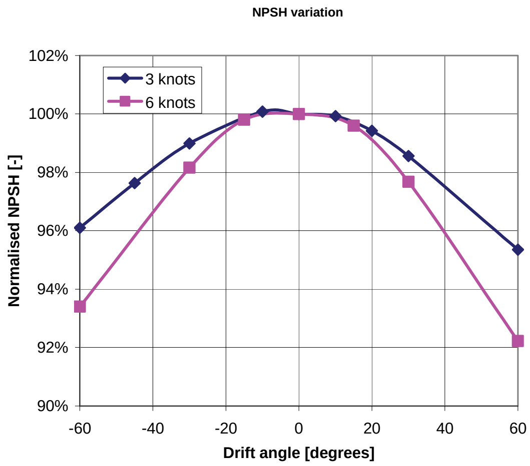

Figure 4: normalised NPSH variation at low speed manoeuvring for 3 and 6 knots

4.2 HIGH SPEED STEERING

The CFD calculations for the high speed steering conditions are carried for 30 and 35 knots. The drift angles are varied between -30 and +30 degrees. It is expected that normal steering will not result in these large drift angles, due to the limitations in the steering angles of the waterjet installations.

Figure 5 shows the normalised torque for both ship speeds. Similar to the results presented in the previous subsection, all results have been normalised with the values found for the zero drift angle.

The asymmetrical behaviour of the torque is in line with the results found for the low speed manoeuvring. Differences between the two ship speeds are negligible for all drift angles.

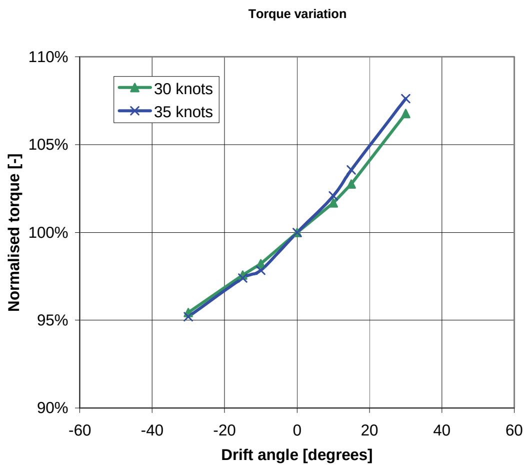

Figure 5: normalised torque variation at high speed steering

Figure 6 shows the normalised NPSH for the high speed steering conditions. Based on eqn. [2], there should be a difference in NPSH for the two ship speeds. However, due to the applied method of normalising the results, both available NPSH values are set to 100% at zero drift angle. It is now clearly shown that the effect of the drift angle is identical for both ship speeds. Comparison of figures 4 and 6 learns that the amount of NPSH reduction at high speed is obtained at lower drift angles. A reduction of 8% at 6 knots is found at a drift angle of 60 degrees, whereas 30 degrees drift angle is found at high speed. In general, the critical margins against cavitation are found below 30 knots. It is therefore concluded that high speed steering is regarded to be a critical off-design condition.

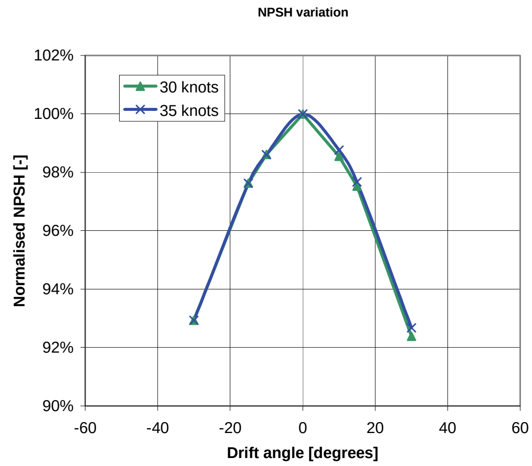

Figure 6: normalised NPSH variation at high speed steering

4.3 Three-jet operation

For the analysis of the effects of three jet operation a series of calculations is made at constant power with varying ship speed. Due to variations in flow rate through the waterjet, also a variation of impeller torque is found. The RPM of the pump has been varied for each ship speed to meet the full power condition.

Figure 7 shows the effect of the ship speed on the impeller torque, for full power operation. The torque has been normalised with the torque at 44 knots, which represents the operating condition as shown before in figure 2. The observed increase of torque for operation at lower ship speeds is only limited. On the other hand, the effect of ship speed on the available NPSH is significant, as shown in figure 8. The quadratic relation of the NPSH with the ship speed as shown in eqn. [2] can be recognised in this chart.

Figure 8 shows that in case of a reduction of the ship speed from 44 to 34 knots, the available NPSH decreases with 27%. This significant reduction causes the large effect on the cavitation margins as shown in figure 2.

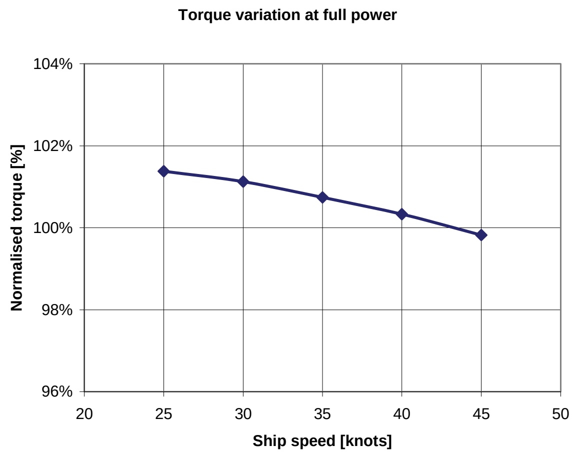

Figure 7: normalised torque at full power for varying ship speed

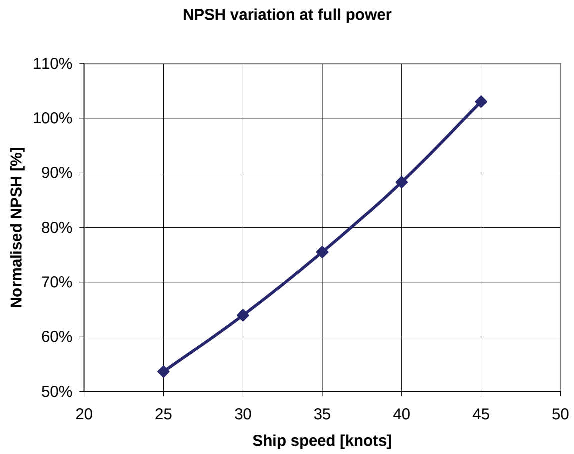

Figure 8: normalised NPSH variation at full power for varying ship speed

5. EFFECT OF IMPROVED CAVITATION MARGINS ON PERFORMANCE

5.1 DESCRIPTION OF NEW PUMP TYPES

The CFD analyses presented in the section before are based on the Lips-Jets E-type waterjet installation, which has been introduced about 10 years ago. Since some years, Wartsila has two new pump types in its portfolio, namely the LJX and the WLD type. One of the main differences between the two new pumps and the conventional E-type is the building type of the pump. The original pump has the typical geometrical shape of a mixed-flow pump, whereas the new pump types are shaped according to axial flow pumps. This is illustrated in figure 9. This figure also shows the effect of the transom flange diameter for identical inlet diameter. The outer diameter of the mixed-flow pump increases from the inlet towards the transom, whereas the axial-flow pump has a constant outer diameter over this part.

The LJX/WLD pump does not only have a different cross-sectional shape, but also the pump specific NPSH κ is better. As a result, the cavitation margins are larger and therefore the cavitation behaviour is improved compared to the E-type.

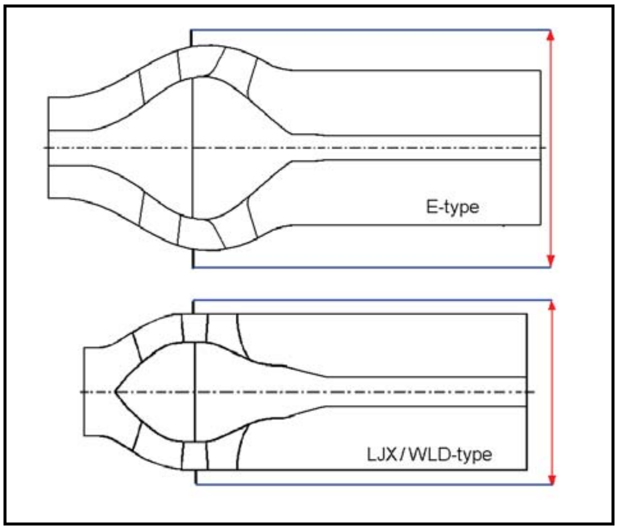

Figure 9: Cross-sectional views of mixed-flow E-type and axial flow LJX/WLD-types

5.1 EFFECT OF IMPROVED CAVITATION MARGINS FOR MANOEUVRING

As shown in figure 2, the cavitation limit at 6 knots is found at 32% of the full power. This represents an available thrust of 69% of the design thrust. Figure 10 shows the comparable thrust diagram for 4 waterjets equipped with the axial flow type pumps. This figure shows that the cavitation limit at 6 knots is now found at almost 41% power, which is equivalent with 83% thrust.

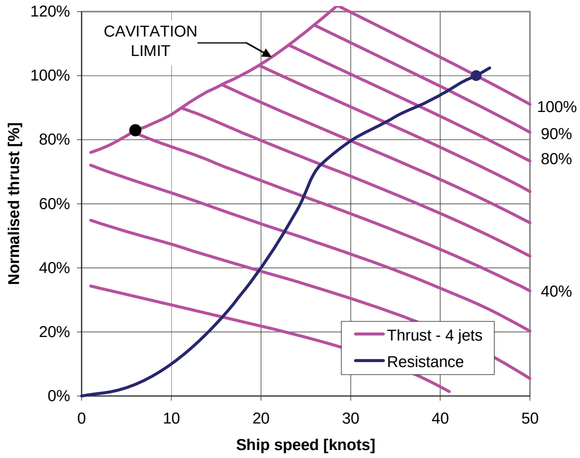

Figure 10: LJX/WLD-type thrust diagram for 4 jets operation for given resistance line

The axial pump can absorb about 28% (41/32) more power at manoeuvring speed of 6 knots before the cavitation margins of the mixed-flow E-type are met. This compensates the effects of the inflow under drift angles by far.

When the benefits of the improved cavitation margins are expressed in the increase of available thrust, an increase of 20% (83/69) is found. Increase in thrust increases the operational envelope of the installation, which will result in better acceleration amongst others.

5.2 EFFECT OF IMPROVED CAVITATION MARGINS FOR THREE JET OPERATION

The evaluation of three jet operation for a given resistance curve, as shown in figure 2, revealed that the available cavitation margins vanished for the E-type pump. The same evaluation is shown in figure 11 for the axial flow pump types. At full power the speed margin is about 6 knots. This is sufficient for good operation of the vessel even at three jets.

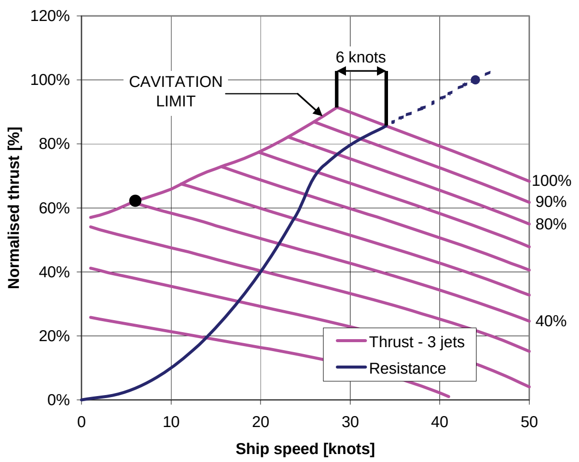

Figure 11: LJX/WLD-type thrust diagram for 3 jets operation for given resistance line

6. CONCLUSIONS

Both at low speed manoeuvring and high speed steering shaft torque of the impeller is influenced by the inflow field under a drift angle. Negative drift results in a decrease of torque and positive drift lead to a higher torque. The variation in torque is related to the presence of pre-swirl in the inlet ducting. If the pump has to operate at large positive drift angles an increase of torque of about 5% is observed. This might lead to overloading of the engine.

The available NPSH is influenced both at low speed manoeuvring and high speed steering. The decrease of NPSH is related to the magnitude of the drift angle. However, the behaviour is more or less identical for negative and positive drift angles.

The effects of drift angles on torque and NPSH are significant at low speed manoeuvring conditions. Available margins for engine overloading and cavitation might not be sufficient for all conditions encountered.

High speed steering seems to be less sensitive to the variations in torque and NPSH under normal conditions. Torque increase at realistic drift angles is only a few percent. In general the cavitation margins are substantial above 30 knots (assumed all jets in operation). Consequently, the decrease of NPSH should not lead to increased cavitation.

When a vessel with four waterjet installations is operated with only three jets, the available cavitation margins at full power decrease significantly and they might even vanish completely. A reduction in NPSH of almost 30% is found when the ship speed drops from 44 knots (with four jets in operation) to 34 knots with three jets.

Two new axial flow pump types, denoted LJX and WLD have been developed with improved cavitation margins.

The axial pump types can absorb almost 30% more power at manoeuvring speeds before the cavitation limits are reached, which results in about 20% more available thrust.

The increased cavitation performance of the axial pump enables operation of a vessel with three jets at full power, whilst keeping sufficient margins against cavitation.

7. REFERENCES

1. Bulten, N.W.H., ‘Numerical Analysis of Waterjet Propulsion System’, PhD thesis, Technical University of Eindhoven, 2006

2. Bulten, N.W.H., Verbeek, R., Van Esch, B.P.M., ‘CFD simulations of the flow through a waterjet installation’, *International Journal of Maritime Engineering*, Vol 148 part A3, pp 23-34, 2006

3. Verbeek, R. & Bulten, N., 'Recent developments in waterjet design', RINA Waterjet Propulsion II conference, Amsterdam, 1998

8. AUTHORS BIOGRAPHY

Norbert Bulten is team leader of the CFD department of Wärtsilä Propulsion Netherlands BV. He has written a PhD thesis at the Eindhoven Technical University (TU/e) about the numerical analysis of a waterjet installation.

Rob Verbeek is responsible for waterjet hydrodynamics and product development within Wärtsilä Propulsion Netherlands BV, formerly known as Lips Jets.

RESEARCH ON THE OPTIMUM BLADES NUMBER OF MIXED FLOW PUMP BASED ON CFD

Qiongfang Yang, **Yongsheng Wang, Zhihong Zhang**, and **Mingmin Zhang**, Naval University of Engineering, China

SUMMARY

Effects of changing the number of pump blades of both rotor and stator on the characteristics of flow pattern and waterjet propulsion performances are principally investigated in this paper, which includes the changes of rotor's blades from 5 to 7 to the effect of Stodola slip factor, of stator's vanes from 9 to 13 to the effect of straightening the outflow of impeller, and of both rotor and stator's blade numbers simultaneously. It shows that, given the condition of fixed pump revolution and vessel speed, the Stodola slip factor, the head, axial-thrust and brake power are all incline as the number of rotor's blades increase, but the efficiencies decline; the circumferential velocity of the nozzle outflow weakens with the increase of number of stator's vanes, but the improvement is approximately unchangeable when it comes to 11. The waterjet performances are close when the stator's vanes are 10 and 11, both of their head and axial-thrust are bigger than that of with 12 or 13 stator's vanes; The waterjet optimum propulsion performances can obtained when 5 blades of rotor match 9 vanes of stator, while the rotor blades are 6 or 7, the best number of stator's vanes both are 11, but the 7 blades and 11 vanes combination presents a better cavitaion performances.

NOMENCLATURE

b_2	Width of rotor outlet (m)
D_{1m}	Average diameter of the rotor at inlet(m)
D_{2m}	Average diameter of the rotor at outlet(m)
D_{2e}	Minimum diameter of the rotor at outlet(m)
D_{2a}	Maximum diameter of the rotor at outlet(m)
$\boldsymbol{f}$	Vector of inertia force (N)
g	acceleration due to gravity (m s^2)
H	Head of pump (m)
l	Blade chord (m)
N	Brake power (kW)
n	Rotating speed of pump (r min^{-1})
n_s	Specific speed ($m^{-3/4}$ $s^{-3/2}$), $n_s = \dfrac{3.65n\sqrt{Q}}{H^{3/4}}$
$NPSH$	Net positive suction head (m)
$NPSH_i$	Incipient net positive suction head (m)
p	Pressure (Pa)
p_1	Upstream (suction) static pressure (Pa)
p_{01}	Upstream (suction) total pressure (Pa)
p_v	Vapor pressure (Pa)
P_V'	Introduced parameter to determine local $p<p_v$ region (Pa)
p_{min}	Minimum pressure in-house the pump (Pa)
Q	Volume flow rate (m^3 s^{-1})
$\boldsymbol{r}$	Vector of space (m)
S_S	Stodola slip factor (-), $S_S = 1 \quad \dfrac{\pi \sin\beta_{b2}}{Z}$
s	Solidity (-), $s = l / t_m$
t	Time (s)
t_m	Cascade interval (m)
$\boldsymbol{U}$	Vector of fluid velocity (m s^{-1})
V_s	Ship speed (m s^{-1})
V	Pump suction speed (m s^{-1})
$\boldsymbol{\omega}$	Vector of angular velocity (rad s^{-1})
Z	Number of blades (-)
α_1	Blade angle at the rotor discharge (°)
α_2	Flow angle on shroud side at rotor outlet (°)
α_3	Flow angle on hub side at rotor outlet (°)
β_{b2}	Mean blade angle at the rotor discharge (°)
β_2	Flow angle at the rotor discharge (°)
ρ	Density of water (kg m^{-3})
μ	Dynamic viscosity (N s m^{-2})
μ_t	Turbulence viscosity (N s m^{-2})
η	Pump efficiency (-), $\eta = \dfrac{\rho g Q H}{N}$

1. INTRODUCTION

The number of pump blades has significant effects on its head, efficiency, and cavitation performances. Generally, the effects present non-linear characteristics, and a given device exist an optimum number of rotating blades in the framework of optimum integrated performances in practical engineering application. Stepanoff (1957) pointed out empirical formulas to analyze the optimum blades number for centrifugal and axial flow pumps. It is important to recognize that the extrusion action of blades and its surface friction loss should be weakened as much as possible when the number of blades is calculated, additionally, the blade passage should be sufficiently extruded to ensure stable flow field and sufficient actions blades act on the flow [2].

The key to design pumps that operate more efficiently, quietly, and reliably at lower cost is a better understanding of, and ability to, predict their hydrodynamics accurately, which requires a detailed scene of the flow fields within the blade passages. Nowadays computational fluid dynamics (CFD) is seeing more and more use successfully in predicting the flow fields in both stationary and rotating blade passages. Miner[3] analyzed the flow field within the first-stage rotor and stator of a two-stage mixed flow pump and made a comparison with the measured data of the rotor's velocity and pressure profiles. Hu et al.[4]

used several models, including single blade to blade channel model and the whole impeller model with or without the shaft and the stator, to compute the flow field in the impeller and nozzle of a waterjet pump and compare the torque with the experimental data. Bulten (2006) made a detailed analysis of a mixed-flow waterjet propulsion system in his Ph.D. dissertation, especially to quantify the effects of the non-uniform inflow and the resulting non-stationary flow on the system performances, and to quantify the forces on the complete waterjet installation in both axial and vertical direction. These cases demonstrate the ability of the CFD method to predict the waterjet pump performances, including the thrust distribution accurately.

This paper with an emphasis on the effects of various number of blades on the waterjet thrust, torque, efficiency and incipient cavitation performances. The governing equations, numerical methods and the suitable computational domain for the waterjet numerical simulation will be presented in section 2. Section 3 will present the validation of numerical method, based on the mesh resolution to obtain reasonable results for such devices flows, by comparing numerically calculated thrust and torque of the waterjet under both design and off-design conditions with the waterjet-ship load-drive characteristics curve. The effects of number of blades to the propulsion performances lie in section 4, which will address 3 cases, (ⅰ) only change the rotor's blades form 5 to 7, (ⅱ) only change the stator's vanes from 9 to 13, (ⅲ) change the rotor and stator's blades simultaneously to reconstruct different devices. Section 5 will present the incipient cavitation performances of the two optimum combination pump above-argumentation. Section 6 will summarize the results that have been obtained in this study.

2. GEOMETRY AND COMPUTATIONAL INVESTIGATIONS

The solver is a cell-centered finite-volume-based code which solves the hydrodynamic equations as a single system, and uses a fully implicit discretization of the equations at any given timestep. Turbulence is modeled using SST turbulence model. It combines the $\kappa-\varepsilon$ and $\kappa-\omega$ models. For the free stream region the $\kappa-\varepsilon$ model is used and for the near wall flow region (y^+<5) the $\kappa-\omega$ model is applied. It has been shown to eliminate the free stream sensitivity problem without sacrificing the $\kappa-\omega$ near wall performance[6]. It is reckoned to perform very well close to walls in boundary layer flows, particularly under strong adverse pressure gradients[6,7].

Equations governing the turbulent incompressible flow within the rotor are formulated in a rotating reference frame. The continuity and momentum equations are:

$$\frac{\partial \rho}{\partial t} + \nabla \cdot (\rho \mathbf{U}) = 0 \tag{1}$$

$$\frac{D}{Dt}(\rho \mathbf{U}) + 2\rho \boldsymbol{\omega} \times \mathbf{U} + \rho \boldsymbol{\omega} \times \boldsymbol{\omega} \times \mathbf{r} = \rho \mathbf{f} \quad \nabla p + (\mu + \mu_t)\nabla^2 \mathbf{U} \tag{2}$$

where $\boldsymbol{f}$ is inertia force, water is sucked from the bottom of the ship with the change of potential energy, so the gravity is taken into account. p is modified to account for effects due to rotation, ρ density, and μ the dynamic viscosity, μ_t the turbulence viscosity. U is the velocity vector, and ω angular velocity vector, r the space vector. As the stator lies in the stationary reference frame, the continuity equation remains the same but the momentum equation changes to

$$\frac{D}{Dt}(\rho \mathbf{U}) = \rho \mathbf{f} \quad \nabla p + (\mu + \mu_t)\nabla^2 \mathbf{U} \tag{3}$$

These equations along with the inlet velocities and outlet pressure boundary condition are solved for the waterjet in-house flow field.

The waterjet consists of inlet duct, a rotor-stator, and nozzle. Considering the effects on inflow caused by the ship speed and hull boundary layer, a sizable region under hull, named flow control volume (FCV), should be chosen with a care. So the stator(including the nozzle), rotor, inlet duct(including the fairing) along with the FCV make up of the whole computational domain of the waterjet, see Fig.1. Fig.2 shows the mixed flow pump geometry.

Fig.1 Computational domain of the waterjet

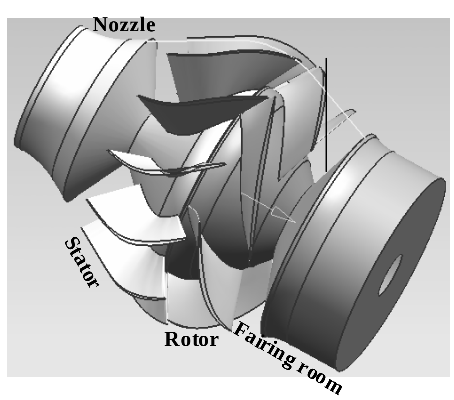

Fig.2 Mixed flow pump geometry

3. VALIDATION OF FLOW FIELD COMPUTATION

The grid used in the computations has about one million. The inlet duct and the FCV are discretized into unstructured cells as a whole. Special emphasis was put on modeling the inlet lip turbulent eddy motion and computing streamwise acceleration of the boundary layer near the hull, so fine grid spacing are used in such local region. The rest solution domain are filled with hexahedral cells. Considering the periodicity of the blade passages, Fig.3 shows the single blade to blade channel surface mesh for both the rotor and stator.

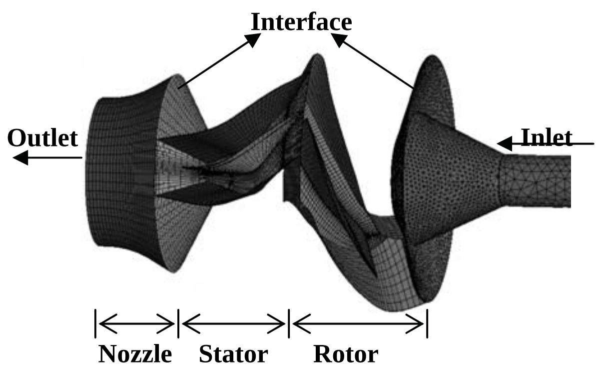

Fig.3 Surface mesh of the waterjet single passage

An appropriate mesh density gives a compromise between the accuracy and the computational cost. Miner [8] made a comparison of the velocity profiles with an axial flow impeller from two meshes, one with 22176 nodes and the other with 40131 nodes, and showed no significant differences. A continuation of work referring to a mixed flow pump (specific speed is 388.54) was performed by him later[3]. Based on the experience gained in the analysis of the axial flow impeller, the rotor model has 26299 nodes and the stator with 20519 nodes, the shapes and magnitudes of the velocity and static pressure profiles were correctly predicted again. As the mixed flow waterjet pump for this study is close to that of Miner both on the specific speed and design parameters, the mesh resolution of the rotor and stator gets 20000 nodes as basic orders of magnitude throughout the computations presented in subsections. The height of the first cell adjacent to the blade surface is approximately 0.00001 D_{1m}, which is 3 to 50 in terms of y^+ for all surfaces, where D_{1m} is the average diameter at the inlet of the rotor. Ten layers of hexahedral cells have been attached to the surface with a grid-stretching ratio equal to 1.1. The number of the computational elements of the inlet duct and FCV domain is approximately 190000 after a comparison. Velocity components of uniform stream with the given inflow speed are imposed. On the nozzle exit boundary, the static pressure is set to background pressure while other variables are extrapolated, which assumes the jet diameter at vena contracta equals to nozzle diameter. The mixed plane interfaces are used to handle with the rotating and stationary domains. Throughout the computations presented in subsections, such schemes are used unless otherwise stated.

Results for the waterjet show comparison between computed and manufacturer global data on design speed and revolution and off-design conditions, see Fig.4, where all wall forces due to pressure and wall shear stress are integrated to get the thrust. All variables are normalized by the design value. The power absorption prediction differs by less than 2%, while the difference for the thrust is a litter higher, but still less than 4%.

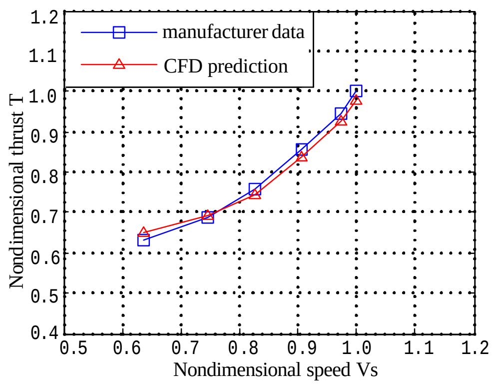

(a)

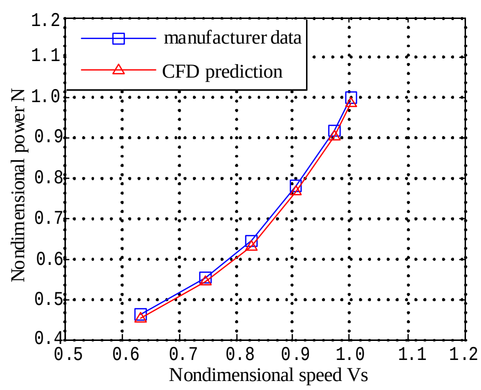

(b)

Fig.4 Thrust and power versus speed: (a) thrust and (b) power

4. EFFECTS OF VARIABLE NUMBLE OF BLADES ON PROPULSION PERFORMANCES

This section will describe different number of blades for rotor-stator interaction on the waterjet performances with three steps. Firstly, just changing only the rotor's blades from 5 to 7, the Stodola slip factor will change subsequently. Secondly, increase of the stator's vanes resulting in different commutating action is of our interest. Finally, several configuration by changing both of the rotor and stator's blades simultaneously, the global quantities are compared with each other in order to select the optimum match of the two components.

4.1 CHANGE ROTOR'S BLADES ONLY

The mixed flow waterjet pump consists of a six blades rotor and an eleven vanes stator. The design parameters of the rotor on design ship speed and rotational speed are specific speed n_s=465.7, average diameter of the rotor at inlet $D_{1m}=0.136m$ and at outlet D_{2m}=0.137m, width of outlet b_2=0.073m, minimum and maximum diameter at outlet D_{2e}=0.887m and D_{2a}=0.950m respectively, the mean blade angel at the discharge β_{b2}=21.6°, and the Stodola slip factor S_S=0.803, which are calculated based on literatures[2,9]. Changing only the rotor's blades, the solidity $s = l / t_m$ will vary significantly, where l is the chord of the blade measured in the developed meridional plane (Fig.5), t_m is the cascade interval, while the response of the other geometrical parameters are entirely negligible[10], see Table1. Fig.5 shows a significant fraction of the geometrical parameters on the meridional plane. On this surface, the subscripts 1 and 2 denote particular values at inlet and discharge, and the corresponding subscripts a , e and m relate to the tip, root and mean span location respectively. The angles, α_1、 α_2 and α_3 are blade angle at the discharge, flow angle on shroud side and on hub side, which can be directly obtained form the schematic in literature[9]. The condition $0.995V_{sdesign}$ and $1.001\,n_{design}$ is used to analyze in the subsequent computations. The corresponding rotor geometrical parameters with different rotor's blades are compared in Table1.

As shown in Fig.5, the flow angle β_2 is not identical to the discharge blade angle β_{b2}, and, therefore, implies an effective slip S , which is due to the non-uniformity in the discharge flow caused by the rotational flow within an individual blade passage. Stodola (1927) was among the first to recognize the importance of the rotational component flow. Busemann (1928) first calculated its effect upon the head/flow characteristic for the case of infinitely thin blades. Stodola also gave the estimated slip factor, S_S , was $S_S = 1 \quad \frac{\pi \sin \beta_{b2}}{Z}$, where Z was the number of blades[11]. As the number of blades gets larger, S_S tends to unity as the rotational flow increasingly weakens, which minimizes the decrease in the head[11]. As shown in Table1, all the three rotor's blade angle at the discharge is approximate 21.6° . Fig.6 shows the three waterjet's head, propulsion efficiency, axial thrust and brake power corresponding to three rotors with different blades. The head-blades relationship is approximately linear. In practice, however, the frictional losses will increase with the number of blades. One popular engineering criterion (Stepanoff 1948) is that Z should be one third of the discharge blade angle (in degrees).

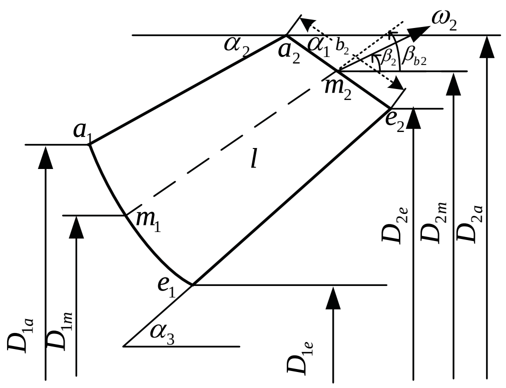

Fig.5 Meridional surface and geometrical parameters

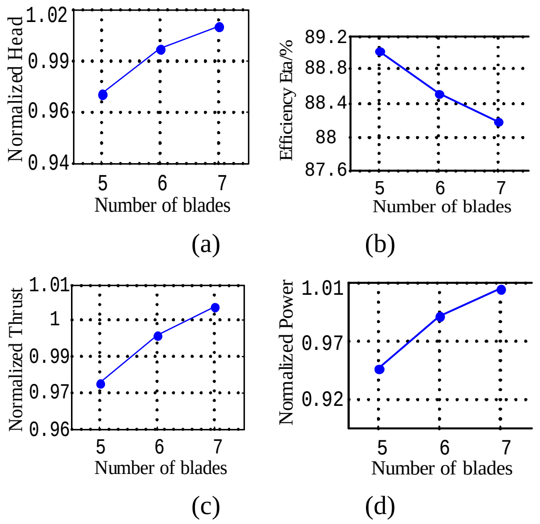

Fig.6 The waterjet propulsion performance curves versus the number of rotor's blades: (a) head, (b) propulsion efficiency, (c) thrust (d) brake power.

As shown in Fig.6, on the off-design condition, the propulsion efficiency of the waterjet is highest in the case of the rotor with five blades, while the lowest with seven blades; but both of the corresponding axial thrust and the brake power show an opposite way. According to the definition of pump efficiency:

$$\eta = \frac{\rho g Q H}{N} \tag{4}$$

where,
Q =flow through the waterjet pump;
H =head of the pump;
N =brake power required from an engine

Although the head is maximum for seven blades, the power absorption increase more rapidly at increased number of blades, hence a decline for the efficiency. According to the operational characteristics of the waterjet, the power required with the seven blades rotor is larger than the delivered engine power, which will result in a heavy condition. On the other side, when the number of rotor's blades turns to five, a light condition will present, the engine is not able to deliver the maximum power again in such a case. Integrating the flow and propulsion predictions, the waterjet device reaches the optimum propulsion performances with the six blades impeller. The same conclusion can also be obtained under the other four off-design points, see Fig.7.

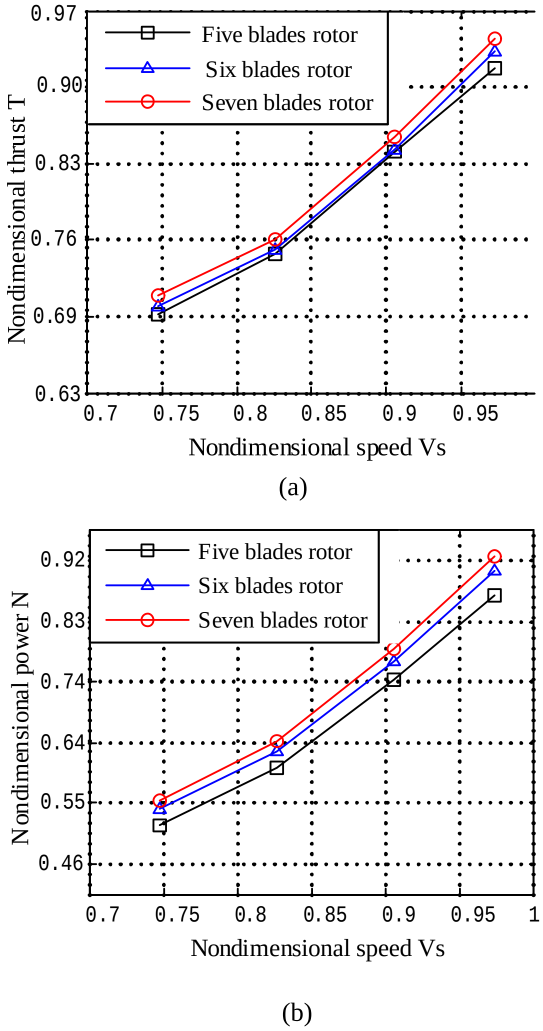

Fig.7 Waterjet propulsion predictions under off-design conditions: (a) thrust versus speed and (b) power versus speed

4.2 CHANGE STATOR'S VANES ONLY

The stator is just downstream of the rotor. It's blade angle is designed to straighten the flow so that the fluid leaves the stator nearly in axial direction. For reasons of continuity, the decrease of the cross-section area of the stator results in an increase of the kinetic energy and a corresponding decrease of pressure. It recovers non-tangential component in idealism. According to the momentum principle, the developed thrust of the waterjet is closely relative to the velocity distribution at the exit of the discharge nozzle, which will be used to reflect the uniformity of the outflow. Considering changing the origin eleven vanes stator, over a range of nine to thirteen vanes, combines the origin six blades rotor to be analyzed. And both of the shroud and hub for the rotor- stator interaction is the same as the origin. The computational condition is the same as section 4.1.

Fig.8 shows the iso-velocity plot distribution at the exit of the nozzle for five waterjet devices with different number of vanes stator, the corresponding predicted thrust and power can be found in Table2. As the number of vanes gets larger, the rotating component of the outflow increasingly weakens, however, it shows no significant difference when it comes to 11. Uniting Table 2, the head, propulsion efficiency, thrust and brake power of the waterjet are close to each other for the ten vanes stator and eleven vanes. It shows the maximum thrust for the eleven vanes, while the efficiency for the nine vanes stator is the highest, due to its minimum frictional losses. Compared to the waterjet with a eleven-vane stator, the thrust and brake power of the waterjet with twelve or thirteen vanes are much smaller, and the hydrodynamic characteristics for the twelve and thirteen vanes are similar at the same time. Integrating the flow and propulsion predictions, the waterjet device reaches the optimum propulsion performances with the eleven-vane stator.

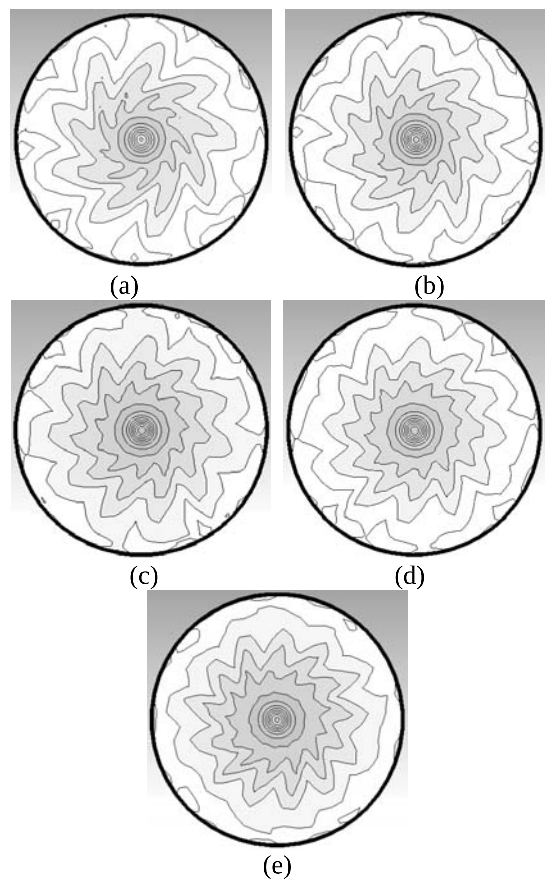

Fig.8 Iso-velocity plot distribution at the exit of the discharge nozzle with different number of vanes: (a) 9; and (b) 10; and (c) 11; and (d) 12; and (e) 13

4.3 CHANGE ROTOR'S BLADES AND STATOR'S VANES SIMULTANEOUSLY

The stator of the mixed flow pump is 3-dimention with a long axial distance but short spanwise. The rotor-stator interaction should be taken into account when the stator's vanes are designed, so the vanes should be matched the discharge of the rotor. Fig.9 shows the pressure distribution of the origin waterjet pump's meridional surface, including both of the rotor and stator. The leading edge of the vane is approximately parallel to the trailing edge of the rotor's blade, and the axial distance between them are very small. Such stator's vanes are generally called with big distortion. The variety of rotor's blades and stator's vanes simultaneous will result in the change of the meridional surface of the pump, hence of the streamline within the blade passage, which will affect the waterjet propulsion performances. The operational point is also the same as that in section 4.1.

For different combination between rotor's blades and stator's vanes, Fig.10 shows the comparison of the head, propulsion efficiency, thrust and the absorbed power of the different waterjet devices. For the waterjet attached by the six blades rotor, all the global quantities lie intermediately compared to that of five-blade rotor and seven-blade rotor matched by five different stator's vanes. Under the same operational point, the head of the waterjet with seven blades rotor gets the maximum value, but its efficiency is the lowest, however, as for five blades rotor, it is just on the contrary, which is the same as just changing the rotor's blades only. All the global quantities of the six blade rotor integrating with the series of stator's vanes vary similarly with that of seven blades rotor. When the rotor's blades is five, the optimum propulsion performances can be obtained by attaching the nine vanes stator. Another optimum match is seven blades rotor and eleven vanes stator, which is the same as the combination for six blades rotor.

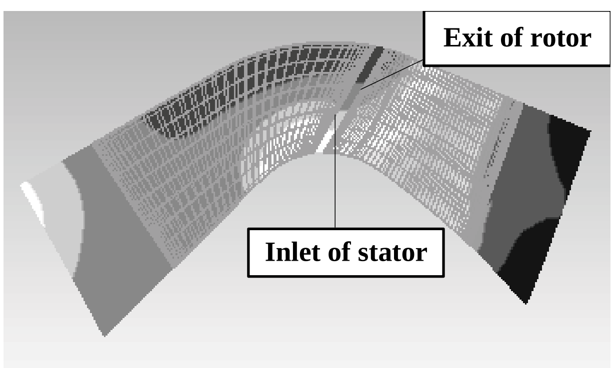

Fig.9 Pressure distribution of the origin waterjet pump's meridional surface

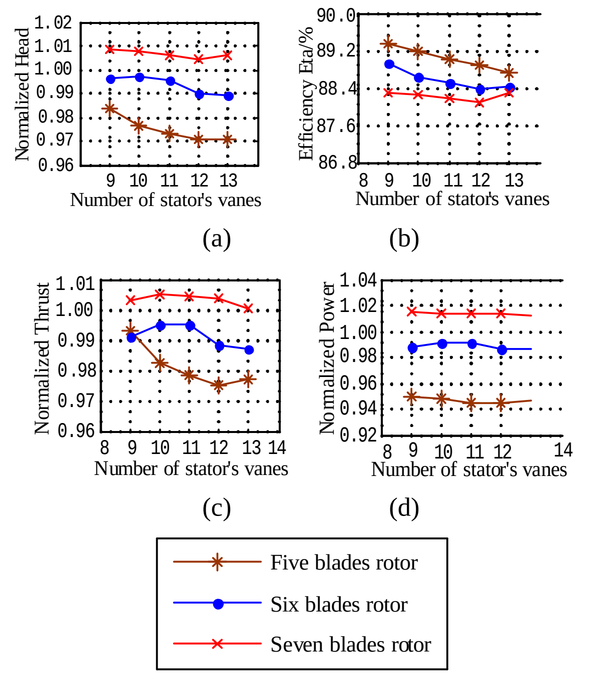

Fig.10 Waterjet propulsion predictions for the different combination between rotor's blades and stator's vanes: (a) head, (b) efficiency, (c) thrust and (d) power

5. COMPARISON OF PUMP INCIPIENT CAVITATION PERFORMANCES WITH 6 BLADES ROTOR TO 7

Since we have concluded that the optimum propulsion performances of the waterjet can be presented by combination of 6 or 7 blades rotor and 11 vanes stator, now form the pump incipient cavitation point of view there are some basic introduce. Cavitation is defined as the process of formation and disappearance of the vapor phase of a liquid when it is subjected to reduced and subsequently increased pressure at constant ambient temperatures. The potential for cavitation is typically evaluated in terms of cavitaion parameters: net positive suction head, NPSH, which is regarded as a measure for the margin against vaporization of the fluid entering the pump. The formula to compute it reads:

$$NPSH = \frac{p_{01} - p_v}{\rho g} \tag{5}$$

In which p_{01} is the upstream (suction) total pressure, p_v is vapor pressure, and g is acceleration due to gravity. The total pressure equals

$$p_{01} = p_1 + \frac{1}{2}\rho V^2 \tag{6}$$

Where p_1 is upstream (suction) static pressure, and V is suction velocity. The incipient cavitation characteristic plays a key role when designing and evaluating rotors with regards to suction performance. By definition (5) one has

$$NPSH_i = \frac{p_{01,i} - p_v}{\rho g} \qquad (7)$$

where $p_{01,i}$ is the total upstream (suction) pressure, associated with the situation that cavitation starts somewhere downstream. At a given condition it exists a minimum pressure $p_{\min}$ at a particular location downstream in-house the pump. Considering the two streamline through point of $p_{\min}$ and p_v respectively, corresponding to the condition of p_1 and $p_{01,i}$. It follows that:

$$p_1 - p_{1,i} = p_{\min} - p_v \qquad (8)$$

Substituting equation (8) in equation (7) and (5) it gets:

$$NPSH_i = \frac{p_{01} - p_{\min}}{\rho g} \qquad (9)$$

Equation (9) stated that incipient NPSH can be obtained with total upstream pressure and the minimum pressure. Here the fluid is assumed to be pure, without dissolved gas.

Next it turns to the waterjet pump. The real inlet duct and ship hull geometry are simplified as a straight suction pipe, see Fig.11, so the inflow velocity distributions are uniform. Bulten(2006) analyzed the influence of non-uniform axial inflow in detail in his Ph.D dissertation. For the origin 6 blades rotor and 11 vanes stator combination, by CFD calculation it states that under the designed rotating speed and capacity condition the axial force of the pump enlarges 20% with the shaft power decreases 0.7% at the same time, so the efficiency of the pump increases with the uniform inflow.

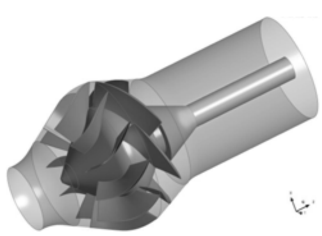

Fig.11 Sketch of waterjet pump with simplified inlet

To determine the region where the local static pressure drops below the vapor pressure,(i.e. $p < p_v$), another parameter $p_v^{'}$ is introduced, with reference to equation (8), the formula reads:

$$p_v^{'} = p_v + (p_1^{'} - p_1) \qquad (10)$$

in which $p_1^{'}$ is the pipe inlet static pressure, see Fig.11. Then, substituting equation (5) and (6) in equation (10) it gets:

$$p_v^{'} = p_{01}^{'} - \rho g NPSH \qquad (11)$$

where $p_{01}^{'}$ is the total pressure of the pipe inlet. So the region $p < p_v$ can be visualized during post-processing after the CFD run through the iso-surface of $p_v^{'}$.

Fig.12 gives an comparison of the local low pressure region above-analyzed between the pumps with 6 blades rotor and 7 blades. For both the pumps the region starts a little distance after the blade leading edge, and has longest streamwise length near the rotor shroud. While the 6 blades rotor pump has the larger region for the bigger single blade load. Fig.13 shows the comparison of blade load at 0.7 times span location of the two pump. The pressure side of the rotor with the number of 6 is higher around the leading edge. The CFD calculation states that the $NPSH_i$ of the 6 blades rotor pump is 114.0m, which is smaller than the 7 blades rotor pump of 126.5m under the same design condition above-argumentation, indicating a easier susceptibility to incipient cavitaion.

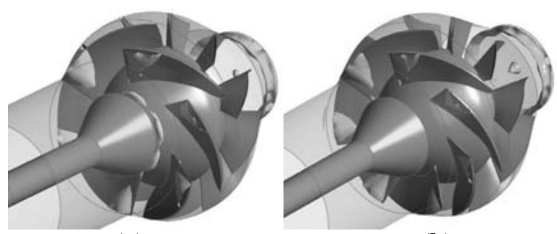

(a) **(b)**

Fig.12 Comparison of the local $p < p_v$ region between the two pump: (a) 6 blades rotor-11 vanes stator; (b) 7 blades rotor-11 vanes stator

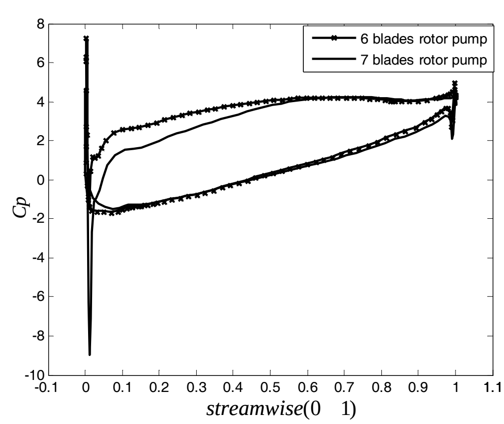

Fig.13 Comparison of the pressure coefficient at 0.7span location between the 6 blades and 7 blades

6. CONCLUSIONS

Based on CFD, the flow pattern and propulsion performances of the waterjet are analyzed on both design and off-design conditions. Effects of the rotor's blades and stator's vanes to the propulsion performances are mainly investigated, and the results obtained are as follows:

(1) Given the operational points with dynamic parameters, the propulsion efficiency reaches the highest with the five blades rotor configuration, the lowest with the seven blades rotor; while both the thrust and brake power are just on the contrast, the lowest with five blades rotor and the highest with seven blades rotor. As the increase of rotor's blades number, the Stodola slip factor gets larger, which weakens the rotational flow within the blade passage, hence results in the increase of the head.

(2) Just changing the stator's vanes only, the rotating discharge flow at the exit of the nozzle tends to uniformity as the vanes' number get larger, but the improvement is approximately unchangeable when the vanes comes to 11, and makes the efficiency decline due to frictional losses at the same time. Under the certain operational point, compared to the waterjet with a eleven-vane stator, the thrust and brake power of the waterjet with twelve or thirteen vanes are much smaller, and the hydrodynamic characteristics for the twelve and thirteen vanes are similarity as well.

(3) Increasing the rotor's blades from five to seven, and changing the stator's vanes from nine to thirteen at the same time, it can reconstruct 15 different waterjet pumps. In which the characteristics for the series of six blades rotor lie intermediately compared to that of five-blade rotor and seven-blade rotor matching five different stator's vanes respectively. The waterjet series with five-blade rotor get the maximum efficiency and minimum head, while the waterjet series with seven-blade rotor are on the contrast. A five blades rotor combining a nine vanes stator can obtained the optimum propulsion performances, when the number of rotor's blades is six or seven, the optimum match is both the eleven-vane stator, while the 6 blades rotor pump's local low pressure region is bigger and so is easier to incipient cavitation.

7. ACKNOWLEDGEMENTS

This research was sponsored by one of the Office of Naval Research Grant under the administration of Dr. Yongsheng Wang and partially supported to prepare this paper by the basic research project in E450.

8. REFERENCES

1. STEPANOFF A J. Centrifugal and Axial Flow Pumps[M]. *New York: John Wiley & Sons.INC.*,1957.

2. GUANG Xingfang. The Master Handbook of Modern Pumps[M]. *Beijing: Press of Astronautics*, 1995.(in Chinese)

3. MINER S M. CFD Analysis of The First-Stage Rotor and Stator in A Two-Stage Mixed Flow Pump[J]. *International Journal of Rotating Machinery*, 2005(1): 23-29.

4. HU P, ZANGENEH M. CFD Calculation of The Flow Through A Waterjet Pump[C]. *International Conference on Waterjet Propulsion III, Sweden: RINA*, 2001: 1-10.

5. BULTEN N. Numerical Analysis of a Waterjet Propulsion System[D]. *PhD dissertation, Library Eindhoven University of Technology, Netherlands*, 2006.

6. LLOYD G, ASTILLEROS E. Best Practice Guidelines for Marine Applications of Computational Fluid Dynamics[R]. *WS Atkins Consultants and members of the NSC, MARNET-CFD Thernatic Network*, 2002: 37-42.

7. MENTER F R. Ten Years of Industrial Experience with SST Turbulence Model[C]. *Fourth International Symposium on Turbulence, Heat and Mass Transfer (ICHMT), Turkey: Antalya*, 2003: 625–632.

8. MINER S M. 3D Viscous Flow Analysis of An Axial Flow Pump Impeller[C]. *International Symposium on Transport Phenomena and Dynamics of Rotating Machinery (ISROMAC'96), Hawaii: Honolulu*, 1996, 2: 336-344.

9. HE Xijie, LAO Xuesu. Design Method of Mixed-Flow Pump Impeller's Blade[J]. *Journal of Hebei Engineering and Technical College*, 2000(1): 1-5.(in Chinese)

10. YAN Bipeng, TANG Fangping. Study on The Performance of Axial-Flow Pump by Changing The Number of Its Blades[J]. *Journal of Yangzhou University*, 1998, 1(3): 53-55.(in Chinese)

11. BRENNER C E. Hydrodynamics of Pumps[M]. *Vermont: Concepts ETI, Inc.*, 1994.

9. AUTHORS BIOGRAPHY

Qiongfang Yang received a B.S. degree (Ship Power Engineering, 2006) and an M.S. degree (Marine Engineering, 2008) from Naval University of Engineering, and now is a Ph.D candidate within the marine engineering realm. He is a member of the Office of New Technology of Marine Propulsion, has received the first scalar award in Hubei province for his B.S. thesis, and has written 8 papers in the area of marine propulsor up to now.

Yongsheng Wang holds the current position of Director at the Office of New Technology of Marine Propulsion. He is Professor of Marine Engineering in the University of Naval Engineering.

Zhihong Zhang holds the current position of Director at the Department of Fluid Mechanics, professor.

Mingmin Zhang is a member of the Institute of Underwater Acoustics, professor, mainly focuses on the underwater radiated noise of the navy machinery.

TABLE 1 Geometrical parameters of the rotor's blade

Number of blades	Specific speed	Width of outlet (m)	Average diameter at inlet (m)	Average diameter at outlet (m)	Velocity meridional at outlet (m/s)	Maximum diameter at outlet (m)	Minimum diameter at outlet (m)	Blade angle (°)	Stodoal slip factor
5	469.390	0.073	0.135	0.135	0.229	0.943	0.881	21.594	0.757
6	466.060	0.073	0.136	0.137	0.228	0.950	0.887	21.606	0.803
7	462.749	0.073	0.136	0.138	0.227	0.953	0.890	21.601	0.829

TABLE 2 Waterjet propulsion prediction with 6 blades rotor attached by different stator's vanes

Number of vanes	Thrust (kN)	Brake power (kW)	Propulsion efficiency (%)	Head (m)
9	71.261	2137.553	88.921	38.266
10	71.583	2143.661	88.612	38.277
11	71.596	2142.872	88.511	38.219
12	71.089	2133.264	88.370	38.007
13	70.962	2132.854	88.434	37.976

A MULTI-OBJECTIVE AUTOMATIC OPTIMIZATION STRATEGY FOR DESIGN OF WATERJET PUMPS

M. Zangeneh, University College London, UK
K. Daneshkhah and **B. DaCosta,** Advanced Design Technology Ltd, UK

SUMMARY

A methodology is presented for designing waterjet pumps to meet multi-objective design criteria. The method combines a 3D inviscid inverse design method with multi-objective genetic algorithm to design pumps which meet various aerodynamic and geometrical requirements. The parameterization of the blade shape through the blade loading enables 3D optimization with very few design parameters. A generic pump stage is used to demonstrate the proposed methodology. The main design objectives are improving cavitation performance and reducing leading edge sweep. The optimization is performed subject to certain constraints on Euler head, throat area, thickness and meridional shape so that the resulting pump can meet both design and off-design conditions. A Pareto Front is generated for the two objective functions and 3 different configurations on the Pareto front are selected for detailed study by 3D RANS code. The CFD results confirm the main outcomes of the optimization process.

1. INTRODUCTION

Waterjets are increasingly being used as the propulsive method of choice for high speed marine vehicles. A pump designed for waterjet application should have high propulsive efficiency, compact size and low entrained water. Furthermore it needs to withstand non-uniform inflow conditions, which have an adverse effect on its hydrodynamic and suction performance. In order to meet these contrasting requirements, a design strategy is required that can consider a large part of the design space and provide information on trade-offs between contrasting design objectives.

Traditionally waterjet pumps are designed based on empiricism and trial and error approach, in which the impeller and diffuser geometry are modified manually by changes to blade angle distribution. The flow through the resulting impeller (or diffuser) is then analysed by some form of quasi-3D (Q3D) or 3D numerical method. For example, in [1] and [2] a lifting surface method is proposed for this purpose. While in [3] a combination of Q3D inviscid method together with a 3D RANS code is proposed. These methods are then used to evaluate the flow in the pump. However, these methods do not provide any guidance on how the blade geometry should be modified in order to improve the flow field and hence the designer has to rely on trial and error. Such a trial and error process, however, by its nature restricts the designer to relatively small part of the design space, limited to blade angle distributions that have worked in the past, and does not allow the easy exploitation of a wide part of the design space.

An alternative approach to the design of the pump stage is to use an inverse method. In such an approach the impeller or diffuser geometry is designed for a specified distribution of pressure distribution or blade loading. Since the viscous losses and cavitation behaviour in the pump is to large extent controlled by the 3D pressure distribution, by using this approach one can obtain a more direct control over the design process.

A 3D inverse design approach, TURBOdesign-1 [4], that has been extensively used in pump design is that proposed in [5], in which a 3D method is used to design the blade geometry subject to specified blade loading distribution and blade thickness. This method has been used to improve exit flow non-uniformity from centrifugal and mixed flow impellers [6] and eliminate corner separation in diffusers [7]. Furthermore it has proved to be very effective in developing a very compact mixed flow pump [8]. Development of a compact pump is particularly important in marine waterjet applications as it reduces the weight of the waterjet system and the amount of entrained water. However, as shown in [8], reduction of volume of the mixed flow pump by 60% is only possible by very careful control of cavitation phenomena. However, a design that improves cavitation may have an adverse effect on performance or on Static or dynamic stresses. Hence the importance of a multi-objective design which takes account of the different contrasting requirements.

TURBOdesign-1 has already been coupled to automatic optimizers and 3D RANS code for minimizing losses [9] and cavitation performance [10]. Parametrizing the blade in terms of blade loading parameters enable one to represent large part of the design space with a few design parameters and hence provide distinct advantages in 3D optimization of turbomachinery blades, see [11]. In this paper we propose a new strategy in which TURBOdesign-1 is coupled with Multi-objective Genetic Algorithm in order to create a Pareto Front for the contrasting design requirements.

2. METHODOLOGY

2.1 INVERSE DESIGN METHOD

The commercial software TURBOdesign-1 [4] is used to parametrically describe the blade geometry. Turbodesign-1 is a three-dimensional inviscid inverse design method, where the distribution of the circumferentially averaged swirl velocity ($r\overline{V}_\theta$) is prescribed on the meridional channel of the blade and the corresponding blade shape is computed iteratively.

The circulation distribution is specified by imposing the spanwise $r\overline{V}_\theta$ distribution at leading and trailing edge and the meridional derivative of the circulation $\partial r\overline{V}_\theta / \partial m$ (blade loading) inside the blade channel. The input design parameters required by the program are the following:

- Meridional channel shape in terms of hub, shroud, leading and trailing edge contours.
- Normal/tangential thickness distribution.
- Fluid properties and design specifications.
- Inlet flow conditions in terms of spanwise distributions of total temperature and velocity components.
- Exit rV_θ spanwise distribution. By controlling its value, the work coefficient (or Euler head) are fixed.
- Blade loading distribution ($\partial r\overline{V}_\theta / \partial m$). It is imposed at two or more span locations between hub and shroud. The code then automatically interpolates in the spanwise direction to obtain the two-dimensional distribution over the meridional channel.
- Stacking condition. The stacking condition must be imposed at a chord-wise location between leading and trailing edge. Everywhere else the blade is free to adjust itself according to the loading specifications.

In this optimization, the meridional shape, blade thickness and Euler head were fixed and the blade loading and stacking conditions were modified. The blade loading parameters are shown in Fig. 1. The values of blade loading can be specified at a number of streamlines. In Fig. 1 the values are shown at the hub and shroud streamlines. The loading on each streamline is defined by a parabolic distribution from leading edge to a user defined point (NC_{HUB} or NC_{SHROUD}) , followed by a straight line section that the user can specify the slope ($SLOPE_{Shroud}$ or $SLOPE_{Hub}$) and then another parabolic section starting from ND that brings the loading down to zero at the trailing edge in order to satisfy the Kutta conditions. The value of loading at the leading edge is an important parameter that affects the blade incidence and hence can be used to adjust the peak efficiency point of the design.

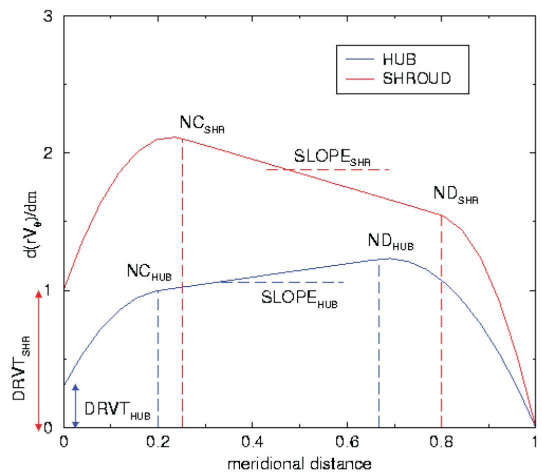

Fig. 1 The blade loading parameters used in the optimization

2.2 MULTI-OBJECTIVE OPTIMIZATION METHODOLOGY

Optimization Technique Description:

A Non-dominated Sorting Genetic Algorithm (NSGA-II) [12] is used for the multi-objective optimization. This technique is well-suited for highly non-linear and discontinuous design spaces. Each objective is treated separately and a pareto front is constructed by selecting feasible non-dominated designs. Standard genetic operation of mutation and crossover are performed on the designs. Selection process is based on two main mechanisms, "non-dominated sorting" and "crowding distance sorting". By the end of the optimization run a pareto set is constructed where each design has the "best" combination of objective values and improving one objective is impossible without sacrificing one or more of the other objectives.

population size	80
number of generations	200
crossover probablity	0.9
crossover distribution index	10
crossover distribution index	20
initialization mode	random

Table 1 – The setting used for optimization using NSGA-II

3. DESCRIPTION OF TEST CASE

The pump stage used for this study is a generic mixed flow stage with specific speed of 946 (based on rpm, m and m^3/min).

3.1 OPTIMIZATION TARGET AND DESIGN PARAMETERS

In this study, the blade loading was specified on 3 streamlines at hub, midspan and shroud. In order to reduce the number of design parameters, the values of NC and ND on all streamlines were fixed at 0.2 and 0.8 (i.e. at 20% and 80% of meridional chord) on each streamline and also the value of leading edge loading on the shroud was fixed at zero so that zero incidence is maintained on the shroud during the optimization. So the design variables modified by the optimizer were as shown in Table 2.

Design Parameter	Main Blade	
	Min	Max
LEH	-0.3	1.0
LEM	-0.2	0.5
SlopeH	-2.0	0.5
SlopeM	-2.0	0.5
SlopeS	-2.0	0.5

Table 2 – Range of Design Parameters used in Optimization

So overall 5 design parameters were used to modify the blade loading. These include the leading edge loading on the hub (LEH) and midspan (LEM) and slope of loading curve on the hub, midspan and shroud (SlopeH, SlopeM and SlopeS). In addition the blade was stacked at the trailing edg. The value of wrap angle was fixed as zero at the hub and varied between -10^o and 10^o at the shroud by the optimizer. So in total 6 design parameters were used.

3.2 DESIGN TARGET

The purpose of this multi-objective optimization is to minimize at the same time criteria for cavitation and impeller leading edge sweep. High leading edge sweep can help cavitation performance but can have an adverse effect on manufacturing or impeller stresses. For cavitation criteria the value of minimum static pressure as predicted by TURBOdesign-1 was used. TURBOdesign-1 provides very accurate prediction of the surface static pressure as compared to measurement and CFD predictions. Hence by asking the optimizer to maximize the minimum static pressure one should arrive at a design that has improved suction performance. The criterion used for leading edge sweep can be more easily defined in terms of the blade shape. In this case we defined ratio of the difference in Cartesian coordinates of the hub to shroud at leading edge divided by the meridional shape difference multiplied by 100. So in the case of no sweep a value of 100 will be obtained and the greater the value of sweep ratio is over 100 the higher is the leading edge sweep.

3.3 CONSTRAINTS

In section 2, it was mentioned that the meridional shape and blade thickness are fixed during the optimization. Another important feature of TURBOdesign-1 is that the Euler head is specified in the program and hence during the optimization process the Euler head and specific work are fixed. In addition to these constraints, which are implicit to the inverse design process and hence do not need to be specified explicitly in the optimizer (which can affect the convergence of the optimizer), 3 additional constraints were imposed in the optimization.

The first constraint was on the throat area. Since the throat area of the impeller can change by changes to blade loading distribution the value of throat was set to vary no more than ±4% of the throat area of the baseline impeller in order to ensure that correct peak efficiency flow rate is maintained. Furthermore, additional constraints were imposed on the diffusion ratio on the shroud, based on the TURBOdesign-1 predicted blade surface velocity distribution, to limit the possibility of flow separation. Constraints were also placed on the maximum value of leading edge sweep to be less than 106, a value slightly more than that of the baseline impeller.

4. RESULTS

The result of the optimization, which correspondes to 16,000 different impeller geometries was obtained in about 31 hour of computation on a single core of a P4 processor PC. The results are summerized in the Pareto front plot, shown in Fig. 3.

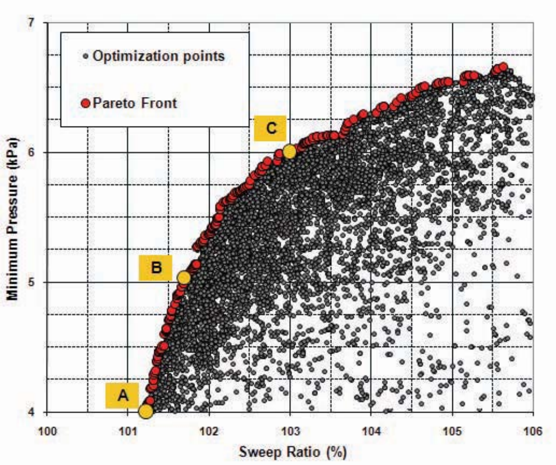

Figure 3: The Pareto Front for the Optimization

In Fig. 3, the minimum pressure (on vertical axis) and sweep ratio (on the horizontal axis) for every single configuration obtained by the optimizer are plotted. Each blue point corresponds to one configuration designed by TURBOdesign-1 through the modification made to blade loading by the optimizer. The higher the minimum static pressure for a configuration, the higher its suction performance. The red dots represent the Pareto Front or the “optimum” sets of configurations for the design space.

Three impeller designs along the Pareto front (shown by A, B and C) are selected for further detailed study. In Fig. 4, comparison of the leading edge shape of the A impeller impeller C is presented. One can see clearly that the A impeller has, as expected, a significantly reduced leading edge sweep as compared to impeller C.

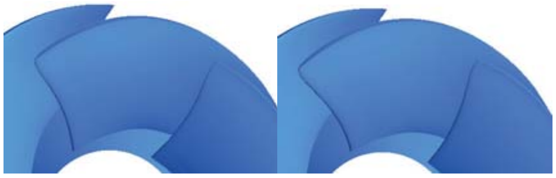

(a) Impeller A (b) Impeller C

Fig. 4: Comparison of the leading edge shape of Impeller A and C

In order to make a detailed comparison of the flow field in the impellers A to C 3D RANS code was used.

4.1 DESCRIPTION OF 3D CFD METHOD

CFD computations are performed using ANSYS CFX which is widely used in industry for turbomachinery flow simulation. The computational domain consists of a rotating domain (impeller) and a stationary domain (diffuser). A structured H-O topology is used to construct the mesh. A tip clearance of 0.5 mm is used for the impeller blade. The mesh consists of 300K and 175 K elements for the impeller and diffuser domains, respectively. Figure 5 shows the details of the computational mesh.

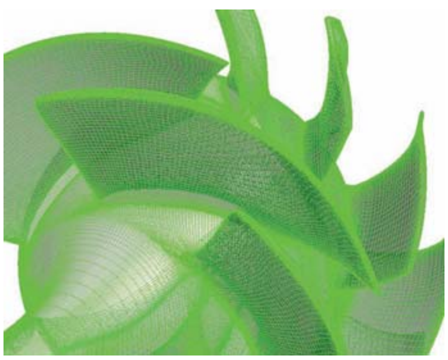

Figure 5: Computational Mesh

The incompressible RANS equations are solved simultaneously for the stage configuration. A two-equation k- turbulence model with scalable wall functions is used. Flow is assumed to be axisymmetric, so that only one passage is modelled in each domain and a non-overlapping mixing plane interface is used between the impeller and the diffuser domains. The inflow boundary conditions are total pressure, total pressure and flow angles and the mass flow rate boundary condition is used at the outflow.

For cavitation analysis, a two phase Rayleigh-Plesset model is used. The interphase transfer is governed by a mixture model where the interface length scale is 1 mm. Flow is assumed to be homogeneous and isothermal at 293.15 K. The saturation pressure is 3619 Pa and the mean nucleation site diameter is 2e-03 mm.

4.2 COMPARISON OF BASIC PERFORMANCE PARAMETERS

The steady CFD computations of the stage were performed at various flow rates to be able to make a comparison of the stage performance with the 3 different impellers obtained from the optimization versus the baseline. In Fig. 5, the normalised pump head versus flow rate of the 3 different stages are shown. In each case, the same diffuser was used. The results indicate that the predicted pump head for impellers A and B is very similar to the baseline values across all the different flow rates. Impeller C, however, seems to have a slightly lower head.

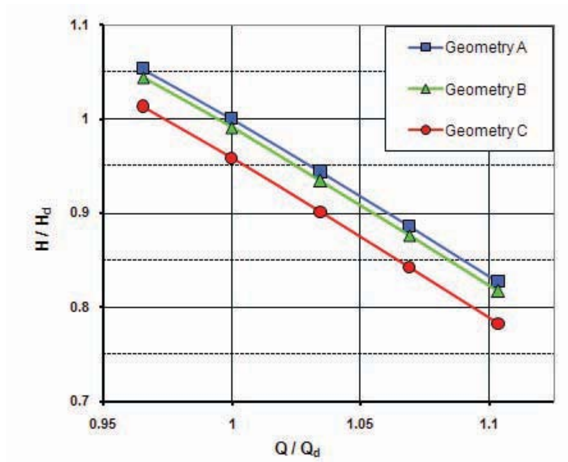

Fig. 5 Comparison of normalised predicted head versus flow rate for different stages.

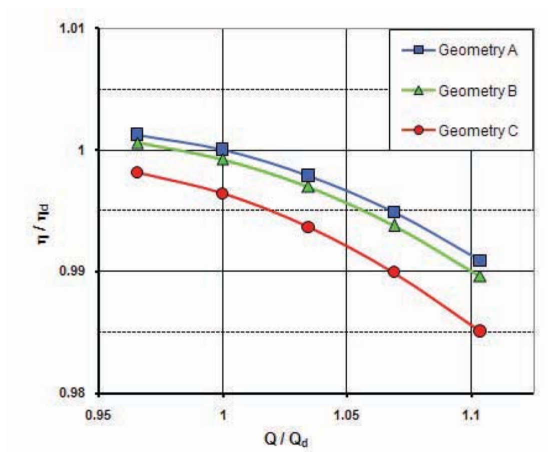

Fig. 6: Comparison of predicted impeller efficiency

In Figure 6 the predicted impeller efficiency for the different cases are compared. Again the results are normalised with the maximum impeller efficiency of impeller A.

Finally the stage efficiency normalised by the maximum efficiency of impeller A are shown in Fig. 7. The results confirm that all 3 optimization cases are achieving the same pump stage peak efficiency flow rate as the specified flow rate.

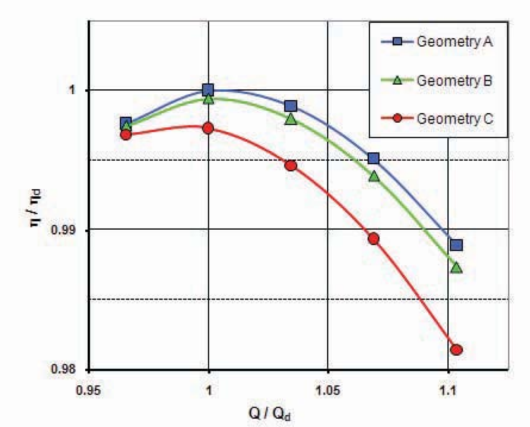

Fig. 7 Comparison of Predicted Stage Efficiency

4.3 COMPARISON OF CAVITATIONS PERFORMANCE

In order to compare the performance of the different impellers in terms of their cavitation performance, two phase cavitation analysis was performed by reducing the inlet total pressure at the design flow rate. The results at a total pressure corresponding to initiation of cavitation at the design flow rate is shown in Fig. 8. The results confirm the trend expected from the Pareto front in Fig. 3, in which impellers A and B have a value of min surface static pressure which is similar, and as expected their cavitation performance is similar. However, impeller C has clearly a better cavitation performance but higher leading edge sweep values.

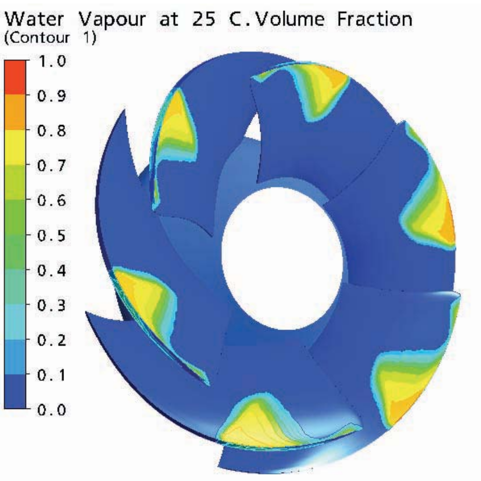

(a) Impeller A

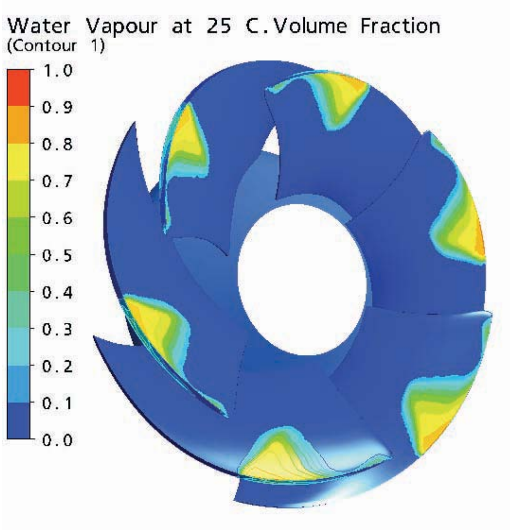

(b) Impeller B

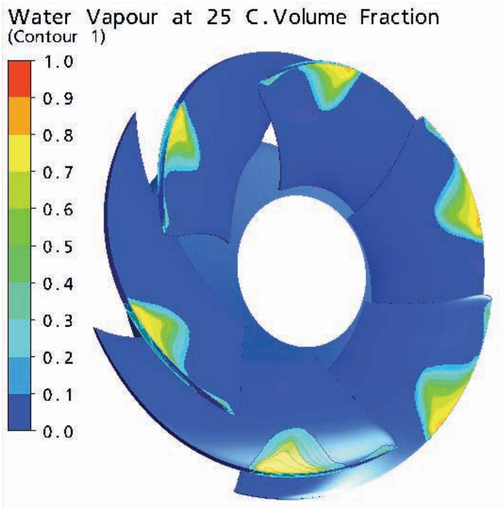

c) Impeller C

Fig. 8. Cavitation Analysis for different impellers

5. CONCLUSIONS

A methodology is presented for multi-objective design of waterjet pumps in which the blade shape is parametrized in terms of blade loading parameters used as input in a 3D inverse design code. By using the 3D inverse design code its possible to perform 3D multi-objective optimization with only 6 design parameters. Computing the performance objectives and constraints directly from the output of the inverse method (3D pressure or velocity field and geometry data) makes the evaluation of each configuration very rapid. A relatively large population of 16000 design configurations can be computed in about 24-33 hours of CPU time on a single processor PC. The results shown confirm that by imposing the correct constraints it is possible to achieve designs that meet both design and off-design objectives. The proposed approach can be used to rapidly and automatically explore a large part of the design space to create impeller or diffuser designs that meet contrasting requirements relating to efficiency, suction performance, manufacturing limitations, mechanical constraints or cost.

6. REFERENCES

1. Taylor, T.E. and J.E. Kerwin (1998), 'Waterjet pump design and analysis using a coupled lifting-surface and RANS procedure', International Conference on Waterjet Propulsion Latest Developments, 22 & 23 October 1998, Amsterdam.

2. Taylor, T.E., and R.W. Kimball (1999), 'Experimental validation of a coupled lifting-surface/RANS procedure', 5th International Conference on Fast Sea Transportation, Seattle, Washington, USA, Sept 1999.

3. Huntsman, I., Hothersall, R., 2001, "Developmet of Quasi 3D Methods and 3D Flow Solvers for the Hydrodynamic Design of Water Jets", Proceedings of Waterjet Propulsion III Conference.

4. Turbodesign-1. Advanced design technology Ltd.

5. Zangeneh, M., 1991, "A 3D Design Method for Radial and Mixed-Flow Turbomachinery Blades", Journal of Numerical Methods in Fluids, **13**, pp. 599-624.

6. Zangeneh, M., Goto, A., Harada, H., 1998, "On the Design Criteria for Suppression of Secondary Flows in Centrifugal and Mixed Flow Impellers", Journal of Turbomachinery, **120**, pp. 723-735.

7. Goto, A., Zangeneh, M., 2002, "Hydrodynamic Design of Pump Diffuser Using Inverse Design Method and CFD", Journal of Fluids Engineering, **124**, pp. 319-328.

8. Goto, A., Ashihara, K., Sakurai, T., Saito, S., 1999, "Compact Design of Diffuser Pumps Using Three-Dimensional Inverse Design Method", ASME Paper FEDSM99-6847.

9. C. Yiu and Zangeneh, 2000, "Three Dimensional Automatic Optimisation method for Turbomachinery blade design" Journal of Propulsion and Power Vol. 16. No. 6, Nov-Dec 2000.

10. Ashihara, K., and Goto, A., 2001, "Turbomachinery Blade Design Using 3D Inverse Design Method, CFD, and Optimization Algorithm," ASME Paper No. 2001-GT-0358.

11. Bonaiuti, D and Zangeneh, M. , 2006, "On the Coupling of Inverse Design and Optimization Techniques for Turbomachinery Blade Design", ASME Paper GT-2006-90897. To be published in ASME Journal of Turbomachinery.

12. Deb,K., Pratap, A., Agarwal,K. and Meyarivan, T. 2002, A Fast and Elitist Multiobjective Genetic Algorithm: NSGA-II, IEEE Transactions On Evolutionary Computation, Vol. 6, No. 2, pp. 182-189.

7. AUTHORS BIOGRAPHY

Mehrdad Zangeneh is Professor of Thermofluids at University College London. His research interest relate to development of design methods for turbomachinery based on 3D inverse design approach and automatic optimization methods.

Kasra Daneshkhah is a senior design engineer at Advanced design technology and has been involved in design of various industrial and marine pumps as well as low speed fans.

Bruno Da Costa was an intern student at Advanced Design Technology from University of Centrale Paris, France.

WATERJET PUMP DEVELOPMENT FOR HIGH PERFORMANCE AND HIGHER POWER DENSITY

R Aartojärvi and **M Heder,** Rolls-Royce AB, Sweden

SUMMARY

This paper presents the development of a new high performance mixed-flow waterjet pump with a higher power density than the previous design. The design objective has been to improve the cavitation performance of the pump in order enable a significant size reduction for a given ship speed and engine power. This will result in lower weight the pump unit as well as for the whole propulsion system. Size reduction has a positive effect also on the inflow to the pump and thereby the interaction between inlet duct and pump. An increase of the power density of the waterjet unit presents a number of challenges. One is to maintain high propulsive efficiency. Another challenge is to cope with the structural loads. The aim of this paper has been to focus on structural issues in the design process of the new pump.

1. INTRODUCTION

A pump designed for a waterjet application should be part of a robust and reliable propulsion unit providing a high propulsive efficiency. This can be accomplished by low weight and small dimensions. The new pump needs to cope with various inflow conditions without cavitation erosion and structural problems. These and other requirements should all have an impact on the design.

A new high performance waterjet pump has been developed. This paper describes the design process where CFD, model tests and structural analysis have been integrated. The result is a mixed flow pump where the leading edges of the impeller blades have been swept forward.

This paper is focused on the development of the impeller as this component presented the greatest challenge. During the development process pressure load obtained by CFD was applied to a FE model of the impeller in order to compute static stress. The result of the FE analysis was then verified by static stress obtained in model test. Dynamic stress of the impeller blades was obtained from model tests under a number of different operating conditions.

Rolls-Royce AB has developed a modern design environment based on waterjet system simulations, advanced pump design tools, the extensive use of analysis tools as well as model scale and full scale experimental testing. The importance of making best use of a combination of analytical and experimental methods is emphasized in this paper.

2. BLADE LOADS BY CFD

The new pump design was developed in three steps using a 3D inviscid design code, 3D RANS simulations and experimental tests at Rolls-Royce Hydrodynamic Research Centre.

The 3D RANS model, illustrated in Fig. 1, is built using a mixing plane approach together with rotationally periodic boundaries. This approach limits the model to only one impeller blade and one guide vane. The computational grid is built using a hexahedral multi block topology including the rotor tip gap. Apart from the boundary conditions the model is set up with SST k-ω turbulence model and higher order discretization schemes for the solver.

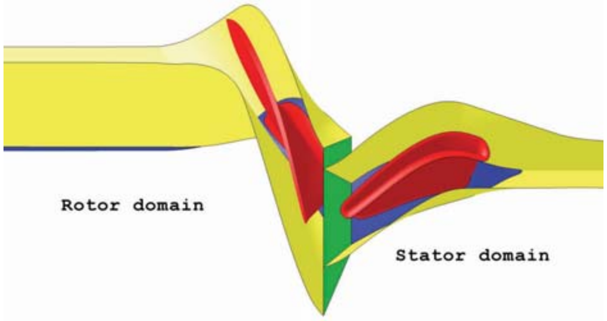

Figure. 1 top view of the CFD model including blades (red), hub (blue) and periodic boundaries (yellow). The mixing plane (green) is also highlighted in the centre.

The results are used both to predict pump performance and to provide a mean load field on the blades later to be used in FE analysis, see Fig. 2. The dynamic load due to non-uniform inflow and cavitation are treated by experimental methods.

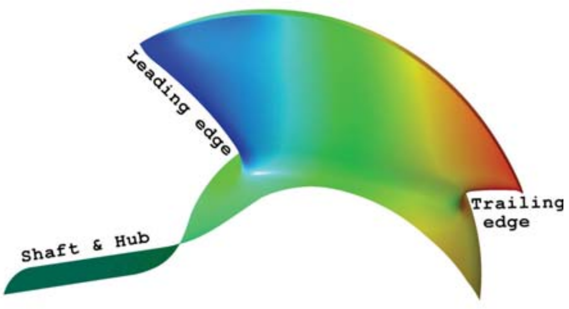

Figure 2. A contour plot of static pressure acting on the rotor blade

3. MODEL TEST

3.1 TEST METHODS

In order to determine the final hydrodynamic performance of the pump a number of model tests need to be carried out to supplement the results from CFD analysis. In this section these methods are described very briefly.

A pump loop test set-up, as shown in Fig. 3, gives the overall performance of the pump in terms of head rise, power, pump efficiency and cavitation performance as a function of the flow rate. This test is however done under ideal conditions since the inflow to the pump is uniform, which is not true for a waterjet application but it is valuable as a starting point and verification of the CFD results.

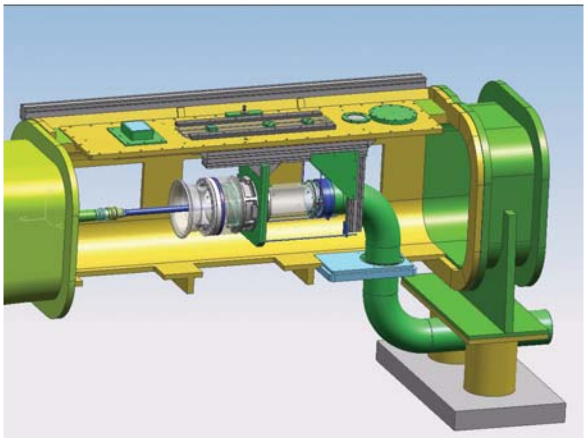

Figure 3. Set-up for pump loop tests at RRHRC.

The effect on pump performance of the inflow non-uniformity needs to be measured in a waterjet system test set-up as shown in Fig. 4. This test gives the interaction between the inlet duct and the pump and can be compared to corresponding system analysis using CFD. The difference to the pump loop results increase with the degree of inflow non-uniformity, which in turn is determined by the operating condition of the waterjet easiest described by the inlet velocity ratio (IVR).

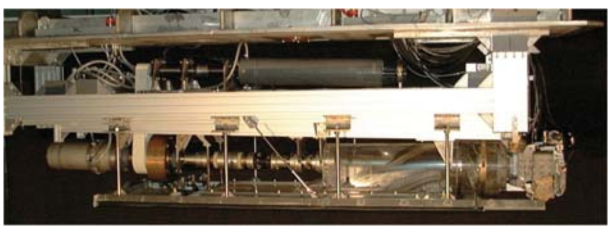

Figure 4. Set-up for waterjet system tests at RRHRC.

The waterjet system test is also essential to adjust the preliminary cavitation performance obtained in the pump loop test. The result is the so-called cavitation zones for the waterjet system describing limitations for operation due to cavitation erosion, thrust breakdown etc.

Another important objective for the waterjet system test is to obtain loads acting on different parts of the structure, with the focus on the impeller. Strain gauge measurements on impeller blades are mainly used to obtain load variations caused by the non-uniform inflow to the pump or the flow interaction with the guide vanes, see Fig. 5.

Figure 5. Strain gauges on impeller pressure side.

3.2 TEST RESULTS FOR THE NEW PUMP

Pump loop tests and waterjet system tests have shown that the main design objective for the new pump, to improve the cavitation performance of the pump to enable a 12% size reduction, was accomplished. In addition the pump efficiency was increased as well as the actual flow rate to head rise ratio. This means that the propulsive efficiency of the new pump is 2-3% higher compared to the previous design, which is quite a significant improvement.

Strain gauge measurements on the pressure side close to the leading edge of an impeller blade gave the strain amplitudes used in the structural analysis together with FE computations of the average strains using pressure loads from CFD analysis in uniform flow.

It is mainly the non-uniformity of the inflow and the cavitation number that determine the strain amplitude in the leading edge of the impeller blade. The effect of cavitation is less straight forward than that of the non-uniformity, since cavitation can reduce the strain amplitude close to the leading edge and transfer load further downstream. Systematic measurements were done to find the decisive load case. A typical strain signal from the measurements is shown in Fig. 6.

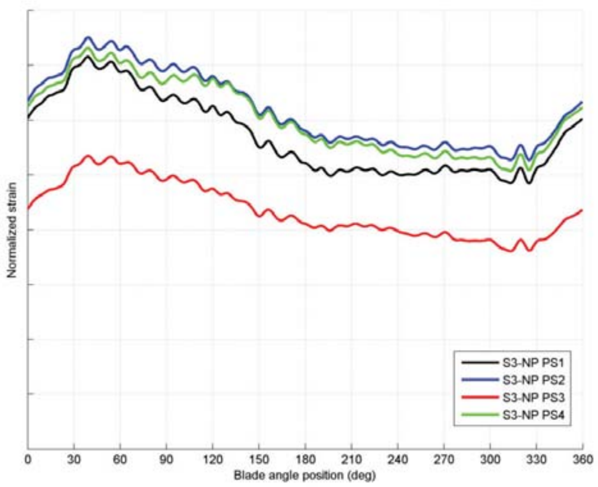

Figure 6. Strain signals from the 4 gauges on the pressure side in Fig. 5.

The gauge named PS1 is located close to the leading edge just outside of the fillet. Gauge PS2 and PS3 are located aft along the chord. PS4 is located further out on the blade, see Fig. 5.

4. FE ANALYSIS OF IMPELLER

The mean stress in full scale has been computed employing a FE model representing the complete impeller, see Fig. 7. The FE model is composed of 10-node parabolic tetrahedrons. One of the blades has been meshed with a finer mesh than the remaining blades in order to reduce the size of the model. The FE model has been constrained in all directions on the pump shaft interface.

Pressure obtained from CFD shown in Fig. 2 has been scaled to full-scale conditions and applied to the outer surface of the FE model. The effect of rotational load has also been included in the analysis.

Fig. 8 shows the resulting principal stress corresponding to a 45 knots operating condition. Due to the forward swept blade the highest stress will occur in the area close to the leading edge. In order to optimize the use of material the blade thickness variation results in a constant stress over a large area. The stress in the hot spot area is considerably lower than the yield strength of the material and well below the design limit for static stress.

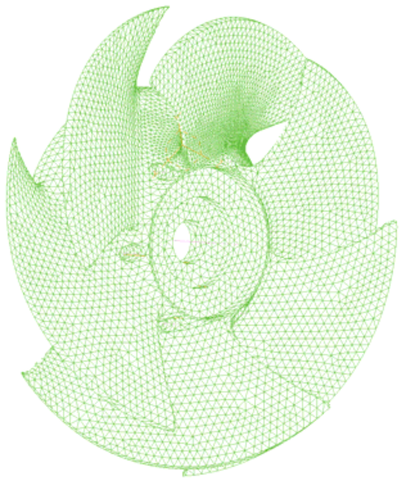

Figure 7. FE model of impeller.

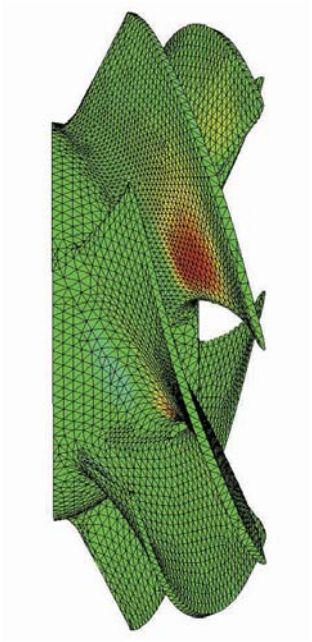

Figure 8. Maximal principal stress of impeller.

The strain obtained in the FE analysis is compared to the result of the model test in Fig. 9, where the strain has been normalized with respect to the highest strain obtained in the model test. The result of the model test has been scaled to correspond to the same size and operating condition. The strain obtained in the FE analysis is computed in the same direction as of the strain gauges. The strain is here compared in four positions, all located within the red area in Fig. 8. The gauges named PS1 – PS3 are all located just outside the fillet on the pressure side, PS1 closest to the leading edge and PS2 and PS3 further aft. The gauge PS4 is located further out on the blade. The location of the gauges can be seen in Fig. 5. The comparison shows a good agreement and the difference between the results is generally within 10%. A number of operating conditions has been analyzed with similar results.

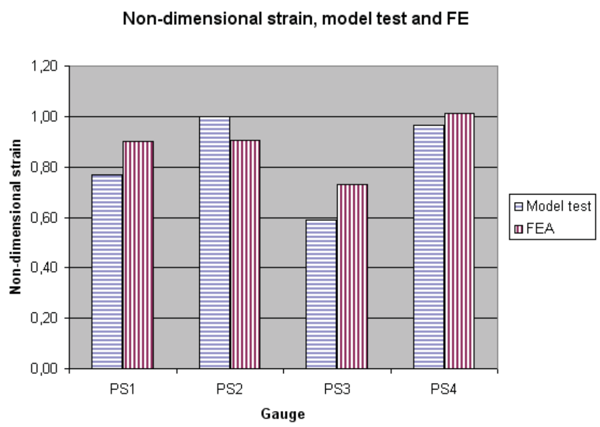

Figure 9. Non-dimensional strain obtained in model scale and by FE analysis.

The smean stress of the new impeller is on approximately the same level as of the present impeller. The resulting stress level is well below the design criteria. Consequently the static stress has not been the main concern in the design process. Instead the focus has been on the dynamic stress and fatigue of the impeller blade.

5. FATIGUE OF IMPELLER BLADES

In the previous section it was shown how mean stress of the impeller employing pressure obtained by CFD can be computed in a good agreement with to the result of model tests. The dynamic stress of the impeller can on the other hand only be obtained by scaling the result of the model test. Factors like the influence of cavitation can presently not easily and efficiently be represented in CFD analysis. Also the number of operating conditions to be studied would render a CFD analysis of the system very time consuming.

At an early stage of the design process it was found that the highest stress amplitude will occur in the same area as the highest mean stress found in the FE analysis. The dynamic stress in this area is caused by pressure fluctuations when the blade is passing the wake in the intake. Therefore the focus of the design process was to carefully choose a thickness distribution of the blade in order to achieve a constant static and dynamic stress spread out over the area close to the leading edge. In this way the material will be utilized in a more efficient way than if a single hotspot would be present.

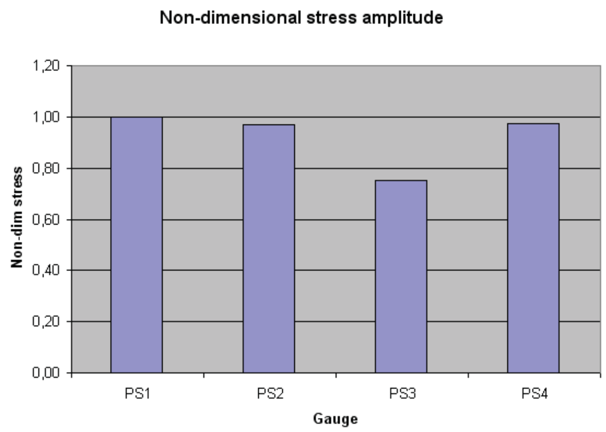

Figure 10. Non-dimensional stress amplitude in gauges.

Fig. 10 shows the non-dimensional dynamic stress obtained in the positions of the strain gauges obtained from Fig. 6. All located were on the pressure side of the blade in the area close to the leading edge, see Fig. 5.

The figure shows the stress amplitude under an operating condition corresponding to a 45 kn ferry. The amplitudes have been normalized against the maximum value in order to show the relative distribution. The result shows that the amplitude is approximately the same in gauge PS1, PS2 and PS4. A tendency of decreasing amplitude along the chord can be seen. This has been confirmed from tests with gauges located close to the trailing edge where very low amplitudes were found. The amplitude in gauge PS4 shows the amplitude is approximately constant in radial direction.

Based on the stress amplitude of the impeller blade the fatigue life can be estimated employing the Palmgren-Miner cumulative damage rule. An SN curve has been established based on a combination of testing and extensive full scale experience. In the fatigue test a specimen of the actual cast duplex stainless steel was subjected to an environment of sea water.

Based on the design life and the operating profile of different vessels the cumulative damaged has been computed under different operating conditions. The resulting cumulative damage is on the same level as of the present Kamewa SII waterjets.

6. CONCLUSIONS

This paper has shown the importance of integrating structural analysis in the development process of a new waterjet pump. By carefully choosing the distribution the blade thickness a good utilizing of the material has been achieved without influencing the hydrodynamic performance. For an impeller with forward swept impeller blades knowledge of the dynamic stress is essential. In order to obtain the impeller stress variation with the effects of non-uniform flow in the intake and cavitation model test are necessary.

7. AUTHORS BIOGRAPHY

Reima Aartojärvi is manager of waterjet hydrodynamics at Kamewa Waterjets, Rolls-Royce AB, Kristinehamn, Sweden.

Mats Heder holds the position of senior structural engineer at Kamewa Waterjets, Rolls-Royce AB, Kristinehamn, Sweden.

RESEARCH ON HYDRODYNAMIC PERFORMANCE OF HYBRID PROPULSION SYSTEM

C Sun, Y Wang and **Z Li**, University of Naval Engineering, China

SUMMARY

Hybrid propulsion systems of waterjet(s) and propeller(s) have many advantages. An existing ship, South African Navy 3500 ton corvette which was reported in Waterjet Propulsion 4, has greatly proven that. When waterjet(s) and propeller(s) are combined in a ship, not only the interactions of waterjet-hull and propeller-hull, but also the interaction between waterjet(s) and propeller(s) should be considered. In this paper, hybrid propulsion system of a waterjet and two propellers is studied particularly. An isolated waterjet propulsion system and open-water propeller performances are studied and results are validated by experimental data. Flow region of the hybrid propulsion system is simulated by solving RANS equations and interactions of the two kinds of propulsors are analyzed. Inflow and outflow of waterjet and propellers are different from isolated conditions. Performances of propellers are changed more widely than the waterjet. Different rotating direction of the propellers will affect the velocity distribution at ducting inlet and then the performance of waterjet. Efficiency of the propulsion system and non-uniformity of pump inflow are better when propellers rotate outward. Both calculation and theory analysis show that propellers are more sensitive to the change of flow field on hybrid propulsion system. More attention should be given to propellers when a hybrid propulsion system is designed.

NOMENCLATURE

A	Propeller disc area (m^2)
A_{nozzle}	Nozzle exit area (m^2)
C_{Tjet}	Waterjet thrust loading coefficient (1/1)
C_{Tprop}	Propeller thrust loading coefficient (1/1)
D	Propeller diameter (m)
J	Advance ratio (1/1)
k_M	Torque coefficient (1/1)
k_T	Thrust coefficient (1/1)
M	Torque (kN m)
n	Rotating speed ($r.s^{-1}$)
p	Pressure ($N\ m^{-2}$)
Q	Flow rate ($m^3\ s^{-1}$)
T	Thrust (kN)
v	Ship speed ($m.s^{-1}$)
v_A	Axial velocity entering propeller ($m\ s^{-1}$)
v_{in}	Average inlet velocity of flow ($m\ s^{-1}$)
v_j	Average nozzle velocity of flow ($m\ s^{-1}$)
v_{pump}	Average axial velocity of pump inflow ($m\ s^{-1}$)
μ	Jet velocity ratio (1/1)
ζ	Non-uniformity of pump inflow(1/1)
ρ	Specific density ($kg.m^{-3}$)

1. INTRODUCTION

Hybrid propulsion systems of waterjet(s) and propeller(s) have been applied on fast yachts, ferries and warships for some time. Higher efficiency and more operation modes are the main characteristics of these applications. From the appearance of such systems, the question of how to tackle the issue of cruising at high overall efficiency with a diesel and/or gas turbine plant is sometimes solved. At low or medium speeds the propellers are driven by diesel(s) so that propellers have good efficiency and diesel engine(s) are loaded in an optimum way. At higher speeds, both waterjets and diesel engines or gas turbines have good efficiencies. For naval vessel, propeller's noise around 20 knots can be optimized without using large propeller diameters which are difficult to mach with the hull geometry.

For the hybrid propulsion system, propellers are arranged near the ducting inlet of waterjet. For isolated propeller or waterjet ships, it is enough when the interaction of propeller-hull or waterjet-hull is considered. When waterjet and propellers work together, the condition is greatly changed. Flow regions of waterjet and propellers affect each other. Inflow and outflow conditions of two kind of propulsors are changed and so are the performances. Such issues should be considered when a hybrid propulsion system is designed.

In this paper the interaction of a waterjet and two propellers is researched by using CFD method. Flow field of the hybrid propulsion system is simulated by solving RANS equations. Positions and rotating direction of propellers are changed to compare the varying of performances. Sensitivity of propellers to the change of flow field is studied particularly in the end.

2. CONCEPT DESIGN INTEGRATION

Parameters of MEKO A-200 Corvette were reported detailed in Waterjet propulsion 4[1]. A simple hybrid propulsion system similar to MEKO A-200 is selected for this research work. Power ratio, diameter ratio of waterjet to propeller are just same as MEKO A-200. However, the selected hybrid propulsion system is small, waterjet and propellers are different from MEKO A-200. Furthermore, the main issue concerned is the interaction of waterjet and propellers so that only stern part of vessel is considered and no particular ship model is used. To further simplify the problem, the ship is truncated at the design waterline, eliminating the need to define the free surface. Table 1 displays the data of selected hybrid propulsion system.

Table 1 Selected Hybrid Propulsion System Data	
Design speed	30knot
Waterjet intake duct diameter	71cm
Propeller diameter	1.15m
Power of propellers in mode III	2*600kW
Power of waterjet in mode III	2000kW
Propeller speed	732rpm
Waterjet speed	850rpm

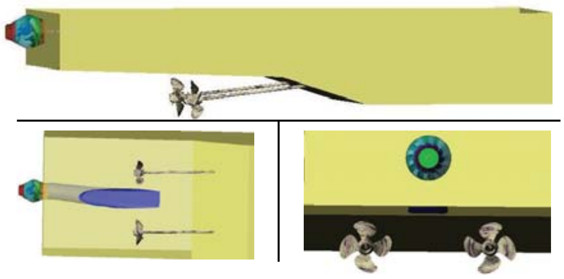

Fig.1 CAD model of hybrid propulsion system

Fig.1 Shows the CAD model of selected hybrid propulsion system. Only a waterjet and two propellers are installed at stern part of ship. With a flat bottom section, the waterjet and the hull join more easily, and the properties of waterjet and propellers are not modified by any built-up surface.

After the model of hybrid propulsion system has been built, CFD method is used to calculate the hydrodynamic performance of it. In order to compare and validate CFD results, isolated waterjet and open water propeller are analysed using CFD method at first.

3. VALIDATION OF CFD RESULTS

The numerical models of the waterjet and propeller are based on a Reynolds-Averaged-Navier-Stokes (RANS) method. Analysis of the flow is made with the commercial CFD code CFX. The CFD code uses the finite volume method to solve the discretised set of equations. Besides the equations for conservation of mass and momentum, two additional equations are solved to model the turbulence. For all simulations the *sst* turbulent model is used.

3.1 VALIDATION OF WATERJET RESULTS

There are many reports using CFD method to calculate the performance of waterjet[2-4]. Norbet W.H.B have done especially comprehensive and detailed calculation about this in his doctoral dissertation[5]. In this paper, the complete waterjet propulsion system is the analysis object. A control volume is constructed around the ship bottom to represent the boundaries of the calculated flow field. The optimum domain of the control volume from my research group is 20D upstream of the inlet, 10D and 8D of width and depth respectively. D is the rotor inlet diameter of waterjet.

The generation of the mesh of the complete waterjet is split into three separate parts; the inlet mesh and the pump meshes with rotor and statorbowl. The mesh of inlet is done with the commercial mesh code ICEM CFD. Near the surface of the ducting, shaft and hull bottom a special procedure is applied to create fine cells at the walls. This ensures good quality of the y+ values.

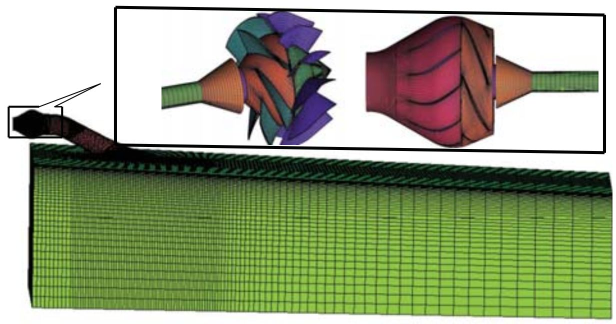

Fig.2 Mesh of complete waterjet propulsion system

The mesh of pump is done with the code of TURBOGRID. The main topology structure of rotor is H model and statorbowl is J model. O-grid is generated around the blades. This complete mesh is shown in fig.2. After meshed, the model is brought into CFX Pre to define the fluid boundaries. The front of the control volume is set as an inlet, introducing water to the control volume at the ship speed. The opposite end of the control volume could have been set as an outlet or an opening, the latter of which is simply a pressure field that allows fluid to flow in or out. In this paper it is defined as an outlet. The outboard boundary and the bottom boundary are set as free slip walls. The hull, ducting and shaft are defined as no-slip walls. Rotation of the impeller can be implemented via the quasi-steady Multiple Frames of Reference method or via the fully transient moving mesh option. The latter is significantly more time consuming, and it is therefore not applied in this analysis. Pump outlet is set as an outlet boundary condition.

The working point of waterjet is determined by the ship speed and the shaft speed of the pump. Many groups of ship speed and shaft speed are set and calculated. Fig.3 shows the comparison of the calculated thrust and results provided by KaMeWa company.

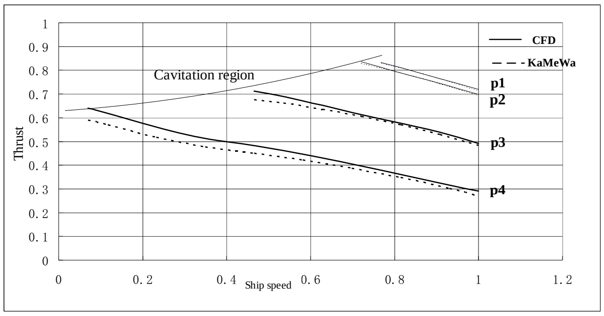

Fig.3 Thrust prediction for waterjet system using CFD code and KaMeWa data

Agreement between the calculated thrust and KaMeWa data is very good for most of the calculated conditions. Near the cavitation zone which is restricted using every year errors become large. It is because cavitation model is not used in this analysis. Over the complete range of calculated conditions, the largest deviations of power and thrust are 3.8% and 8.6%.

3.2 VALIDATION OF OPEN WATER PROPELLER RESULTS

The CFD analysis of the open water propeller is described in 2 parts. First the generation of the numerical model will be discussed. Then the CFD predictions of thrust and torque will be compared with experimental data.

The present simulations are performed on a 4 blades propeller with the diameter D=0.25m. The computational domain has been identified with a cylinder surrounding the propeller and aligned with the shaft axis. The inlet is 4D upstream, the outflow 6D downstream, the diameter of the lateral cylindrical boundary is 5D. The whole domain is spilt into 2 parts to generate mesh. One domain is just around the propeller which is filled with tetrahedral cells, ten lays of prismatic cells have been attached to the blades and hub surface. Another domain is meshed by hexagonal cells. The mesh is shown in fig.3.

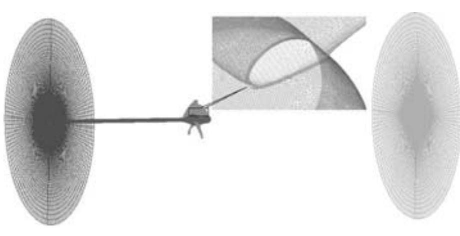

Fig. 3 Mesh of the open water propeller

Boundary conditions are set to simulate the flow around a rotating propeller in open water: on the inlet boundary, velocity components of uniform stream with the given inflow speed are imposed; on the exit boundary, the static pressure is set; on the outer boundary, the opening boundary condition is imposed; on the blade and hub surface, the no-slip condition is imposed.

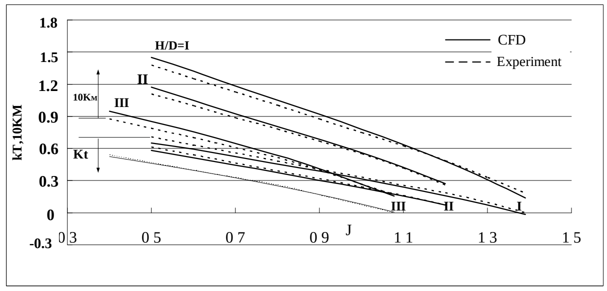

Fig.4 CFD results and experimental data

To analyze the computational results, the thrust and torque coefficients, k_T and k_M, are selected as the global quantities of interests:

$$k_T \quad T/(\rho n^2 D^4)\,;\, k_M \quad M/(\rho n^2 D^5)\,;\, J \quad v/(nD)$$

The comparison with the experimental data for both thrust and torque coefficients is illustrated in Fig.4. The results agree reasonably well with experiment data. The maximum errors of k_T and k_M are 8%.

4. CFD ANALYSIS OF HYBRID PROPULSION SYSTEM

After the computational results of isolated waterjet and open water propeller are validated, the hybrid propulsion system is analyzed. Mesh is generated according to the isolated waterjet and the open water propeller system, the mesh is shown in fig.5. Most boundary conditions are same as the isolated waterjet and propeller. For lack of better option, the top surface (which would otherwise be the free surface) was set as a symmetry plane. This restricts the water available to the inlet by denying the ability for the inlet to draw water from above the waterline.

Fig.5 Mesh of hybrid propulsion system

4.1 FLOW CHARACTERISTICS OF HYBRID PROPULSION SYSTEM

Figure 6 shows the streamline of hybrid propulsion system. There is an important difference with the isolated waterjet and propeller. For hybrid propulsion system, both waterjet and propeller are sucking water from the same direction and origin. Space between two propellers is narrower than inflow width of the isolated waterjet plus propellers. The suction flow of propellers are inclined to the side of the ship. After water been accelerated by propellers and ducting inlet, they flow to the stern part of the ship. However, velocity of water around the ducting inlet is higher than the water accelerated by propellers, shapes of propellers' streamline are seriously distorted.

Furthermore, propellers' blades pressure distribution are greatly changed. Pressure distribution on four blades is not identical. Fig. 7(a) shows the pressure coefficient of blade 1 and blade 3 at four different blade spans. Pressure coefficient on blade 1 which is near the ducting inlet is lower than blade 3. Cavitation should be restricted at blade 1 and 4, especially at the region near the hub.

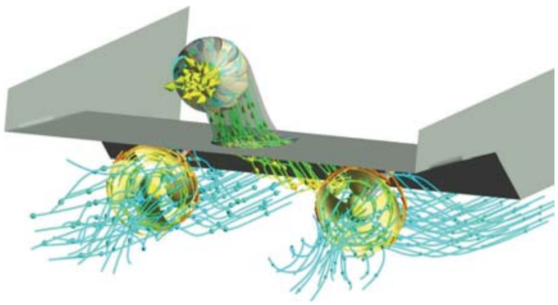

a. view from the afterbody of ship

b. view from the bottom of ship

Fig. 6 Streamline of hybrid propulsion system(inward rotating)

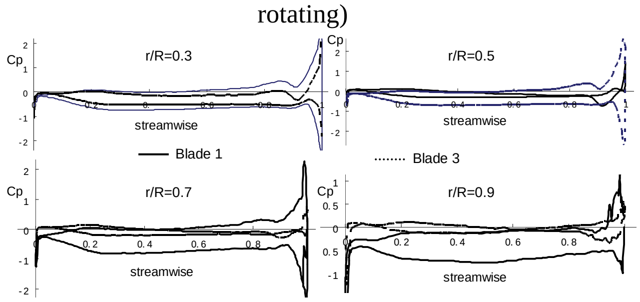

a. pressure values of blade 1 and blade 3.

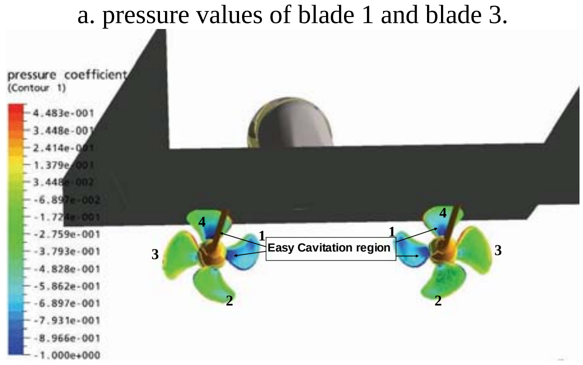

b. pressure contours of propellers' blades

Fig. 7 Pressure distribution of propellers blades

4.2 INFLUENCE OF THE RELATIVE POSITION OF PROPELLERS AND WATERJET

For hybrid propulsion system, the waterjet permits to be moved as far aft in the ship as desired without the problem of unacceptable large inclination of the shaftline and the engine foundation. So the relative position between waterjet inlet and propellers can be changed more widely. In this paper, performances of five different positions of propellers are analyzed. The sketch map of propellers' positions is shown in figure 8. From position 1 to position 5, propellers are close to the ducting inlet gradually. When the calculations are done, mesh size is identical for five positions.

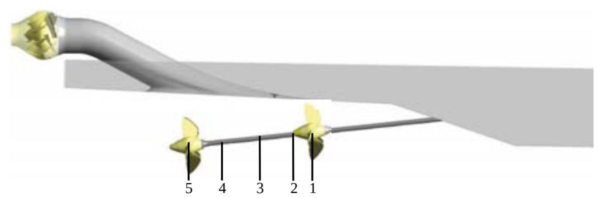

Fig 8. Sketch map of propeller positions.

It is expected that the change of propellers' positions will result in a varying flow conditions of the waterjet and propellers and thus their performances. Fig. 9(a) shows the torque and thrust of waterjet at five different propellers' positions. The results have been normalised with values of the isolated waterjet. It can be observed that the effect of propellers' positions on waterjet performance is small. Torque is nearly constant at five propellers' positions. Thrust fluctuates at the range of 2%. Two causes contribute to the fluctuation of thrust. One is the varying of mass flow rate which can be seen from fig.9(d). From momentum balance we know that the thrust is related to the square of the volume flow rate. Consequently, a relatively small change of the volume flow rate can lead to a large change in the thrust of the installation. The other is the change of wake fraction. When a waterjet and two propellers work together, velocity at the region of ducting inlet is higher than the isolated condition and wake fraction is larger. For the two reasons we can learn that thrust of hybrid propulsion is smaller than the isolated conditions and some fluctuations may exist, it can be seen in figure 9(a). Furthermore, pressure distribution along the cutwater is changed. Analysis of the pressure in figure 10 shows that although the two locations of the stagnation point and minimum value are almost the same for five propellers' positions, pressure values are different. Minimum pressure of position 5 is lowest.

Compared with the waterjet, thrust and torque of propellers fluctuate widely. The deviation can reach to 6%, it is shown more detail in figure 9(b). This is mainly due to the decrease of advance ratio. Figure 9(d) shows the velocity at propeller disc plane of five positions. From position 1 to position 5, velocity decreases gradually and thus the advance ratio. We can derived the change of thrust and torque from the open water propeller diagram.

Over the complete propellers' positions of calculated conditions, performances of waterjet and propellers are all changed. However, there are only a rather limited varying of efficiency. This is shown in figure 9(c).

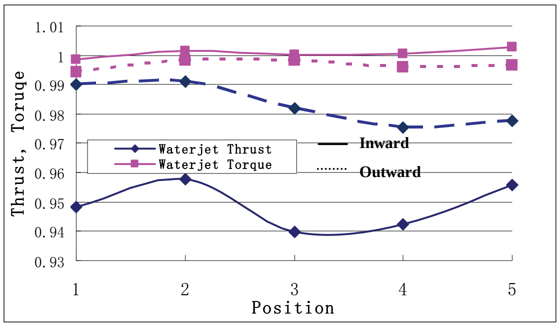

a waterjet thrust and torque

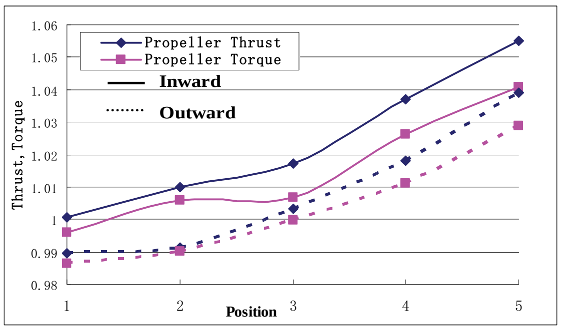

b propeller thrust and torque

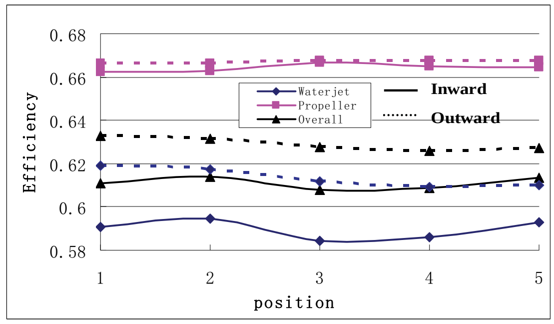

c efficiency of waterjet and propeller

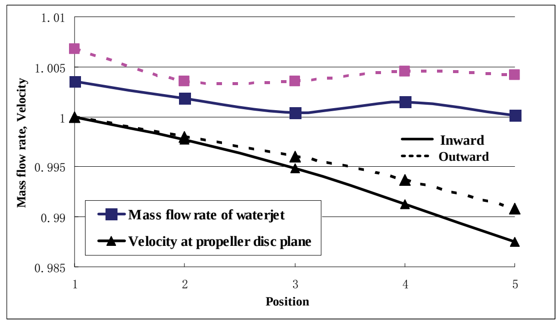

d mass flow rate and velocity

Fig. 9 Comparison of calculations of some results for five different propellers' positions

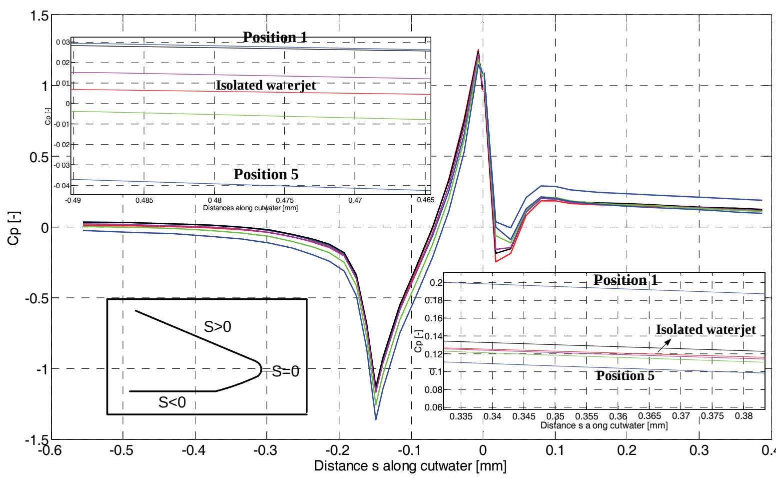

Fig. 10 Calculated pressure coefficient Cp along the cutwater for different positions of propellers.

4.3 INFLUENCE OF PROPELLER SHAFT ROTATING DIRECTION

For current most vessels the normal propulsion is two propellers driven by diesels and/or gas turbines. The rotating direction of propeller shaft is mainly associated with ship manoeuvring ability. However, influence of propellers' rotation direction on waterjet and propellers' hydrodynamic performance will be researched particularly in this paper. For the above calculation, the starboard and port propellers are left-handed and right-handed. It is called inward rotating propellers, and the reverse is called outward rotating propellers. Fig. 11 shows the streamline of hybrid propulsion system at the condition of outward rotating propellers. Differences between figure 6 and figure 11 show that outward rotating propellers' streamlines are assembled under the ducting inlet while dispersed of inward rotating propellers. Pressure and velocity distribution under the hull are different at two cases. Figure 9 displays the comparison of the results of two cases. Obviously, thrust and torque of waterjet is more close to isolated condition when propellers rotate outward. This is mainly due to varying of wake fraction for the increase of mass flow rate when propellers rotate outward cannot change the values so much.

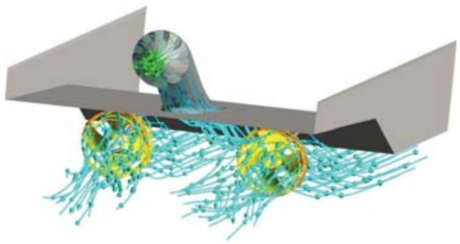

a. view from the afterbody of ship

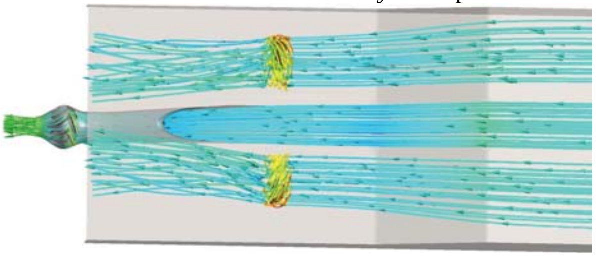

b. view from the bottom of ship

Fig. 11 Streamline of hybrid propulsion system(outward rotating)

For further comparison of different propellers rotation directions , the level of non-uniformity is expressed as a single value ζ [6].

$$\zeta \quad \frac{1}{Q}\int\sqrt{(v \quad v_{pump})^2}\,dA$$

where v is the local axial velocity and v_{pump} the average axial velocity. Non-uniform pump inflow velocity distribution can cause flow rate fluctuations through an impeller channel and the variations of the inflow angle at the leading edge of the blade[5]. Obviously, the non-uniformity should be kept minimal from a hydrodynamic point of view. Calculation results show that the level of non-uniformity of outward rotating propellers is smaller than inward rotating propellers (fig.12). That's because when propellers rotate outward, water is gathered under the ducting inlet, hull boundary is destroyed and can't play a role in the non-uniformity. From this point of view, the case of outward rotating propellers is better.

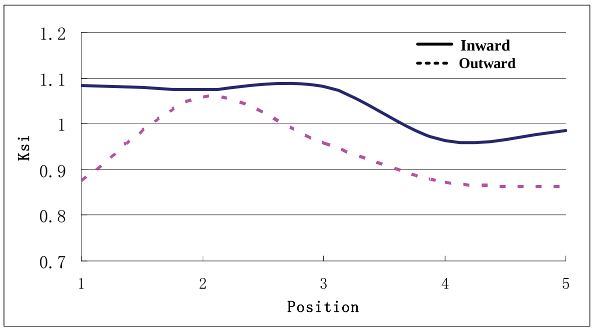

Fig. 12 Comparision of non-uniformity at two propeller rotation direction

5. MOMENTUM BALANCE FOR BOTH AN OPEN PROPELLER AND A WATERJET

Some hydrodynamic performances of hybrid propulsion system have been discussed above, from which we know that flow shapes of waterjet and propellers are different from each isolated condition and performance of propellers changed more widely. In fact, thrust of waterjet and propeller can be derived from the momentum balance for an incompressibility fluid. In this section, in order to explain propeller is more sensitive in hybrid propulsion system, thrust of waterjet and open propeller will be analysed from theory.

5.1 OPEN PROPELLER THRUST

Assume that the propeller is an actuator disc, i.e. a disc with diameter D and area A, causing a sudden increase in pressure Δp . The propeller acts on a circular column of fluid. Upstream, the flow is undisturbed and has a velocity of advance v_A while passing though area A_0 with diameter D_0 . Downstream the flow has contracted; the diameter has decreased to D_1 and the speed has increased to $v_A + \Delta v$. The pressure in the slipstream is the same as the pressure in the undisturbed flow. Figure 13 shows a sketch of the control volume of an open propeller with the nomenclature of the velocities.

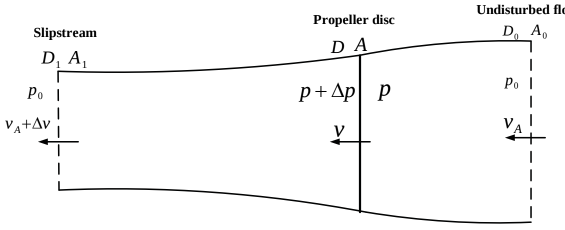

Fig 13The propeller as actuator disc: the momentum theory

If Bernoulli’s law is applied, It can be got:

Aft of propeller:

$$p+\Delta p+\frac{1}{2}\rho v^2 = p_0+\frac{1}{2}\rho(v_A+\Delta v)^2$$

Ahead of propeller:

$$p+\frac{1}{2}\rho v^2 = p_0+\frac{1}{2}\rho {v_A}^2$$

If the second equation is subtracted from the first, the pressure rise over the propeller disc can be solved:

$$\Delta p = \frac{1}{2}\rho(v_A+\Delta v)^2 - \frac{1}{2}\rho {v_A}^2$$

Assume that the thrust T exerted by the propeller on the fluid is uniformly distributed so the pressure increase at the disc is the same in every position.

$$T = \Delta p.A = [\frac{1}{2}\rho(v_A+\Delta v)^2 - \frac{1}{2}\rho {v_A}^2].A$$

Define the non-dimensional thrust loading coefficient as:

$$C_{Tprop} = \frac{T_{prop}}{1/2\rho {v_A}^2 A_{prop}}$$

Where A_{prop} is the cross-sectional area of the propeller disk, based on the propeller diameter. Jet velocity ratio μ is defined as:

$$\mu=\frac{v_{in}}{v_{out}}$$

So,

$$C_{Tprop}=\frac{T_{prop}}{1/2\rho {v_A}^2 A_{prop}}=\frac{(v_A+\Delta v)^2}{{v_A}^2} - 1=\frac{1-\mu^2}{\mu^2}$$

5.2 WATERJET THRUST

For the determination of the thrust of a waterjet in general the same approach as for the open propeller is used. The waterjet thrust is defined as:

$$T = \rho Q(v_j - v_{in})$$

The thrust loading coefficient based on nozzle exit area is discussed in [8]. With the nozzle area as reference area, the relation between jet velocity ratio and the thrust loading coefficient becomes:

$$C_{Tjet} = \frac{T}{1/2\rho {v^2}_{ship} A_{nozzle}} = \frac{2(1-\mu)(1-w)^2}{\mu^2}$$

Where w is the wake fraction. The wake fraction becomes zero, when the inflow velocity is equal to the ship speed. This is equivalent with an open water test of a propeller with uniform inflow. The resulting loading coefficient for a waterjet with undisturbed inflow yields:

$$C_{Tjet} = \frac{2(1-\mu)}{\mu^2}$$

Comparison with the open propeller thrust loading coefficient reveals a difference between the waterjet and the open propeller. This is due to the fact that a waterjet is an internal flow machine. For a waterjet the ratio between the inlet and nozzle area is fixed, whereas it is related to the thrust for an open propeller. For a hybrid propulsion system of waterjet(s) and propeller(s), propeller flow condition is greatly disturbed while waterjet flow condition only has small changes. This can be seen from the streamline of hybrid propulsion system. So propeller is weaker in hybrid propulsion system, more attention should be given to it.

6. CONCLUSION

Behavior of the flow pattern though a hybrid propulsion system of a waterjet and two propellers is simulated and some results are analyzed. Results show that hydrodynamics of hybrid propulsion are obviously different from the isolated conditions. Flow field of waterjet and propellers interact on each other. Efficiency and non-uniformity of pump inflow in outward rotating condition are better than in inward condition. Both calculation and theory analysis show that propellers are more sensitive to the change of flow field on hybrid propulsion system. More attention should be given to propellers when a hybrid propulsion system is designed.

7. REFERENCES

[1] Juergen Wessel, 'Waterjet Propulsion for a 3500 Ton Corvette from BLOHM+VOSS', International Conference on Waterjet Propulsion, RINA, London, 2004

[2] Seil G.J., 'The Effects of the Shaft Rotation and Scale on the Flow in Waterjet Inlets', International Conference on Waterjet Propulsion III, RINA, Gothenborg, Sweden 2001

[3] Park, W.G et al., 'Numerical Analysis of Intake Flow of Waterjet Pump', The 2nd PNU International Colloquium on Waterjet, Pusan, Korea, pp.171-178

[4] Bulten N.W.H, Verbeek, R., 'CFD simulation of

the flow through a waterjet installation', International Conference on Waterjet Propulsion 4, RINA, London, 2004

[5] Bulten N.W.H., 'Numerical Analysis of a Waterjet Propulsion System'. PhD thesis, Technical University of Eindhoven ,2006

[6] Roberts J L，WalkeG J R, 'Boundary Layer Ingestion Effects in Flush Waterjet Intakes', International Conference on Waterjet Propulsion, RINA, The Netherlands, 1998

[7] Hans K.Woud, Douwe S., 'Design of Propulsion and Electric Power Generation Systems'. The Institute of Marine Engineering, Science and Technology, London, 2002

[8] MacPherson, D.M., ‘A universal parametric model for waterjet performance’, Proceedings FAST’99 conference, pp. 879-882, Seattle, 1999

8. AUTHORS BIOGRAPHY

Cunlou Sun is a Ph.D. candidate of Marine Engineering at the University of Naval Engineering, P. R. China. Last year he got his master degree and his master thesis is about waterjet numerical analysis.

Yongsheng Wang is a Professor at the University of Naval Engineering, P. R. China. Since 1982 he has published more than 80 papers and his main research interests are marine power plant and its characteristics analysis.

Zhuying Li is a assistant professor at the University of Naval Engineering, P. R. China. Her main research interest is material mechanics.

TESTING AIR-AUGMENTED WATERJET PROPULSION

A Gany, A Shemer, A Gofer and **D Har-Lev**, Faculty of Aerospace Engineering, Technion – Israel Institute of Technology, Haifa, Israel

SUMMARY

A unique concept of an air-augmented waterjet propulsion system has been successfully tested, resulting in a remarkable increase in the system's thrust. This research may present a conceptual revolution for increasing boost capability and maximum attainable speed from a given waterjet system, similarly to the role played by an after-burner in a jet engine. Static tests in a water-tank have been conducted using a Yamaha jet-ski waterjet propulsion unit. Data obtained from the original motor operation at different rpm's have been used as a reference. Air injection in the air-augmented tests has been done through an extension section specially designed and installed between the pump and the nozzle exit cone. Typical thrust increase in the range of 15-30% and more compared to the original thrust has been obtained due to the injection of air bubbles, without affecting the pump operation and without causing cavitation problems. Such a capability may have significant implications on improving vessel's maneuvering, boost and speed.

1. INTRODUCTION

Marine two-phase jet propulsion has been studied extensively at the Technion - Israel Institute of Technology for nearly two decades. The main idea of the two-phase jet propulsion is that gas or air bubbles injected into the water flow within the propulsion unit convert their expansion work, $\int \mathrm{PdV}$, into kinetic energy of the flow, hence increasing the exhaust jet speed and generating thrust.

The thrust generated by both aeronautical and marine jet engines, including the marine two-phase jet propulsor, can be expressed by

$$F = \dot{m}(u_e - u) \qquad (1)$$

where F is the thrust, $\dot{m}$ the fluid mass flow rate, u is the cruise velocity, and u_e is the exhaust velocity. Equation (1) assumes that the pressure at the nozzle exit is equal to the ambient pressure (adapted nozzle). In the case of marine two-phase jet propulsion one may take into account the fact that the air mass flow rate is almost negligible compared to the water flow rate, $\dot{m}_a << \dot{m}_w$, hence the fluid flow rate through the propulsion unit is practically equal to the water flow rate.

Earlier research was focused on the operating mode of marine two-phase ramjet (Figure 1). Water enters to the marine ramjet as a result of the vessel motion. Internal pressure increases due to deceleration of the flow in the inlet diffuser. Then, air bubbles are injected into a mixing chamber, forming a two-phase flow which accelerates while flowing in the nozzle. The high speed exhaust jet generates thrust without any moving parts in contact with the water. Past works [1-3] discussed the subject of marine ramjet. Patents by Varshay and Gany [4, 5] described the concept in detail. Gany [6, 7] presented the theoretical thermodynamic cycle as well as experimental

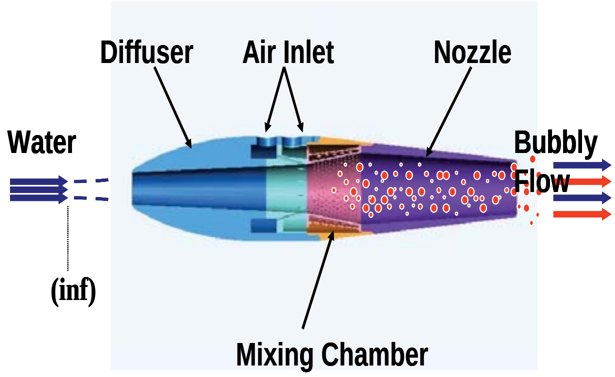

Figure 1: Illustration of a marine two-phase ramjet propulsion unit.

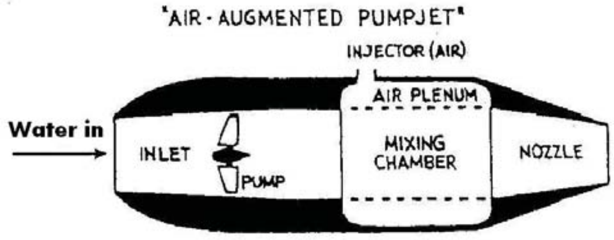

Figure 2: Schematic of marine air-augmented waterjet.

results. Albagli and Gany [8] and Mor and Gany [9, 10] analyzed and solved the two-phase flow characteristics with relation to marine ramjet. The marine ramjet may be an elegant and efficient propulsion solution for high-speed cruise regime. One should note, however, that generally ramjet engines cannot start from rest and have relatively low boost capability.

The objective of the present article is to present concept and testing of another operating mode of two-phase marine propulsion, namely, a boost mode, comprising air-augmented waterjet (Figure 2). A similar option is mentioned in [11]. The idea of the air-augmented waterjet is to combine the operation of a standard waterjet propulsion unit to a thrust augmentation section based on air injection which causes further increase of the exhaust jet speed. The combination acts like an after-burner in an aeronautical turbojet engine. It can provide additional thrust from an existing waterjet propulsor when necessary, e.g., to increase vessel acceleration, to increase maximum speed, or to overcome a resistance hump without affecting the regular waterjet pump operation. In this way one can upgrade the waterjet propulsion, extracting more thrust from the same unit and avoiding cavitation problems which would occur if thrust increase were done by operating the existing waterjet engine at a higher power. An example revealing how thrust augmentation by air injection can avoid operation in cavitation regime for overcoming a resistance hump is shown in Figure 3. One can see that instead of increasing waterjet engine power, implying operation under cavitation in the waterjet pump (Figure 3a), one may operate at a lower engine power (avoiding cavitation), adding the necessary thrust via air injection (Figure 3b). In this sample case, the addition of 15% thrust by the air system is sufficient to overcome the resistance hump, staying away from cavitation problems. Thus, one does not have to install a larger waterjet unit, yet enjoying the augmented thrust by using a small air supply unit.

In the following sections experiments done and results obtained, revealing the feasibility and actual performance of thrust augmentation by air injection will be presented.

2. TEST FACILITIES

Tests have been conducted in a water tank with connection to air supply. A 50 kW Yamaha jet-ski waterjet propulsion unit has been used for the tests. Thrust at static operation was measured using a load cell at the jet-ski front. Pressure downstream of the pump as well as motor rpm and airflow rate have been recorded continuously. Schematic of the test installation is presented in Figure 4.

3. RESULTS AND DISCUSSION

3.1 BASIC WATERJET OPERATION

A number of test series have been conducted. For baseline data the original waterjet was operated at different rpm's in a regular manner, without air injection. Then, a cylindrical section was installed (to enable introduction of air) between the pump section and the nozzle cone section. The engine with this installation was run again without air to compare the results with the original arrangement. Figure 5 presents the results of thrust versus motor rpm for the two installations. One can see that the thrust data overlap one another and no apparent practical difference is detected.

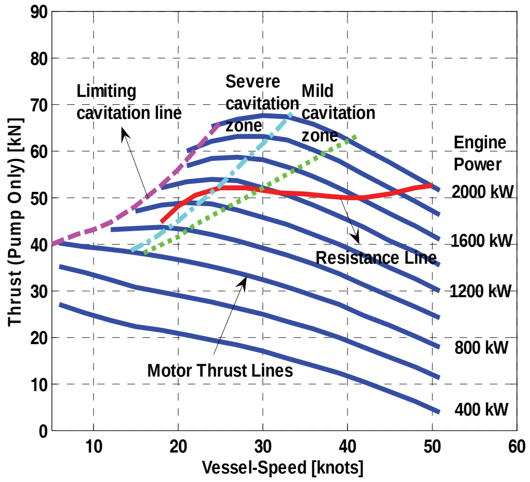

(a)

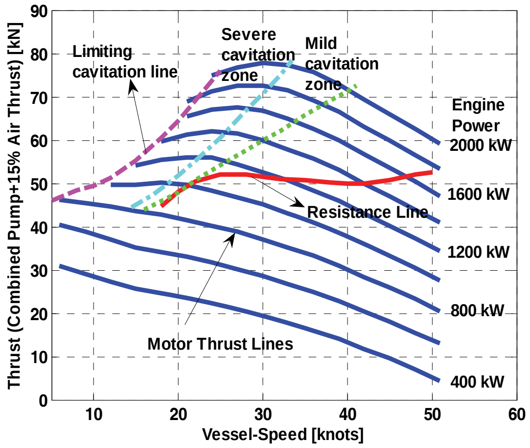

(b)

Fig. 3: Sample of thrust vs. vessel-speed maps: (a) Regular waterjet, requiring operation in the cavitation zone to overcome resistance hump. (b) Air-augmented waterjet, avoiding operation in cavitation regime.

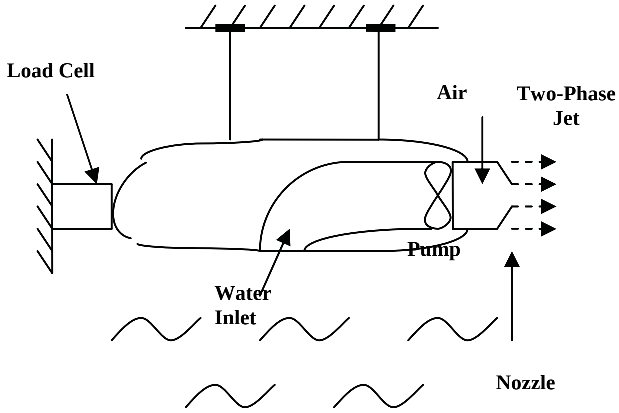

Fig. 4: Schematic of the test installation for the air-augmented waterjet.

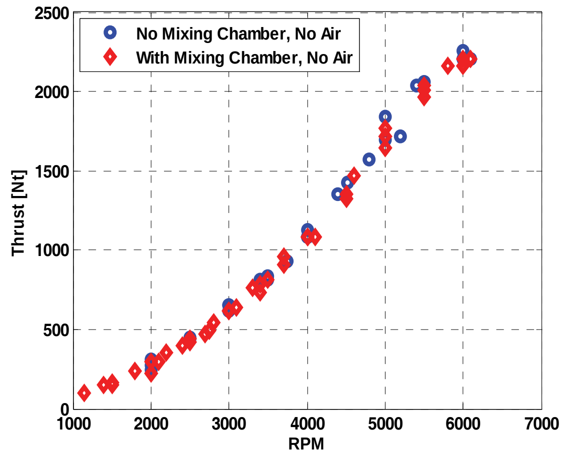

Figure 5: Thrust vs. rpm for the original waterjet and for the waterjet with a mixing chamber extension. No air injection.

3.2 THRUST AUGMENTATION BY AIR INJECTION

Thrust increase due to air injection has been studied by introducing the air from 16 ports at the extension section (mixing chamber) casing into the water flow.
Ideal isothermal gas expansion in the nozzle is associated with expansion work w_{ep} per unit mass of air as follows,

$$w_{\exp} = RT \ln r \qquad (2)$$

where R is the specific gas constant, T is the water temperature, and r is the ratio between the pressure after the pump and the ambient pressure. It is predicted that an effective fraction of the air expansion work $\eta w_{\exp}$ per unit mass of air is converted to additional kinetic energy of the exhaust jet (at efficiency η). For optimal design, the nozzle exhaust plane has to be adjusted according to the air-to-water mass flow rate ratio and the vessel speed. As stated before, all tests have been conducted in static conditions (zero vessel speed).

Figure 6 presents the thrust ratio with and without air as a function of airflow rate, for waterjet engine operating at 2000 rpm. A theoretical line with air expansion work conversion efficiency $\eta = 70\%$ seems to reflect the actual performance. Note that for this low rpm, thrust increase may be as high as 55%. In this rpm the nozzle was adjusted to the low airflow rate ($60 g/\sec$), hence, somewhat better efficiency can be observed in that range. Figures 7-9 make a similar presentation for 3000, 4000, and 5000 motor rpm, respectively. One can see that the theoretical line with 70% air expansion efficiency gives a good correlation in all cases. The thrust ratio decreases at higher rpm's for the same airflow rate, as expected by the theory. Note that the air expansion work efficiency seems to be somewhat better at the higher rpm, where the nozzle is adjusted to higher airflow rates.

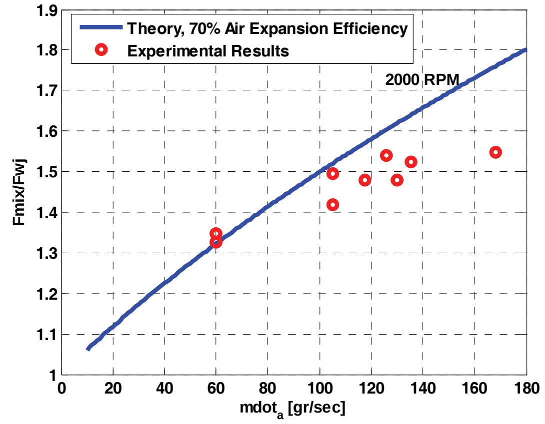

Figure 6: Thrust ratio of waterjet engine with and without air injection vs. airflow rate. Engine at 2000 rpm.

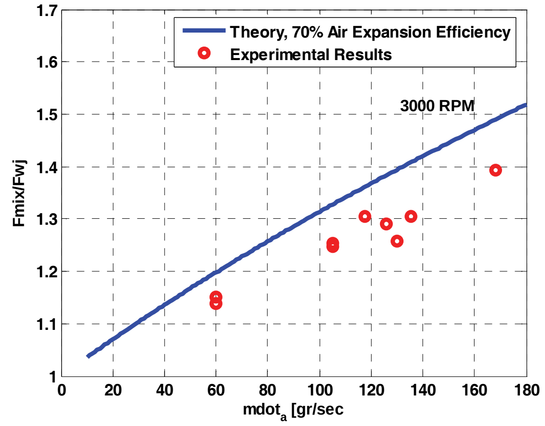

Fig. 7: Thrust ratio of waterjet engine with and without air injection vs. airflow rate. Engine at 3000 rpm.

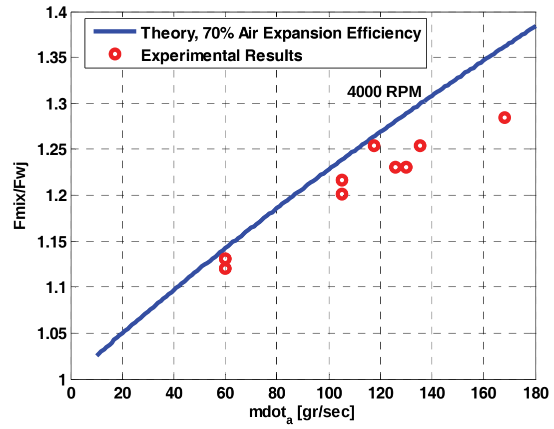

Fig. 8: Thrust ratio of waterjet engine with and without air injection vs. airflow rate. Engine at 4000 rpm.

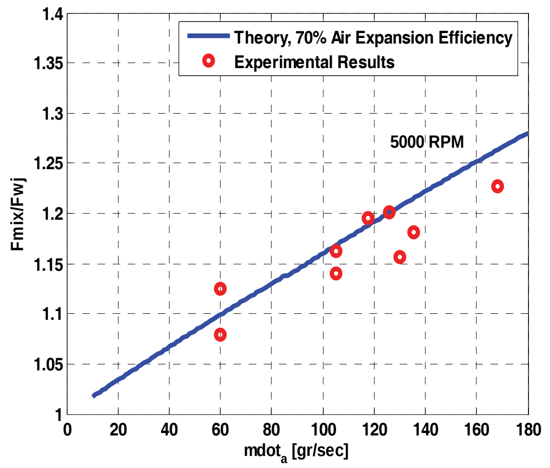

Fig. 9: Thrust ratio of waterjet engine with and without air injection vs. airflow rate. Engine at 5000 rpm.

4. CONCLUSIONS

Concept and testing of air augmented waterjet propulsion have been presented. It is shown that by injecting air provided by a relatively small air compressor into the nozzle section of a waterjet unit, one can increase the waterjet thrust without affecting the pump and engine operation. The additional thrust is produced in a way parallel to the operation of an after-burner in an aeronautical turbojet engine. The main advantage is the possibility to increase of boost and speed, and overcoming resistance hump without the use of a larger waterjet unit and with avoiding cavitation problems.

The tests conducted using 50 kW Yamaha waterjet unit reveal static thrust increase of 15%-50%, depending on air flow rate and motor rpm, demonstrating air expansion work efficiency of about 70%.

The concept of air-augmented waterjet is very promising for upgrading waterjet systems.

5. REFERENCES

1. MOTTARD, E.J., and SHOEMAKER, C.J., “Preliminary Investigation of an Underwater Ramjet Powered by Compressed Air,” *NASA Report TND9*, December 1961.

2. WITTE, J.H., “Predicted Performance of Large Water Ramjets,” *AIAA 2nd Advanced Marine Vehicles and Propulsion Meeting, Seattle, WA, USA*, 1969.

3. CHERNYY, I.M., “Optimal Parameters and Efficiency of Gas-Water Jet Engines Operating on Cold and Hot Gas,” *Fluid Mechanics – Soviet Research*, Vol. 6, No. 2, pp. 87-105, 1977.

4. VARSHAY, H. and GANY, A., “Underwater Two-Phase Ramjet Engine,” *United States Patent Number 5,598,700*, Feb. 4, 1997.

5. VARSHAY, H. and GANY, A., “Underwater Two-Phase Ramjet Engine,” *United States Patent Number 5,692,371*, Dec. 2, 1997.

6. GANY, A., "Analysis of a New Thermodynamic Power Cycle for a Two-Phase Waterjet," *International Conference Waterjet Propulsion 4, RINA*, London, UK, May 26-27, 2004.

7. GANY, A., "Two-Phase Marin Ramjet Propulsion Research," *The Australian Naval Architect*, Vol. 12, No. 2, pp. 36-40, May 2008.

8. ALBAGLY, D. and GANY, A., “High Speed Bubbly Nozzle Flow with Heat, Mass, and Momentum Interactions,” *International J. of Heat and Mass Transfer*, Vol. 46, pp. 1993-2003, 2003.

9. MOR, M. and GANY, A., “Analysis of Two Phase Homogeneous Bubbly Flows Including Friction and Mass Addition,” *J. of Fluid Engineering Transactions of ASME*, Vol. 126, pp. 102-109, 2004.

10. MOR, M. and GANY, A., “Performance Mapping of Bubbly Water Ramjet,” *International Journal of Maritime Engineering*, Vol. 149, Part A1, pp.45-50, 2007.

11. MUENCH, R.K. and GARRETT, J.H., “A Review of Two-Phase Marine Propulsion,” *AIAA Paper No. 72-589, AIAA/SNAME/USN Advanced Marine Propulsion Meeting*, Annapolis, MD, USA, July 17-19, 1972.

6. AUTHORS BIOGRAPHY

Alon Gany is a Professor, holding the Lena and Ben Fohrman Chair in Aeronautical Engineering and heading the Sylvia and David IA Fine Rocket Propulsion Center at the Faculty of Aerospace Engineering, Technion – Israel Institute of Technology, Haifa, Israel. Prof. Gany has published numerous papers in the field of Propulsion in general and marine two-phase jet propulsion in particular. Prof. Gany is a fellow of RINA.
Email: gany@tx.technion.ac.il

Arik Shemer is currently an M.Sc. student at the Faculty of Aerospace Engineering, Technion – Israel Institute of Technology, Haifa, Israel. His research deals with air-augmented waterjet. He obtained a B.Sc. degree in marine technology from the University of Newcastle, UK (2000). He is the owner of a company Shemer Marine Engineering in Israel.
Email: info@yacht4sale.co.il

Aviad Gofer is an M.Sc. student at the Faculty of Aerospace Engineering, Technion – Israel Institute of Technology, Haifa, Israel. His B.Sc. degree (2006) was also obtained from the Technion. His main research

subject is compressibility and transport phenomena in two-phase bubbly flow and two-phase marine jet propulsion.
Email: aviad.gofer@gmail.com

Doron Har-Lev is the Lab Engineer of the Sylvia and David IA Fine Rocket Propulsion Center, Faculty of Aerospace Engineering, Technion – Israel Institute of Technology, Haifa, Israel. He received his B.Sc. degree in Mechanical Engineering from Tel Aviv College of Engineering (2002).
Email: doron@aerodyne.technion.ac.il

SIMULATION OF DYNAMIC CHARACTERISTICS OF WATERJET AND ITS APPLICATION ON TROUBLESHOOTING

Yongsheng Wang and **Jiangming Ding**, University of Naval Engineering, China;
Zhirong Liu and **Wenshan Xu**, Guangzhou Marine Engineering Corp., China

SUMMARY

A mathematical model describing the dynamic characteristics of a marine waterjet propulsion plant was built up. The rotating-speed vs. power curves of the diesel engine from a test-bed and the vessel speed vs. thrust curves of waterjet were modeled by means of the neural networks. Other components of the waterjet propulsion plant, such as reduction gearbox, were also modeled by manufacture's data. These main components models were integrated as a whole waterjet propulsion system in a simulation program for dynamic characteristic analyses on MATLAB platform. In a case that searching the reason of a friction clutch failure in the reduction gearbox during maneuvering operation of a waterjet-propelled fast vessel, the applications of dynamic characteristic simulation in the troubleshooting of waterjet propulsion system was played a very important role in locating main causes for the failure.

1. INTRODUCTION

System simulation is widely used in Marine Engineering, for example, analysis of steady-state and dynamic characteristics, setting of parameters and selecting of control strategy of control systems, predictions of rapidity and maneuverability of ship, daily and emergent operations of marine power plant.

Marine waterjet propulsion is different from marine propeller propulsion, and there are some differences in their operating principles and characteristics. For example, the absorbed power by propeller depends not only on propeller's rotating speed but also ship speed, under the condition of the same the rotating speeds of propeller but different ship speeds, there are much obvious different propeller loads. On the contrary, the absorbed power by waterjet depends mainly on waterjet's rotating speed and much less on ship speed[1,2]. Therefore the waterjet principle and corresponding characteristics should be applied in the dealing with some issues of waterjet propulsion related to design of waterjet propulsion, setting down the operating rules， troubleshooting of failure.

The neural network method is used in modeling of waterjet characteristics which integrated with models of main diesel engine, governor, transmission components and hull into a whole waterjet propulsion system. Based on the whole waterjet propulsion model the steady-state and dynamic characteristics of the waterjet propulsion system can be simulated and analyzed. This simulation system is effectively applied in some troubleshooting as a case study.

2. MATHEMATICAL MODEL OF WATERJET PROPULSION SYSTEM

The mathematical model of the waterjet propulsion system should be built up first of all before the steady-state and dynamic characteristics of the system are simulated and analyzed. For the ordinary waterjet propulsion system in the form of indirect-driven mode there are two subsystems, a subsystem in a rotating movement of "main engine—waterjet " and a subsystem in a translation movement of "waterjet—hull"

2.1 MATHEMATICAL MODELS OF TWO SUBSYSTEMS IN WATERJET PROPULSION SYSTEM

A differential equation for the subsystem in the rotating movement of "main engine—waterjet is as following:

$$iM_e - M_f - M_p = J\frac{d\omega}{dt} \qquad (1)$$

Where M_e is a main engine torque, M_f is a friction torque in transmission system, M_p is a waterjet's torque, i is a reduction ratio of gearbox, J for waterjet shaft motion is a total moment of inertia of the whole subsystem, ω is an angular velocity of waterjet shaft.

A differential equation for the subsystem in the translation movement of "waterjet—hull is

$$nT \quad R \quad \Delta R \quad m\frac{dV_s}{dt} \qquad (2)$$

Where T is thrust of a set of waterjet propulsion, n is number of sets of operating waterjets, R is a hull's resistance. ΔR is an added resistance from trailing waterjet, m is mass included in hull's mass and added water mass, V_s is ship speed.

The （1）and（2）are two basic governing equations in simulation of the dynamic characteristics of waterjet propulsion. In order to describe the dynamic characteristics with accuracy it is a key that all parameters and coefficients and their relations in the two basic governing equations should be determined with accuracy. In arriving at this goal a first step is to well and truly develop components' models of the waterjet propulsion system, i.e. the models of speed governor, diesel engine, reduction gearbox and shaft, waterjet, hull resistance. Then these models are well and truly integrated into the whole model of the waterjet propulsion system.

2.2 MATHEMATICAL MODELS OF COMPONENTS IN WATERJET PROPULSION SYSTEM

Emphases in simulation of waterjet propulsion system should be placed on the system characteristics and interaction among the system components. From the view point of system engineering a mathematical modeling based on external characteristics of components can meet the demand of study on propulsion characteristics with satisfied accuracy. The external characteristics (or curves) of components are usually provided by manufacturer. The modeling of all components in this paper makes use of their external characteristics (or curves) from manufacturers or designers.

Models of governor, diesel engine, reduction gearbox and shaft, hull in the waterjet propulsion system are very common in simulation of propeller propulsion system and there are lots of references about them. The only difference in waterjet propulsion system with propeller propulsion system is propulsor.

A quasi-steady-state method and external characteristics of waterjet from manufacturer are used in modeling of the absorbed power and thrust of waterjet in the paper. One curve is waterjet rotating speed vs. ship speed at constant absorbed power (Figure 1, called the rev. speed curve), another is waterjet thrust vs. ship speed at constant absorbed power (Figure 2, called the thrust curve).

In Figure1 and Figure2 the rev-speed characteristic and the thrust characteristic of waterjet within an operating envelope are described by series of curves. It is needed to interpolate and extrapolate data among series of curves because any data among series of curves are needed in simulation. This task can be done by the neural network. The details of modeling of characteristic curves of some marine fluid coupling were investigated in references [3-6].

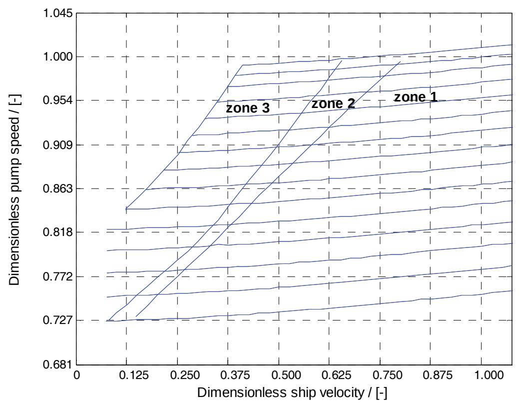

Figure 1: The Rev. Speed Characteristic of Waterjet

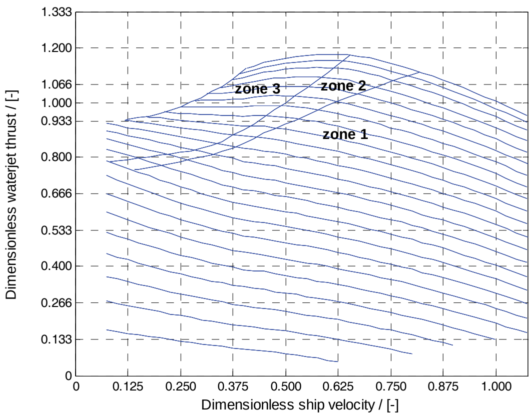

Figure 2: The Thrust Characteristic of Waterjet

A simulation model of the external characteristics by the neural network method is built up in this paper shown in Figure 3[7]. First the inputs, the rotary speed of the waterjet and the ship speed, into the block of Neural Network Model for Waterjet Power Calculation can produce the absorbed power of the waterjet. Then the inputs, the absorbed power of the waterjet and the ship speed, into the block of Neural Network Model for Waterjet Thrust Calculation can produce the thrust of the waterjet.

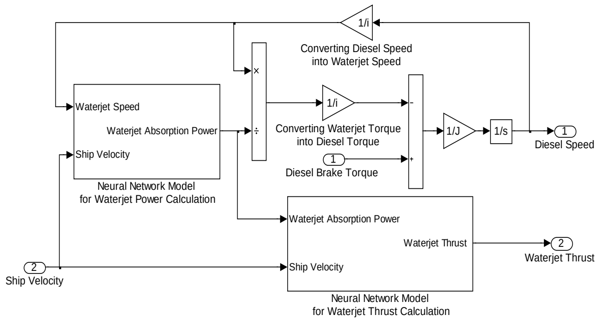

Figure 3: Simulation Model of Waterjet

The rotary direction of waterjet is not changed when ship experiences crash-stop maneuver. A reversing force is obtained by deflect the jet of water. Thrust reversal is achieved by a position setting of a reversing bucket. The thrust is reversed by gradually moving the bucket into the jet of water and thus deflecting a gradually increasing proportion of the jet in a forward & downward direction. The thrust can be varied continuously from zero to maximum ahead or astern by setting the bucket in an intermediate position. During the reversal of the jet of water there is a loss of flow energy, thus the reversing force (going astern) is smaller than the forwarding force (going ahead) at the same rotary speed of the waterjet. A ratio of the reversing force to the forwarding force depends on type of waterjet and its rotary speed. Here the ratio 0.52~0.55 is selected according to some type of waterjet test data. The process of adjusting the reversing bucket from ahead to astern lasts around 6 seconds. The forwarding force or the reversing force at any bucket's position between ahead and astern is linearly interpolated from 1 to -.52 within 6 seconds. The mathematical model of the processes for acceleration, deceleration and crash stop is based on waterjet control diagram (Figure 4).

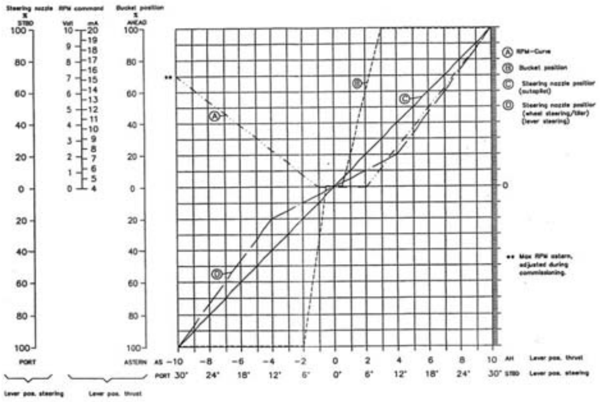

Figure 4: Some Waterjet Control Diagram

3 SIMULATION APPLICATIONS IN TROUBLESHOOTING

Features of propeller propulsion are very better known by ordinary people, and lots of experiences have been accumulated. Therefore some people are apt to apply the experience of propeller propulsion to troubleshooting of waterjet propulsion, and sometimes mistakes occur. Dynamic simulation of waterjet propulsion system based on its property could conveniently and correctly be used to do troubleshooting. In this paper a case study of troubleshooting based on dynamic simulation of waterjet is introduced.

Four sets of waterjet units are adapted in a fast boat, in which a main diesel engine drives a waterjet through a reduction gearbox in each set. In a maneuvering four sets of waterjet units in sea trial were accelerated in step from idling to full speed with 15 seconds. Then a deceleration was done from the full speed to the idling with 8 seconds after the ship design speed was achieved. During the deceleration the rotary speeds of three sets of waterjet units decreased in accordance with each other but the rotary speed of the remaining one was kept unchanged.

Finding the unusual situation and wanting to correct it an operator put the control lever back to the full speed position, ant then try a second deceleration. During the second deceleration the rotary speed of the remaining one still remained unchanged, and then an overspeed occurred. An emergent stop of the diesel engine was triggered off and at the same time a report came from engine room that white smoke came from the reduction gearbox in which the friction discs were destroyed.

There were lots of opinions to the fault and what was a cause to the fault. The primary opinion among them to the fault analysis was that a load to the friction disks in the reduction gearbox is larger than the design load because the remaining one did not change the rotary speed due to malfunction of the control system, and bore much larger load when the three sets of waterjets decreased the rotary speed.

Towards the primary opinion this whole operating process are simulated by the dynamic simulation model based on the four sets of waterjet propulsion units, and analysis of simulation results are done in order to find out the cause of this fault. The first layer of the dynamic simulation model is demonstrated in Figure 5 [5].

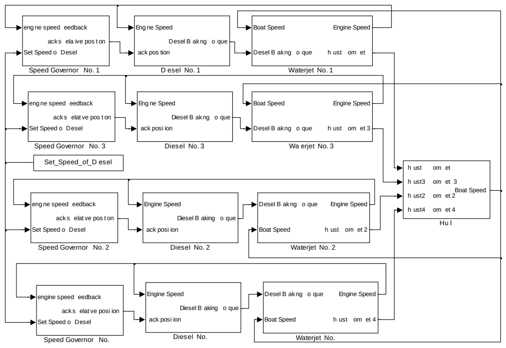

Figure 5: First Layer of Waterjet Propulsion Model

Figure 6 and Figure 7 show the curves of ship speed and engine torque of the waterjet propulsion system when the four sets of waterjet propulsion units are first decelerated and then accelerated in step. In the deceleration process the ship speed and engine torque are also decreased, and then they are increased in the acceleration process. Because of different acceleration rates, that is, the shaft speed increase much fast than the ship speed does, the propulsion system is in state of low ship speed and high shaft speed, thus the engine torque is higher than the design torque in a short period within the acceleration. In the short period within the acceleration the maximum torque is larger 4.4% than the design torque.

Figure 8 and Figure 9 show curves of engine torques in another dynamic process. The dynamic process is similar to the above mentioned fault process in which three sets of waterjet units first were decelerated from full rotary speed to idling speed and then accelerated to full rotary speed and at the same time the remaining waterjet unit was kept at full rotary speed. The engine torque in three sets of waterjet units decrease during the rotary speed decoration; in the middle process the engine speed keeps at the constant idling speed and ship speed still decreases, which makes the engine torque a little bit increased. Then the engine torque increases with the increased rotary speed of the engine and exceeds the design torque when ship speed has not reach the maximum speed. In company with increased ship speed the engine torque returns to the design value. The maximum torque is larger 3.1% than the design torque during the process. The rotary speed of the remaining waterjet units kept at the full rotary speed during the process and its torque increases firstly with the decreased ship speed and then returns to the design torque. Its maximum torque is larger 3.5% than the design torque.

The common property can be drawn from Figure 7 and 8 that the maximum of engine torque is not much larger than the design torque and the increment of the torque is less than 5%. In fact this increment would not cause damage to the friction disks because the maximum torque of engine does not exceed the maximum torque of the friction disks in the safety mode. It is reasonable that the load torque during the malfunction process was not the main cause which overloaded the friction disks and destroyed them. The conclusion is in agreement to characteristic of waterjet propulsion. As we all know waterjet is a propulsor with internal flow and propeller with external flow. Ship speed mainly decides advance velocity of propeller which and the circumferential speed determine an angle of attack and a relative water velocity approaching to propeller blade. The advance velocity is a main factor to affect propeller's load i.e. torque. This is why ship speed will remarkably affect propeller torque. In waterjet the flow enter impeller after water-flow is reformed or reshaped through inlet duct. Thus an influence of ship speed to an angle of attack and a relative water velocity approaching to impeller blade become weak. This is why ship speed will weakly affect waterjet torque. Now we can understand why the torque of waterjet changes a little when ship speed changes a lot as waterjet speed maintains constant.

The scope for searching through the reason triggered the fault is narrowed after the waterjet torque is excluded the possibility of troublemaker.

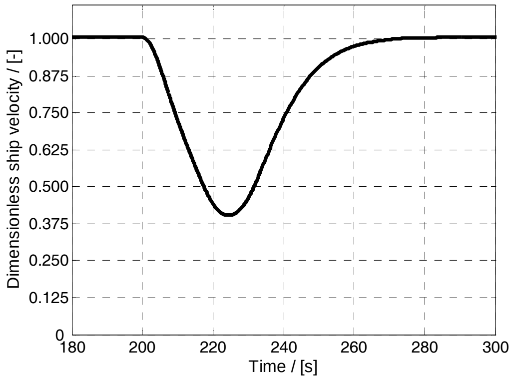

Figure 6: Ship Speed during Normal Maneuver

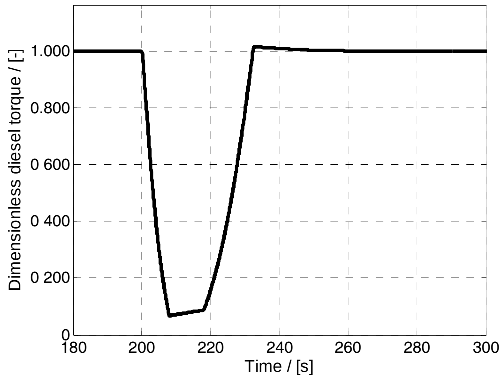

Figure 7 Engine Torque during Normal Maneuver

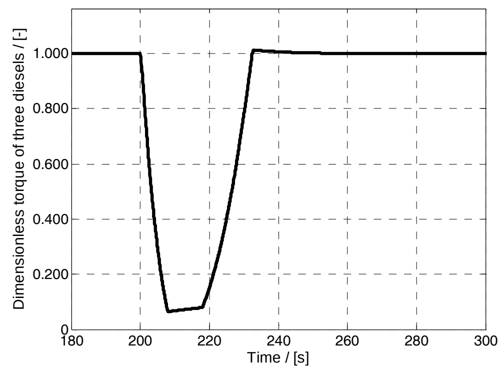

Figure 8 Engine Torque during Abnormal Maneuver

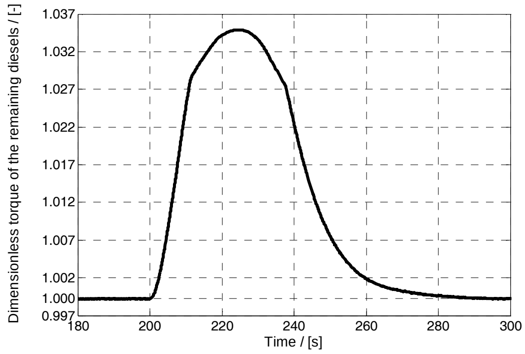

Figure 9: The Remaining Engine Torque during Abnormal Maneuver

4. CONCLUSIONS

（1）Characteristics of waterjet are much different from propeller. Steady-state and dynamic properties of waterjet during maneuvers can be studied by modeling and simulation. This kind of simulation can be applied in design, optimization and troubleshooting of waterjet propulsion. A case study in the paper is one application of them.

（2）The only difference between the waterjet propulsion and propeller propulsion is propulsor, and so waterjet modeling is a key component in modeling of whole waterjet propulsion system. Manufacture's maps or external characteristics of thrust curves and rotary speed curves can be utilized to waterjet's modeling by quasi-steady-state method.

5. REFERENCE

[1] Keith Alexander, 'Waterjet versus Propeller Engine Matching Characteristics', Naval Engineering Journal [J], May 1995.

[2] Yongsheng Wang, Jiangming Ding, Huaqing Chen, et al. 'Research on the Relationship between Waterjet Power Absorption and Ship Speed', Symposium of International Waterjet Conference. RINA, 2004.

[3] Jiangming Ding, Yongsheng Wang, 'Research on Mathematical Model of Fluid Coupling Based upon Physical Principle and Test Curves' (In Chinese), Shipbuilding of China, Vol.47, No.1, 2006.

[4] Yongsheng Wang, Shaozeng Wang, Jiangming Ding, 'Transformation of Input Characteristic of Fluid Coupling and Their Engineering Applications '(In Chinese), Chinese Journal of Mechanical Engineering [J], Vol.42, No.4, 2006.

[5] Yongsheng Wang, Jiangming Ding, 'Research on Approach to Develop Mathematical Model of General External Characteristic of Fluid Coupling' (In Chinese)'. Chinese Journal of Mechanical Engineering, Vol.41, No.4, 2005.

[6] Yongsheng Wang, Huaqing Chen, Chenyang Ao, et al. 'Neural Network Model of Fluid Coupling Used in Ship Power Plant' (In Chinese), Shipbuilding of China, Vol.44, No.4, 2003.

[7] Jiangming Ding, Yongsheng Wang, 'Characteristic Research on Diesel Load during Turning Course of Waterjet-driven Ship' (In Chinese), Shipbuilding of China, Vol.46, No.3, 2005.

6. AUTHORS BIOGRAPHY

Yongsheng Wang, Professor in the University of Naval Engineering in China.

Jiangming Ding, Ph.D. candidate of Marine Engineering in the University of Naval Engineering in China.

Zhirong Liu, Senior Engineer & Chief Designer of marine power plant in the Guangzhou Marine Engineering Corp. in China

Wenshan Xu, Senior Engineer & Chief Designer of naval architect in the Guangzhou Marine Engineering Corp. in China

NUMERICAL SIMULATION AND ANALYSIS OF CAVITATION PERFORMANCE OF WATERJET

Chengjiang Liu, Yongsheng Wang and **Zhihong Zhang,** Naval University of Engineering, China

SUMMARY

With *SST* turbulent model, hydrodynamic performance of a waterjet at non-cavitation conditions is obtained by calculating *RANS* equations with computational fluid dynamic (CFD) method firstly. The comparison between calculation results and data from manufacturer shows that the numerical model and method is creditable. Then, cavitation performance of the waterjet is calculated and analyzed with mixture homogeneous cavitation model based on Rayleigh-Plesset equations. Numerical results, such as power and thrust, agree well with manufacture data. The critical inlet velocity ratio (IVR*)*, when cavitation occurs, is obtained. The calculation results show that mass flow rate and total head of the waterjet pump are reduced when cavitation occurs on rotor blades, and thrust declines. The cavitation on rotor blades gets stronger as IVR falls at constant power condition. Inlet duct cavitation lags behind the rotor cavitation, and nozzle cavitation in form of spatial cavitation occurs ahead of the rotor cavitation, but there is no cavitation on nozzle wall. Finally, a conclusion is obtained that the limiting cavitation line is a constant suction specific speed line.

NOMENCLATURE

NPSH: Net Positive Suction Head [m]
ρ: Density [kg m^{-3}]
C: Velocity [m s^{-1}]
α: Local volume fraction [-]
p: Pressure [Pa]
R: Radius of the bubble [m]
V: speed [m s^{-1}]
N: Rotating speed of pump [rev min^{-1}]
IVR: Inlet velocity ratio = V_s/V_P [-]
ε: Inlet loss coefficient [-]
ω: Wake fraction [-]
h_j: Nozzle elevation above the waterline [m]
v_0: Absolute velocity just in front of inlet of blade [m s^{-1}]
w_0: Relative velocity just in front of inlet of blade [m s^{-1}]
λ: Dimensionless coefficient [-]
m: mass [kg]
N_{ss}: Suction specific speed [-]
Q_v: Volume flow rate, [m^3 s^{-1}]
D: Diameter of pump inlet [m]

SUBSCRIPT

a: available
r: required
m: mixture
n: the nth phase
v: vapor
w: water
nuc: nuclei
l: liquid
s: ship
max: maximum
p: pump
∞: ambient

1. INTRODUCTION

As in aerospace the propeller has been replaced by the jet engine, which was necessary to reach higher speeds, application of waterjets in marine vessels shows a similar trend where the waterjet helps vessels reach higher speeds. Theory and many relations which describe the principles of waterjet propulsion are derived more or less directly from propeller theory, with the same nomenclature[1,2]. However, there are some significant differences between propeller and waterjet propulsion. With the limitation of cavitation, propeller is not allowed to work at high speeds, so the vessels propelled by conventional propellers are hard to reach the speed higher than 35 knot. But waterjet can help vessels overcome this speed limit as the essential working assembly of a waterjet which has the property of a general pump can work at high rotating speeds. As long as the inlet duct in front of the pump can supply enough available net positive suction head (*NPSHa*), cavitation will not occur in the pump. *NPSHa* will increase as ship speeds up, so there is no risk of cavitation at high speeds of waterjet. This is a remarkable difference between waterjet and propeller, and this is the main reason for waterjet suitable to high-speed vessels.

Although the waterjet is prior to the propeller in the application of high speed vessels and has good cavitation property, a waterjet would work with risk of cavitation if it works at high rotating speed with low vessel speed. Because at some conditions such as rapid boost, fast turning and back astern, the *NPSHa* supplied by inlet duct may be lower than the net positive suction head required (*NPSHr*) by pump. As known to all, cavitation will cause breakdown of waterjet performance. So, it is very significance to research the cavitation performance of the waterjet.

In earlier years, model test and full-scale trial were the main means to investigate waterjet performance. Nowadays, computational fluid dynamic (CFD) becomes more and more important in the research of waterjet performance and cavitation phenomena. Some institutes have carried out many researches with wind tunnel and water tunnel[3,4,5], and in the meantime numerical simulation of cavitation is becoming a popular topic in recent years. Based on plenty of tests, researchers have developed several cavitation models to simulate different kinds of cavitations, which have used to two-dimensional hydrofoils, propellers and radial flow pumps[6~12]. However, there are little reports of numerical simulation of cavitation performance of a whole waterjet propulsion system.

In this paper performance prediction of a whole waterjet propulsion system at non-cavitation conditions is completed firstly. Then, numerical simulation and analysis of cavitation performance of it is carried out on the basis of the creditable model and method approved above. Some conclusions are obtained in the end.

2. NUMERICAL MODEL

2.1 GOVERNING EQUATIONS AND CAVITATION MODEL

Leading edge cavitation, known as attached cavitation, also usually called sheet cavitation, occurs at depression zones of the blade surface.

Cavitation and especially leading edge cavitation have a well mixed multiphase behavior at cavity closure region, where the interface between liquid and vapor is not clearly identified, and the two-fluid modeling in sense of resolving each phase separately leads to unrealistic small scales resolution. With these limitations the two-fluid model returns automatically to a mixture model, and the latter appears to be the best choice regarding the computation effort for leading edge cavitation modeling[5]. So the homogeneous mixture model is used to simulate the turbulent cavitation flow in a waterjet propulsion system.

The basic concept of the mixture model is to consider the mixture as a whole. This formulation is more simple than the two-fluid model, which is formulated by considering each phase separately and expressed in terms of two sets of conservation equations governing the balance of masses, momentum and energy for each phase.

2.1 (a) Governing Equations

The governing continuity and momentum equations for a classical RANS and homogeneous mixture multiphase flow are described as below.

The mixture continuity equation can be written as follows:

$$\frac{\partial \rho_m}{\partial t} + \vec{\nabla} \cdot (\rho_m \vec{C}_m) = 0 \qquad (1)$$

where the mixture quantities are defined as:

$$\rho_m = \sum_{n=1}^{2} \rho_n \alpha_n \qquad (2)$$

$$\vec{C}_m = \sum_{n=1}^{2} \frac{\rho_n \vec{C}_n}{\rho_m} \qquad (3)$$

$$p_m = \sum_{n=1}^{2} p_n \alpha_n \qquad (4)$$

where α_n is the local volume fraction.

The general formulation of the conservation of momentum has the same form as the single phase theory for the whole mixture:

$$\frac{\partial}{\partial t}(\rho_m \vec{C}_m) + \rho_m (\vec{C}_m \cdot \vec{\nabla}) \vec{C}_m = -\vec{\nabla}(p_m) + \vec{\nabla} \cdot (\bar{\bar{\tau}} + \bar{\bar{\tau}}_t) + \vec{M}_m + \vec{f} \qquad (5)$$

$\bar{\bar{\tau}}$ denotes the viscous stress tensor, $\bar{\bar{\tau}}_t$ the Reynolds stress tensor, $\vec{M}_m$ the interfacial momentum source and the surface tension term is neglected, and $\vec{f}$ the body force term which represents typically the gravitational field in hydraulic systems.

Using a mixture model for modeling a turbulent cavitation flow, the system needs two closure assumptions: one for the turbulent terms in the momentum equation and the other for the inter-phase mass source for the mixture density (i.e. volume fraction equation).

2.1 (b) Mass-Fraction Transport Equation

The governing equations describe the cavitation process involving 2-phase 3-component system, where we assume no-slip between two phases. The three components are: vapor (v), water (w), and non-condensable gas in the form of micro-bubbles nuclei (nuc). The relative quantity of each of the components is described by a volume fraction scalar, as:

$$(\alpha_w + \alpha_{nuc}) + \alpha_v = 1 \qquad (6)$$

In many cavitation cases, the non-condensable gas phase is assumed to be well mixed in the liquid phase with a constant volume fraction α_{nuc}. On this assumption the mass fractions α_w and α_{nuc} can be combined and treated as one. The volume scalar α_l is introduced as: $\alpha_w + \alpha_{nuc} = \alpha_l$. Choosing the scalar α_l to solve the transport equation, the governing equation for the liquid phase including non-condensable gas becomes:

$$\frac{\partial}{\partial t}\left(\alpha_l \rho_l\right)+\vec{\nabla}\cdot\left(\alpha_l \rho_l \vec{C}_m\right)=\Gamma_l=\dot{m}_l^v+\dot{m}_l^c \qquad (7)$$

where $\alpha_v = 1-\alpha_l$ and $\dot{m}_l^v$, $\dot{m}_l^c$ are the source terms respectively associated to the vaporization and condensation processes (i.e. growth and collapse). Their units are kg m^{-3} s^{-1} and account for mass exchange between the vapor and liquid during cavitation.

2.1 (c) Rayleigh-Plesset Source Term

The cavitation model is implemented based on the use of the Rayleigh-Plesset equation to estimate the rate of vapor production. For a vapor bubble nucleated in a surrounding liquid, the dynamic of the bubble can be described by the R-P equation, by neglecting viscous terms and surface tension, such as:

$$\rho\left[R\ddot{R}+\frac{3}{2}\dot{R}^2\right]=p_v-p \qquad (8)$$

where R is the radius of the bubble, p_v the vapor pressure in the bubble, p the pressure in the surrounding liquid, and ρ_l the liquid density. The first order approximation is used, where the growth or collapse of a bubble follows the RP equation, neglecting higher order terms and bubbles interactions ($\dot{R}=\sqrt{(2\cdot|p_v-p|)/(3\cdot\rho_l)}$).

In practice, the vaporization and condensation processes have different time scales. Empirical constants, F^c and F^v , are introduced to take into account these constraints. The source terms $\dot{m}_l^v$, $\dot{m}_l^c$ can be expressed as:

$$\dot{m}_l^v=-F^v\,\frac{3\rho_v\alpha_{nuc}\alpha_l}{R_0}\sqrt{\frac{2}{3}Max\left(\frac{p_v-p}{\rho_l},0\right)} \qquad (9)$$

$$\dot{m}_c^v=-F^c\,\frac{3\rho_v\left(1-\alpha_l\right)}{R_0}\sqrt{\frac{2}{3}Max\left(\frac{p-p_v}{\rho_l},0\right)} \qquad (10)$$

2.2 TURBULENCE MODEL

A problem with the original $k-\omega$ model is its strong sensitivity to free-stream conditions. In order to solve the problem, a blending between the $k-\omega$ model near the surface and the $k-\varepsilon$ model in the outer region was developed by Menter[13],which was called Shear Stress Transport model (*SST* model). This turbulent model is adopted in this study.

2.3 SELECTION OF CONTROL VOLUME

In this paper simulation and analysis are based on the geometry of a waterjet equipped in a full-scale ship. Figure 1 shows the waterjet's configuration. Considering the effects on inflow caused by ship speed and hull boundary layer, a large region under hull is needed, which makes up of the whole computation region with the factual waterjet and defined control volume, shown in Figure 2. By calculation and analysis, the depth of the region under the hull is about 8D based on the reasonable distribution of internal flow patterns, the width 10D and the length 30D, where D is the pump nominal diameter[14].

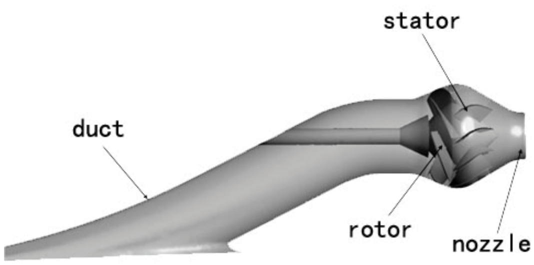

Figure 1: Waterjet configuration sketch

Figure 2: Control volume for waterjet numerical simulation

2.4 MESH AND BOUNDARY CONDITIONS

Each part of the model is meshed by structural hexahedral cells. Near the surface of duct and hull a special procedure is applied to create fine cells at the walls to get the satisfied y^+ values. Close to the blade an O-grid is applied to get high quality cells in the blade boundary layer. The complete mesh consists of about 2.1M hexahedral cells as shown in figure 3. The computation domain is extended some distance upstream duct inlet. At the inflow plane a non-uniform velocity profile is prescribed according to a certain hull boundary layer thickness. At all other boundaries of the domain, a constant pressure condition is applied. Duct and hull are set to no-slip walls. Nozzle outlet and outflow of control volume are set to atmospheric pressure. Rotation of the impeller can be implemented via the quasi steady Multiple Frames of Reference Method[2,15,16].The equations are solved by full imply multi-grid solve strategy.

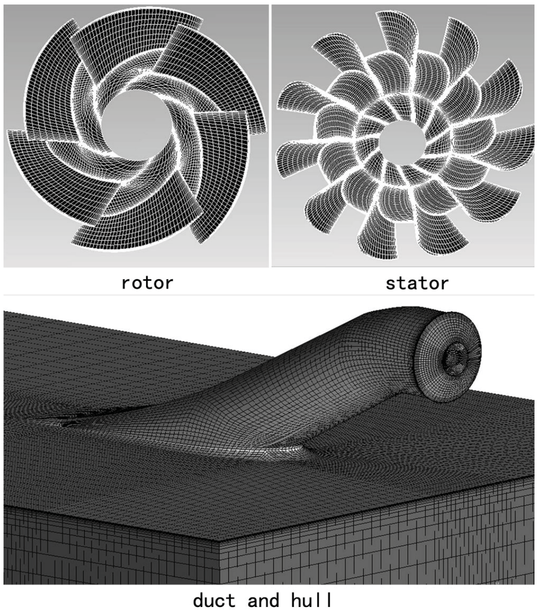

Figure 3: Mesh of each part of waterjet

3. PERFORMANCE PREDICTION AT NON-CAVITATION CONDITIONS

Operation with the vessel should comply with the waterjet operation limitations. On the ship speed - shaft speed diagram with constant power there are three zones with different limitations (Figure 4). They are:

Zone 1: Continuous operation, limited by maximum engine brake power.
Zone 2: Intermittent operation with a limited operating time. Maximum annual operating hours is 500.
Zone 3: Intermittent use only, with a limited operating time. Maximum annual operating hours is 50.

Should zone 3 be entered during emergent acceleration or turning, so the time delay for zero-speed to full-power needs to be increased in the engine speed governor. When the waterjet works at a high rotating speed with low ship speed, such as emergent acceleration and fast turning, zone 3 will be entered and cavitation will occur in waterjet.

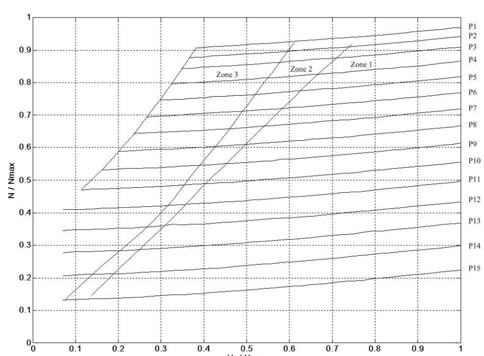

Figure 4: Relation of ship speed and shaft speed

The main work of this section is to predict the performance of the waterjet working in zone 1. Some operation points on constant power lines such as P1, P2, P9, P15 and the resistance curve not shown in the figure are calculated. In the calculation procedure, cavitation model is not included, for there is no cavitation at these operating conditions in zone 1.

Calculation results of waterjet thrust and power agree well with data from manufacture as shown in Table 1 to 5. The error of thrust prediction at design operation point is 0.078% and the error of power prediction 2.898%. The biggest error of thrust prediction is 8.964%, and the biggest error of power prediction 4.189% at all operation points in zone 1. In the tables, *Vs* denotes the actual ship speed, V_{max} the maximum ship speed, *N* the rotating speed of pump, N_{max} the maximum rotating speed of pump.

Table 1: Error of predicted power and thrust on constant power line P1 in zone 1

Ship speed Vs/V_{max}	Pump speed N/N_{max}	Error of power (%)	Error of thrust (%)
1.000	0.989	2.674	2.802
0.930	0.987	2.775	1.512
0.814	0.982	1.790	0.477

Table 2: Error of predicted power and thrust on constant power line P2 in zone 1

Ship speed Vs/V_{max}	Pump speed N/N_{max}	Error of power (%)	Error of thrust (%)
1.000	0.980	0.365	0.492
0.930	0.977	-0.043	-0.454
0.814	0.972	-0.181	0.635

Table 3: Error of predicted power and thrust on constant power line P9 in zone 1

Ship speed Vs/V_{max}	Pump speed N/N_{max}	Error of power (%)	Error of thrust (%)
1.000	0.889	3.170	5.167
0.930	0.886	3.276	3.252
0.814	0.881	2.617	1.941
0.698	0.876	1.898	1.825
0.581	0.873	1.351	2.875

Table 4: Error of predicted power and thrust on constant power line P15 in zone 1

Ship speed Vs/V_{max}	Pump speed N/N_{max}	Error of power (%)	Error of thrust (%)
1.000	0.741	3.862	6.137
0.930	0.738	4.189	8.964
0.814	0.733	3.111	5.436
0.698	0.728	2.198	3.453
0.581	0.723	1.909	3.078
0.465	0.719	0.919	3.447
0.349	0.716	0.557	5.698
0.233	0.713	0.267	6.240
0.116	0.711	-0.229	5.611

Table 5: Error of predicted power and thrust on the resistance curve

Ship speed Vs/V_{max}	Pump speed N/N_{max}	Error of power (%)	Error of thrust (%)
0.505	0.721	1.294	3.495
0.591	0.749	1.819	2.837
0.699	0.799	2.337	1.796
0.771	0.842	2.548	0.796
0.824	0.881	2.687	0.333
0.870	0.917	2.858	0.066
0.909	0.951	2.959	0.096
0.935	0.977	2.898	0.078
0.945	0.987	2.876	0.012

The numerical model and method is validated after the comparison between calculation results and manufacturer's data.

4. PERFORMANCE PREDICTION AT CAVITATION CONDITIONS

It is very significant to predict the cavitation performance of a waterjet mounted on a vessel. But it is an arduous task to simulate and predict the cavitation performance of a waterjet by CFD method because the waterjet mounted on a vessel is a complex system, and it is not mature to simulate cavitation flow by numerical method. After completing numerical simulation of non-cavitation performance of a waterjet and cavitation flow around a hydrofoil successfully[17], authors have tried to simulate and predict cavitation performance of a waterjet by CFD method in this study and some useful results obtained.

4.1 CALCULATION RESULTS AND ANALYSIS

In this section, the calculations mainly aim at the operating conditions in zone 2 and 3, where cavitaion would occur. The operating conditions are also on constant power lines P1, P2, P9 and P15. The CFD code with cavitation model is conducted to complete the calculation by making the results without cavitation model as the initial input, and convergent results are obtained in the end. The comparison between calculation results and manufacturer's data is shown in table 6 to 9, where the normal body data are results without cavitation model and the italic bold body data are results with cavitation model.

Table 6: Error of predicted power and thrust on constant power line P1 in zone 2 and 3

Ship speed Vs/V_{max}	Pump speed N/N_{max}	Error of power (%)	Error of thrust (%)
0.698	0.978	-1.466	0.859
0.698	***0.978***	***-0.671***	***-0.629***
0.581	0.974	-1.813	3.911
0.581	***0.974***	***0.960***	***2.967***
0.465	0.971	-2.232	10.741
0.465	***0.971***	***3.188***	***7.388***
0.381	0.969	-2.343	18.912
0.381	***0.969***	***1.722***	***9.851***

Table 7: Error of predicted power and thrust on constant power line P2 in zone 2 and 3

Ship speed Vs/V_{max}	Pump speed N/N_{max}	Error of power (%)	Error of thrust (%)
0.698	0.968	-1.427	0.928
0.698	***0.968***	***-0.184***	***0.729***
0.605	0.966	-1.535	2.913
0.605	***0.966***	***-1.344***	***2.470***
0.535	0.963	-2.001	5.593
0.535	***0.963***	***-0.520***	***4.638***
0.465	0.961	-2.201	9.973
0.465	***0.961***	***0.239***	***7.602***
0.372	0.959	-2.364	19.135
0.372	***0.959***	***-0.308***	***8.299***

Table 8: Error of predicted power and thrust on constant power line P9 in zone 2 and 3

Ship speed Vs/V_{max}	Pump speed N/N_{max}	Error of power (%)	Error of thrust (%)
0.465	0.869	-2.214	4.939
0.465	***0.869***	***-1.172***	***3.414***
0.349	0.866	-2.412	11.237
0.349	***0.866***	***-0.877***	***8.241***
0.233	0.864	-2.565	15.925
0.233	***0.864***	***0.063***	***11.902***
0.202	0.863	-2.629	17.652
0.202	***0.863***	***0.229***	***12.487***

Table 9: Error of predicted power and thrust on constant power line P15 in zone 2 and 3

Ship speed Vs/V_{max}	Pump speed N/N_{max}	Error of power (%)	Error of thrust (%)
0.093	0.711	-2.919	8.464
0.093	***0.711***	***-2.549***	***7.323***
0.076	0.711	-2.960	8.457
0.076	***0.711***	***-2.689***	***7.059***

The prediction results of power and thrust show that it is feasible to calculate cavitation performance of the waterjet with CFD method. From table 1 to 4 and table 6 to 9 we can see that the prediction errors at cavitation conditions are larger than the ones at non-cavitation conditions. This is because that the cavitation flow is more complex, and its simulation is more difficult.

At cavitation conditions, the thrust calculated with cavitation model is much more close to data from manufacturer than the one without cavitation model. The former is more creditable for taking into account cavitation. A cavity will firstly form on the suction surface of the rotor blades, which can initially increase the blade camber—and, thus, the flow turning and blade lift—and cause a small increase in the powering parameters. The phenomenon has been validated by the numerical simulation for the power calculated with cavitation model is larger than the one without cavitation model.

4.2 ANALYSIS OF CAVITATION PERFORMANCE

Generally, cavitation incidence of pump is determined by cavitation test. Characteristics of waterjet pump is also recognized by test. However, numerical simulation can be another way to know of the performance of a waterjet. Due to the effect of non-uniform inflow, the performance of waterjet pump installed on vessel is different from the one on test-bed. So it is necessary to know of the performance of the pump integrated in a waterjet by test measure or numerical simulation.

In order to prevent cavitation the waterjet pump needs a certain pressure at the inlet of the pump. This required pressure is expressed as the required net positive suction head (*NPSHr*). Pump operation is allowed as long as the available *NPSHa* exceeds the required *NPSHr*. The available suction head is the total head at the inlet of the pump minus the vapor pressure of the liquid. For a waterjet installation the available *NPSHa* is determined by the waterjet operation point. The *NPSHa* can be expressed as function of the ship speed:

$$NPSHa = \frac{p_\infty - p_v}{\rho g} + \frac{V_s^2}{2g}(1-\varepsilon)(1-\omega)^2 - h_j \qquad (11)$$

where p_∞ represents the ambient pressure, p_v the vapor pressure of water, V_s the ship speed, ε the inlet loss coefficient, ω the wake fraction and h_j the nozzle elevation above the waterline. The *NPSHr* can be expressed as follows:

$$NPSHr = \frac{v_0^2}{2g} + \lambda \frac{w_0^2}{2g} \qquad (12)$$

where v_0 is the absolute velocity just in front of inlet of blade, w_0 the relative velocity just in front of inlet of blade and λ a dimensionless coefficient. It is unpractical to get the value of *NPSHr* from equation (10), as the velocities and coefficient are not easy to get. So the equation (12) can be replaced by equation (13) below to obtain the *NPSHp* at the inflow face of the pump as *NPSHr*:

$$NPSHr = NPSHp = \frac{p_s - p_v}{\rho g} + \frac{V_p^2}{2g} \qquad (13)$$

where V_p represents the mass average velocity at the inflow face of the pump, $V_p = \sum (V \cdot m) / \sum m$, where V the local velocity and m the local mass.
The pump will perform well as long as the required inlet suction head *NPSHr* is below the available inlet suction head *NPSHa*:

$$NPSHr \leq NPSHa \qquad (14)$$

Combination of equations (11) and (13), with the requirement of equation (14), yields:

$$\frac{p_s - p_v}{\rho g} + \frac{V_p^2}{2g} \leq \frac{p_\infty - p_v}{\rho g} + \frac{V_s^2}{2g}(1-\varepsilon)(1-\omega)^2 - h_j \tag{15}$$

Substitution of equation $IVR = V_s / V_p$ in equation (15) and rearranging of all variables gives:

$$IVR \geq \sqrt{\frac{\rho V_s^2}{2(p_\infty - p_s) + \rho V_s^2 (1-\varepsilon)(1-\omega)^2 - 2\rho g h_j}} \tag{16}$$

On the other hand, if IVR which is used to denote the flow conditions in the waterjet inlet duct is below a critical value, cavitation will occur in the waterjet pump.
Figure 5 shows the relations of the *NPSHr* and *NPSHa* with IVR on the constant power line P1. The critical value of IVR is about 1.2 when *NPSHr* equals to *NPSHa*. When IVR is bigger than 1.2, the *NPSHa* exceeds the *NPSHr*, The bigger is the IVR, the bigger is the difference of *NPSHa* and *NPSHr*, and consequently the possibility of cavitation is smaller. On the contrary, when IVR is smaller than 1.2, the *NPSHa* is lower than the *NPSHr*, so the cavitation occurs. The smaller is the IVR, the bigger is the difference of *NPSHa* and *NPSHr*, and consequently more serious is the cavitation.

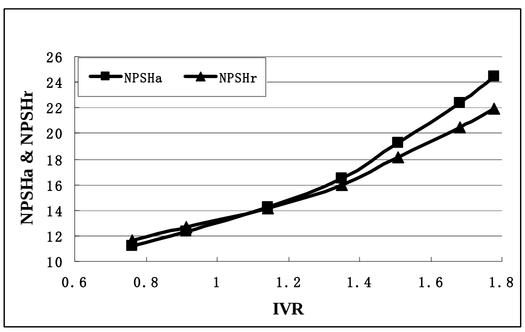

Figure 5: The relation of *NPSHr* and IVR and the relation of *NPSHa* and IVR on constant power line P1

Except for the prediction results of power and thrust at different ship speed in section 3.1, analysis of mass flow rate and total head as functions of IVR is carried out in this section. Figure 6 shows the relation of mass flow rate and IVR on constant power line P1. At low IVR smaller than 1.2 the decrease of mass flow rate occurs due to cavitation blocking a certain portion of the impeller channel before finally resulting in performance breakdown. The smaller is IVR, the severer is the decrease of mass flow rate, which indicates that the severer is cavitation. Figure 7 shows the relation of total head and IVR on constant power line P1. If cavitation were not considered, total head would increase as IVR decreases; on the other hand, total head would increase as mass flow rate decreases. This is not actual. But when cavitation is considered, it is absolutely opposite. At low IVR smaller than 1.2, the total head will decrease due to the cavitation, and it will decrease rapidly with the cavitation severer, i.e. smaller IVR. The decrease of both mass flow rate and total head means the decrease of working capability of the waterjet pump. This is the reason for the decrease of thrust at cavitation condition.

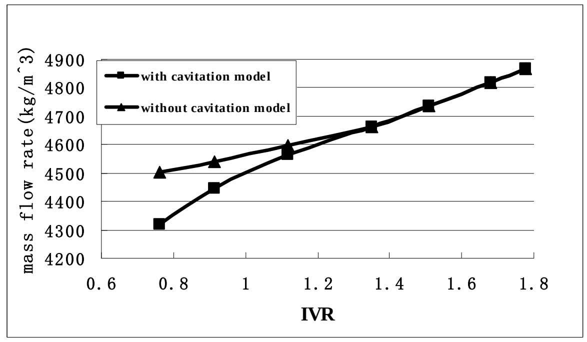

Figure 6: The relation of mass flow rate and IVR on constant power line P1

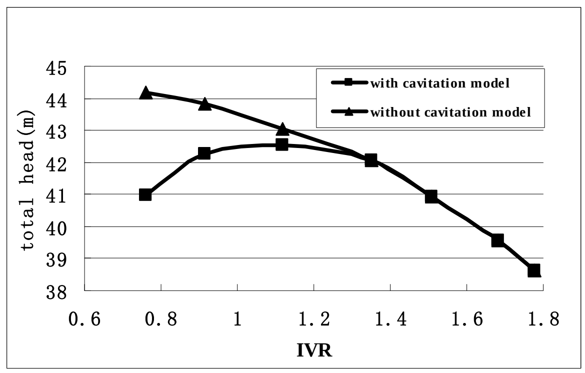

Figure 7: The relation of total head and IVR on constant power line P1

Figure 8 shows the distributions of vapor fraction in token of cavitation at different IVR on constant power line P2. As IVR decreases, area of isosurface of vapor fraction becomes larger. This illuminates that cavitation in the waterjet pump is severer. Cavitation at the operation point in zone 3 is much severer than in zone 2, and even exists in the space away from wall.

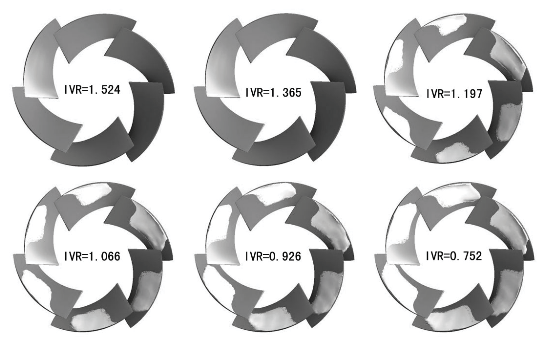

Figure 8: Distribution of vapor fraction in token of cavitation at different IVR on constant power line P2

4.3 CAVITATION IN INLET DUCT AND NOZZLE

A waterjet is mainly composed of inlet duct, pump and nozzle. At some certain inflow states (or operation states), cavitation occurs in waterjet pump. Similarly, at some certain inflow states (or operation states), cavitation may occur in inlet duct and nozzle. In this section, the cavitation in inlet duct and nozzle will be discussed.

Figure 9 is the pressure distribution of the mid-section plane in inlet duct at different IVR. There are two depression zones: one is located at lower side of pipe bend labeled 1 and the other one is located in the vicinity of the lip. The former is nearly constant, and hardly changed with IVR. The latter is changed obviously with IVR. At high IVR, it is located at the hull side of the lip, and with IVR decreasing, the location is moved up along the tip, and finally located at the top side of the tip. When IVR is smaller than 1.0, the lowest pressure is smaller than vapor pressure, so cavitation occurs in inlet duct. It is obvious that cavitation in inlet duct lags behind in waterjet pump, for the latter occurs at IVR smaller than 1.2.

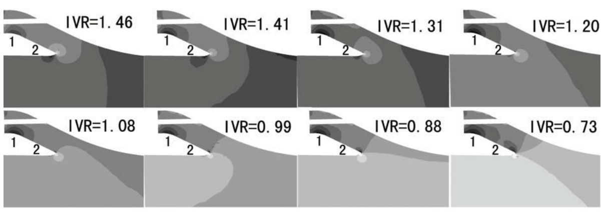

Figure 9: Pressure distribution at mid-section plane of inlet duct at different IVR

Figure 10 shows the vapor fraction and pressure distributions in nozzle. The pressure is lower where nearer to the nozzle outlet but there is no cavitation on nozzle wall even at very low IVR for the lowest pressure is always above the vapor pressure. However the spatial cavitation caused by eddy flow after the stator hub exists even at high IVR

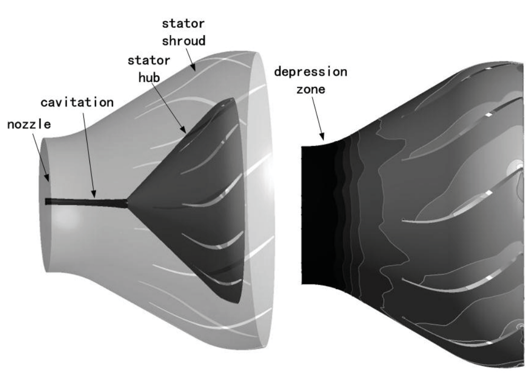

Figure 10: Vapor fraction and pressure distribution in nozzle

4.4 CAVITATION DIVISION LINES

The numerical prediction of operation points on the cavitation division lines mentioned in section 3 is conducted by CFD code with cavitation model in this paper. Calculation results of suction specific speed at every operation points are listed in table 10 to 12. The suction specific speed is expressed as:

$$N_{ss} = \frac{5.62N\sqrt{Q_v}}{NPSHr^{3/4}} \qquad (17)$$

where N is the rotating speed of pump, rev min^{-1}, Q_v the volume flow rate, m^3 s^{-1}.

Table 10: Suction specific speed of different operation points on cavitation division line 1

Variables	Values			
Vs/V_{max}	0.495	0.625	0.708	0.769
N_{ss}	1266	1290	1284	1270

Table 11: Suction specific speed of different operation points on cavitation division line 2

Variables	Values		
Vs/V_{max}	0.425	0.519	0.610
N_{ss}	1361	1395	1406

Table 12: Suction specific speed of different operation points on cavitation division line 3

Variables	Values		
Vs/V_{max}	0.201	0.296	0.381
N_{ss}	1544	1584	1619

Table 10 to 12 show that the suction specific speed on the same cavitation division line is nearly a constant, so the cavitation division line can be called a constant suction specific speed line, which is the same as mentioned in references[1,2,18]. The three values are respectively 1277.5 for cavitation division line 1, 1387.3 for cavitation division line 2 and 1582.3 for cavitation division line 3.

5. CONCLUSION

In this paper the numerical simulation and analysis of a waterjet propulsion system in cavitation condition are carried out by CFD method, which is a helpful approach to model the cavitation performance of a waterjet. The work and conclusions of this work are:

Firstly, based on the validation of the numerical model and method used in predicting the performance of a waterjet at non-cavitation conditions, the prediction results of its cavitation performance have good accordance with the data from manufacturer. The relation of *NPSHa* and IVR and the relation of *NPSHr* and IVR are obtained, and the critical IVR for cavitation occurrence is obtained with the value about 1.2. When cavitation exists, the mass flow rate and the total head both decrease obviously. The distribution of vapor fraction can help observe the cavitation state in the waterjet pump. It also indicates that the cavitation becomes severer with IVR decreasing on constant power line.

Secondly, cavitation in inlet duct and nozzle are analyzed. At some certain inflow conditions or operating conditions cavitation may occur in inlet duct, lagging behind cavitation in waterjet pump. But cavitation in nozzle existing in form of spatial cavitation occurs in advance of that in waterjet pump, with no cavitation on nozzle walls. Thirdly, the cavitation division lines are discussed with the conclusion that the cavitation division line is a constant suction specific speed line. This is consistent with references [1,2,18].

6. REFERENCES

1 ALLISON J. L., 'Marine waterjet propulsion', SNAME Transactions, Vol. 101, 1993.
2 NORBERT B., 'Numerical analysis of a waterjet propulsion system', Netherlands: Library Eindhoven University of Technology, 2006.
3 MURRIN N. D. C., BOSE N., Chin S. N., 'Waterjet system wind tunnel test', International Conference on Waterjet Propulsion 4, RINA, London, 2004.
4 PARK W. G., 'Numerical flow and performance analysis of waterjet propulsion system', Ocean Engineering 32, 2005.
5 BOUZIAD Y. A., 'Physical modeling of leading edge cavitation: computational methodologies and application to hydraulic machinery', DEA de conversion de l'énergie: Université Paris VI, 2006.
6 SAITO Y., NAKAMORI I., IKOHAGI T., 'Numerical analysis of unsteady vaporous cavitating flow around a hydrofoil', Fifth International Symposium on Cavitation, Osaka: Scientific Committee, 2003.
7 KAWAMURA T., SAKODA M., 'Comparison of bubble and sheet cavitation models for simulation of cavitating flow over a hydrofoil', Fifth International Symposium on Cavitation, Osaka: Scientific Committee, 2003.
8 KINNAS S. A., SUN H., 'Numerical analysis of flow around the cavitating cav2003 hydrofoil', Fifth International Symposium on Cavitation, Osaka: Scientific Committee, 2003.
9 POUFFARY B., PATELLA R. F., REBOUD J. L., 'Numerical simulation of cavitating flow around a 2d hydrofoil: a barotropic approach', Fifth International Symposium on Cavitation, Osaka: Scientific Committee, 2003.
10 TAKAYUKI W., TAKAFUMI K., 'Simulation of steady and unsteady cavitation on a marine propeller using a RANS CFD code', Fifth International Symposium on Cavitation, Osaka: Scientific Committee, 2003.
11 MASASHI F., TOMOYOSHI O., YOSHIAKI T., 'Prediction of cavitation performance of axial flow pump by using numerical cavitating flow simulation with bubble flow model', Fifth International Symposium on Cavitation, Osaka: Scientific Committee, 2003.
12 ZGOLLI R., AZOUZ H., 'Numerical approach to the prediction of cavitation in pumps', Fifth International Symposium on Cavitation, Osaka: Scientific Committee, 2003.
13 MENTER F., 'Two-equation eddy-viscosity turbulence models for engineering applications', AIAA-Journal 32, 1994.
14 CHENGJIANG L., YONGSHENG W., ZHIHONG Z., 'Study on flow control volume in numerical simulation of waterjet' Journal of Hydrodynamics (Ser.A), Vol. 5, 2008.
15 NORBERT B., VERBEEK R., 'CFD simulations of the flow through a waterjet installation', International Conference on Waterjet Propulsion 4, RINA, London, 2004.
16 NORBERT B., BART E., 'Review of thrust prediction method based on momentum balance for ducted propellers and waterjets', 'Proceedings of FEDSM2005', Houston: ASME, 2005.
17 CHENGJIANG L., YONGSHENG W., JUBIN L., 'Numerical simulation of cavitationg flow around two-dimensional hydrofoil', Journal of Navel University of Engineering, Vol. 5, 2008.
18 LAURENCE B., 'Specialist Committee on Cavitation-Final Report and Recommendations to the 25th ITTC', Fukuoca: 25th ITTC, 2008.

7. AUTHORS BIOGRAPHY

Chengjiang Liu is a Ph.D. candidate of Marine Engineering at the Naval University of Engineering, P. R. China. He has accomplished the research tasks "Research on prediction of power and thrust characteristics of a waterjet" and "Research on cavitation prevention and repair method of a waterjet".

Yongsheng Wang is Professor and holds the current Director in office of New Technology of Marine Propulsion in the Naval University of Engineering, P. R. China. Since 1982 he has published more than 90 papers and his main research interests are marine power plant.

Zhihong Zhang holds the current Chair in Department of Fluid Mechanics, Professor at the Naval University of Engineering, P. R.

Overview of Recent Developments in Testing of Waterjets at NSWCCD

M Donnelly and **S Gowing,** Naval Surface Warfare Center, Carderock Division, W.Bethesda, MD, USA

SUMMARY

In the past decade the U.S. Navy has gained much experience with waterjet-propelled ships. Existing propeller test facilities have been modified to accommodate waterjet pump tests. The 24 inch and 36 inch water tunnel facilities have incorporated bell-mouth flow nozzles into the tunnel contraction to measure total flow rate, and different impedance schemes have been added to change the waterjet flow coefficient. Numerous tow tank self-propulsion tests of both high speed catamarans and large waterjet-propelled monohulls have been carried out. These tests use extensive LDV measurements of inflow boundary layers, pump internal flows and nozzle discharge flows to determine flowrates and quantify nonuniformity factors in accordance with ITTC recommendations for powering predictions. The ITTC approach is augmented with an inlet wake scaling procedure to make full-scale predictions from tow-tank self-propulsion tests. These predictions are compared to power estimates based on pump loop tests and assumed wake, thrust deduction and inlet loss factors. The pump power and tow tank derived predictions match well, and details of the waterjet/hull flow show interactions that affect overall performance.

NOMENCLATURE

[Symbol]	[Definition] [(unit)]
B_{M1}	*combined coefficient for momentum flux at ITTC Station 1*
B_{M6}	*combined coefficient for momentum flux at ITTC Station 6*
C_{p1}	*average pressure coefficient at ITTC Station 1*
C_{p6}	*average pressure coefficient at ITTC Station 6*
D_3	*pump inlet diameter (m)*
$E3$	*energy at ITTC Station 3*
$E5$	*energy at ITTC Station 5*
g	*acceleration due to gravity (m^2/s)*
H^*	*head coefficient*
KQ	*torque coefficient (Torque / $\rho n^2 D^5$)*
n	*impeller revolutions per second*
$N^*_{1\%}$	*non-dimensional NPSH required*
$NPSH_R$	*net positive suction head required*
Q	*flowrate (m^3/s)*
Q^*	*flow coefficient*
P^*	*power coefficient*
p_t	*total pressure*
p_s	*static pressure*
t	*thrust deduction*
T	*torque*
U_x	*axial velocity measured at a point*
$\overline{U}_x$	*average axial velocity from LDV*
$V0$	*ship speed or system test tunnel velocity*
V_1, $V1_{bar}$	*average velocity in the capture area*
$V3_{bar}$	*average velocity at Station 3*
V_6	*average jet velocity*
w	*wake fraction*
β_M	*momentum non-uniformity factor*
β_E	*energy non-uniformity factor*
η	*pump efficiency*
λ	*scale ratio*
ρ	*density (kg/m^3)*
ζ_{13}	*inlet loss coefficient*

Abbreviations

IVR	inlet velocity ratio
JHSS	Joint High Speed Sealift
LDV	laser Doppler velocimetry
NSWCCD	Naval Surface Warfare Center, Carderock Division
PIV	particle image velocimetry
SPIV	stereo particle image velocimetry

1. INTRODUCTION

Waterjets have become popular propulsors because of their ability to exceed 40 knots without thrust breakdown limitations typical of propellers in the 30-35 knot range. Their use has been well-established for commercial ferries and transports, catamarans especially. Waterjets also provide shallow draft and high manoeuvrability via steerable nozzles and fast-acting reversing buckets.

In the past decade the U.S. Navy has gained much operational experience with waterjet-propelled ships. Starting from modified ferries HSV-X1 and HSV-2, to development of its own high-speed research platform, FSF-1 Sea Fighter, the Navy is now acquiring waterjet-propelled Naval combatants, LCS-1 and LCS-2, and evaluating waterjet propulsion for high speed sealift, JHSS. With support from the United States Office of Naval Research (ONR) and the Naval Sea Systems Command (NAVSEA), the Naval Surface Warfare Center Carderock Division (NSWCCD) has undertaken an extensive waterjet testing program. The program focus has been evaluation of commercial waterjet designs and comparison of waterjets to classical shafted propeller or podded propulsors. The interactions of waterjet flows on hulls (trim and sinkage changes, wakefield and wave effects) and modified hull flows on waterjets (air or polymer lubricated boundary layers) have also been studied.

Existing propeller test facilities have been modified to accommodate waterjet tests and create pump loops. These modifications enable tests of rotor, stator, and nozzle designs. Either the pump model has been integrated into the tunnel shell to control the pump flow with auxiliary pump head from the tunnel impeller, or the model has been installed as a separate unit mounted on a strut in the test section. In the Navy's Large Cavitation Channel (LCC), an entire waterjet system has been installed above the test section ceiling. This configuration is used to test flow non-uniformity effects at the pump entrance and the inlet, including inflow variations from a rotating shaft wake and ingested hull boundary layers. All these facilities can be used to quantify pump headrise and power input versus flowrate, and measure cavitation breakdown. In addition to typical torque dynamometry and static pressures, laser Doppler velocimetry (LDV) and stereo particle image velocimetry (SPIV) are used to calibrate the flow nozzles and map flow field variations.

NSWCCD has also undertaken numerous tow tank self-propulsion tests of both high speed catamarans and large waterjet-propelled monohulls designed for sealift operations. The tow tank models have been modified extensively to enable waterjet data measurements. LDV systems using scanning techniques have been installed in up to four waterjet units to measure integrated flow data, harmonic content, inflow velocity profiles, and quantify non-uniformity factors in accordance with ITTC recommendations for powering predictions [1]. Hull pressure variations have been measured with pressure scanners and capacitance probe rakes used to survey wake surfaces behind the transom.

For full scale power predictions, the ITTC approach is augmented with an inlet wake scaling procedure developed by NSWCCD to scale tow tank self-propulsion tests. This modified procedure is compared to a waterjet vendor's approach based on matching waterjet system thrust to vessel resistance curve. The vendor approach prescribes the input power levels and determines the vessel performance from pump curves and input coefficients for wake fraction, inlet loss coefficient, and thrust deduction.

2. MODEL TEST ARRANGEMENTS

2.1 (a) Tow Tank Models

The sizes of waterjet pumps tested at Carderock spans a wide range. Small, 2 in. to 3 in. (50.8 mm to 76.2 mm) diameter units are typically used for tow tank models because they fit well in models with scale ratios of 20 to 50. These units are rarely geosim models of the pumps designed for the ship being tested, however, because of the cost and time of manufacturing them or absence of a final pump selection from which the model could be made. At the low Reynolds numbers of pump flows used in tow tank tests, the scale effects on pump performance (head vs. rpm) are severe and these data would be difficult to use anyway. Surrogate pumps are used instead, and these may be units designed for use in radio-control boats, or small pumps used in other tests that will fit in the model. Recent developments in sintered metal and Stereo Lithography manufacturing are making geosim models easier to manufacture. Geosim pump models do have the advantage of fitting easily into the hull. It is NSWCCD standard practice to use a geosim inlet, and a scaled inlet and nozzle diameter to enable a more direct scaling of powering results.

2.1 (b) Water Tunnel Models

Larger waterjet pump models are tested in water tunnels at higher speeds to reduce Reynolds effects and test cavitation behavior. These models range from 7.5 in. to 12 in. (190.5 mm to 304.8 mm) and are made with aluminum rotors and stators and clear acrylic housings and nozzles for cavitation viewing. The pumps are driven from upstream or downstream, depending on the tunnel propeller shaft arrangements. Rotor torque is measured with the shaft dynamometer and piezometer rings are used to measure wall pressures at the various pump stations. Three types of tunnel installations have been used at Carderock and are described below.

The 24 inch and 36 inch water tunnel facilities have incorporated bell-mouth flow nozzles into the tunnel contraction to measure total flow, and different impedance schemes have been used to change the waterjet flow coefficient. Shaft line video cameras, LDV, SPIV, and Kiel probes are used to measure flow and pressure fields and examine cavitation breakdown.

The first is a pump loop in which the tunnel flow is funnelled through the pump model, typically through an upstream bellmouth flowmeter. The flowmeter serves to measure the flow rate and provide a uniform velocity profile via area contraction to the rotor inlet. The pump discharge flows through the nozzle and into the open jet test section and tunnel diffuser in the form of a submerged jet. This arrangement is called a 'flow through' arrangement and is shown in Figure 1. The pump flow rate or flow coefficient will be fixed for a specific rpm and this is termed the 'bollard' condition, and this coefficient is usually close to the design point. The flow is adjusted by varying the tunnel impeller speed to pressurize the inlet plane and force more flow through the pump, or installing impedance devices downstream of the pump (screens, rods or plates) to decrease the flow rate. Often the best control is realized by using an impedance scheme to decrease the pump flow below its un-impeded bollard flow rate, and then increase the flow through the bollards condition and beyond using the tunnel impeller. The under and over bollard flows represent accelerating and decelerating conditions, respectively. Other laboratories achieve flow control by piping the pump discharge out of the tunnel entirely through a bypass line fitted with a secondary pump for flow adjustment and a turbine flowmeter. The bypass is then fed back into the tunnel elsewhere in the circuit.

The second tunnel installation that has been used is to mount the waterjet pump centered in the open jet test section but allow the tunnel flow to pass around the pump as well as through it. The model looks like a turbojet engine on a test stand. A flowmeter is again fitted upstream of the rotor to measure flowrate, but the contraction of the nozzle and the pressure drop is limited to avoid blocking the annular tunnel flow around it. The tunnel impeller can be used to vary the flowrate, but the dynamic range of flow adjustment is more limited because the tunnel flow can bypass the pump versus passing through it. This arrangement is called a 'bypass' scheme and is shown in Figure 2.

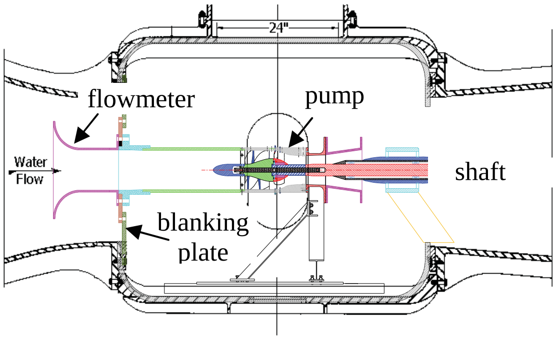

Figure 1: Flow through pump arrangement (24 in WT)

The third tunnel installation scheme is to mount the model pump with an inlet above the ceiling of the closed jet test section. The inlet is faired flush with the ceiling and the discharge nozzle is mounted in a box that deflects the flow back down into the test section. This is referred to as a 'system' test installation because it enables testing of the inlet, pump, and nozzle. Figure 3 shows this arrangement from the behind, showing the nozzle in a simulated transom.

Each of these installations offers advantages and disadvantages.

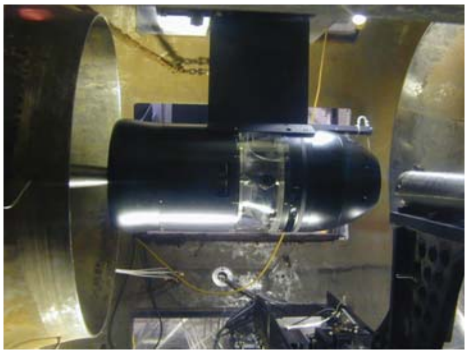

Figure 2: Bypass pump arrangement (36 in WT)

Figure 3: System test installation in the Large Cavitation Channel**.**

2.2 FLOWRATE MEASUREMENT

The first scheme provides for simple flow rate measurement via the bellmouth flowmeter, and accurate flow rate measurement is essential for estimating pump power characteristics. The flowmeter pressure drop can be calibrated in place against internal flow surveys with LDV, PIV or Pitot tubes, and the inlet velocity and pressure profile is nearly uniform except near the bellmouth wall and the shaft. The large space in the upstream contraction into which the bellmouth flowmeter is placed allows the bellmouth to be built with contours that are standard for flowmeters (ASHRAE, ASTM). The bypass scheme also uses a flowmeter, but the area contraction and resulting pressure drop are small and a uniform flow profile into the rotor is not guaranteed. Pressure taps can be fitted into the discharge nozzle for any of these installations and the resulting pressure drop used to measure flow, but this involves extensive calibrations because radial pressure gradients can exist in the nozzle from flow rotation and rapid area changes. For the through flow arrangement, the calm water envelope outside the pump casing allows probe measurements at the rotor inlet, rotor/stator plane, or nozzle exit, and this advantage can also be used for attic installations. Detailed surveys for the bypass installation can be achieved with LDV, but the optical probes are more distant to be out of the annular flow.

2.3 FLOW COEFFICIENT CONTROL

At first glance the first scheme seems simple for flow control – simply ramp up the tunnel impeller to drive the flow coefficient higher. But the model pump flowrate is a small fraction of the tunnel flowrate, hence the tunnel impeller operates severely off-design when used to increase pump flowrate. Sometimes the impeller must be run from 50% to 80% of maximum speed to achieve the desired pump flow, causing facility noise, vibration, and perhaps impeller cavitation. Pressure control of the waterjet model for cavitation testing can be difficult because increased flows beyond the bollard condition require increased inlet pressure, forcing further reduction of the tunnel pressure to bring the model back to the same point. The tunnel pressure is essentially vented to the nozzle discharge and that becomes the control point in the model. The bypass installation enjoys the advantage of having the impeller operate more closely to its design, resulting in less noise and vibration. Of all the test schemes, the attic installation offers complete freedom for altering pump flows over varied free-stream speeds. The tunnel impeller is un-affected by the waterjet flow.

2.4 INLET EFFECTS

Variations of inlet flows have been tested both with the attic installations and pump loop installation. The attic installation will ingest a facility-dependent boundary layer depending on the test section ceiling, and this can be modified with obstacles (blocks or struts) to thicken the ingested layer and mimic a profile predicted for a particular ship condition. The advantage is that the boundary layer can be reasonably predicted and LDV or probes can measure the layer to insure that it is correct. The attic installation also offers the easiest way to test added boundary layer features such as polymers and air layers. For the pump loop installation, there is no inlet, and the velocity field at the rotor inlet must be predicted with a RANS calculation that predicts the rotor inlet flow based on the evolution of the inlet boundary layer flowing through the inlet. The spinning shaft wake complicates this calculation. If a test budget is insufficient for an attic installation, the pump loop performance can be altered by non-uniformity factors which account for the gradient due to the ingested boundary layer and wake of the rotating shaft..

3. DISCUSSION OF RESULTS

3.1 PUMP PERFORMANCE TESTS USING PUMP LOOPS

A pump-loop is used to evaluate pump performance with a uniform inflow. Performance characteristics are the flow coefficient, Q*, the head coefficient, H*, and the power coefficient, P*, expressed as:

$$Q^* = \frac{Q}{n\ D_3{}^3}$$

$$H^* = \frac{g\ H}{n^2 D_3{}^2}$$

$$P^* = \frac{2\pi\ T}{\rho\ n^2 D_3{}^5}$$

H is defined as the total headrise across the impeller / stator, from ITTC Stations 3 to 5 [1]. Because of the non-uniform pressure and velocity fields at Station 5, this value is re-defined as the total headrise from Station 3 to Station 6, the nozzle exit. This approach adds the nozzle loss into the pump headrise, but nozzle losses are typically small, and the simplicity and accuracy of measuring the velocity and pressure at the nozzle exit versus downstream of the stator make this approach more useful. With pump performance defined in this manner, pump efficiency becomes

$$\eta = \frac{Q^* H^*}{P^*}.$$

Representative results from the 36in WT pump-loop are shown in Figure 4 for headrise normalized by the values measured at the design flow. Results are

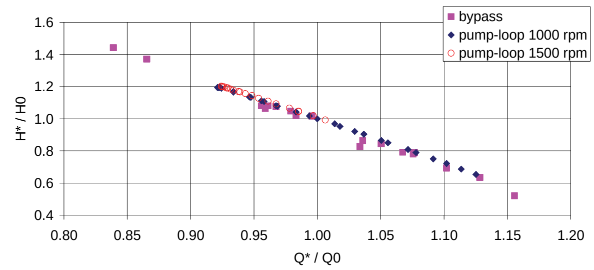

Figure 4: Pump performance data from the 36in WT.

shown for both the bypass configuration and the setup in which all of the tunnel flow passes through the pump. Comparison of the results shows excellent agreement, indicating that both configurations are suitable for pump performance tests. For the bypass configuration, different flowrates were obtained by changing the discharge nozzle with exit areas of 60%, 80%, 100%, and 120% of design. These combinations provided a range of flow coefficient from -4% to +26% of the design value, but with a limited number of flowrates for each nozzle. By varying the tunnel impeller speed with the flow-through configuration, flowrates from 100% to 120% of design were achieved. Numerous blockage schemes were investigated to throttle the flowrate below the design value. Preliminary configurations used impedance devices that were either too close to the nozzle exit, or imposed a non-uniform blockage, as shown by non-uniformity in the four static pressures measured independently at the nozzle exit. Figure 5 shows the final blocking scheme which used a large flat plate mounted on the tunnel diffuser and an orifice plate further downstream. By changing the diameter of the orifice and varying the tunnel impeller speed, a range of flow coefficients covering ± 20% of the design value could be tested. This range was sufficient to locate the peak efficiency of the pump.

The use of a pump-loop facility in which the pump casing is mounted in the open jet test section of a cavitation tunnel also offers advantages for additional measurements. These include velocity and pressure profiles at each stage of the pump, enabling evaluation of the pump components (rotor, stator, nozzle) separately.

Figure 5: Final test configuration blockage plates.

Figure 6 shows the efficiencies of the rotor and stator stages of a pump, using LDV and Kiel probes to measure the inlet and exit planes, and compares the data to CFD predictions [2].

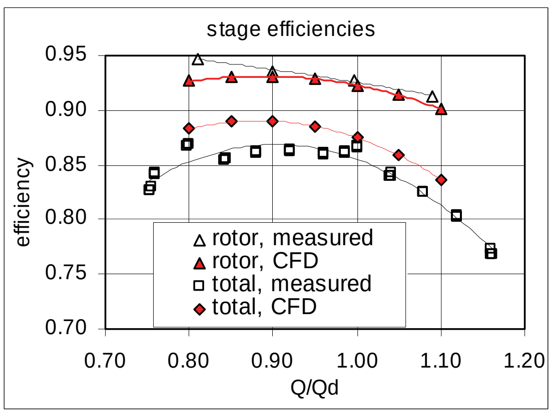

Figure 6: Rotor and stator efficiencies measured in the 24in WT.

Using an upstream bellmouth as a flowmeter provides real time measurement of the flowrate and allows the nozzle to discharge unimpeded into the test section. This better simulates a full-scale installation and allows optical access with either a submerged LDV system or SPIV system. These types of detailed flow measurements can be used to validate stator designs, which are intended to remove swirl imparted by the impeller, and to determine non-uniformity factors of momentum and energy that feed into predictions of full-scale waterjet performance on a given hullform. An example of a stereo particle image velocimetry measurement is shown in Figure 7. Stator wakes and swirl from a hub vortex are clearly visible.

The pump-loop facilities at Carderock are also used to evaluate cavitation and thrust breakdown using the facility pressure control systems. NSWCCD uses the definition of a 1% loss in torque from the non-cavitating condition to define breakdown. This boundary is normally defined as a 1% loss in efficiency or 3% loss in headrise. Because these are calculated quantities impacted by measurement inaccuracies a more direct measurement approach has been taken. By decreasing

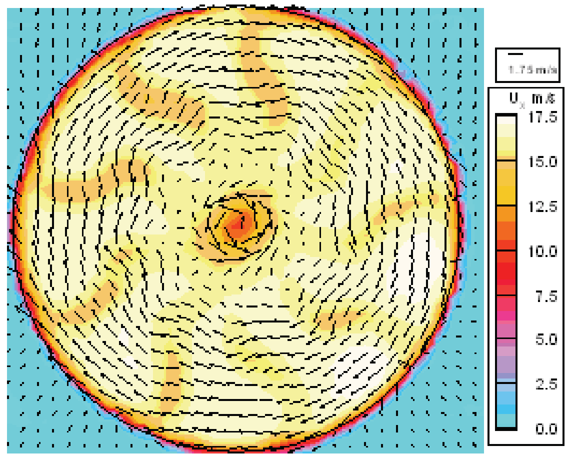

Figure 7: LDV measurements of the nozzle discharge, from 36in WT flow-through setup.

tunnel static pressure at several flow coefficients until the 1% loss in torque is reached, a curve of Q* versus $N^*_{1\%}$ can be determined, in which $N^*_{1\%}$ is the non-dimensional equivalent of NPSH required i.e.:

$$N^*_{1\%} \quad \frac{g\ NPSH_R}{n^2 D_3^{\,2}}$$

In-house developed LabVIEW data acquisition software is used to plot these results in real-time such that sufficient data can be acquired to accurately define this value. Plots of thrust breakdown from both a uniform inflow and a system test are shown in Figure 8, and the horizontal axis on the plot has been normalized by the design flow coefficient. The vertical axis has been removed to protect proprietary data. Based on limited overlapping data, cavitation breakdown does not appear to be affected by the non-uniform inflow of a system test as shown in Figure 9. The NSWCCD system test facility is discussed in the next section of this paper.

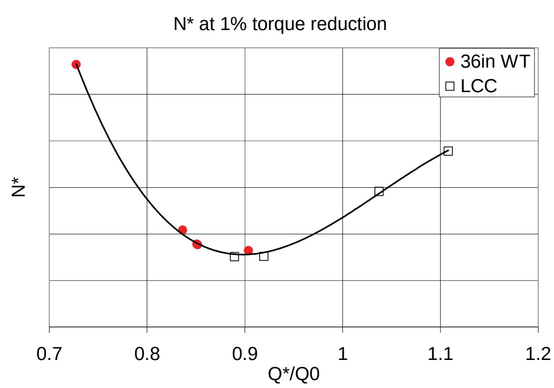

Figure 8: Comparison of cavitation breakdown data from pump-loop and system tests.

3.2 SYSTEM TESTS

A waterjet system test can be used to evaluate inlet designs and the impact of non-uniform inflow on pump performance and cavitation breakdown. The approach NSWCCD has taken is to utilize the 12 in (304.8 mm) inlet diameter pumps from the 36in WT tests and incorporate them with a flush inlet into the attic of the William B. Morgan Large Cavitation Channel test section (LCC). Flow from the pump nozzle discharges into a void section of the attic and is deflected back down into the test section flow. The LCC is a closed-loop re-circulating water tunnel with variable pressure control. The test section is 10 ft x 10 ft (3.05 m x 3.05 m) with diagonal corners to accommodate viewing windows. The nozzle is shown in Figure 3 protruding through the simulated transom. The inlet can be seen as the dark rectangle further upstream.

To evaluate pump performance the impeller is run through a range of rotational speeds at a constant tunnel speed, from no flow (bollards) to 30 knots (15.4 m/s). In the pump-loop facility the impeller was run at a constant speed of 1400 rpm while adjusting the flowrate with blockage and the water tunnel impeller. The flowrate through the pump and the range of flow coefficient achieved with the system test encompass the range attained in the pump loop tests.

An initial comparison of pump performance between the pump-loop and the system test indicated a shift in the head (H*) and power (P*) curve. This shift can be attributed to the effects of flow non-uniformity quantified by the parameters β_M, and β_E for momentum and energy, respectively. These parameters are determined from measurements of the flowfield using LDV. Measurements at the rotor inlet are shown in Figure 9. The ingested boundary layer is apparent as velocity gradient across the inlet with the wake of the rotating shaft superimposed. The boundary layer was later thickened by adding blocks upstream to simulate the thicker boundary layer expected for this pump in the full-scale condition.

Preliminary pump performance results were computed from

$$p_t \quad p_s + \frac{1}{2}\rho \overline{U}_x^{\,2} .$$

Final results incorporated the non-uniformity factor, β_E, into calculations of energy,

$$p_t \quad p_s + \beta_E \cdot \frac{1}{2}\rho \overline{U}_x^{\,2}$$

in which β_E is defined as

$$\beta_E \quad \frac{\int U_x U^2 dA}{\overline{U}_x^{\,3} A} .$$

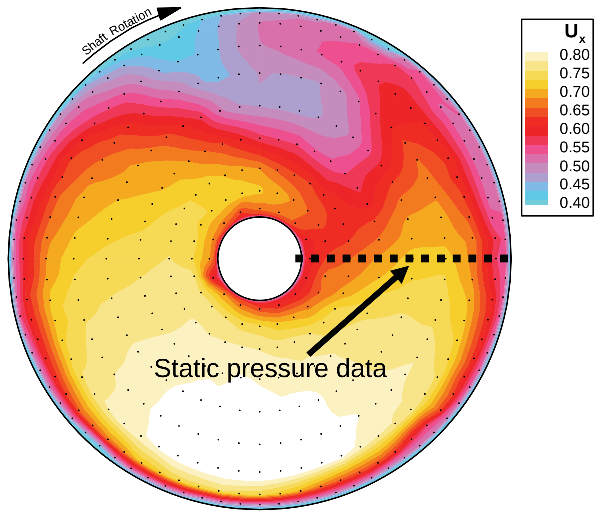

Figure 9: LDV measurements at Station 3 taken at the LCC.

The non-uniformity shown in Figure 9 yields a β_E value of 1.125, which means that the dynamic head is actually 12.5% more than the uniform flow approximation. By correcting the pump performance to account for the non-uniform inflow, the performance is in good agreement with results from the uniform inflow pump-loop facility. However, these equations still assume a constant static pressure at this flow plane. To check for non-uniformity in the static pressure, Kiel probe measurements were taken in a line from the pump casing to the shaft. These measurement locations are shown in Figure 9. Their location does not correspond to the location of the maximum wake deficit as they were limited by the experimental layout. The static pressure was computed by subtracting the dynamic pressure based on the LDV data from the total pressure measured by the Kiel probe. The results are shown in Figure 10. The symbols represent the flow field static pressures and the solid lines indicate the average of

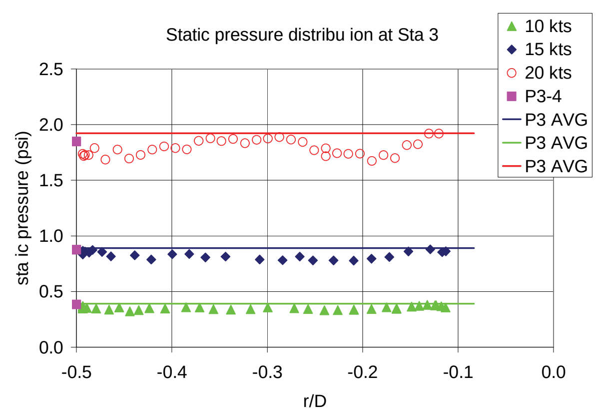

Figure 10: Static pressure measurements at Station 3, inflow to the impeller.

the four static wall pressures measured in the pump casing at the same location. The data at r/D = -0.5 correspond to the individual pressure measurements at the closest wall pressure tap and agree well with the first measurement taken by the Kiel probe. The average pressures used in the performance calculations (wall taps) over-estimate the field-point measurements, based on this one line survey. Calculations of the entire flow-field using CFD could demonstrate the magnitude of errors caused by the non-uniformity in static pressure at Station 3. The initial comparisons between the system test and pump-loop facility show good agreement indicating this correction is small.

Measurement of inlet performance is an important advantage of system tests. Figure 11 shows the inlet loss coefficient versus the inlet velocity ratio, IVR. Inlet loss coefficient is defined as the energy lost from Station 1, the pump capture area, to Station 3 non-dimensionalized by the dynamic pressure at Station 1 times the flowrate through the pump. The measured losses are smaller than what is normally reported for inlets, but this can be attributed to the elliptical upper lip and smoothly defined surfaces used in this particular design. Manufacturer's representatives considered this inlet to be too difficult to build for a practical installation. The minimum value of the loss coefficient should be similar to the friction factor which is in the order of 1% for this inlet flow. Results from two CFD calculations are indicated on the plot as U2NCLE and TENASI. Both under predict the loss coefficient.

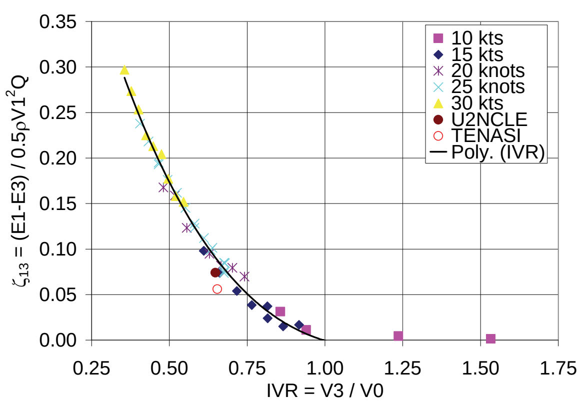

Figure 11: Inlet loss coefficient for flush mounted inlet used in ONR FNC WJ testing.

3.3 TOW-TANK SELF-PROPULSION

NSWCCD also uses tow-tank models operated at self propulsion as part of the overall waterjet test program. The scalability of results from tow-tank models running at Froude-scaled speeds has been a topic of debate. To resolve these scaling issues, detailed tow-tank measurements on a proposed high speed sealift platform (JHSS) were conducted. A scanning LDV system was developed that was capable of mapping the entire flow field simultaneously in four jets within 1 to 2 minutes. The optic assemblies had to be moved to capture data on both sides of the shaft for the inlet flow, but the nozzle flows could be mapped in one to two passes down the basin. LDV provided the most accurate measure of flowrate for this type of test, and the scanning procedure enabled measurements close to the wall. The pressure measurement system was enhanced with an automated back-flushing system to keep air out of pressure lines and taps installed above the static waterline. By utilizing these advances in measurement techniques, a comprehensive, high-quality data set was obtained from which conclusions could be made regarding the need for self-propulsion tow tank tests for full-scale powering predictions of waterjet ships. These data also revealed physics of the waterjet-hull flow interactions. Errors were evaluated for previous tow tank practices such as nozzle-mounted Kiel probes, bollard tests, and collection tank calibrations for flow measurement.

The primary focus of the waterjet testing was on two proposed hullforms, one using mixed flow pumps and the other using axial flow waterjets. The smaller diameter of the transom mounting flange for the axial flow waterjets allowed a narrower and shallower transom for the axial flow hull versus the mixed flow design. The expected result would be an axial flow hull offering a lower bare hull resistance, but with a reduced inlet spacing. The results of these tests are discussed in more detail in Jessup et al. [3], and Fry et al [4].

Chesnakas et al [5] showed that Reynolds effects at model scale conditions cause poor pump performance that cannot be scaled for full-scale predictions. However, the wake fraction and thrust deduction are valid outcomes of these tests and provide essential information in understanding the waterjet-hull interaction. For a waterjet propelled vessel, the wake fraction is defined as the average velocity in the upstream flow captured by the pumps, divided by the ship speed. Full scale wake fractions are lower than model scale fractions because of thinner boundary layers, hence the wake fraction from the Froude scale tank test is scaled using an inlet wake scaling procedure [6]. Results from this approach also agree with preliminary estimates of wake fraction made using an assumed boundary layer profile at a full-scale Reynolds number. The other tow tank datum, thrust deduction factor, is considered free of scale effects. The thrust deduction 1-t is defined as the hull resistance minus the applied tow force divided by the net system thrust. Savitsky [7] made the assumption that this factor has no scale effects, and the 24th ITTC explored this issue further [1]. It is hypothesized that the only component of thrust deduction which scales with Reynolds number is the change in hull resistance from the missing hull area at the waterjet inlets, and this area is typically negligible.

The model-scale wake fraction is determined from LDV measurements at ITTC Station 1 and a scaled trapezoidal capture area to bound the ingested pump flow. The dimensions of the trapezoid are initially assumed to be

Base = 1.5 x D3
Top = 0.75 x D3
Height = 0.65 x D3

These initial dimensions are then scaled by a constant factor until the integrated flowrate through the trapezoid matches the flowrate determined for the operating pump. Comparisons from the axial flow hull with capture areas computed using a steady RANS code with a reflection plane at the free-surface are shown in Figure 12.

The overall area and average velocities from these two techniques are in good agreement even though the trapezoids penetrate further into the boundary layer and do not capture all the flow being ingested from the outboard waterjets. Exchanging the capture areas in the powering predictions causes only a 0.2% change in the delivered horse power. In the case of the axial flow hull the width of the capture area is constrained by the inlet spacing.

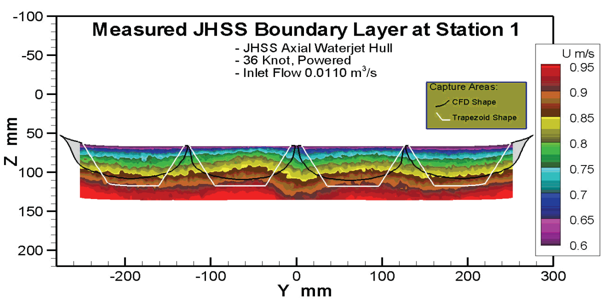

Figure 12: Comparison of capture areas for CFD Boundary Layer at St 1.

For the mixed flow hull with wider inlet spacing, there was concern that the assumed initial base length would not accurately capture the correct flow area because it did not span across the entire inlet spacing. How much this could impact the final powering result was also unknown. To investigate this further, additional CFD calculations on the mixed flow hullform were conducted. The computed capture areas for the axial and mixed flow hullforms are shown in Figure 13. The mixed flow capture areas are wider, expanding to fill the larger inlet spacing, and ingest more lower-momentum fluid from the boundary layer. These results indicate that the current practice of defining the trapezoidal capture area as only a function of the inlet diameter may be inadequate. NSWCCD is integrating the CFD capture areas into the mixed flow hull powering predictions to quantify this effect. The vertical offset in the capture areas, shown in Figure 13, shows the added depth of the mixed flow hull at ITTC Station 1.

Results for thrust deduction factor for the axial and mixed flow hull forms are shown in Figure 14. The net system thrust is determined from a control volume approach which determines the net change in momentum from ITTC

Figure 13: Comparison of computed Station 1 capture areas, axial to mixed flow hullform.

Station 1 to the nozzle exit, Station 7. This approach is discussed in more detail in Scherer et al. [8]. The thrust deduction fraction, t, becomes negative for the mixed flow hull above 30 knots. This added benefit from thrust deduction is assumed to result from the larger inlet spacing on the mixed flow hullform. Ongoing analysis is also attempting to correlate the sinkage and trim differences between the two hullforms on this parameter.

The differences of the full-scale powering predictions for the axial and mixed flow hullforms are shown in Figure 15. These powering predictions utilize the inlet scaled wake fraction, thrust deduction, and non-uniformity factors determined from the tow-tank self-propulsion tests. For full-scale ship speeds above 30 knots, the benefit of reduced resistance of the axial flow hull is offset by the negative thrust deduction on the mixed flow hull. This is counter-intuitive to the initial assumption that a more slender hull will need less power because of its lower resistance. These insights are an advantage of tow tank testing that is sometimes absent in vendors' designs. Additional details regarding the full-scale powering predictions are discussed in the next section.

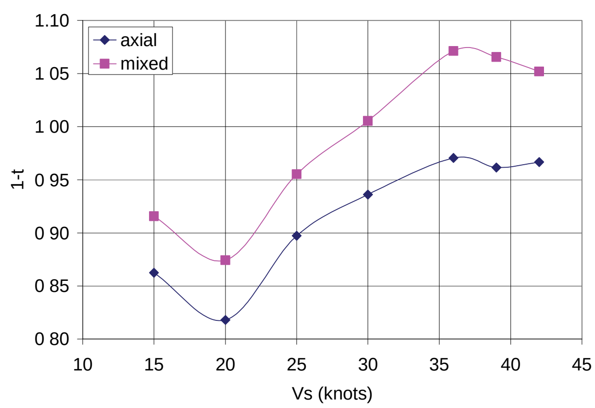

Figure 14: Thrust deductions of the mixed and axial flow JHSS hullforms from self-propulsion tests.

4. POWERING PREDICTIONS

Two approaches to powering predictions were used for the JHSS ship and are compared here. The first approach, equivalent to vendor provided predictions, matches the jet system thrust to the hull resistance. For a constant input power the jet system thrust is computed

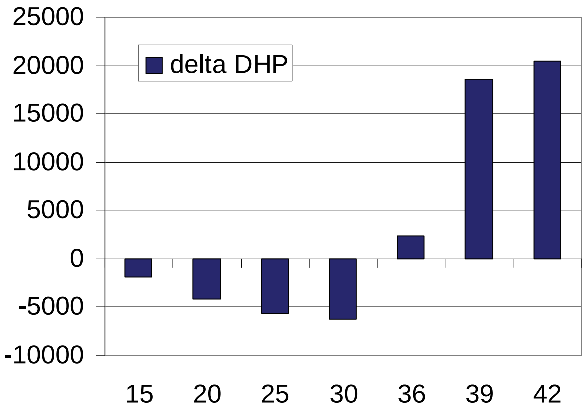

Figure 15: Difference in full-scale powering prediction for JHSS, AxWJ - MxWJ hullforms.

for a range of flow coefficients utilizing the result of a pump-loop test for Q*, H*, and P*. It is assumed that the pump inlet and nozzle diameter have already been determined from a pump sizing study. Values for the thrust deduction, wake fraction, and inlet loss coefficient are either estimated or calculated.. At a set power level and flow coefficient, the jet system thrust defined as

$$thrust \quad (1 \quad t)\ \rho\ Q\ (V_6 \quad V_1)$$

The thrust value that matches the hull resistance determines the operating point flowrate Q*. At this flow coefficient, P8 is computed from the pump performance curves and with the input power is used to determine impeller rpm. In addition, the results from the cavitation breakdown tests conducted in the pump-loop facility can be used to determine the location of the cavitation zone boundaries relative to the operating curve.

The tow tank and system tests provide additional options for improving the full-scale power predictions from this approach. The initial values of the wake fraction, thrust deduction, and inlet loss coefficient can now be replaced by measured values over a range of speeds. This is important for ships outside of the experience base of industry. The JHSS monohull, with a waterline length of 980 ft (298.7 m), is larger than most waterjet ships, operating at a lower Froude number. The tests also yield values for flow non-uniformities that can improve the system thrust prediction, specifically β_{M1}, Cp1 for the inlet momentum and β_{M6}, Cp6 for the nozzle momentum. It is interesting that measurements of β_{M6} are nearly equal in both the system test and pump-loop facilities, indicating that the non-uniformity ingested by the inlet is not passed through the impeller/stator. Incorporating both B_{M6} and B_{M1} into the equation for jet system thrust should provide a more accurate thrust value than using area averaged parameters, V_6 and V_1 only. The equation becomes:

$$thrust \quad (1 \quad t)\ \rho\ Q\ (B_{M6}\, V_6 \quad B_{M1}\, V_1)$$

where

$$B_{Mi} = \beta_{Mi} + 0.5\ C_{pi}$$

The second approach for predicting full-scale power is to directly scale the results from the headrise and flowrates measured in the tow-tank self propulsion tests. Again, an inlet wake-scaling procedure is used to account for the difference in wake fraction. The model-scale hydraulic pump power is used with an assumed full-scale pump efficiency to determine power, and pump performance curves are not utilized at all. The effective pump power E5-E3, or the energy rise across the impeller/stator, is scaled using the following equation to obtain delivered power.

$$DPH \quad \left(\frac{\rho_{ship}}{\rho_{model}}\right)\left(\frac{E5 \quad E3}{\eta_{pump}}\right)\lambda^{3\ 5}/550$$

The definition of E3 and E5 incorporates the measured static pressures and non-uniformity factors determined from LDV measurements. These values are also recomputed after the inlet wake scaling procedure to reflect the higher flowrate required to account for the reduced momentum at ITTC Station 1. Additional details regarding the derivation of these equations can be found in Scherer et al [8], and Scherer and Wilson [6].

The results from these two approaches, including the various improvements, are compared in Figure 16. The scaled results from the tow-tank self propulsion tests are used as a baseline and error bands from this approach are shown as the envelope of dashed black lines. The other predictions are shown as the percent difference relative to these tow tank baseline results.

Powering results from the pump-loop tests with tow tank/system test values of wake fraction, thrust deduction, and inlet loss coefficient are labelled “original”. Refining these predictions with the non-uniformity factors changes them little, as shown in the data labelled “original with betas”. Both of these curves are within 4% of the tow tank predictions. It is only fortuitous that the pre-test prediction falls largely within the error bands because large errors in the predicted hull resistance were offset by errors in the assumed 1-w, 1-t, and inlet loss coefficient values. If these assumed parameters had been applied to the measured hull resistance, the power predictions would have been low by as much as 15%, as shown by the “corrected resistance” curve. Additional analysis of these results indicates that the primary difference in powering performance is the thrust breakdown, as the pre-test prediction for wake-fraction and inlet loss coefficient were in good agreement with measured results.

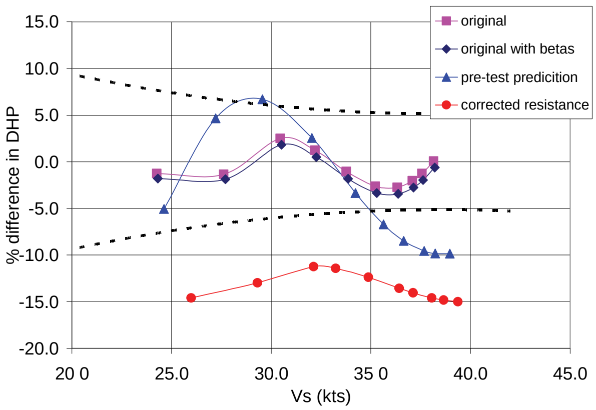

Figure 16: Percent difference in powering prediction approaches.

5. SUMMARY

Extensive modifications were undertaken to NSWCCD's propeller testing facilities in order to evaluate commercial waterjet designs for the proposed ship, JHSS. Two pump-loop facilities designed to accommodate testing at two different scales were evaluated and the results validated by comparison. Cavitation breakdown testing in a uniform flow facility versus a system test, which includes the ingested the hull boundary layer and rotating shaft wake, are shown to be equivalent for a limited overlapping range. While this conclusion is significant because it indicates that cavitation breakdown performance can be predicted from a pump-loop facility, it does not eliminate the fact that the growth and collapse of unsteady cavitation in a non-uniform inflow could contribute to additional cavitation erosion, The execution of a detailed self-propulsion tow tank test for a waterjet propelled vessel provided a high quality data set which can be used to evaluate the usefulness of these test in predicting full-scale required power. Application of new measurement techniques including scanning LDV investigated the lower bound of uncertainty in flowrate quantification. An evaluation of powering prediction methods indicates a combined approach is essential when a hull design falls outside the experience for full-scale predictions of thrust deduction.

6. ACKNOWLEDGEMENTS

The authors would like to acknowledge the significant contribution of numerous engineers to the work presented here including Dr. Chris Chesnakas, Mr. Keegan Delaney, Mr. Michael Ebert, Dr. David Fry, Dr. Stuart Jessup, Mr. Otto Scherer, and Dr. Michael Wilson.

7. REFERENCES

1. ITTC, "Report of the Specialist Committee on Validation of Waterjet Test Procedures," Proceedings of the 24th ITTC Triennial Meeting, Edinburg, Scotland UK, 2005.

2. Gowing, S., "CCDoTT Waterjet Pump Test in the 24" Water Tunnel," Naval Surface Warfare Center, Carderock Div. Rept. NSWCCD-50-TR-2005/103, December 2005.

3. Jessup, S., Donnelly, M., Fry, D., Cusanelli, D., and Wilson, M., "Performance Analysis of a Four Waterjet Propulsion System for a Large Sealift Ship," 27th Symposium on Naval Hydrodynamics, Seoul, Korea, October 5-10.

4. Fry, D., Jessup, S., Delaney, K., "JHSS Waterjet Performance Evaluation with Scanning Laser Doppler Velocimetry," Carderock Division Report NSWCCD-50-TR-2008/042, August, 2008.

5. Chesnakas, C., Donnelly, M., and Jessup, S., "Testing of a Waterjet at a Range of Scales," 27th Symposium on Naval Hydrodynamics, Seoul, Korea, October 5-10.

6. Scherer, J. and Wilson, M, "Waterjet Inlet Wake Scaling," Carderock Division Report NSWCCD-50-TR-2008/051, Oct 2008.

7. Savitsky, D., (Chairman) "Report of the High Speed Marine Vehicle Committee," 18th ITTC, pp. 304-313, Kobe, Japan.

8. Scherer, O, et.al.," Procedure for Conducting a Towing Tank Test of a Waterjet Propelled Craft Using Laser Doppler Velocimetry to Determine Momentum and Energy Flux, American Towing Tank Conference, July, 2001.

8. AUTHORS BIOGRAPHY

Martin Donnelly holds the current position of mechanical engineer in Code 5800, Resistance and Propulsion Division at the Naval Surface Warfare Center, Carderock Division. His current responsibilities include the execution of naval propulsor evaluations including the development of cavitation erosion predictions. His previous experience is in experimental fluid mechanics, and test data acquisition development.

Scott Gowing holds the current position of mechanical engineer in Code 5800, Resistance and Propulsion Division at the Naval Surface Warfare Center, Carderock Division.. He is responsible for research and development of fluid systems, propulsors, and test and evaluation of naval concepts. His previous experience includes work with two-phase flows, ventilated waterjets, composite propellers, and service with the ITTC Specialist Committee on Cavitation.

ACTIVE RUDDER CONTROL

Nils Morén, MJP Marine Jet Power AB, Sweden
Stanislav Pavlov, MTD Company, Ltd., Russia

SUMMARY

Most fast craft with water jet propulsion do not have hull appendages, which makes them significantly less course-stable compared to similar vessels with propellers and rudders. Deflecting the steering nozzle of a waterjet to stabilize heading of a fast craft when moving in a seaway, causes thrust losses up to (especially in following seas) 40% at maximum deflection angles.

MJP Waterjets suggest that fast craft with water jet propulsion can be fitted with specially designed auxiliary rudders. These rudders are intended for directional control of the vessel at operational speeds while steering nozzles remain fixed in their neutral position. The algorithm of active rudder control is implemented in the MJP Waterjets' Vector Control System and tuned so that all steering at high speed is achieved by active rudder control only. That means that at high speeds, the waterjet operates as a booster unit and constantly produces the claimed thrust and efficiency, thus increasing the vessel's operational efficiency. In theory the active rudder control is applicable for most fast waterjet driven vessels but before implementation each vessel's characteristics should be studied to determine best solution since it in some cases is enough with interceptors.

1. STEERING BY WATERJET

Deflecting the steering nozzle of a waterjet, both to provide a steering control input and to stabilize heading of a fast craft when moving in a seaway, causes thrust losses that are increasing with higher deflection angles. Generally, fast craft with waterjet propulsion do not have large hull projections, which makes them less course-stable compared to similar vessels with conventional propulsion and steering devices.

In real sea conditions, steering is always activated with the result that the actual propelling thrust value is always lower than that claimed by the manufacturer (i.e. determined for ideal conditions and with the steering nozzles not engaged – in so-called "booster" mode).

Motion analysis of fast craft moving in a seaway, even if the significant wave height is 1 m or more, shows that the actual efficiency of the waterjet, considering the increased yawing of the vessel (due to worse course-keeping ability) and the deflections of the waterjet steering nozzles required to compensate for it, is reduced by ~10% and more while wave height increasing.

This effect is particularly noticeable when the vessel is moving in following seas. This causes reduction in the vessel's speed or makes increase the engine output to compensate for loss of efficiency. In a heavy seaway, the waterjet efficiency may drop up to 30% compared to the claimed one.

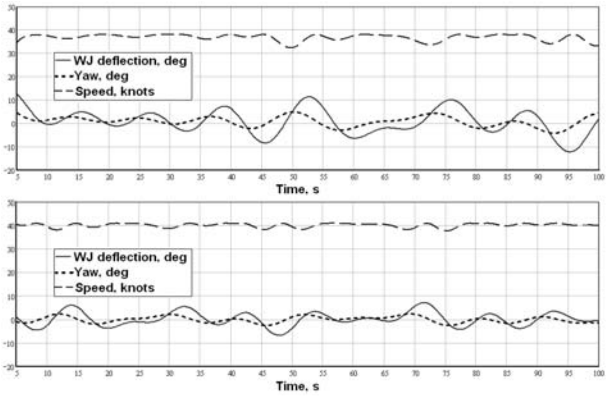

Figure 1: Motion parameters

The diagrams (Figure 1) show the motion parameters for two similar vessels in the same weather conditions. The top diagram refers to the vessel with waterjet propulsion system only, and the bottom diagram to the vessel equipped with active rudder control. The average speed of the vessel steered with waterjet nozzles is 36.8 knots against 40.1 knots for the vessel steered with active rudder control.

Another drawback of the directional stabilization by means of steering nozzles only is the insensitivity of these devices to smaller deflection angles. There is a dead zone of about ±5° complemented with a non-linear variation of steering force with deflection angle. This insensitivity is due to a gap between the boundaries of the jet and the steering nozzle. This is made to avoid the jet being distorted and thus to ensure the maximum thrust on a straight course.

Thereby, such directional stabilization requires that the steering nozzles be deflected by much larger angles to compensate also for small course deviations. Lack of vessel response to small nozzle deflections often makes the master put on excessive amount of wheel thus causing the vessel deviate from its course in the opposite direction instead of keeping it on course.

Generally, the efficiency of steering control at speed is considerably lower compared to rudders.

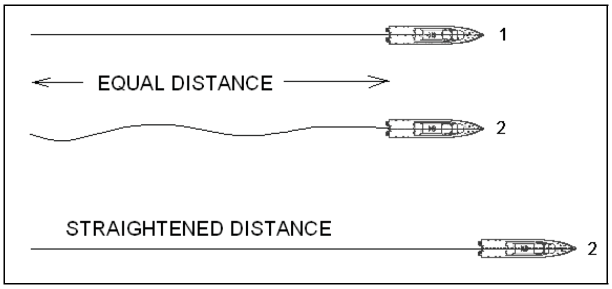

Figure 2: Straightened distance

The vessel No.1 in the Figure 2 is equipped with waterjet propulsion and active rudder control, the vessel No.2 has waterjet propulsion and no rudders. It is clear to understand that the average speed on a given distance is higher for No.1 vessel.

2. MJP ACTIVE RUDDER CONTROL

2.1 HOW IS THIS TO BE DEALT WITH?

To eliminate this effect, MJP Waterjets can suggest fast craft with waterjet propulsion to be fitted with one or two auxiliary rudders in case use of interceptors is not sufficient. These auxiliary rudders are specially designed and shaped and have comparatively small area compared to 'normal' rudders and are intended for directional control of the vessel at operational speeds while steering nozzles remain fixed in their neutral position.

That means that at high speeds, the waterjet operates as a booster unit and always produces the claimed thrust and efficiency (regardless of the weather conditions), see Figure 3. At lower speeds both rudders and steering nozzles are used for steering the vessel, ensuring high maneuvering capabilities.

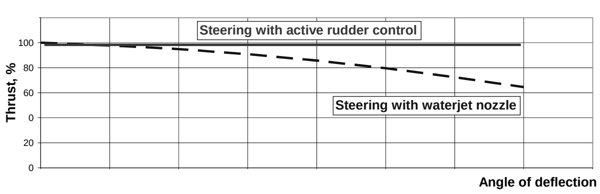

Figure 3: Thrust losses

A sufficiently wide dead zone (Figure 4) inherent to waterjet steering control leads to larger nozzle deflection angles needed to provide the same steering force as is produced by the rudders.

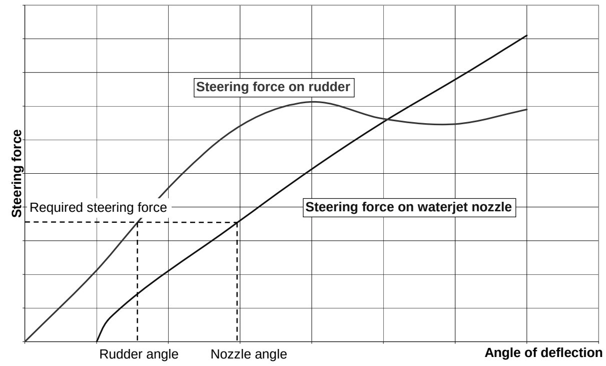

Figure 4: Steering force

2.2 MJP ACTIVE RUDDER CONTROL

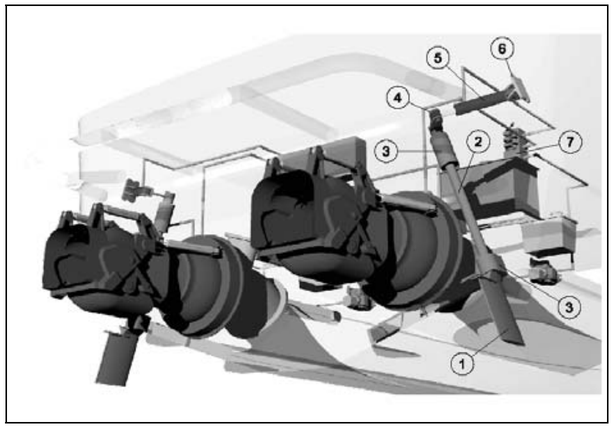

Figure 5: Active rudder control

The active rudder control is presented in Figure 5. The reference numbers in Figure 5 denote the following: 1-Rudder blade; 2-Rudder stock; 3-Rudder stock basement; 4-Tiller; 5-Actuator; 6-Actuator basement; 7-Hydraulic unit

2.3 INCREASED COURSE STABILITY – LOWER FUEL CONSUMPTION

Use of active rudder control increases the vessel course stability even at rough sea, thus minimizing the way to target point while maintaining high performance of the waterjet propulsion system.

Active rudder control requires less hydraulic power to steer the vessel compared to waterjets-only steering and has a favorable effect on the hydraulic system lifetime.

2.4 INCREDIBLE MANEUVERABILITY

The vessel with waterjet propulsion and active rudder control can perform sharp turns with minor speed losses compared to full turns typical for the vessels with waterjets steering nozzle only. Speed loss while turning is about negligible.

2.5 INTEGRATION IN MJP CONTROL SYSTEM

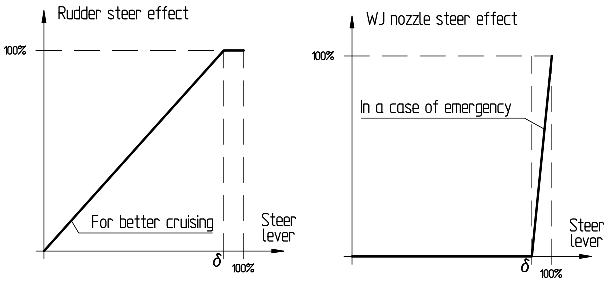

Figure 6: Control system

The algorithm of active rudder control is implemented in the MJP Waterjets' Vector Control System (Figure 6). The algorithm is "tuned" so that all steering at high speed is achieved by active rudder control only, with the waterjets operating in booster mode to provide maximum thrust and efficiency. It should be noted that in emergency this control algorithm will enable a combined deflection of the auxiliary rudders and the steering nozzles even during high-speed operation (by putting helm to maximum angle) to turn away from the danger in the shortest time, thus improving the safety of operations.

2.6 SUPPLY AND INSTALLATION

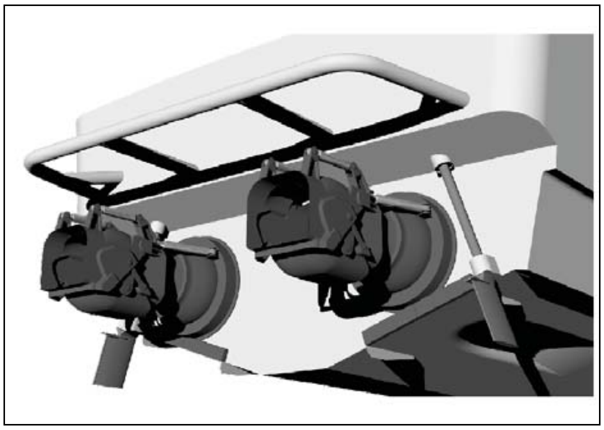

Figure 7: Transom arrangement

The purpose-designed rudder blades and rudderstocks can either be manufactured by the shipyard using the documentation provided by MJP Waterjets or supplied by MJP Waterjets. The rudderstocks are usually located after the transom (Figure 7) and their mounting is not too complicated, but they can also be installed on the bottom of the vessel similar to a conventional rudder. The hydraulic equipment is supplied by MJP Waterjets. The rudder actuators are integrated in the hydraulic system and waterjet control system. The hydraulic cylinders of the rudder actuators are manufactured from stainless steel and have built-in feedback sensors of contactless type. The cylinders can also be mounted after the transom. Since most current fast craft have "Deep Vee" hulls and the rudder blades are comparatively small, the auxiliary rudders do not generally increase the vessel draught at all.

2.7 RETROFITTING

Compact size, easy mounting and the same or updatable control system allow the active rudder control to be retrofitted on the existing vessels equipped with MJP propulsion system.

3 OPERATING EXPERIENCE

Several mono and twin-hulled vessels are currently fitted with MJP Waterjets steerable propulsion systems featuring auxiliary rudders (see Figures 8-10). The available operating experience has shown a substantially higher quality of steering control compared to the standard version, particularly when moving in following seas. In some cases, an annual fuel economy of 8-10% has been achieved.

Figure 8: Superfoil passenger ferry

Figure 9: High speed patrol boat

Figure 10:Coast Guard Ship

4. CONCLUSIONS

An effective auxiliary steering system – active rudder control – has been suggested by MJP as a possible option for high speed craft with waterjet propulsion. The system has been successfully implemented on several mono and twin-hulled vessels and shown its high performance capability. For some vessels the solution is not needed or desired depending on vessel size, hull design, speed range and operating waters. Also project budget and complexity should be evaluated before implementation. In cases where applicable however, the active rudder control is a very efficient solution that is highly recommended.

5. AUTHORS BIOGRAPHY

Mr. **Nils Morén** is an Aeronautical Engineer and holds the current position of Sales and Marketing Manager at MJP Marine Jet Power AB in Österbybruk, Sweden. MJP deliver complete waterjet propulsion systems specialized for heavy duty and high performance applications. The business areas are in the fields of Commercial, Navy, Coast Guard and Yacht.

Mr. Morén has many years of experience from various positions within the Marine industry and before joining MJP in 1995 he worked for the Swedish shipyard Marinteknik AB as Design Engineer and Project Manager.

Mr. **Stanislav Pavlov** is a naval architect and holds the current position of Director at MTD Company Ltd. in Saint Petersburg, Russia, specialized in the design of fast marine craft including related research activities.

After graduation of the Leningrad Shipbuilding Institute in 1975 he started his career with one of the Russia's major naval design bureaus and performed a great variety of tasks in the area of feasibility studies, hydrodynamic and hull form design and propulsion (incl. waterjets) of fast marine craft. After its establishing in 1995, MTD Company Ltd. is closely collaborating with MJP Waterjets of Sweden.

SCALING OF WATERJET PROPULSOR INLET WAKES

M B Wilson, Naval Surface Warfare Center, Carderock Division (NSWCCD), USA

SUMMARY

There are significant scale effect problems involved with waterjet self-propulsion model testing, even without obvious pump-related issues. Model hull boundary layers are relatively thicker than those at full scale, and model frictional drag is relatively larger. Model hull flow velocity distributions are not as full as those developed at high Reynolds number on the ship, so the average of inlet velocities must be relatively higher. This paper presents a description and application of a procedure for dealing with one aspect of the scaling problem by adjustment of the model-scale flow rate so that the full-scale values may be estimated while maintaining the same thrust loading developed by the waterjet. Results from a specific example of a self-propulsion test are presented.

NOMENCLATURE

A Cross section area
A_1 Hull inlet or capture area at Station 1a
A_6 Nozzle area, at Station 6
A_7 Jet section area at vena-contracta
B_E Combined coefficient for energy flux
B_M Combined coefficient for momentum flux
C_{pJ} Pressure coefficient at Station J
C_A Correlation allowance
C_F ITTC ship-model correlation line coeff.
C_{Th} Thrust loading coefficient
D_6 Diameter of jet nozzle, Station 6
D_{M1} Ratio of nondim. momentum velocities
E Energy flux
F_D Estimated model scale tow force
F_n Froude number
JVR_0 Jet velocity ratio, based on V_0
K Ratio of combined momentum flux coeffs
L Waterline length, reference length
M Momentum flux
p Static pressure
Q_J Waterjet system flow rate; flow rate at Station J
R_i Model ideal resistance = $R_{Tm} - F_D$
R_T Total resistance
S Hull wetted surface area
t Thrust deduction fraction
T, T_{sys} Jet system thrust
u Local total velocity
$\overline{V}$ Mean velocity (general)
V_0 Vehicle speed, free stream velocity
$\overline{V}_1$ Capture area mean inlet velocity
$\overline{V}_7$ Mean jet velocity at Station 7
$\overline{V}_M$ Mean momentum velocity

α Angle of jet discharge from shaft line
β_E Energy non-uniform velocity factor
β_M Momentum non-uniform velocity factor
λ Model scale ratio
ρ Mass density

Subcripts

J Station number, measurement station
JSE Effective jet system
M Momentum-related factor
m Model
s Ship; full scale
tot Total

Abbreviations

ATTC American Towing Tank Conference
ITTC International Towing Tank Conference
JHSS Joint High Speed Sealift
LDV Laser Doppler Velocimetry
NAVSEA Naval Sea Systems Command

1. INTRODUCTION

When conducting tests on a scale model of a waterjet-propelled craft, the model will normally have a lower Reynolds number than the full size ship. In a Froude-scaled model test the Reynolds number will be reduced approximately as the scale ratio to the 3/2 power. This leads to a proportionally higher friction drag and thicker boundary layer on the model than on the ship. In towing basin tests, the difference in frictional resistance can be partially accounted for by applying a tow force to the model as it travels down the tank. Other drag components not included on the model such as still air drag, bilge keels, etc must be accounted for with a correlation allowance added to the ship friction drag. Under these conditions, the propulsor supplies a thrust corresponding to the scaled full size ship thrust. This is the procedure normally used in testing propeller-driven ships and is recommended by the International Towing Tank Conference [1] for conducting waterjet propulsion tests.

However, because the waterjet thrust is proportional to the change in momentum flux between the discharge and inlet, a change in the relative inflow velocity pattern will have an effect on the resulting flow rate required to develop the intended thrust. Since the scale model inflow velocity distribution is not the same as on the full size ship, the model will never have a geometrically scaled flow field. This paper concerns a method for correcting the model results to give an estimate of the full scale performance.

The 21st ITTC Quality Manual [2] specifies the stations where measurements are to be made for a waterjet propulsion system. These stations are now defined as:

- Station 0: Far ahead of the ship in undisturbed flow
- Station 1a: At one inlet width upstream of the tangency
- Station 2: At the aft lip of the inlet
- Station 3: Just ahead of the pump blade tips
- Station 4: Between pump rotor and stator
- Station 5: Just aft of the pump stator
- Station 6: At the nozzle outlet plane
- Station 7: Where static pressure is near ambient in jet

Control point location definitions given in the 23rd ITTC Specialist Committee Report [3] are shown in Figure 1, and indicate that Station 1a is the designation of the inlet capture area measurement plane.

2. SELF-PROPULSION TESTING AND WAKE SCALING METHOD

2.1 GENERAL

As noted above, the idea is to conduct the model powering test with a make-up tow force F_D, at the correct Froude number, so that the 'ideal' model resistance represents the total ship resistance at model scale. The resulting model scaled resistance is designated as

$$R_i = R_{Tm} - F_D \,, \qquad (1)$$

where R_{Tm} is the total measured drag force on the model hull without active propulsion, with the inlets covered, and R_i is the target model-scale drag force to be balanced by the total model scale propulsion thrust. The notation R_i is chosen to agree conceptually with current NSWCCD model powering test terminology. The self-propulsion condition for a model is determined when the target tow force is matched by the measured tow force in a towing basin test. Main results from the self-propulsion test are the model-measured shaft rotation speeds, various average flow velocity magnitudes and distributions, and certain pressures needed to estimate total jet system thrust. Because waterjet system thrust is very difficult to measure by direct means, we must use the calculated thrust force derived from the change in momentum flux between the discharge and inlet planes of the system flow path region. Total model thrust $T_{m,tot}$ is the sum of the calculated thrust values of all the active waterjet units, and is found to be related to the ideal model resistance by an experimentally derived factor termed the thrust deduction factor defined as:

$$(1-t) = \frac{R_i}{T_{m,tot}} \,. \qquad (2)$$

It is assumed that the thrust deduction factor determined on the model scale is the same for full scale when the condition of Equation (1) is maintained. (see the 24th ITTC Waterjet Report [4]).

A non-dimensional thrust loading coefficient, based on vehicle speed V_0 and jet area A_7, is defined as

$$C_{Th} = \frac{T}{\frac{1}{2}\rho V_0^2 A_7} \,. \qquad (3)$$

The present development is founded on the concept that to achieve correct model-to-full scale propulsion-flow similarity the model propulsor should be run at the same non-dimensional jet system thrust loading as for full scale

$$(C_{Th})_{ship} = (C_{Th})_{model} \qquad (4)$$

2.2 REFINED JET SYSTEM THRUST ANALYSIS

With the guidance provided by the general outline given in the ITTC Waterjets Group Report [1], the initial published details of a refined set of formulas for analysis of waterjet performance were developed and presented by Scherer, et al. [5], and then streamlined in Scherer and Wilson [6]. The refinements consist of accounting for both local pressures and non-uniform velocity effects in the momentum flux at the end-stations of the propulsor flow path. The discussion here is concerned only with the thrust as obtained from the analysis of test data at the intake and discharge stations.

Jet system thrust for each waterjet unit is determined from the difference in momentum flux, written as

$$T_{unit} = \rho_m (Q_J)[(B_{M7})\overline{V}_7 \cos\alpha \quad (B_{M1})\overline{V}_1] \,, \qquad (5)$$

where Q_J is the waterjet unit volume flow rate. Area-averaged (mean) velocities $\overline{V}_1$ and $\overline{V}_7$, and the combined coefficients B_{M1} and B_{M7} are determined at Station 1a and Station 7, respectively. Note that throughout, quantities subscripted with 1 refer to the capture area plane at Station 1a.

$$B_{M1} = \beta_{M1} + \tfrac{1}{2} C_{p1},$$
$$B_{M7} = \beta_{M7} + \tfrac{1}{2} C_{p7}, \qquad (6)$$

where β_{M1} and β_{M7} are momentum non-uniform velocity factors at Station 1a and 7, and C_{p1} and C_{p7} are the local static pressure coefficients referred to the same ambient pressure and made non-dimensional by the local station mean velocity squared. The coefficient C_{p7} is typically taken as zero because of its location at the vena-contracta of the jet.

Definitions for area-averaged velocity and momentum non-uniform velocity factors at Station J are

$$\bar{V}_J = \frac{1}{A_J} \iint (u_x)_J \, dA_J, \quad \beta_{MJ} = \frac{1}{A_J} \iint \left(\frac{u_x}{\bar{V}} \right)_J dA_J \qquad (7)$$

The thrust equation can also be written as

$$T_{unit} = \rho(Q_J)[\bar{V}_{M7}\cos\alpha \quad \bar{V}_{M1}], \qquad (8)$$

where the average momentum velocities are defined as

$$\bar{V}_{M7} = (B_{M7})\bar{V}_7, \qquad \bar{V}_{M1} = (B_{M1})\bar{V}_1.$$

These two momentum velocities are useful in definitions used in the wake scaling procedure.

2.3 EFFECTIVE JET SYSTEM POWER

The 21st ITTC Waterjet Group Report [1] provided the definition of effective jet system power as the increase in energy flux between Station 7 and Station 1a, which can be written as

$$P_{JE} = \tfrac{1}{2}\rho(Q_J)\left[B_{E7}\bar{V}_7^2 - B_{E1}\bar{V}_1^2 \right], \qquad (9)$$

where the combined energy coefficients are given in simplified form as

$$B_{E1} = \beta_{E1} + C_{p1},$$
$$B_{E7} = \beta_{E7} + C_{p7}, \qquad (10)$$

and the general form of the energy non-uniform factor for Station J is

$$\beta_{E} = \frac{1}{A_J} \iint \frac{u_x(u_x^2 + u_t^2 + u_r^2)_J}{(\bar{V})^3} dA_J. \qquad (11)$$

The contributions to the total kinetic energy come from the squares of the axial, tangential, and radial velocity components in the jet. The dominant effect is from the x-component. Previous discussions of C_{p1} and C_{p7} apply here. The jet system power P_{JE} is the hydraulic power added to the flow between the intake and the discharge jet. It does not include the inlet or nozzle losses, and is thus only a part of the total power required by the pump to drive the flow through the unit. It is included here only as an indicator of the trend of power performance.

2.4 SCALING CAPTURE AREA FLOW RATE

2.4(a) Thrust Loading Equivalence

The non-dimensional thrust loading of Equation (3) can be written in general terms as

$$C_{Th} = 2\left(\frac{\bar{V}_7}{V_0}\right)\left\{ \frac{\bar{V}_7}{V_0} B_{M7}\cos\alpha - \frac{\bar{V}_1}{V_0} B_{M1} \right\}. \qquad (12)$$

Now the objective of the inlet wake scaling procedure can be stated as follows: under the provision that both the model and full-scale waterjet systems are producing the same non-dimensional thrust, we can determine the full-scale jet velocity $(\bar{V}_7)_s$ from measurements of the model jet velocity $(\bar{V}_7)_m$, the model inlet velocity $(\bar{V}_1)_m$, as well as the representative average static pressures and velocity non-uniformity factors at Stations 7 and 1a. The factors B_{M7} and B_{M1} represent the ratios of mean momentum velocity-to-mean velocity for flows at Stations 7 and 1a, respectively, and generally have values that are close to 1.0. It is assumed that the changes of these factors between the model and ship are minor. Therefore, we assume that model values can be substituted for the full-scale values in the thrust loading equivalence equation. Also, this substitution is made because usually we can only conveniently determine the model values. The equal thrust loading equation can then be written as a quadratic equation for the ship factor $(\bar{V}_7/V_0)_s$ in terms of coefficients based on obtainable model data. The solution to the quadratic equation for the ship jet velocity ratio is

$$\left(\frac{\bar{V}_7}{V_0}\right)_s = \left(\frac{D_{M1}}{2}\right) K \left(\frac{\bar{V}_1}{V_0}\right)_m +$$
$$\tfrac{1}{2}\left[\left(2\left(\frac{\bar{V}_7}{V_0}\right) - K\left(\frac{\bar{V}_1}{V_0}\right) \right)^2 + (D_{M1}^2 - 1)K^2 \left(\frac{\bar{V}_1}{V_0}\right)^2 \right]_m^{\frac{1}{2}}, \qquad (13)$$

where D_{M1} is the ratio of normalized ship-to-model momentum velocities at Station 1a

$$D_{M1} = \frac{(\bar{V}_{M1}/V_0)_s}{(\bar{V}_{M1}/V_0)_m} \approx \frac{(\bar{V}_1/V_0)_s}{(\bar{V}_1/V_0)_m}, \qquad (14)$$

and $$K = B_{M1} / B_{M7}\cos\alpha \qquad (15)$$

It can be shown from Equation (13) that if the factor D_{M1} is equal to one, that the model and ship have proportionally similar boundary layers entering the inlet, and the ship and model have the same jet velocity ratio. Determination of the value of the factor D_{M1} is the key to the present method of inlet wake scaling.

2.4(b) Effect of Reynolds Number on Inlet Flow

Since waterjet system thrust is proportional to the change in momentum flux between the discharge and the intake, a change in the relative inflow velocity between model and full scale will have an effect on the resulting flow rate and energy flux required to develop the desired thrust.

We assume that the momentum and energy deficits at the inlet measurement plane (Station 1a) are attributable to the viscous flow over the hull ahead of the inlet. In order to quantify this loss, we assume that the momentum deficit is proportional to the estimated skin friction coefficient C_F. With the free stream momentum flux and momentum flux at Station 1a given by

$$M_0 = \rho(A_7\overline{V}_7)V_0 \,, \quad \text{and} \quad M_1 = \rho(A_7\overline{V}_7)\overline{V}_{M1} \,, \qquad (16)$$

the momentum flux deficit at Station 1a is

$$(M_0 - M_1) = \rho(A_7\overline{V}_7)(V_0 - \overline{V}_{M1}) \,. \qquad (17)$$

When this equation is made non-dimensional by the factor $\frac{1}{2}\rho A_7 V_0^2$, we have

$$(C_{M0} - C_{M1}) = 2\left(\frac{\overline{V}_7}{V_0}\right)\left(1 - \frac{\overline{V}_{M1}}{V_0}\right) . \qquad (18)$$

The ratio of ship-to-model momentum deficits can be written in terms of flat plate friction coefficients (assumed to be estimated from the ITTC correlation line) as

$$\frac{(C_F + C_A)_s}{C_{Fm}} = \frac{[(\overline{V}_7/V_0)(1 - \overline{V}_{M1}/V_0)]_s}{[(\overline{V}_7/V_0)(1 - \overline{V}_{M1}/V_0)]_m} \,. \qquad (19)$$

Note that a correlation allowance C_A is included with the ship friction coefficient. This is because the correlation allowance is generally considered as an additional surface roughness drag effect and so adds to the momentum deficit. Equation (19) can be solved for the ratio of ship-to-model inlet momentum velocity ratio D_{M1}, to give

$$D_{M1} \equiv \frac{(\overline{V}_{M1}/V_0)_s}{(\overline{V}_{M1}/V_0)_m} = \frac{1}{(\overline{V}_{M1}/V_0)_m} + \left(\frac{(C_F + C_A)_s}{C_{Fm}}\right)\left(\frac{(\overline{V}_7/V_0)_m}{(\overline{V}_7/V_0)_s}\right)\left\{1 - \frac{1}{(\overline{V}_{M1}/V_0)_m}\right\} , \qquad (20)$$

where $$\left(\frac{\overline{V}_{M1}}{V_0}\right)_m = B_{M1}\left(\frac{\overline{V}_1}{V_0}\right)_m .$$

Equations (13) and (20) form a pair of simultaneous equations for the ship-scale jet velocity ratio and the factor D_{M1}. From these factors, the scaled flow rate Q_J and mean velocity wake factor $(1 \;\; w) \;\; (\overline{V}_1/V_0)_s$ can be determined.

2.5 SUMMARY OUTLINE OF THE METHOD

The inlet wake scaling procedure can be summarized here as an outline:

- A model waterjet propulsion test conducted at Froude-scaled speeds and at the appropriate self-propulsion conditions should determine for each unit: the thrust force, the Station 1a capture area velocity ratio $(\overline{V}_1/V_0)_m$, the jet velocity ratio $(\overline{V}_7/V_0)_m$, and the propulsion flow rate Q_J.

- Data should be collected for the non-uniform velocity characteristics and representative flow pressures at the capture area planes and at the jet discharge planes in order to determine the momentum factors β_{M1} and β_{M7}, as well as the averaged pressure coefficients. The combined coefficients B_{M1} and B_{M7} are determined from these data.

- The various factors are inserted into Equations (13) and (20), and the expressions are solved simultaneously to determine the inlet velocity ratio factor D_{M1} and the scaled jet velocity ratio $(\overline{V}_7/V_0)_s$.

- Results for the main performance factors of inlet wake scaling are the jet velocity, and thus the flow rate $(Q_J)_s = (\overline{V}_7)_s(A_7)_s$; the capture area velocity ratio $(\overline{V}_1/V_0)_s = (\overline{V}_1/V_0)_m D_{M1}$, and thus the mean velocity inlet wake factor $(1 \;\; w) = (\overline{V}_1/V_0)_s$; and the inlet momentum velocity ratio $\overline{V}_{M1}/V_0$.

- The thrust deduction factor $(1 \;\; t) = R_i/T_{m,tot}$ determined at model scale remains the same at full scale because the scaling method is based on the principle of constant thrust loading.

3. EXAMPLE CASE

3.1 THE MODEL

The example for this discussion was chosen from the recently published study of waterjet propulsion applied to large sealift-type ships with design speeds of 36 knots or higher [7]. Principal particulars of the NSWCCD Model 5662-1 and the full scale ship are given in Table 1, and the hull form body plan is shown in Figure 2. The model hull, constructed of fiberglass, was sized with scale ratio λ = 34.121, and fitted with flush inlets for the four waterjet units arranged in a line across the stern. Model pump inlet diameter and nozzle exit diameter were 8.93 cm (3.517 in.) and 5.58 cm (2.2 in.) respectively. Figure 3 is a photograph of Model 5662-1.

3.2 MODEL MEASUREMENTS AND TESTING

Basic towing basin test measurements were made for the calm water resistance, heave, and trim on the unpowered model with covered inlet openings. For the model tests with active waterjet propulsion, the measurements included the pump rotor axial force, torque, and RPM. Results of these basic tests for the ship speed range of 15 to 42 knots are reported in Cusanelli, et al. [8].

For characterizing the waterjet thrust performance, measurements of wall or surface static pressures were made on the hull at Station 1a (capture area plane), on the inner wall of the casing at Station 3, and near the end of the jet nozzle at Station 6. LDV measurements of the axial velocity distributions were conducted on all four units at Station 1a, and at Station 3. At Station 6, LDV measurements were made on the port inboard and on the starboard outboard nozzles. Results for the nozzles where velocities were not measured were estimated by assuming symmetry. A full presentation of the LDV results is given by Fry and Jessup [9].

Flow rate calibrations using the bollard-thrust method were conducted at zero model speed, from which was developed the technique of determining very accurate volume flow rates from numerical integration of the Station 6 velocities out to the wall of the nozzle. The same approach was used for handling the Station 6 LDV measurements collected during the underway testing.

Model self-propulsion testing consisted of a series of over-and under-propelled runs in the towing basin that bracketed the desired operating condition for each speed. Model self-propulsion operation was determined at the point where the measured tow force matched the target tow force. These tests employed the conventional tow force estimate using flat plate skin friction coefficients calculated from the ITTC ship-model correlation line, and the correlation allowance coefficient C_A = 0.

3.3 ANALYSIS

At Station 6, the area-averaged velocities $\overline{V}_6$ passing through the nozzle area A_6 for each speed condition were used to calculate the flow rate values for each unit. The LDV velocity distributions were also used to compute β_{M6} and β_{E6}, and these, together with the nozzle pressures coefficients C_{p6} were used to estimate the jet velocities $\overline{V}_7$ and the jet velocity ratios JVR_0 at the simulated vena contracta. Analysis of the flow factors at Station 1a depended on the flow rate values determined at Station 6. Capture area values A_1 for each waterjet were estimated using self-similar trapezoidal shapes that were adjusted for the appropriate flow rate. Results for the Station 1a flow factors include the area-averaged inlet velocity ratio $\overline{V}_1/V_0 = (1 \quad w)$, β_{M1}, β_{E1}, and the combined factor momentum velocity ratio $\overline{V}_{M1}/V_0 = [(\beta_{M1} + \frac{1}{2}C_{p1})\overline{V_1}]/V_0$.

The refined jet system thrust for each unit was calculated from the momentum flux difference expression given in Equation (5).

3.4 RESULTS OF INLET WAKE SCALING

For the two sample ship speeds of 25 and 36 knots, Tables 2 and 3 summarize the details of self-propulsion operating conditions, the flow-factors, and the important velocity ratios at Stations 1a and 7. The first column of each table presents the refined results of the model self-propulsion tests with no wake scaling applied. Results in the second column of each table show the same performance features for the model scale, but with values modified by the Reynolds number scaling method presented in Section 2.4. While the total system thrust T_{unit} and thrust deduction factor $(1 \quad t)$ remain the same (with slight round-off differences), the self-propulsion flow rates, inlet capture area velocity ratio, and the jet velocity ratio are all increased by the wake scaling procedure. The third columns of Tables 2 and 3 show the effects of both the capture area wake scaling and the size-scaling on the performance results for the full-scale ship.

Figures 4 through 7 are included to show how the average over the four waterjet units of selected interaction factors vary within the ship speed range of 20 to 42 knots. Figure 4 shows that the inlet velocity ratios $\overline{V}_1/V_0$ and $\overline{V}_{M1}/V_0$ are nearly constant over these speeds. The jet velocity ratio JVR_0 varies within a fairly narrow range, dropping slightly to a minimum of 1.45 between the values of near 1.6. Figure 5 indicates the nearly constant values of both the energy and momentum non-uniformity factors over the speed range. Figure 6 shows that the nozzle pressure coefficient for Station 6 is consistently small and negative over the entire speed range, while the pressure coefficient at Station 1a displays a considerable variation from negative values at low speeds to moderate positive values at the high speeds.

Figure 7 displays the averaged thrust deduction fraction t -values determined for the current example model test results plotted versus the ship length Froude number. As a sample comparison between the trends of the present model and some available full scale estimation for this interaction factor, three spots for the 'correlation' thrust deduction fraction

$$t' = \text{(ship thrust–ship resistance)/ship thrust}$$

are also plotted in Figure 7. These points were obtained from analyzed trial results on a large semi-planing monohull ferry --- the MDV 3000 JUPITER class ship --- reported on by Svensson, et al. [10].

4. SUMMARY

This paper describes a waterjet inlet wake scaling procedure based on the similarity concept of equal thrust loading coefficient for self-propulsion at model and full scale.

For the example model test case provided, at the ship speeds of 25 knots and 36 knots, application of the inlet wake scaling method produces, respectively, the following changes: for the total system flow rate --- increases of 6.4% and 5.9%; for the jet velocity ratio --- increases of 6.6% and 5.8%; for the average capture area wake velocity ratio --- increases of 19.7% and 15.9%; for the average inlet momentum velocity ratio --- increases of 19.7% and 15.9%; and for the effective jet system power --- increases of 10.9% and 9.5%.

The total jet system thrust and thrust deduction factor remain unchanged (within round off accuracy) by the application of wake scaling.

The comparison of the general trends of t factor versus Froude number shown in Figure 7 was intended only to check if the orders of magnitude of the model test-derived values were reasonable. There is no ready explanation for the similarity of curves with respect to the parameter ship length Froude number, F_n .

Clearly, Reynolds number wake-scaling introduces significant changes in basic model-predicted thrust interaction factors. These results are viewed as part of the ongoing accumulation of information and experience at NSWCCD that should be useful for promoting understanding and assessing future waterjet propulsion projects involving large ships.

5. ACKNOWLEDGEMENTS

The author gratefully acknowledges the support of several programs and funding organizations. Initial impetus for the scaling method came during a project sponsored by the Gulf Coast Region Maritime Technology Center (CGRMTC) at the University of New Orleans, funded by an Office of Naval Research (ONR) Cooperative Agreement. Support for the work on the wake scaling of a specific example was provided by the NAVSEA PMS 385 Joint High Speed Sealift (JHSS) Program and from ONR through Dr. K-H Kim. Thanks go to Dr. Martin Donnelly, Dr. David Fry, and Mr. Dominic Cusanelli for providing data and photographs acquired during the waterjet powering experiments conducted for the JHSS project investigations [7].

6. REFERENCES

1. ITTC, "Report of the Waterjets Group, Appendix A," Proc of the 21st ITTC Triennial Meeting, Bergen and Trondheim Norway, 1996.

2. ITTC, "ITTC-Quality Manual for High Speed Marine Vehicles, Waterjets," 21st ITTC Documentation, 1996.

3. ITTC, "Report of the Specialist Committee on Validation of Waterjet Test Procedures," Proc. of the 23rd ITTC Triennial Meeting, Venice, Italy, 2002.

4. ITTC, "Report of the Specialist Committee on Validation of Waterjet Test Procedures," Proc. 24th ITTC Triennial Meeting, Edinburgh, Scotland UK, 2005.

5. Scherer, J.O., Mutnick, I., and Lanni, F., "Procedure for Conducting a Towing Tank Test of a Waterjet Propelled Craft Using Laser Doppler Velocimetry to Determine Momentum and Energy Flux," Proc. 26th ATTC Triennial Meeting, Glen Cove NY, July 2001.

6. Scherer, J.O. and Wilson, M.B., "Waterjet Inlet Wake Scaling," NSWC Carderock Division Report NSWCCD-50-TR-2008/051, 2008.

7. Jessup, S., Donnelly, M., Fry, D., Cusanelli, D., and Wilson, M., "Performance Analysis of a Four Waterjet Propulsion System for a Large Sealift Ship," Proc. of 27th Symposium on Naval Hydrodynamics, Seoul Korea, Oct 2008.

8. Cusanelli, D.S., Carpenter, S.A., and Powers, A.M., "Axial Waterjet (AxWJ) Model 5662 and Mixed-Flow Waterjet (MxWJ) Model 5662-1: Comparisons of Resistance and Model-Scale Powering with Propulsion Nozzle Designs," NSWC Carderock Division Report NSWCCD-50-TR-2007/076, 2007.

9. Fry, D.J. and Jessup, S., "JHSS Waterjet Performance Evaluation with Scanning Laser Doppler Velocimetry,"

NSWC Carderock Division Report NSWCCD-50-TR-2008/042, 2008

10. Svensson, R., Brizzolara, S., and Grossi, L., "Trial Result Including Wake Measurements From the World's Largest Waterjet Installation," Proc. RINA 98, International Conference on Waterjet Propulsion--Latest Developments, Amsterdam Netherlands, Oct 1998.

7. AUTHOR BIOGRAPHY

Dr Michael B Wilson is a senior naval architect in the Resistance and Propulsion Division at NSWCCD. His recent work is concerned with developing and executing projects on waterjet hull/propulsor interactions.

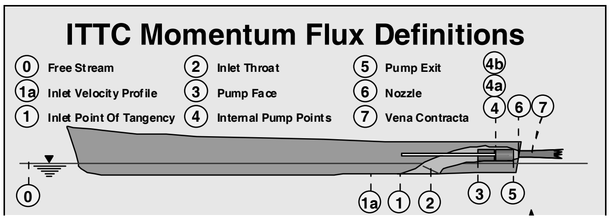

Figure 1. Waterjet Measurement Stations
{Station 1a is the Inlet Capture Area Plane}

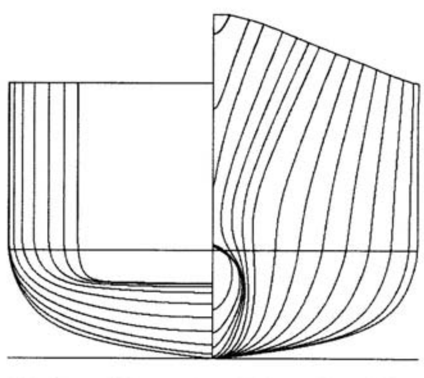

Figure 2. Body Plan of Model 5662-1 Hull Form

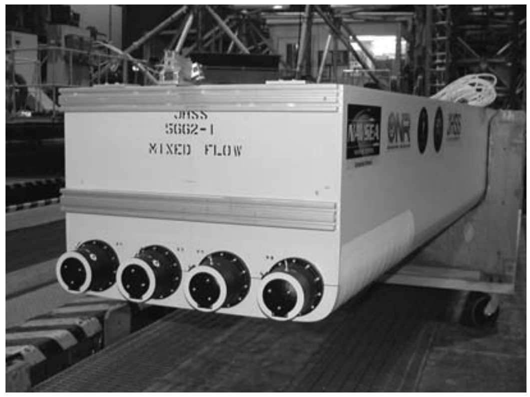

Figure 3. Stern View of Model 5662-1

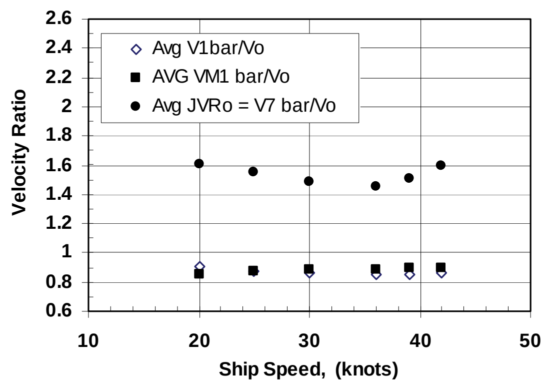

Figure 4. Inlet Wake Velocity Ratios and JVR_0

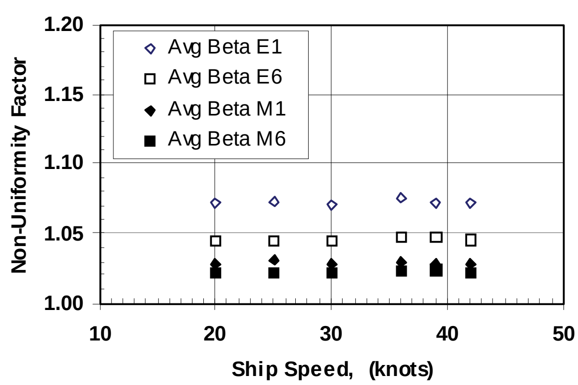

Figure 5. Average Non-Uniform Velocity Factors

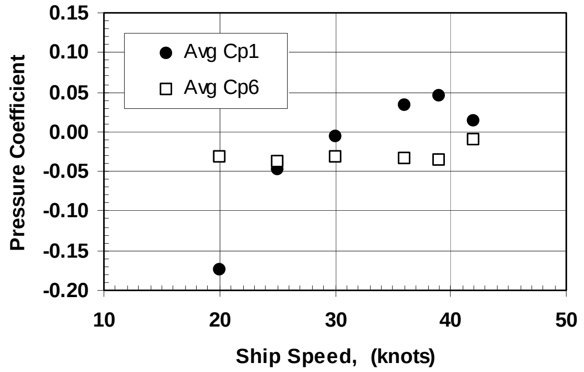

Figure 6. Average Pressure Coefficients at Station 1a and Station 6

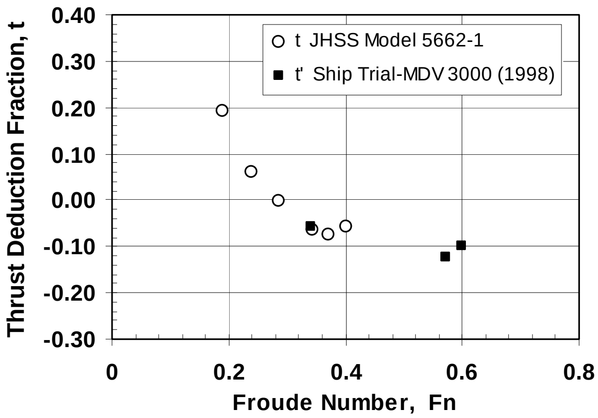

Figure 7. Comparison Plot of Model 5662-1 Thrust Deduction Fraction Values With Published Full Scale Trial Values for a Semiplaning-Type Mohonhull (from [10])

Table 1. Principal Particulars of Model 5662-1 and Ship

	Model	**Ship**
Length WL, L	8 76 m	298 8 m
Beam, B_X	0 9364 m	31 95 m
Draft (even keel), T_X	0 253 m	8 62 m
Displaced Volume	0 9098 m^3	36140 m^3
Displacement	0 9333 mt	37075 mt
Wetted Surface Area	7 77 m^2	9046 m^2
Max Sect Area, A_X	0 1885 m^2	219 5 m^2
Design Speed (Froude No)	6 16 knots (0 342)	36 knots (0 342)
Transom Area Ratio A_T/A_X	0 163	
Transom Draft Ratio T_T/T	0 247	
Transom Beam Ratio B_T/B_X	0 540	
Hull Length/Beam	9 352	
Hull Beam/Draft	3 706	
Hull Block Coeff	0 447	
Hull Prismatic Coeff	0 560	
Hull Max Section Area Coeff	0 797	
L / (Volume)$^{1/3}$	9 038	
Scale Ratio, λ	34 121	

Table 2. Summary of Example Waterjet Inlet Wake Scaling Results for Ship Speed 25 knots

	Model Unscaled Inlet Wake	**Model Scale for Ship Results** Scaled Inlet Wake	**Ship** Scaled Inlet Wake
Ship Speed, V_0 knots	4 295	4 295	25 1
Froude Number, F_n	0 238	0 238	0 238
Total Flow Rate, Q_J [4 units] m^3/s	0 03225	0 03432	233 4
Total Model Resistance, R_{Tm} N	76 24	76 24	
Model Ideal Resistance, R_i N	50 75	50 75	
Total Ship Resistance, R_{TS} N			2072100
Tow Force, F_D N	25 49	25 49	
Total Jet System Thrust [4 units], N	54 0	54 05	2207700
Effective Jet System Power (P_{JSE}) kW	0 1323	0 1467	34990
Average β_{M1}	1 031	1 031	1 031
Average $\beta_{M7} = \beta_{M6}$	1 022	1 022	1 022
Average β_{E1}	1 073	1 073	1 073
Average $\beta_{E7} = \beta_{E6}$	1 045	1 045	1 045
Avg Capture Velocity Ratio, $\bar{V}_1/V_0$	0 726	0 8687	0 8687
Avg Inlet Mom Vel Ratio, $\bar{V}_{M1}/V_0$	0 731	0 875	0 875
Avg Jet Vel Ratio, $\overline{V_7}/V_0$ JR 0	1 46	1 556	1 556
Thrust Deduction Factor, (1-t)	0 94	0 939	0 939
Thrust Deduction Fraction, t	0 06	0 06	0 06

Table 3. Summary of Example Waterjet Inlet Wake Scaling Results for Ship Speed 36 knots

	Model Unscaled Inlet Wake	**Model Scale for Ship Results** Scaled Inlet Wake	**Ship** Scaled Inlet Wake
Ship Speed, V_0 knots	6 182	6 182	36 1
Froude Number, F_n	0 343	0 343	0 343
Total Flow Rate, Q_{JT} [4 units] m^3/s	0 04349	0 04607	313 4
Total Model Resistance, R_{Tm} N	141 9	141 9	
Model Ideal Resistance, R_i N	93 23	93 23	
Total Ship Resistance, R_{TS} N			3806400
Tow Force, F_D N	48 65	48 65	
Total Jet System Thrust [4 units], N	87 32	87 41	3570000
Effective Jet System Power (P_{JSE}) kW	0 3002	0 3287	78390
Average β_{M1}	1 03	1 03	1 03
Average $\beta_{M7} = \beta_{M6}$	1 023	1 023	1 023
Average β_{E1}	1 075	1 075	1 075
Average $\beta_{E7} = \beta_{E6}$	1 048	1 048	1 048
Avg Capture Vel Ratio $\bar{V}_1/V_0$	0 733	0 8496	0 8496
Avg Inlet Mom Vel Ratio, $\bar{V}_{M1}/V_0$	0 767	0 889	0 889
Avg Jet Vel Ratio, $\overline{V_7}/V_0$ JR 0	1 37	1 45	1 45
Thrust Deduction Factor, (1-t)	1 0677	1 0666	1 0666
Thrust Deduction Fraction, t	-0 0677	-0 0666	-0 0666

CALCULATION AND ANALYSIS FOR VORTEX-INDUCED VIBRATION OF WATERJET GRID

Shuping Chang, **Yongsheng Wang** and **Zhiyang Pang,** Naval University of Engineering, China
Wenshan Xu, Guangzhou Marine Engineering Corporation

SUMMARY

When a waterjet ship sails in water areas which are full of wastes, the grid is usually needed to be installed at the mouth of the inlet duct so as to prevent the wastes entering into waterjet system and damaging the impeller. There are some instances at home that the grid was broken, and the shedding parts were sucked into the pump, which damaged the blades. This article aims at discovering the real cause that leads to a broken grid. Vortex-induced vibration may be one of the most important reasons. The control fluid volume, made up of the pump, the inlet, the grid and the hull, is defined and meshed by hexagonal structured elements. CFD method and LES turbulence model are employed to simulate the unsteady flow field. The results show that there are vortexes shedding from the grid. Fluctuant vortex-induced forces are acting on the grid. Model computation is carried on by FEA means at the same time. The comparison between the vortex-induced force frequency and the nature vibration frequency shows that vortex-induced vibration is one of the most important reasons which will cause a violent vibration of the structure, and then, the grid would be severely broken sooner or later. The results can provide suggestions to optimizing the configuration of the grid. Waterjet ships should be used appropriately so as to avoid vortex-induced vibration.

1. INTRODUCTION

As a special propelling way, waterjet uses the counter force generated by water flow at a high speed to keep the ship sailing[1-3]. The flow in the inlet duct has a big velocity. In the water areas which are full of wastes, a grid needs to be installed at the mouth of flow passage in order to prevent the wastes entering into waterjet propulsion system and damaging the pump when the ship is sailing at high speed[4, 5]. There are an abundance of instances at home now that the grid is damaged in a ship equipped with high-speed waterjet pumps. The damaged parts were sucked into waterjet pumps and caused badly damages to the blades or shaft system. In the end, the ship was unable to run normally and a huge economic loss was brought up.

Both the ship designer and waterjet pump manufacturer want to know the real reason why the grid was broken. Many experts have been pursuing for it from many aspects. Some experts figured out that the grid has sufficient strength ability. Some pointed out that coarse jointing would lead to a case of being destroyed. Some asserted that vibration resonance was the terminal reason after material investigations. Vortex-induced forces may produce violent vibration of the grid. But there is no detailed research work on this point of view up to the present.

Accurate hydrodynamic forces should be gained because they are the basic precondition for discovering the right answer. The grid works in a turbulent flow environment, both theory analysis and experimental research can't provide a better value. And vortexes are usually come into being when water flows around a slender object, so there are unsteady forces in existence. Vortex-induced vibration is often a reason of great importance that makes structures broken, such as fluid-conveying pipes, deep sea risers and submerged floating tunnels[6]. The grid is also a slender body and endures direct hydrodynamic forces. It's an exigent problem that whether vortex-shedding phenomena would occur when water flows around the grid.

The article will analyze vortex-induced vibration of the grid and make a judgment whether it's a vital reason. Firstly, a geometrical model is established. The model is constituted of waterjet pump, the inlet, the grid and the hull. The flow control volume is divided by hexagonal structured meshes. And then CFD method is employed to simulate the flow field of waterjet propulsion system and forecast its performance. The computational results agree well with experimental data, which indicate that the numerical model is authentic and creditable. It's observed that there are vortexes shedding from surface of the grid and a fluctuant force just acting on the grid. Meanwhile, the vibration models are extracted by using FEA method. The author will give a clear verdict whether vortex-induced vibration brings a bad grid structure after the comparison between vortex-induced force frequency and its nature vibration frequency. In the end, a suggestion is provided for optimizing the grid framework. Waterjet equipments should also be used rationally so that the malfunction wouldn't take place again.

2. INTRODUCTION OF RESEARCH OBJECT

An actual ship is propelled by four waterjet thrusters and four grids are installed. Every one of the grids has a configuration just as Figure 1. It's mainly composed of six grid pieces and a transverse bar. The cross section of the grid pieces is an unsymmetrical hydrofoil (Figure 2), and the bar is just a cylinder stick. Every component is connected with the inlet duct by bolts.

The four grids of this ship have come through two broken experiences when working at normal sailing conditions. The first time, the bar had 14 cracks and two sects had fallen off, three grid pieces had shed too. So the designer replaced them of new ones. But the new grids were broken only after ten hours the ship had navigated. Figure 3 is one broken grid of this ship. So it's urgent that the real reason should be found as soon as possible.

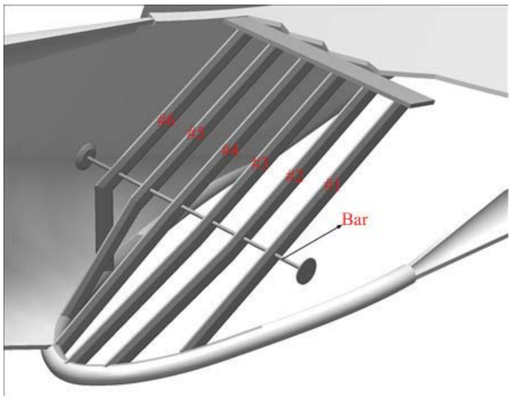

Figure 1 Framework of the grid

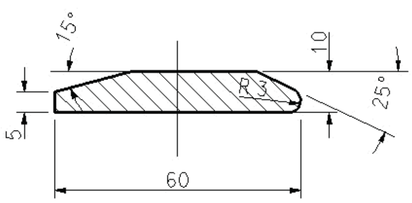

Figure 2 Cross-section of the grid

Figure 3 One broken grid

3. CALCULATION OF VORTEX-INDUCE FORCE

3.1 BASIC THEORY OF CFD

Generally speaking, there are three types of numerical models that are used in CFD realm. They are Reynolds-averaged Navier-Stokes simulation (RANS), direct numerical simulation (DNS) and large eddy simulation (LES). RANS usually ignores flow details and can't capture fine field, such as flow separation, vortex shedding phenomena et al. DNS method needs very small special step and time step, and a powerful enough computer or workstation is in necessary. Nowadays DNS only can solve simple issues, often two-dimensional problems. LES can give a more accurate result than RANS, and the computational time is in the tolerance range of the user. So LES is an approach full of vitality.

LES has a special solving idea. Firstly, it separates flow variables into big-scale ones and small-scale ones. Then the big-scale variables are solved by computing Navier-Stokes equation directly. Sub-grid scale model is used to express the relation between big-scale variables and small-scale variables. Nowadys, LES method has already been applied in many flow issues, which indicate that LES can usually give a good answer. Muralami[7] and Breuer[8] et al had studied flow around blunt bodies by employing LES method, and the results agreed well with experimental data. The author will adopt LES later.

3.2 CONTROL VOLUME AND MESH

In this paper, simulation and analysis are based on the geometry of a waterjet equipped in a full-scale ship. The geometrical model consisted of waterjet pump, the inlet duct, the grid and the hull is established. Considering the effects on inflow caused by ship speed and hull boundary layer, a large region under hull is needed, which makes up of the whole computation region with the factual waterjet and defined control volume, shown in Figure 4. By calculation and analysis, the depth of the region under the hull is about 8D based on the reasonable distribution of internal flow patterns, the width 10D and the length 30D, where D is the pump nominal diameter[9]. Figure 5 shows the matching correlation between the inlet duct and the grid.

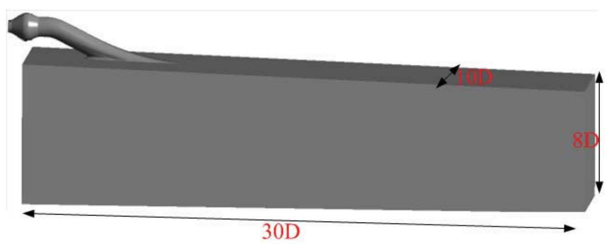

Figure 4 Control volume of waterjet

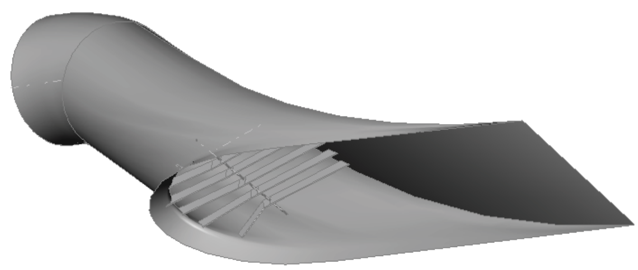

Figure 5 Matching of waterjet inlet duct and the grid

The whole control volume is divided by hexagonal structured mesh. Around the cross-sections of the blades, an O-grid is used to ensure good orthogonality of the boundary layer cells along the impeller surface. These cells are also used in the region near the hub surface. The remainder of the volume between the impeller blades is filled with additional hexagonal cells. The stator bowl is meshed with another group of hexagonal cells, which follow the guide vanes curvature. The layer of extruded cells fills the tip region between the impeller blades. In this way, water can flow over the tip from pressure to the suction side of the blade.

Several thin layers of O cells are created at the inlet duct walls and the grid walls to get the satisfied y+ values. It will do a great help to get high quality cells in the boundary layers and simulate the intricate flow field. The number of the whole computational region is 3,100,000. Figure 6 shows surface mesh of different components of waterjet propulsion system.

(a) Surface mesh of waterjet pump

(b) Surface mesh of the inlet

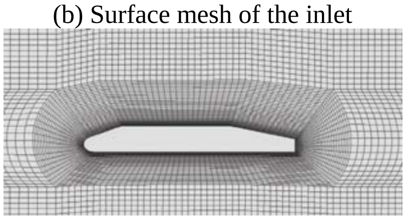

(c) Mesh around the grid

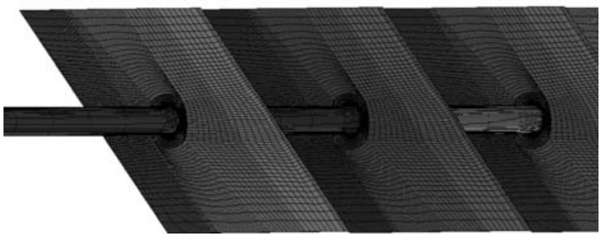

(d) Surface mesh of the grid

Figure 6 Surface mesh of different components

3.3 NUMERICAL APPROACH

The rotor is a revolving component, and its revolving frequency has a big distinction with vortex-induced force frequency. There is no appropriate time step for both of them. The author has no good choice but to design a new scheme just as the follows.

Above all, turbulence model is set as SST $k \quad \omega$ model. Rotation of the impeller can be implemented via the quasi steady Multiple Frames of Reference Method[10,11,12] so as to save much computational time. The region of rotor is in a relatively revolving reference, the other regions are in an absolutely stationary reference. The numerical domain is bounded by a number of surfaces at which different types of boundary conditions are imposed. At the inflow plane a non-uniform velocity profile is prescribed according to a certain hull boundary layer thickness. The opposite end of the control volume could have been set as an outlet or an opening, the latter of which is simply a pressure field that allows fluid to flow in or out. In this paper it is defined as an outlet. The outboard boundary and the bottom boundary are set as free slip walls. The hull, the inlet duct and the grid are defined as no-slip walls. A prescribed static pressure condition is applied at the nozzle outlet plane.

The hydrodynamic forces of all the components of the grid are observed in a monitor window during the whole computational process. The data will be extracted only after the monitor curves are steady. The numerical results of thrust and power agree well with characteristic curves supplied by manufactures, the maximal warp is smaller than 5%. All indicate that the method of using CFD to predict and analyze performance of waterjet propulsion system is feasible and credible.

And then, in order to save computational time, waterjet pump is taken out of the control volume. But the boundary variable distributions of the pump inlet are picked out, which will be used as boundary conditions of the duct outlet. The control flow volume is only left by the inlet, the grid and the hull. Unsteady computation is carrying on by LES model, the time step is prescribed as 5×10^{-5}s. The force monitor will do a great favour to determinant whether the computation is in convergence state. Another hundred of periods are calculated after the force monitor curves fluctuate regularly.

3.4 ANALYSIS OF VORTEX-INDUCED FORCE

The calculated results show that there are vortexes shedding from the grid. The wakes of flow around the grid swing from left to right or from right to left time after time. Figure 7 expresses that the vortex-induced force is pulsate. The lateral lift force of a grid piece is much greater than its drag. The lift will play a more important roll in arousing strong vibration.

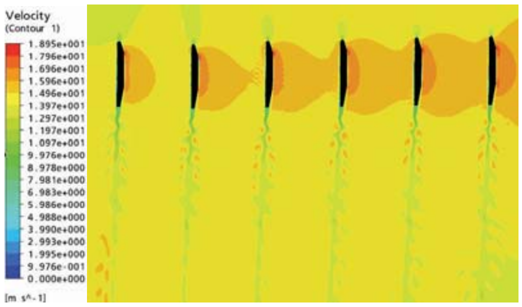

Figure 7 Velocity distribution of flow around the grid

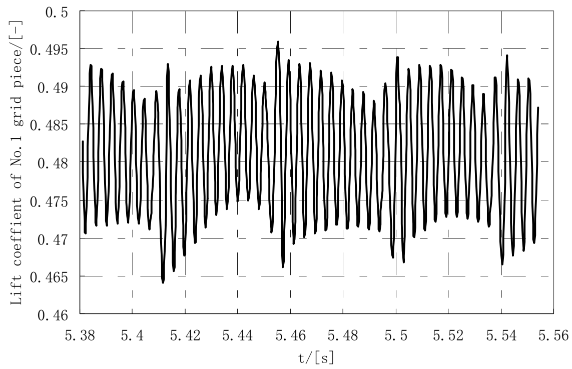

Figure 8 Lift force coefficient of No. 1 grid piece vs. time when at full power advancing five working condition

Evaluation of the periodic behaviour of the solution is based on a Fourier transformation of the fluctuations. Because the grid have a complex framework and the author will analyze vortex-induced force of every component separately. Table 1 tells different component has a diverse vortex-induced force frequency. The vortex shedding frequency will go up with the increase of sailing speed.

Table 1 Vortex-induced force frequency at different working conditions(Hz)

Working conditions	#1 piece	#2 piece	#3 piece	#4 piece	#5 piece	#6 piece	bar
Full power advance one	131 59	140 12	133 36	151 16	156 08	146 90	124 25
Full power advance one	157 51	176 74	185 91	189 85	198 82	182 46	156 24
Full power advance one	225 56	235 99	246 18	247 23	231 15	236 15	208 64
Full power advance one	299 14	308 79	325 85	316 69	319 58	327 87	265 73
Full power advance one	349 86	355 19	376 97	386 24	377 58	375 04	341 38
Part power advance one	116 25	120 25	127 35	125 66	134 58	142 39	115 16
Part power advance two	157 55	168 17	175 47	173 24	186 78	161 94	147 18
Part power advance three	247 01	258 71	280 73	286 49	257 69	270 21	217 80

4. MODEL ANALYSIS OF THE GRID

The FEA model is established for modal analysis. The grid pieces are divided into many hexahedron elements and the transverse bar is substituted by a line which has the property of standing for a beam. The total number of nodes is 35,846 and the total number of FEA elements is 25,464. Based on the fixing criterion, every node of both ends of the grid pieces and the transverse bar are restricted in fastness, just as Figure 9.

MSC. NASTRAN software and Lanczos method are employed to computing vibration frequencies. Figure 10 shows the first rank vibration shape, only the No.3 grid piece is vibrating. Figure 11 tells that the bar will metamorphose greatly when grid pieces have a vibration direction vertical to the whole grid plan. In the frequency range of 430Hz to 450Hz, every component has a big vibration deformation, just as Figure 12.

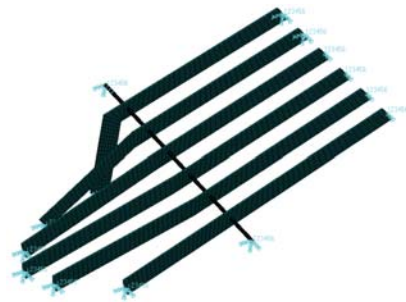

Figure 9 Mesh and boundary condition of FEA model

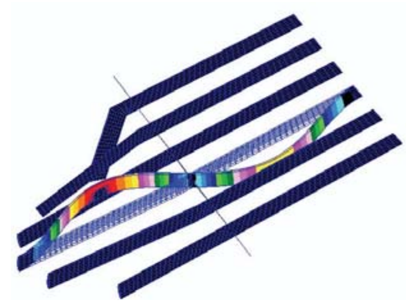

Figure 10 Vibration deformation of the first rank

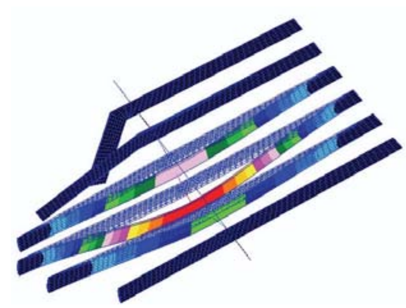

Figure 11 Vibration deformation of the bar

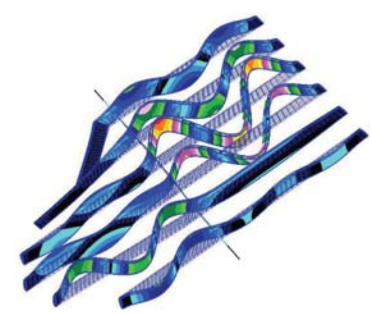

Figure 12 Vibration deformation of all components

5. ANALYSIS OF VORTEX-INDUCED VIBRATION

The grid has various kinds of vibration model due to its intricate framework. But usually there is only one component which is in the state of vibration. So it's necessary to analyzing every part individually.

There is a parameter η that can judge whether vortex-induced vibration will happen or not. It's defined as

$$\eta = \left|\frac{f_i - f_e}{f_e}\right| \times 100\%$$

In this expression, f_i presents the nature vibration frequency, f_e presents the frequency of the actuator, η is called frequency remaining parameter which shows the difference between f_i and f_e. If η is smaller than 30%, it's often thought that the structure is at stake in engineering.

The results show that there are big gaps between vortex-induced force frequency and every grid piece's first rank vibration frequency. But the second and third rank would also arouse an intense oscillation and bring a broken structure. The author will keep on analyzing vibration model further.

Table 2 The second rank modal analysis

The grid piece	f_i (Hz)	Working conditions	f_e (Hz)	η
#1	164 12	Full power advance one	131 59	19 82
		Full power advance two	157 51	4 03
		Part power advance one	116 25	29 17
		Part power advance two	152 55	7 05
#2	93 83	Part power advance one	119 05	26 88
#3	88 97			
#4	100 17	Part power advance one	125 66	25 45
#5	144 54	Full power advance one	156 08	7 98
		Part power advance one	134 58	6 89
		Part power advance two	186 78	29 22
#6	198 305	Full power advance one	146 90	25 92
		Full power advance two	182 46	7 99
		Full power advance three	236 15	19 08
		Part power advance one	142 39	28 19
		Part power advance two	161 94	18 34

Table 3 The third rank modal analysis

The grid piece	f_i (Hz)	Working condition	f_e (Hz)	η
#1	172 69	Full power advance one	131 59	23 80
		Full power advance one	157 51	8 79
		Part power advance two	152 55	11 66
#2	156 58	Full power advance one	140 12	10 51
		Full power advance two	176 74	12 88
		Part power advance one	119 01	23 97
		Part power advance two	168 17	7 40
#3	139 60	Part power advance one	127 35	8 78
		Part power advance two	175 47	25 69
#4	156 58	Full power advance one	151 16	3 46
		Full power advance two	189 85	21 25
		Part power advance one	125 66	19 75
		Part power advance two	173 24	10 64
#5	231 54	Full power advance two	198 82	14 13
		Full power advance three	231 15	0 17
		Part power advance two	186 78	19 33
		Part power advance three	257 68	11 29
#6	250 85	Full power advance two	182 46	27 26
		Full power advance three	236 15	5 86
		Part power advance three	270 21	7 72

Table 4 Modal analysis of the bar

Rank	f_i (Hz)	Working conditions	f_e (Hz)	η
1	139 60	Full power advance one	124 25	10 996
		Full power advance two	156 24	11 92
		Part power advance one	115 16	17 51
		Part power advance two	147 18	5 43
2	156 58	Four power advance one	124 25	20 65
		Full power advance two	156 24	0 22
		Part power advance one	115 16	26 15
		Part power advance two	147 18	6 01
3	172 69	Full power advance one	124 25	28 05
		Full power advance two	156 24	9 53
		Full power advance three	208 64	20 24
		Part power advance one	115 16	33 31
		Part power advance two	147 18	14 77
		Part power advance three	217 80	26 12

Table 5 Modal analysis of the whole grid

Rank	f_i (Hz)	Working conditions	η
1	443 36	Full power advance five	Every component has a η smaller than 30%
2	459 71	Full power advance five	Every component has a η smaller than 30%

Table 2 tells that the vortex-induced force wouldn't bring a strong vibration to No. 3 grid piece. But it's only an exception. All the other grid pieces have a similar vortex-induced force frequency with their second rank nature vibration frequency. Table 3 shows that every grid piece can't escape from the fate of the third rank vortex-induced vibration. There are a lot of vortex-induced force frequencies close to the bar's vibration frequencies of the first three ranks. As a whole, the nature vibration frequency is smaller that vortex-induced force frequency.

But the vortex-induced frequency of low speed working conditions is small too, and they are prone to approach each other. Relatively speaking, low-speed working is easier to bring bad ending. But high-speed sailing conditions such as full power advancing five, every component will be in the state of vortex-induce vibration, which also has fatal damages.

6. CONCLUSIONS

In this paper, a method for identifying vortex-induced forces on the grid has been proposed and a prediction model for vortex-induced vibration of the waterjet grid is developed. The numerical technique is used to obtain a relatively exact vortex-induced force frequency, which can be conveniently used to predict whether vortex-induced vibration is taking place or not. CFD and FEA methods can play an important role in forecasting vortex-induced vibration. The prime conclusions are as follows.

(a) CFD method offers an effective implement to depict the complex flow around the waterjet grid. It provides both steady force and fluctuant force which will do a great help to mouse out the real reason for which the grid was broken.

(b) There are existing vortexes shedding from the grid, which give a fluctuant force to the structure of the grid. The vortex-induced force frequency has a wide rang. There are many situations on which the vortex-induced force frequencies of different grid pieces are close to their low-level nature vibration frequency, such as the second and the third rank. The transverse bar also has an analogical vibration frequency with its vortex-induced frequencies of the first three ranks. The frequency distinction is even smaller than 10%, which would lead a broken grid piece and a broken bar sooner or later.

(c) The grid pieces are sensitive to lower pulsating frequencies, but the transverse bar is sensitive to higher ones. Relatively speaking, the transverse bar is more prone to be damaged.

(d) The section shape of the grid piece should be modified and optimized for reducing the lift force. So that the vortex-induced vibration won't be so violent and the grid can't be broken too easily.

6. REFERENCES

1 YONGSHENG W., JIANGMING D., 'Research on the relationship between waterjet power absorption and vessel speed', International Conference on Waterjet Propulsion 4, London, RINA, 2004.

2 BLOUNT D. L., BARTEE R. J., 'Design of propulsion systems for high-speed craft', Marine Technology, Vol. 34, 1997.

3 ALLISON J. L., 'Marine waterjet propulsion transaction', Society of Naval Architects and Marine Engineers, Vol. 101, 1993.

4 CHANG Z., SHILIAN Z., 'The finite element calculation and analysis for strength and mode of intake grid', China Offshore Platform, Vol. 6, 2007.

5 ZHONG L., ZHIJIAN C., CHUNSHENG S., 'Vortex-induced effect and structural strength of the channel grating in waterjet propulsion', Ship Engineer, Vol. 2, 2007.

6 GUOHE J., KAIXIANG F., ZHENFU G., 'Influence factor analysis for the vortex-induced vibration of towed-cable model', Journal of Vibration and Shock, Vol. 24, 2005.

7 MURALAMI S., 'On turbulent vortex shedding flow past 2D square cylinder predicted by CFD', Journal of Wind Engineering and Industrial Aerodynamics, Vol. 54, 1995.

8 BREUER M., 'A challenging test case for large eddy simulation: high Reynolds number circular cylinder flow', Heat and Fluid Flow, Vol. 21, 2000.

9 CHENGJIANG L., YONGSHENG W., ZHIHONG Z., 'Study on flow control volume in numerical simulation of waterjet' Journal of Hydrodynamics (Ser.A), Vol. 5, 2008.

10 NORBERT B., 'Numerical analysis of a waterjet propulsion system', Netherlands: Library Eindhoven University of Technology, 2006.

11 NORBERT B., VERBEEK R., 'CFD simulations of the flow through a waterjet installation', International Conference on Waterjet Propulsion 4, RINA, London, 2004.

12 NORBERT B., BART E., 'Review of thrust prediction method based on momentum balance for ducted propellers and waterjets', Proceedings of FEDSM2005, Houston, ASME, 2005.

7. AUTHORS BIOGRAPHY

Shuping Chang is a master graduate student of Marine Engineering at the University of Naval Engineering, P. R. China. This year he will get his master degree and his master thesis is about vortex-induced vibration of waterjet grid.

Yongsheng Wang is a professor at the University of Naval Engineering, P. R. China. Since 1982 he has published more than 80 papers and his main research interests are marine power plant and its characteristics analysis.

Zhiyang Pang holds the current Chair in Department of Mechanics Rngineer, a associate professor at the Naval University of Engineering, P. R. China. His main research interests are marine power plant and its characteristics analysis.

Wenshan XU is a senior engineer of Guangzhou Marine Engineering Corporation. Her main research interests are ship designing and marine power plant.

AUTHORS' CONTACT DETAILS

D Borrett,
Hamilton Jet, New Zealand
Dick.Borrett@hamjet.co.nz

N Bulten,
Wärtsilä Propulsion Netherlands BV, The Netherlands
Norbert.Bulten@wartsila.com

Q Yang,
Naval University of Engineering, China
yqfhaijun2008@126.com

M Zangeneh,
University College London, UK
m.zangeneh@ucl.ac.uk

M Heder,
Rolls-Royce AB, Sweden
mats.heder@rolls-royce.com

C Sun,
University of Naval Engineering, China
sclhgd@126.com

A Gany,
Israel Institute of Technology, Haifa, Israel
gany@techunix.technion.ac.il

Y Wang,
University of Naval Engineering, China
yongshengwang666@126.com

C Liu,
Naval University of Engineering, China
riverlcj@163.com

M Donnelly,
Naval Surface Warfare Center, Carderock Division, W.Bethesda, MD, USA
martin.donnelly@navy.mil

P Modig,
MJP Marine Jet Power AB, Sweden
patrik.modig@mjp.se

M Wilson,
Naval Surface Warfare Center, Carderock Division (NSWCCD), USA
michael.b.wilson@navy.mil

S Chang,
Naval University of Engineering, China
changshuji@yahoo.com.cn

MTD MARINE TECHNOLOGY DEVELOPMENT Ltd.

MJP WATERJETS
AN COMPANY

Active Rudder Control

WATERJET PROPULSION 5

RINA, December 2008, London

Introduction

MJP Waterjets presents **active rudder control** intended to improve overall

performance and

maneuverability

of the vessels with waterjet propulsion

Why it is necessary?

Deflecting the steering nozzle of a waterjet

- Provides steering control input
- Stabilise heading

In real sea conditions, steering is always activated with the result of

- Substantial thrust losses
- Increased yawing of the vessel
- Reduction in the vessel's speed or increase in the engine output to compensate for loss of waterjet efficiency

Why it is necessary?

Speed performance analysis

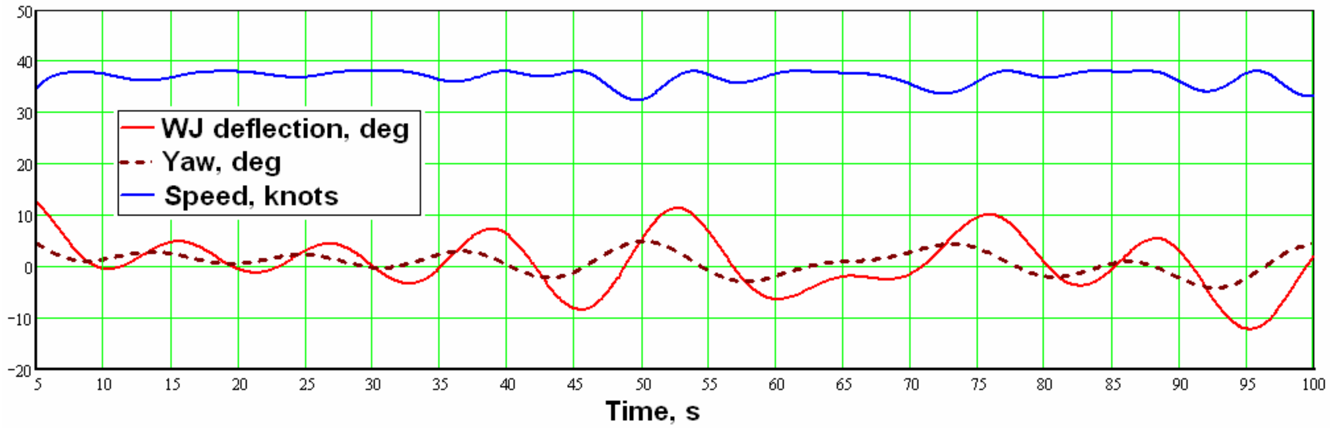

Vessel steered with waterjet nozzles

Average speed 36.8 knots

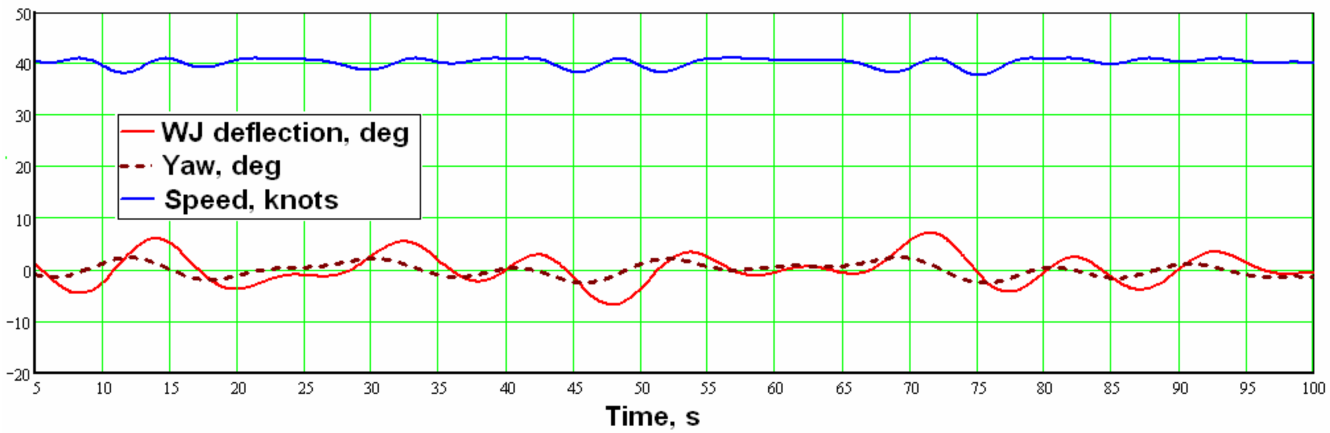

Vessel steered with ***active rudder control***

Average speed 40.1 knots

MTD MARINE TECHNOLOGY DEVELOPMENT Ltd.

MJP WATERJETS AN OO COMPANY

How is this to be dealt with?

Active rudder control:

- one or two auxiliary rudders, specially designed and shaped
- small area compared to ‘normal’ rudders
- directional control of the vessel at operational speeds
- waterjet steering nozzles remain fixed and waterjet operates as a booster unit with the claimed thrust and efficiency

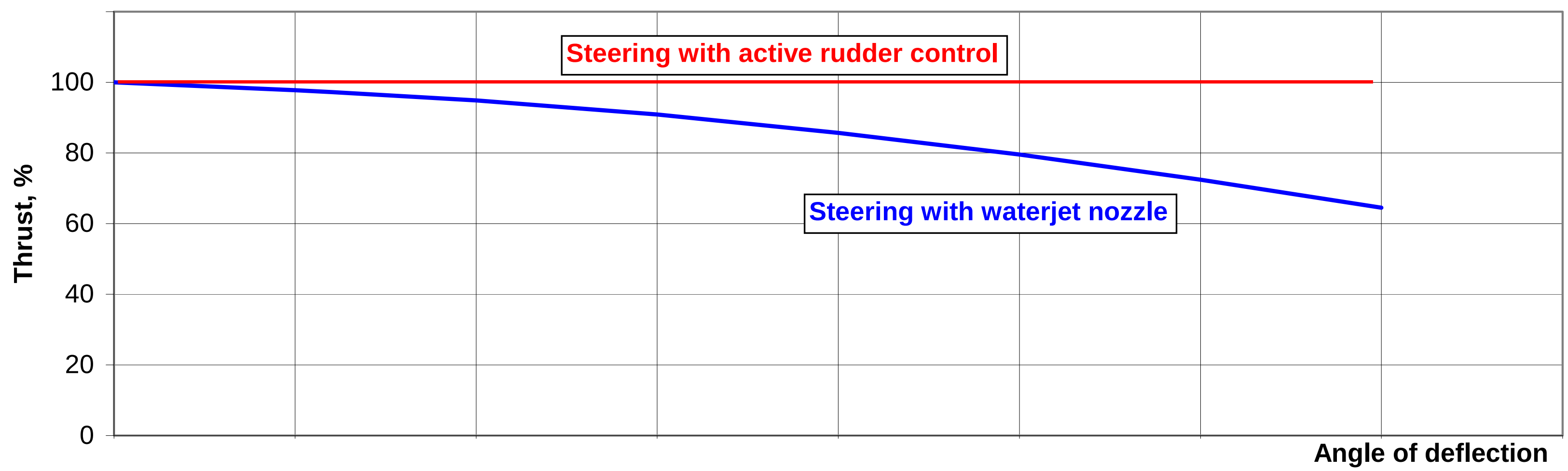

How is this to be dealt with?

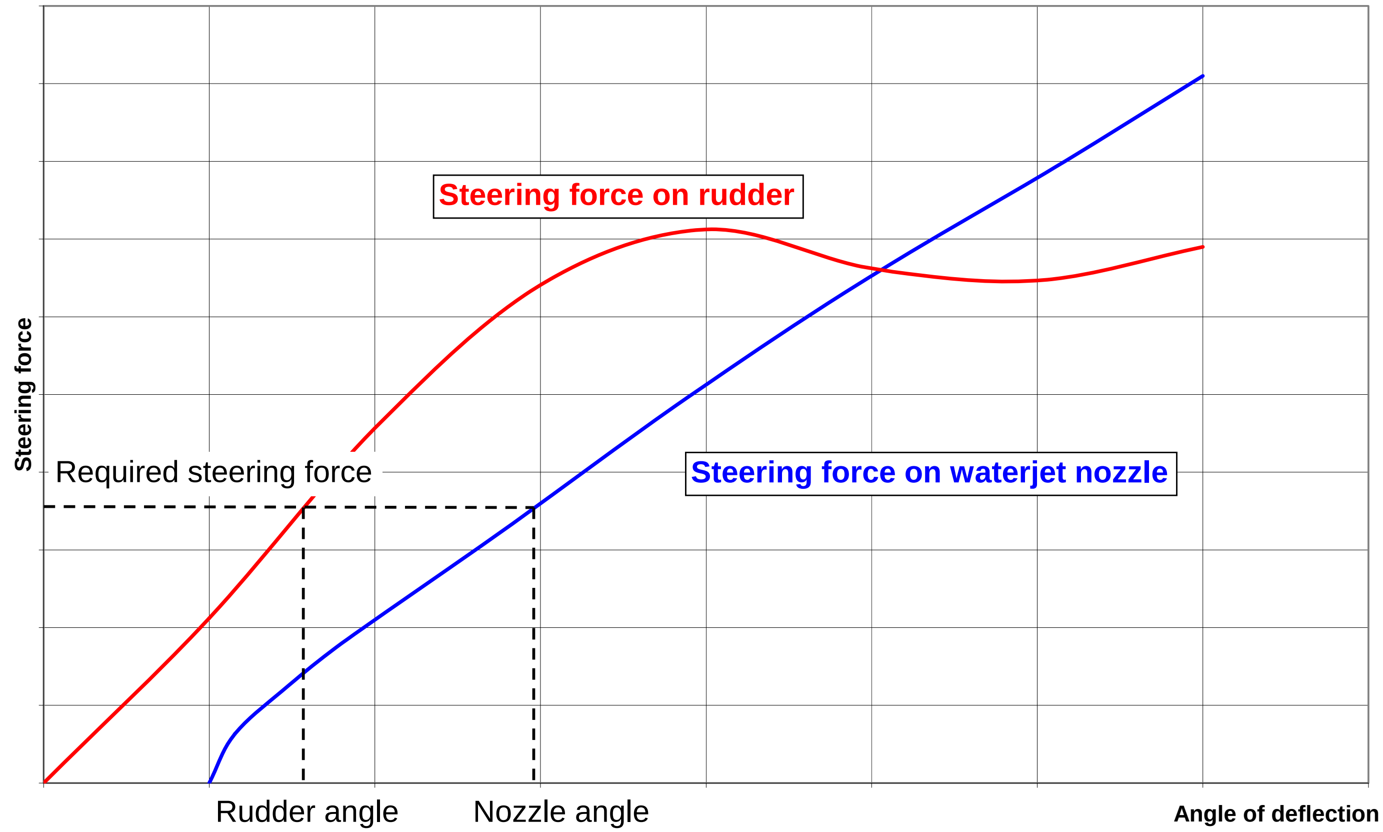

Active rudder control requires less hydraulic power to steer the vessel compared to waterjet-only steering and has a favourable effect on the hydraulic system lifetime

MJP active rudder control

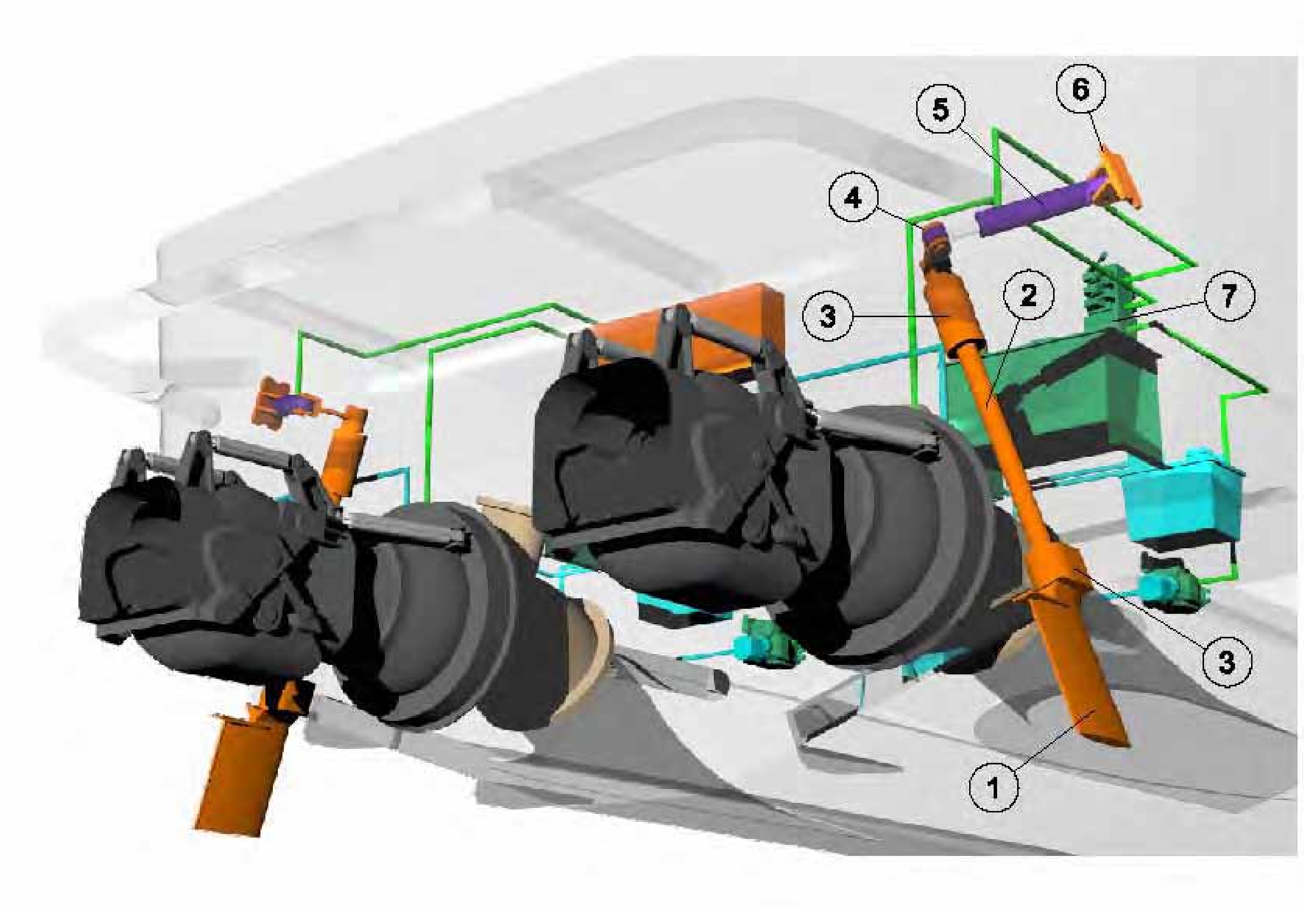

1-Rudder blade

2-Rudder stock

3-Rudder stock basement

4-Tiller

5-Actuator

6-Actuator basement

7-Hydraulic unit

Increased course stability – lower fuel consumption

Use of **active rudder control** makes it possible to keep the vessel on its course even at rough sea, thus minimising the way to target point while maintaining high performance of the waterjet propulsion system

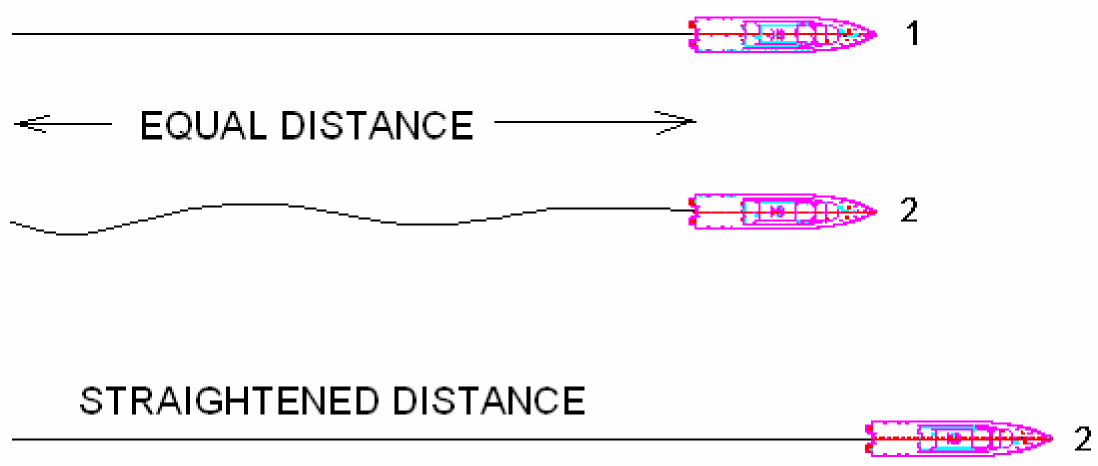

*1. Vessel steered with **active rudder control***

2. Vessel steered with waterjet nozzles

It is clear to understand that the average speed on a given distance is higher for No.1 vessel

MTD MARINE TECHNOLOGY DEVELOPMENT Ltd.

MJP WATERJETS AN COMPANY

Incredible maneuverability

The vessel with waterjets propulsion and **active rudder control** can perform sharp turns with minor speed losses compared to full turns typical for the vessels with waterjets steering nozzle only.

Combined steering by waterjet nozzles and rudders at lower speeds, ensuring high maneuvering capabilities

Integration in MJP Control System

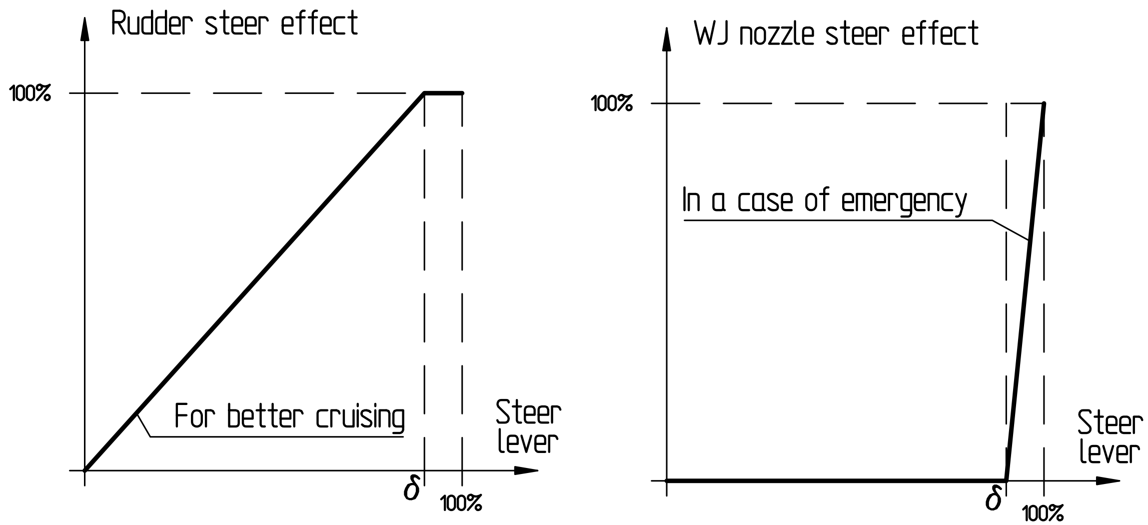

- The algorithm of **active rudder control** is implemented in the MJP Waterjets' Vector Control System.
- Steering at high speed by **active rudder control** only
- Combined steering in emergency improves the safety of operations

Supply and installation

- The rudder blades and rudderstocks manufactured by the shipyard or supplied by MJP Waterjets.
- The hydraulic equipment is supplied by MJP Waterjets.
- Integration in the hydraulic system and waterjet control system.
- Easy mounting on the transom or on the bottom of the ship.
- No change in vessel draught

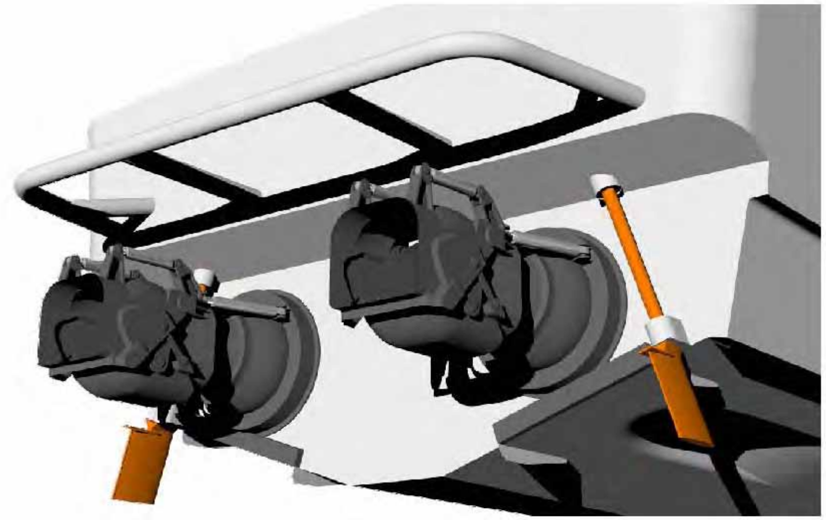

MTD MARINE TECHNOLOGY DEVELOPMENT Ltd.

MJP WATERJETS AN COMPANY

Retrofitting

Compact size, easy mounting and the same or updatable control system allow the **active rudder control** to be retrofitted on the existing vessels equipped with MJP propulsion system

Operating experience

- Several mono and twin-hulled vessels are currently fitted with MJP Waterjets steerable propulsion systems featuring auxiliary rudders.
- The available operating experience has shown a substantially higher quality of steering control compared to the standard version, particularly when moving in following seas.
- An annual fuel economy up to 8-10% has been achieved

Installation examples

Coast Guard Ship

Installation examples

SuperFoil Passenger Ferry

Installation examples

High Speed Patrol Boat

Waterjet Propulsion 5-International Conference

RINA-The Royal Institution of Naval Architects

Calculation and Analysis of Vortex-induced Vibration of Waterjet Grid

Shuping Chang
Ph.D. Candidate
Naval University of Engineering
P.R. China

OUTLINE

1. Introduction
2. Calculation of vortex-induced force
3. Analysis of vortex-induced force
4. Modal analysis
5. Analysis of vortex-induced vibration
6. Conclusions

1. Introduction

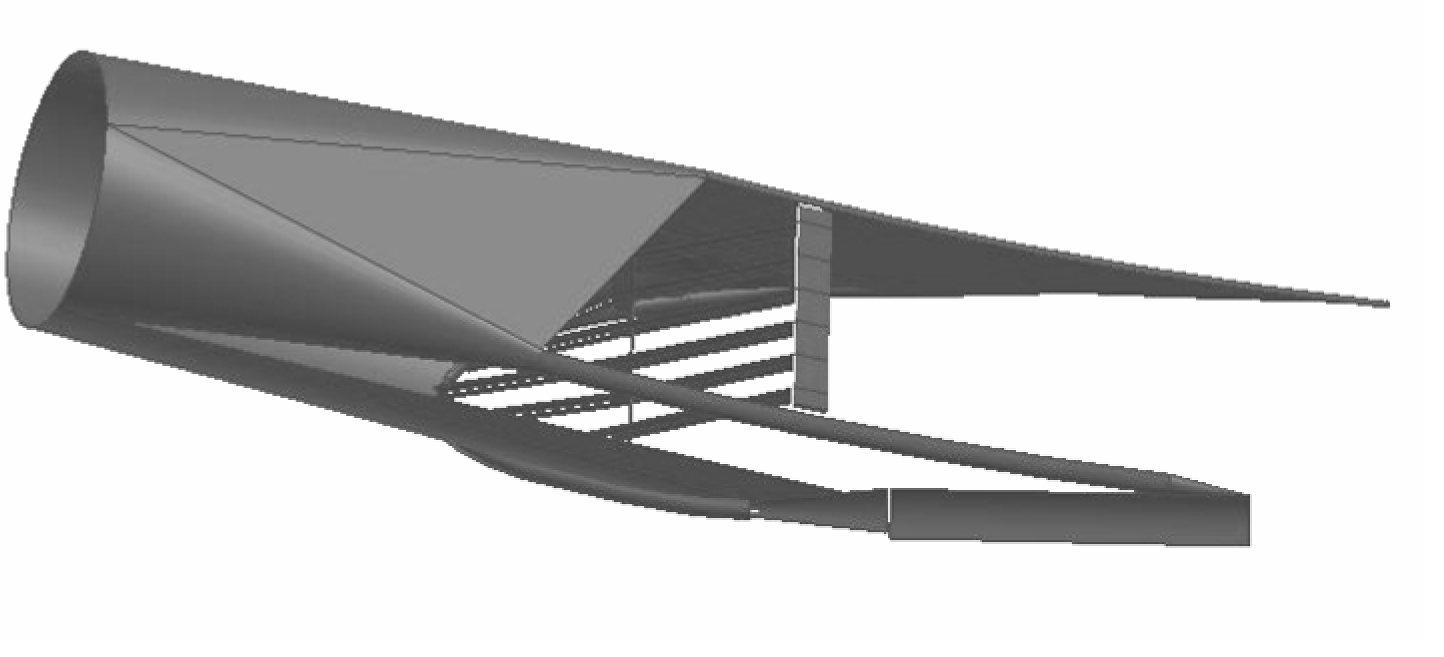

Waterjet inlet and the grid

1. Introduction

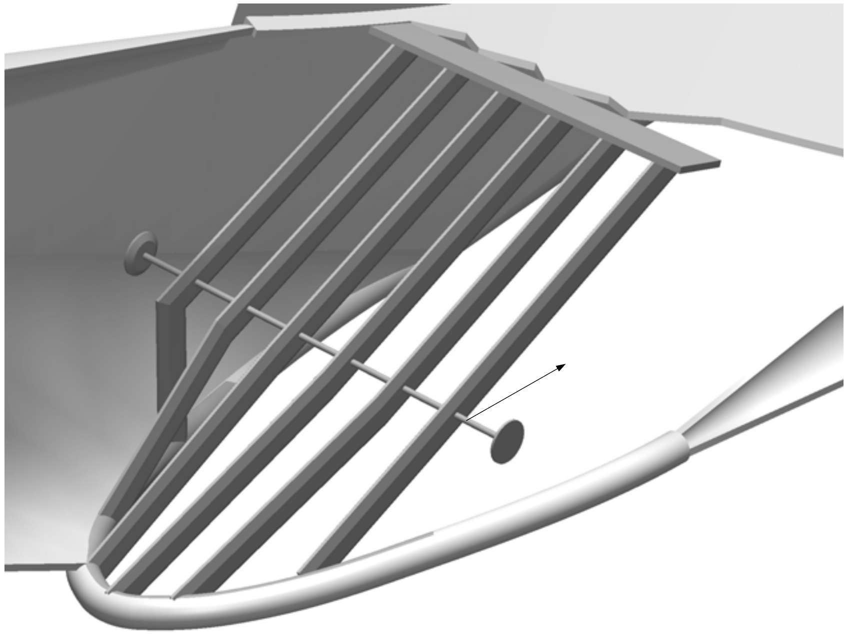

Framework of the grid

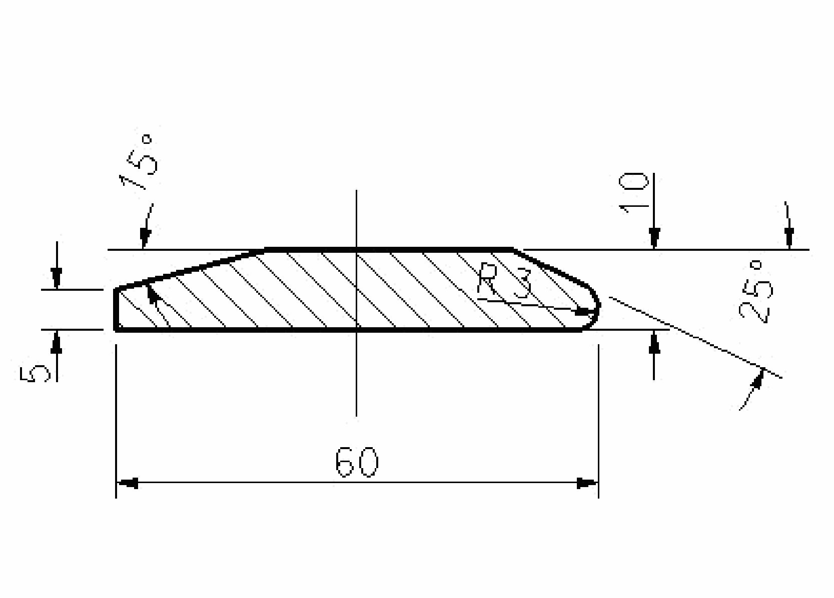

Cross-section of the grid

1. Introduction

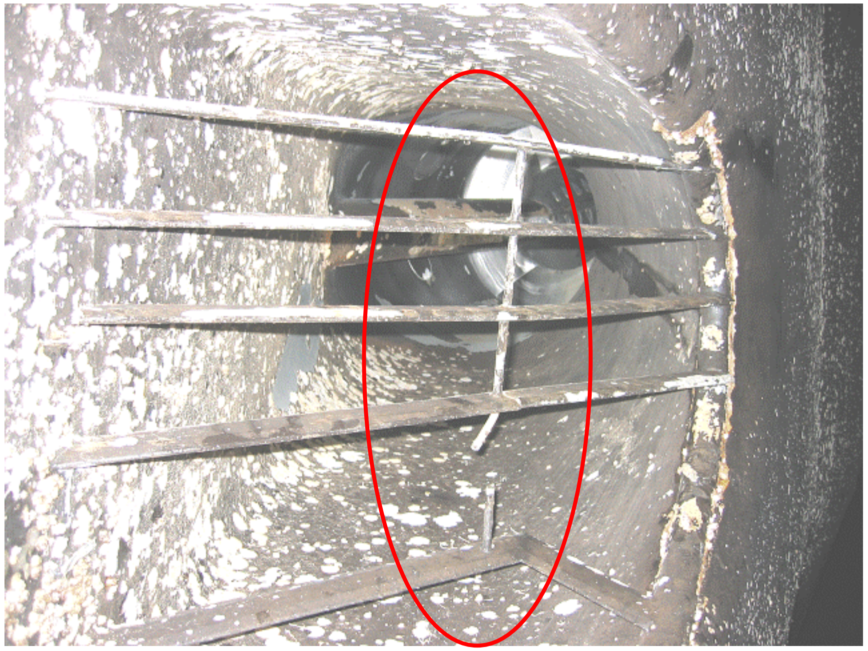

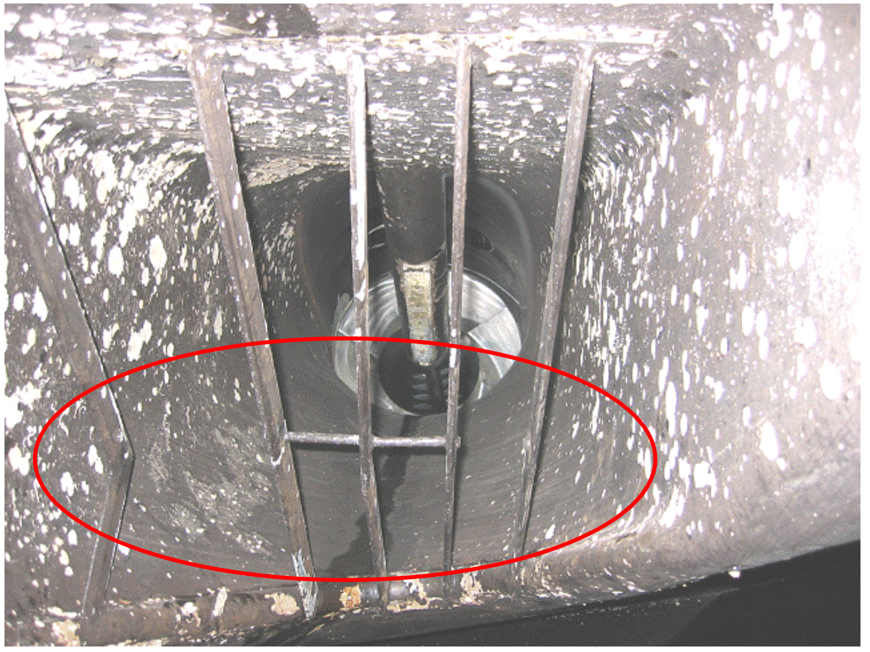

The broken grid

2. Calculation of vortex-induced force

Geometrical modeling

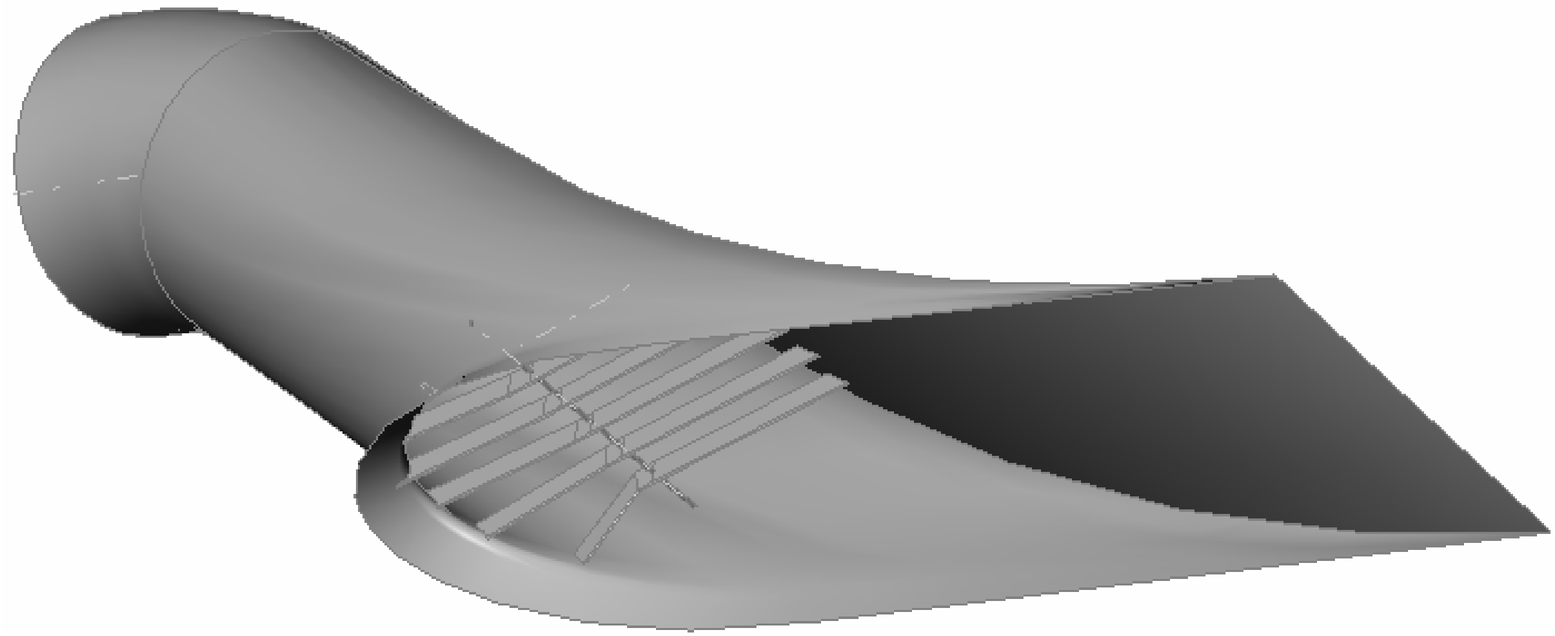

Matching of waterjet inlet duct with the grid

2. Calculation of vortex-induced force

Geometrical modeling

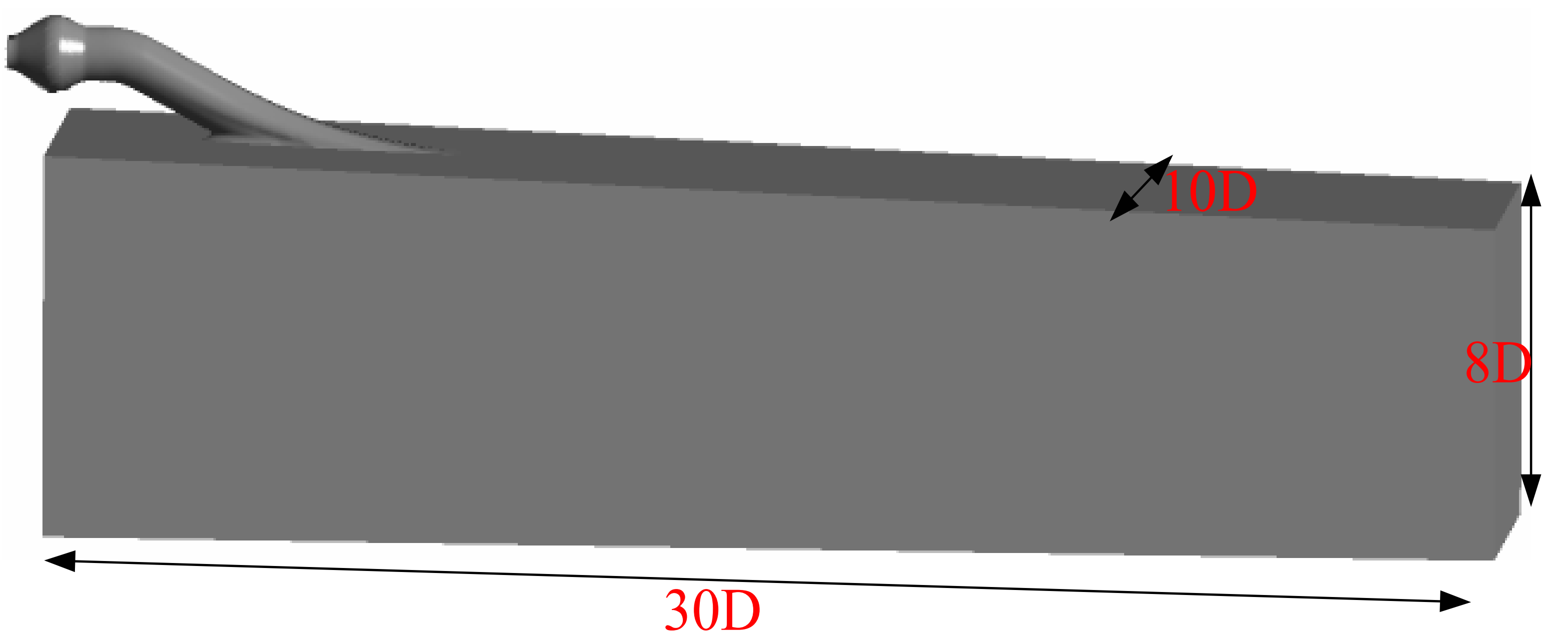

The control volume of waterjet propulsion system

2. Calculation of vortex-induced force

Mesh

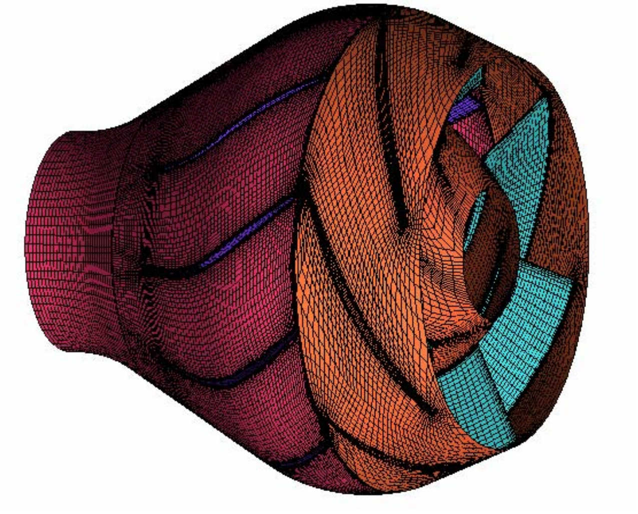

Surface mesh of waterjet pump

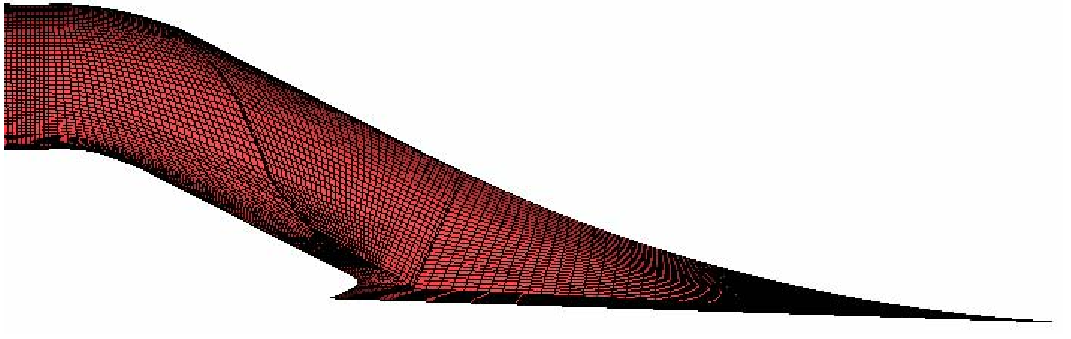

Surface mesh of the inlet duct

2. Calculation of vortex-induced force

Mesh

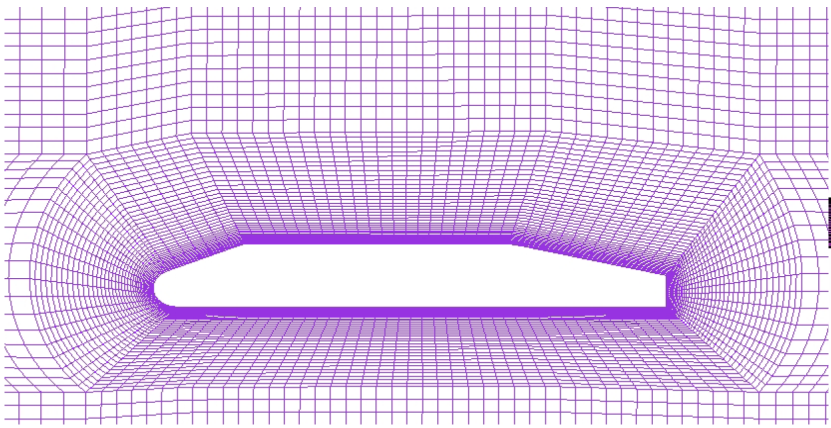

Mesh around the grid

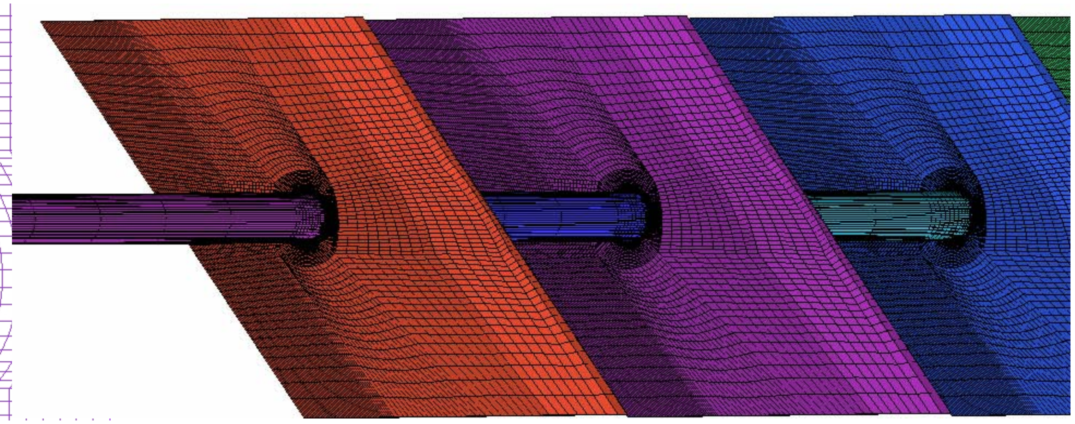

Surface mesh of the grid

2. Calculation of vortex-induced force

Numerical approach

Firstly, turbulence model is set as SST and a quasi-steady approach with MFR method is employed to simulate the flow through whole waterjet propulsion system.

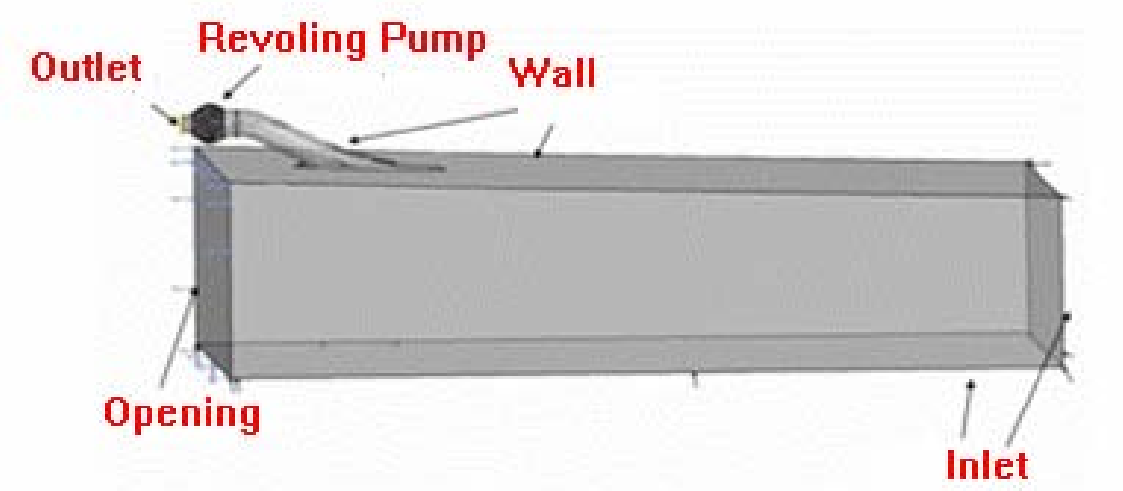

The maximal warp is smaller than 5%.

2. Calculation of vortex-induced force

Numerical approach

Secondly, The waterjet pump is taken out of the control volume. and the variable distributions of the pump inlet are picked out to be used as boundary conditions of the duct outlet. Turbulence model is set as LES, transient computation begins.

3. Analysis of vortex-induced force

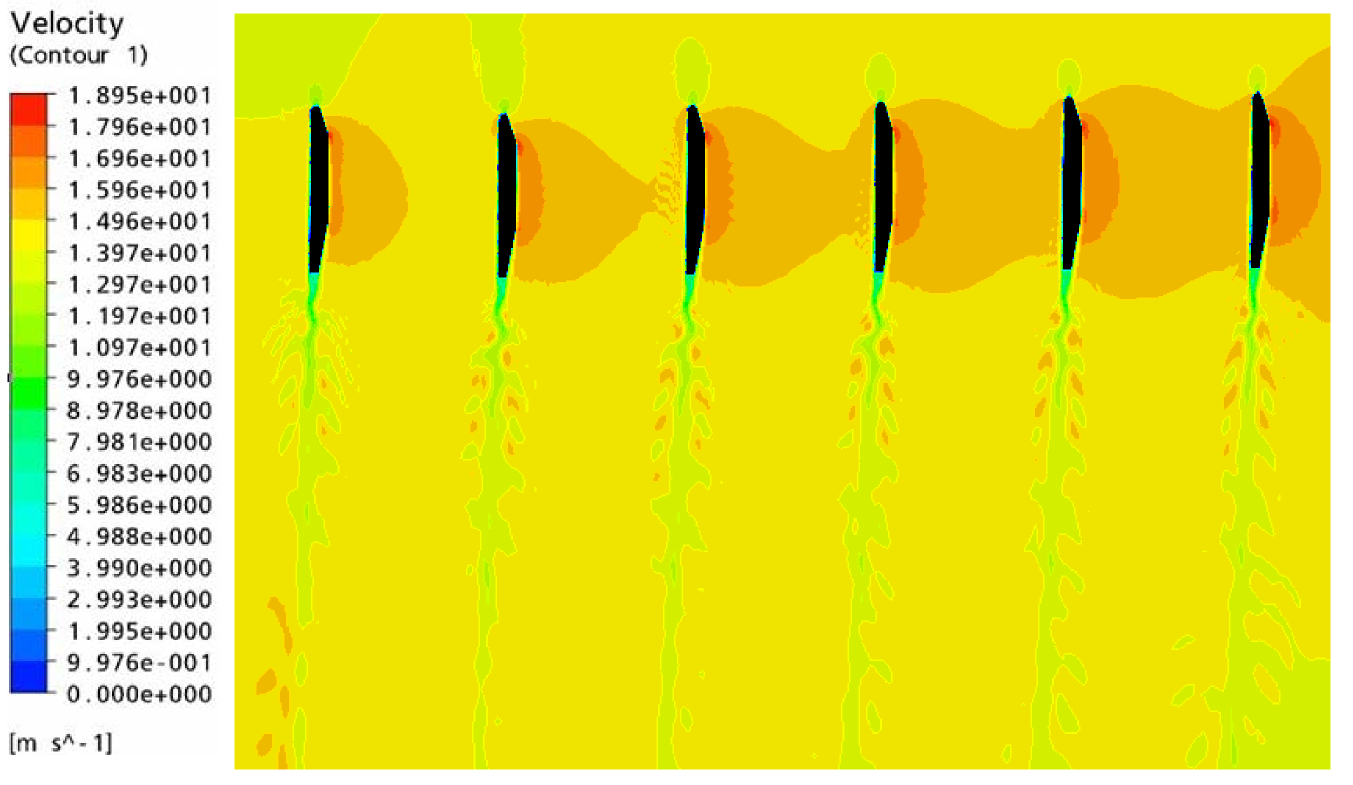

Velocity distribution of flow around waterjet grid

3. Analysis of vortex-induced force

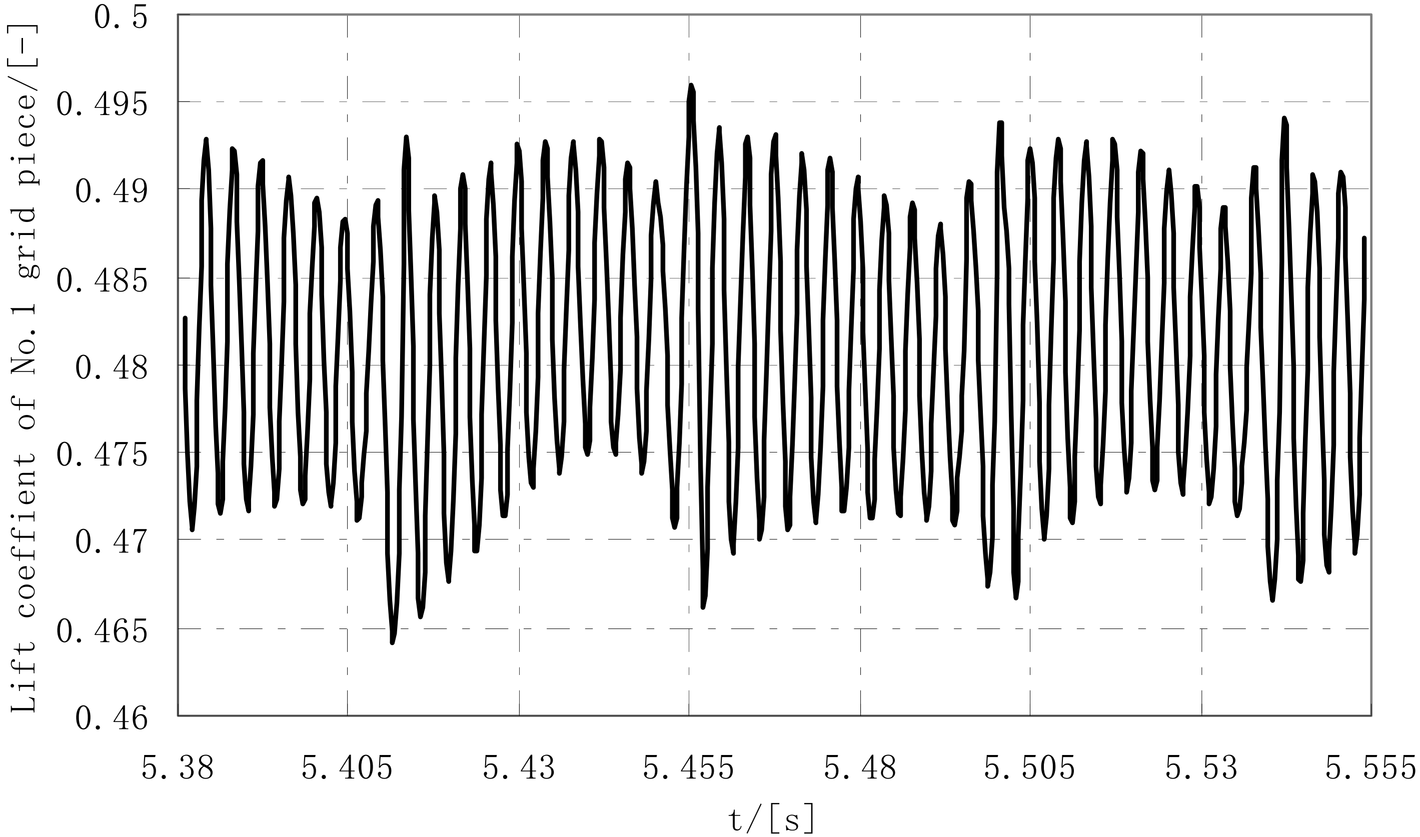

Lift force coefficient of No. 1 grid piece with time

3. Analysis of vortex-induced force

Vortex-induced force frequency at different working conditions(Hz)

Working conditions	#1 piece	#2 piece	#3 piece	#4 piece	#5 piece	#6 piece	bar
Full power advance one	131.59	140.12	133.36	151.16	156.08	146.90	124.25
Full power advance two	157.51	176.74	185.91	189.85	198.82	182.46	156.24
Full power advance three	225.56	235.99	246.18	247.23	231.15	236.15	208.64
Full power advance four	299.14	308.79	325.85	316.69	319.58	327.87	265.73
Full power advance five	349.86	355.19	376.97	386.24	377.58	375.04	341.38
Part power advance one	116.25	120.25	127.35	125.66	134.58	142.39	115.16
Part power advance two	157.55	168.17	175.47	173.24	186.78	161.94	147.18
Part power advance three	247.01	258.71	280.73	286.49	257.69	270.21	217.80

4. Modal analysis

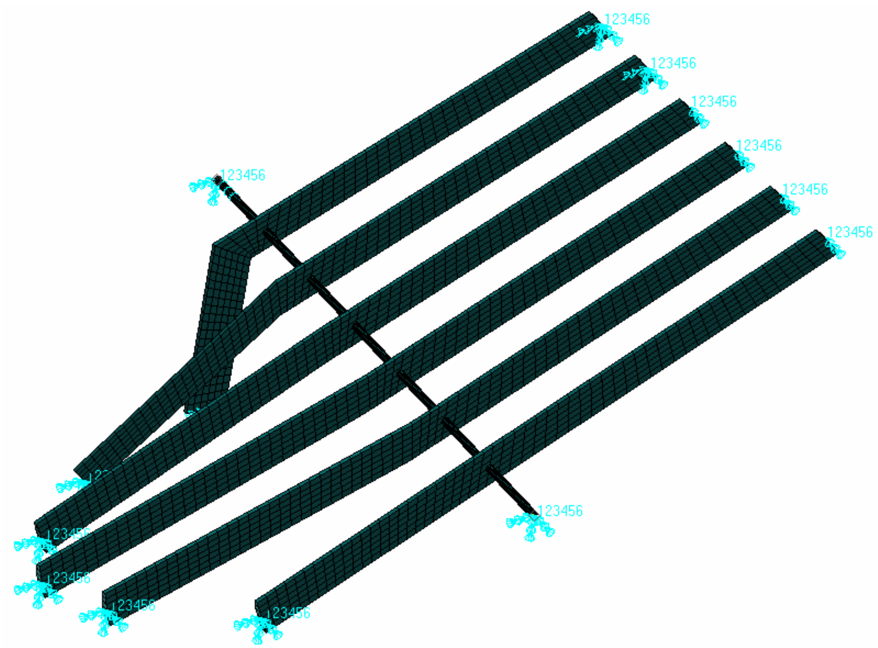

Mesh and boundary condition of FEA model

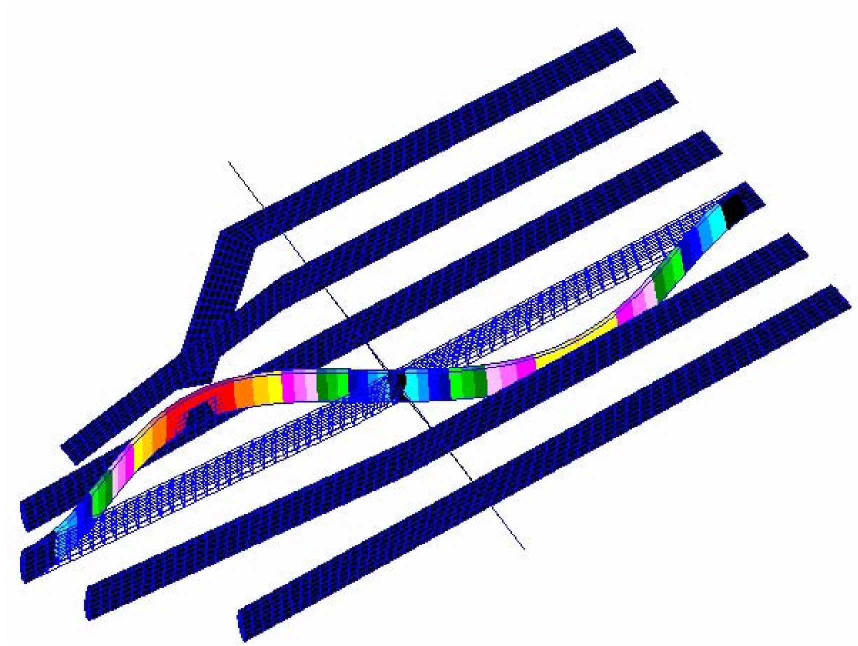

The first rank vibration deformation

4. Modal analysis

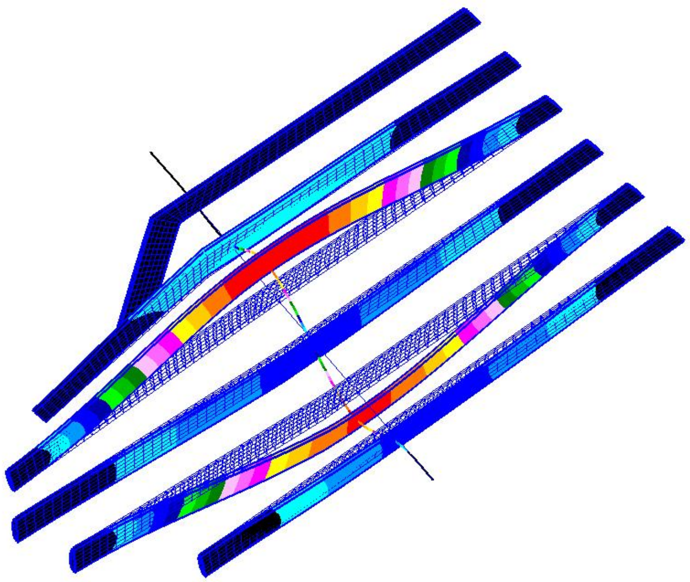

Vibration deformation of the bar

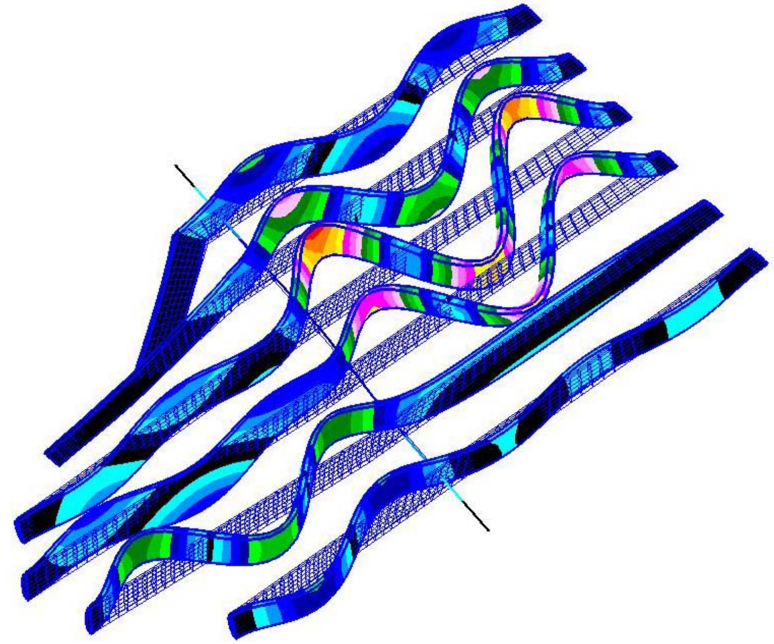

Vibration deformation of whole grid structure

5. Analysis of vortex-induced vibration

$$\eta = \left| \frac{f_i - f_e}{f_e} \right| \times 100\%$$

f_i ——the nature vibration frequency

f_e ——the frequency of the actuator

If η is smaller than 30%,

it's often thought the structure at stake in engineering.

5. Analysis of vortex-induced vibration

The grid has various kinds of vibration deformations due to its intricate framework. But usually there is only one component which is in the state of vibration. So it’s necessary to analyzing every part individually.

The results show that there are gaps between vortex-induced force frequency and every grid piece’s first rank vibration frequency. But the second and third rank would also arouse an intense oscillation and bring a broken structure. The author will keep on analyzing vibration model further.

5. Analysis of vortex-induced vibration

The second rank modal analysis of grid pieces

Number of grid pieces	f_i (Hz)	Working conditions	f_e (Hz)	η
#1	164.12	Full power advance one	131.59	19.82
		Full power advance two	157.51	4.03
		Part power advance one	116.25	29.17
		Part power advance two	152.55	7.05
#2	93.83	Part power advance one	119.05	26.88
#3	88.97			
#4	100.17	Part power advance one	125.66	25.45
#5	144.54	Full power advance one	156.08	7.98
		Part power advance one	134.58	6.89
		Part power advance two	186.78	29.22
#6	198.305	Full power advance one	146.90	25.92
		Full power advance two	182.46	7.99
		Full power advance three	236.15	19.08
		Part power advance one	142.39	28.19
		Part power advance two	161.94	18.34

5. Analysis of vortex-induced vibration

The third rank modal analysis

Number of grid pieces	f_i (Hz)	Working condition	f_e (Hz)	η
#1	172.69	Full power advance one	157.51	8.79
		Part power advance two	152.55	11.66
		Full power advance one	140.12	10.51
		Full power advance two	176.74	12.88
		Part power advance two	168.17	7.40
#3	139.60	Part power advance one	127.35	8.78
#4	156.58	Full power advance one	151.16	3.46
		Full power advance two	189.85	21.25
		Part power advance one	125.66	19.75
		Part power advance two	173.24	10.64
#5	231.54	Full power advance two	198.82	14.13
		Full power advance three	231.15	0.17
		Part power advance two	186.78	19.33
		Part power advance three	257.68	11.29
#6	250.85	Full power advance three	236.15	5.86
		Part power advance three	270.21	7.72

5. Analysis of vortex-induced vibration

Modal analysis of the bar

Rank	f_i (Hz)	Working conditions	f_e (Hz)	η
1	139.60	Full power advance one	124.25	10.996
		Full power advance two	156.24	11.92
		Part power advance one	115.16	17.51
		Part power advance two	147.18	5.43
2	156.58	Four power advance one	124.25	20.65
		Full power advance two	156.24	0.22
		Part power advance two	147.18	6.01
3	172.69	Full power advance two	156.24	9.53
		Full power advance three	208.64	20.24
		Part power advance two	147.18	14.77
		Part power advance three	217.80	26.12

Modal analysis of the whole grid

5. Analysis of vortex-induced vibration

Rank	f_i (Hz)	Working conditions	η
1	443.36	Full power advance five	Every component has a η smaller than 30%.
2	459.71	Full power advance five	Every component has a η smaller than 30%.

6. Conclusions

- **A prediction model for vortex-induced vibration of the waterjet grid is presented by uniting CFD and FEA together.**

- **There are vortexes shedding from the grid. There are many situations on which the vortex-induced force frequencies of different grid pieces are close to their low-level vibration frequency. Vortex-induced vibration is one of the most important reason that lead damages to the grid structure.**

- **The grid pieces are sensitive to lower pulsating frequencies, but the transverse bar is sensitive to higher ones. Relatively speaking, the transverse bar is more prone to be damaged.**

- **The cross-section shape of grid pieces should be modified to avoid bigger lift force and violent vibration caused by lift force.**

The End

Thanks for your attention

Numerical simulation and analysis of cavitation performance of waterjet

Chengjiang Liu
Ph.D. Candidate
Naval University of Engineering
P.R. China

OUTLINE

- Introduction
- Numerical Model
- Performance prediction at non-cavitation conditions
- Performance prediction at cavitation conditions
- Conclusion

INTRODUCTION

- **Waterjet is prior to the propeller in the application of high speed vessels, and has good cavitation property .**
- **Risk of cavitation: works at high rotating speed with low ship speed.**
- ***NPSHa* & *NPSHr***
- **Cavitation simulation on hydrofoils, propellers and radial flow pumps**
- **Numerical simulation of cavitation performance of a waterjet**

NUMERICAL MODEL

- Governing equations and cavitation model: homogeneous mixture multiphase flow
- Turbulence model: SST
- Selection of control volume

Mesh and boundary conditions

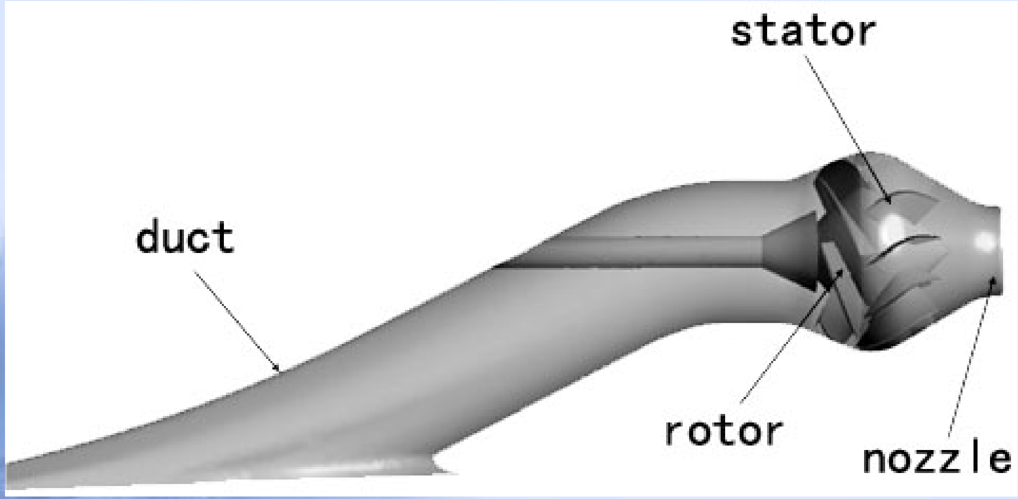

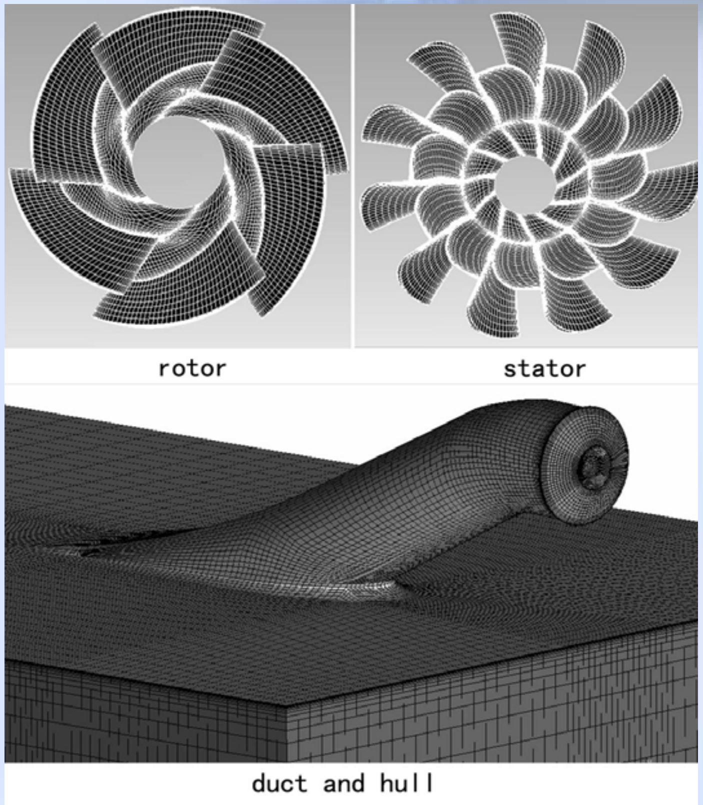

PERFORMANCE PREDICTION AT NON-CAVITATION CONDITIONS

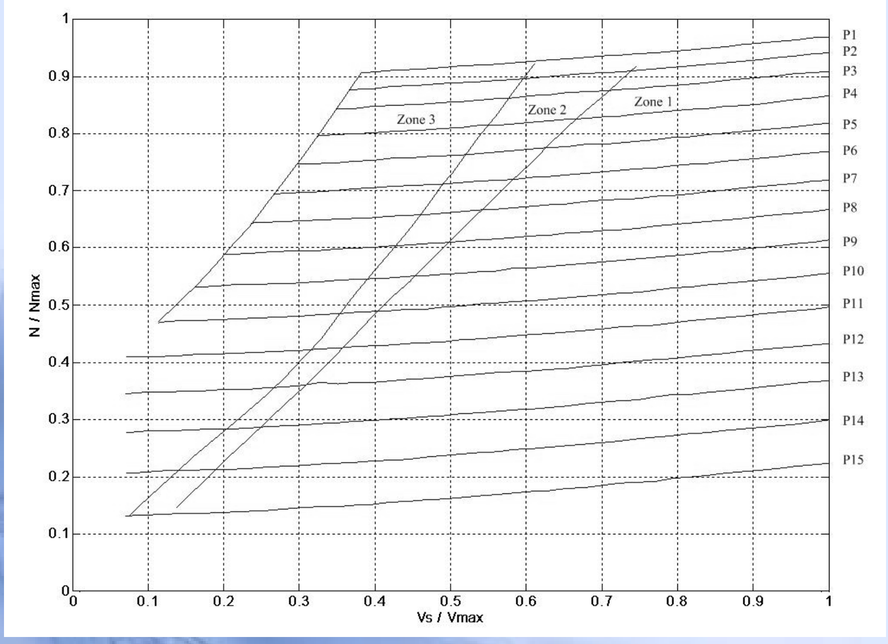

- predict the performance of the waterjet working in zone 1.
- some operation points on constant power lines such as P1, P2, P9, P15 and the resistance curve not shown on the figure

Calculation results

Ship speed Vs/V_{max}	Pump speed N/N_{max}	Error of power (%)	Error of thrust (%)
1.000	0.989	2.674	2.802
0.930	0.987	2.775	1.512
0.814	0.982	1.790	0.477

Ship speed Vs/V_{max}	Pump speed N/N_{max}	Error of power (%)	Error of thrust (%)
1.000	0.980	0.365	0.492
0.930	0.977	-0.043	-0.454
0.814	0.972	-0.181	0.635

Ship speed Vs/V_{max}	Pump speed N/N_{max}	Error of power (%)	Error of thrust (%)
1.000	0.889	3.170	5.167
0.930	0.886	3.276	3.252
0.814	0.881	2.617	1.941
0.698	0.876	1.898	1.825
0.581	0.873	1.351	2.875

Ship speed Vs/V_{max}	Pump speed N/N_{max}	Error of power (%)	Error of thrust (%)
1.000	0.741	3.862	6.137
0.930	0.738	4.189	8.964
0.814	0.733	3.111	5.436
0.698	0.728	2.198	3.453
0.581	0.723	1.909	3.078
0.465	0.719	0.919	3.447
0.349	0.716	0.557	5.698
0.233	0.713	0.267	6.240
0.116	0.711	-0.229	5.611

Calculation results

Ship speed Vs/V_{max}	Pump speed N/N_{max}	Error of power (%)	Error of thrust (%)
0.505	0.721	1.294	3.495
0.591	0.749	1.819	2.837
0.699	0.799	2.337	1.796
0.771	0.842	2.548	0.796
0.824	0.881	2.687	0.333
0.870	0.917	2.858	0.066
0.909	0.951	2.959	0.096
0.935	0.977	2.898	0.078
0.945	0.987	2.876	0.012

- The numerical model and method is approved feasible after the comparison between calculation results and manufacturer's data.

PERFORMANCE PREDICTION AT CAVITATION CONDITIONS

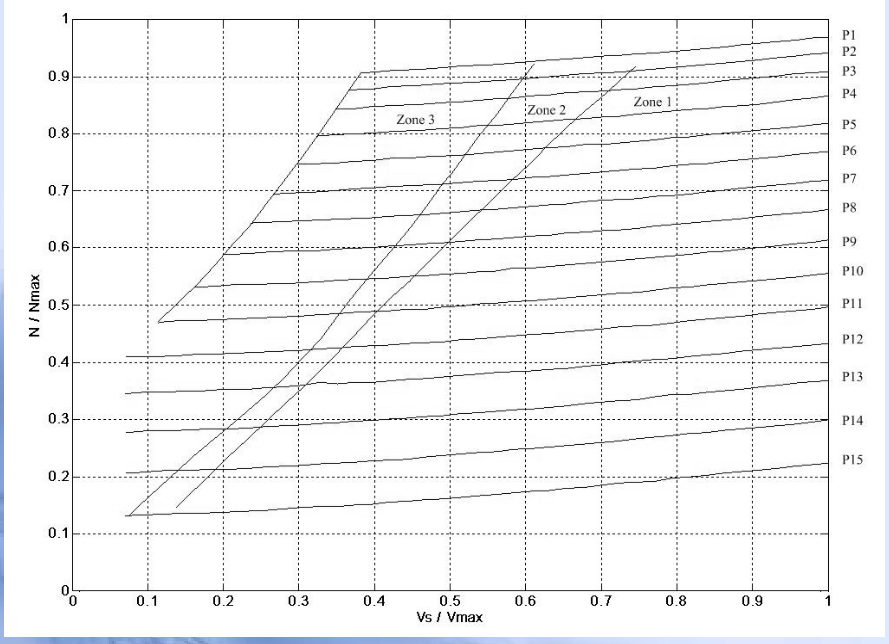

- **operating conditions in zone 2 and 3, where cavitaion would occur**
- **also on constant power lines P1, P2, P9 and P15**
- **results without cavitation model as the initial input**
- **cavitation flow is more complex, and its simulation is more difficult**

Calculation results

Ship speed Vs/V_{max}	Pump speed N/N_{max}	Error of power (%)	Error of thrust (%)
0.698	**0.978**	**-1.466**	**0.859**
0.698	***0.978***	***-0.671***	***-0.629***
0.581	**0.974**	**-1.813**	**3.911**
0.581	***0.974***	***0.960***	***2.967***
0.465	**0.971**	**-2.232**	**10.741**
0.465	***0.971***	***3.188***	***7.388***
0.381	**0.969**	**-2.343**	**18.912**
0.381	***0.969***	***1.722***	***9.851***

Ship speed Vs/V_{max}	Pump speed N/N_{max}	Error of power (%)	Error of thrust (%)
0.465	**0.869**	**-2.214**	**4.939**
0.465	***0.869***	***-1.172***	***3.414***
0.349	**0.866**	**-2.412**	**11.237**
0.349	***0.866***	***-0.877***	***8.241***
0.233	**0.864**	**-2.565**	**15.925**
0.233	***0.864***	***0.063***	***11.902***
0.202	**0.863**	**-2.629**	**17.652**
0.202	***0.863***	***0.229***	***12.487***

Ship speed Vs/V_{max}	Pump speed N/N_{max}	Error of power (%)	Error of thrust (%)
0.698	**0.968**	**-1.427**	**0.928**
0.698	***0.968***	***-0.184***	***0.729***
0.605	**0.966**	**-1.535**	**2.913**
0.605	***0.966***	***-1.344***	***2.470***
0.535	**0.963**	**-2.001**	**5.593**
0.535	***0.963***	***-0.520***	***4.638***
0.465	**0.961**	**-2.201**	**9.973**
0.465	***0.961***	***0.239***	***7.602***
0.372	**0.959**	**-2.364**	**19.135**
0.372	***0.959***	***-0.308***	***8.299***

Ship speed Vs/V_{max}	Pump speed N/N_{max}	Error of power (%)	Error of thrust (%)
0.093	**0.711**	**-2.919**	**8.464**
0.093	***0.711***	***-2.549***	***7.323***
0.076	**0.711**	**-2.960**	**8.457**
0.076	***0.711***	***-2.689***	***7.059***

ANALYSIS OF CAVITATION PERFORMANCE

$$NPSHa = \frac{p_\infty - p_v}{\rho g} + \frac{V_s^2}{2g}(1-\varepsilon)(1-\omega)^2 - h_j$$

$$NPSHr = NPSHp = \frac{p_s - p_v}{\rho g} + \frac{V_p^2}{2g}$$

$$NPSHr \le NPSHa$$

$$\left.\begin{array}{l} \\ \\ \\ \end{array}\right\} \quad IVR \ge \sqrt{\frac{\rho V_s^2}{2(p_\infty - p_s) + \rho V_s^2 (1-\varepsilon)(1-\omega)^2 - 2\rho g h_j}}$$

Cavitation occurs when $IVR < \sqrt{\frac{\rho V_s^2}{2(p_\infty - p_s) + \rho V_s^2 (1-\varepsilon)(1-\omega)^2 - 2\rho g h_j}}$

Pump Cavitation

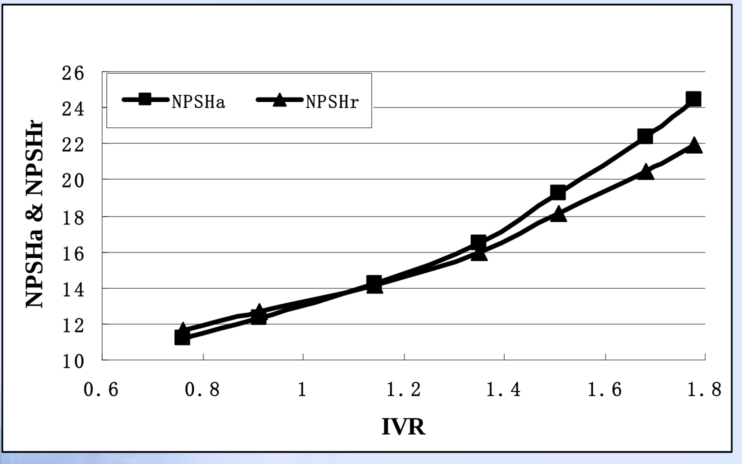

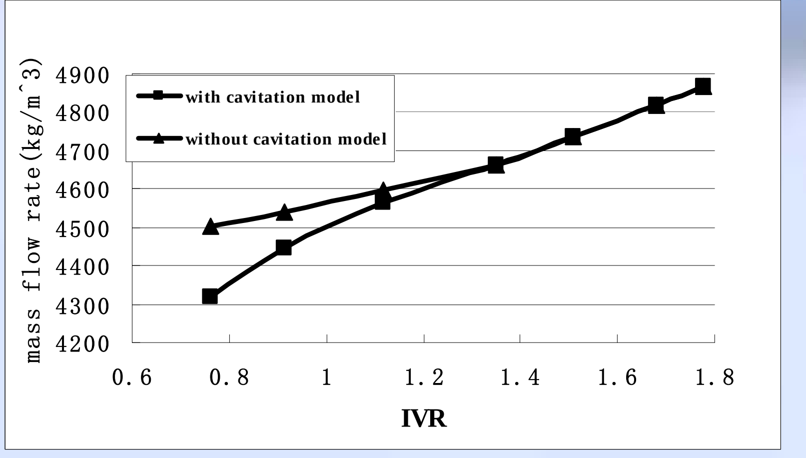

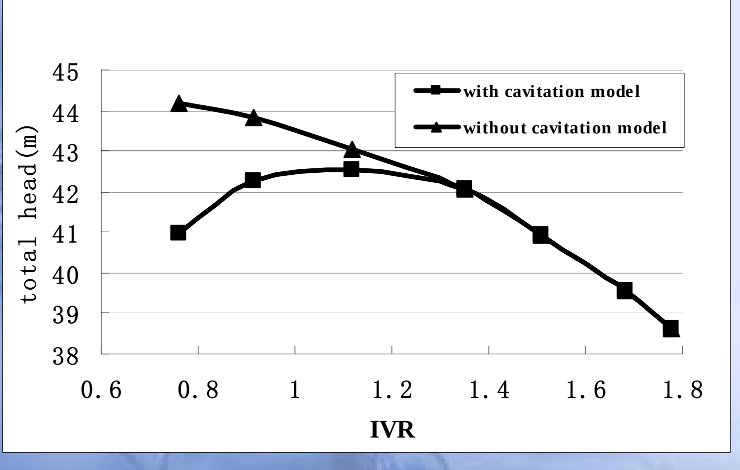

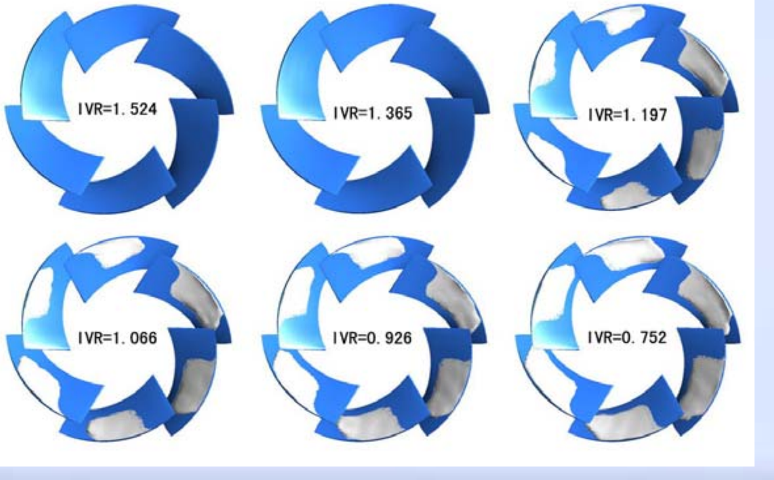

Inlet cavitation

Nozzle cavitation

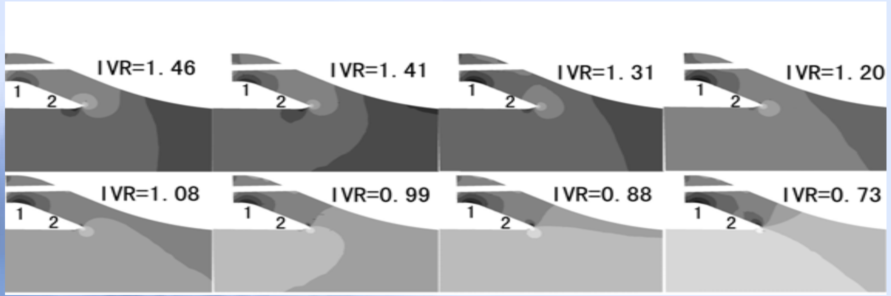

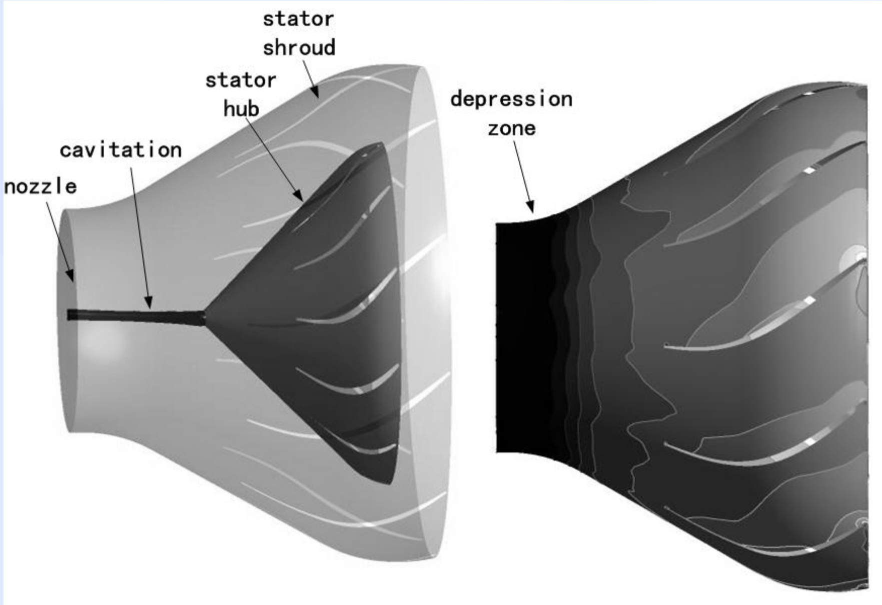

Cavitation division lines

$$N_{ss} = \frac{5.62 N \sqrt{Q_v}}{NPSHr^{3/4}}$$

limiting cavitation line 1

Variables	Values			
Vs/V_{max}	0.495	0.625	0.708	0.769
N_{ss}	1266	1290	1284	1270

limiting cavitation line 2

Variables	Values		
Vs/V_{max}	0.425	0.519	0.610
N_{ss}	1361	1395	1406

limiting cavitation line 3

Variables	Values		
Vs/V_{max}	0.201	0.296	0.381
N_{ss}	1544	1584	1619

CONCLUSION

- The relation of *NPSHa* and IVR and the relation of *NPSHr* and IVR are obtained, and the critical IVR for cavitation occurrence is obtained with the value about 1.2.
- When cavitation exists, the mass flow rate and the total head both decrease obviously.
- Cavitation becomes severer with IVR decreasing on constant power line.

CONCLUSION

- Cavitation may occur in inlet duct, lagging behind cavitation in waterjet pump.
- Cavitation in nozzle existing in form of spatial cavitation occurs in advance of that in waterjet pump, with no cavitation on nozzle walls.
- The cavitation division line is a constant suction specific speed line.

Thank you very much!

Off-design behaviour of waterjets

RINA Waterjet Propulsion 5 conference

By
Norbert Bulten

WÄRTSILÄ

Topics

- Introduction
- Applied methodology
- Effects of off-design operation on performance
- Development of new axial-flow pump
- Performance improvements with axial-flow pump
- Conclusions

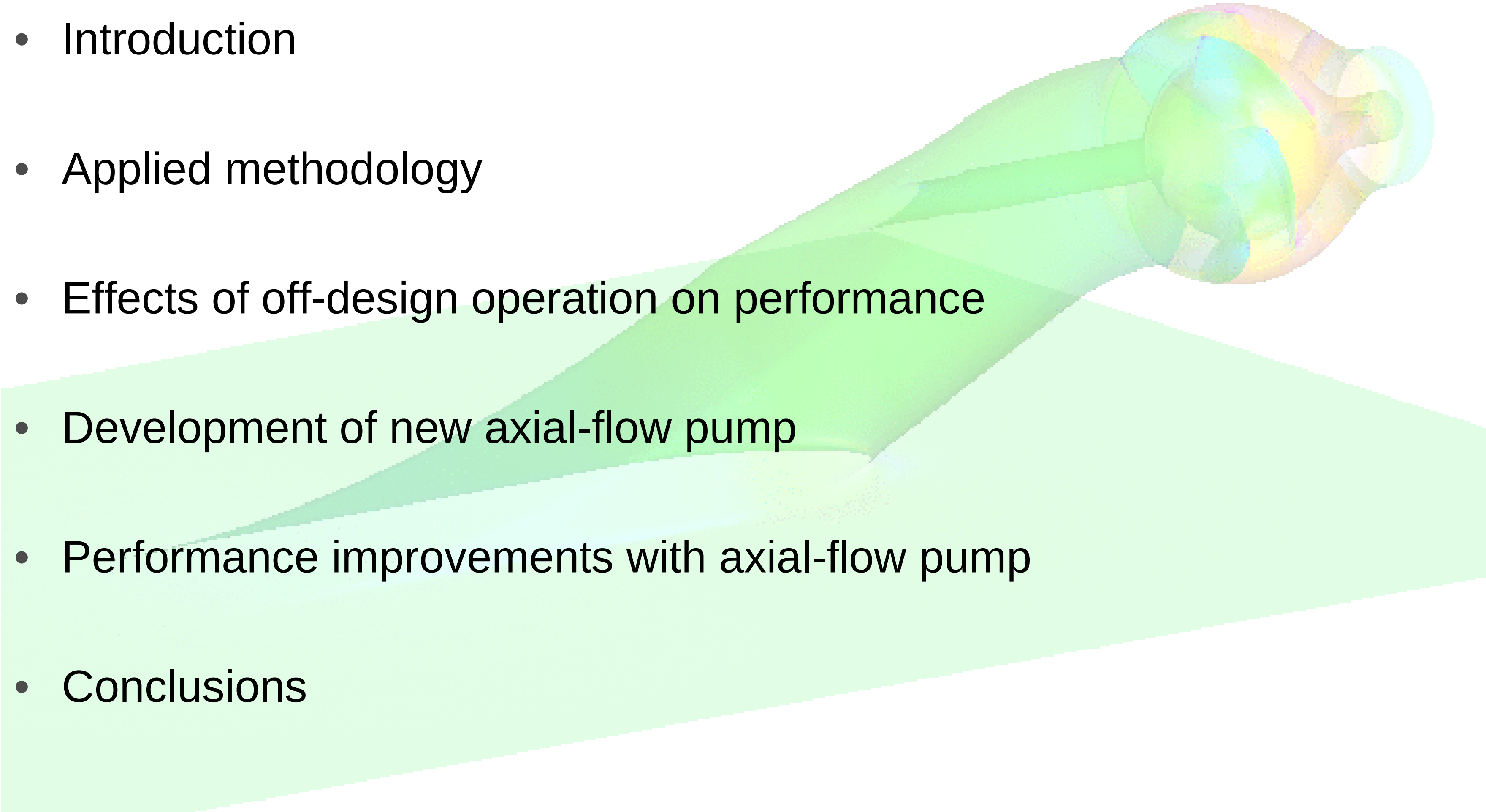

  11 December 2008 RINA Waterjet Propulsion 5 conference / Norbert Bulten

WÄRTSILÄ

Introduction

- Design is focussed on high speed sailing (40+ knots) in straight ahead course

However:

- Steering and manoeuvring performance is important for total trip time as well

- Ships do sometimes have to operate with limited number of installations

Off-design conditions

- Low speed manoeuvring in port
  - Up to 10 knots
  - 360 degrees vectoring
- High speed steering
  - 30 – 35 knots
  - Up to 20 degrees steering
- Three-jet operation
  - Engine failure

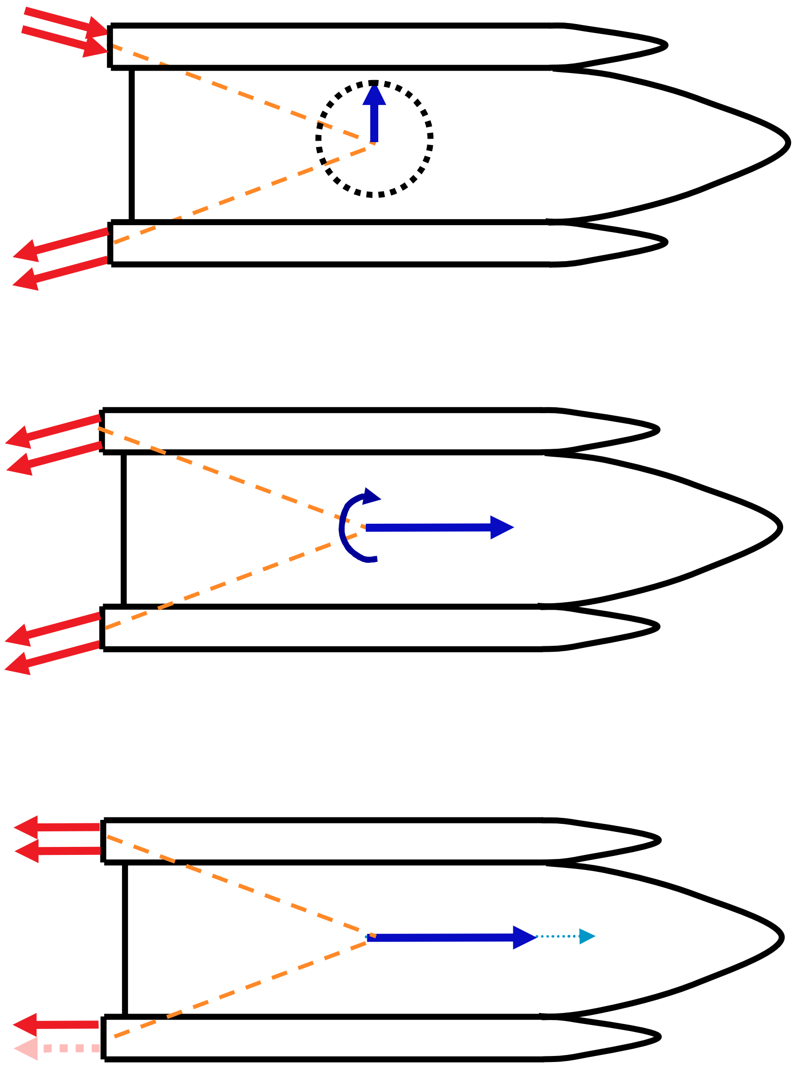

Expected phenomena

- At off-design the following phenomena can occur:
  - Reduced cavitation margins
  - Increase of power consumption: engine overload
  - Decrease of power consumption: light running
- Phenomena are caused by:
  - Increased viscous losses in inlet
  - Reduced flow rate through waterjet
  - Swirl of the flow upstream of pump

Methodology: CFD

- CFD = Computational Fluid Dynamics
- Research based on numerical analysis of the flow through a complete waterjet installation
- Reynolds-Averaged Navier-Stokes equations used; thus taking viscous effects into account
- Turbulence modelling:
  k-ε with wall-functions

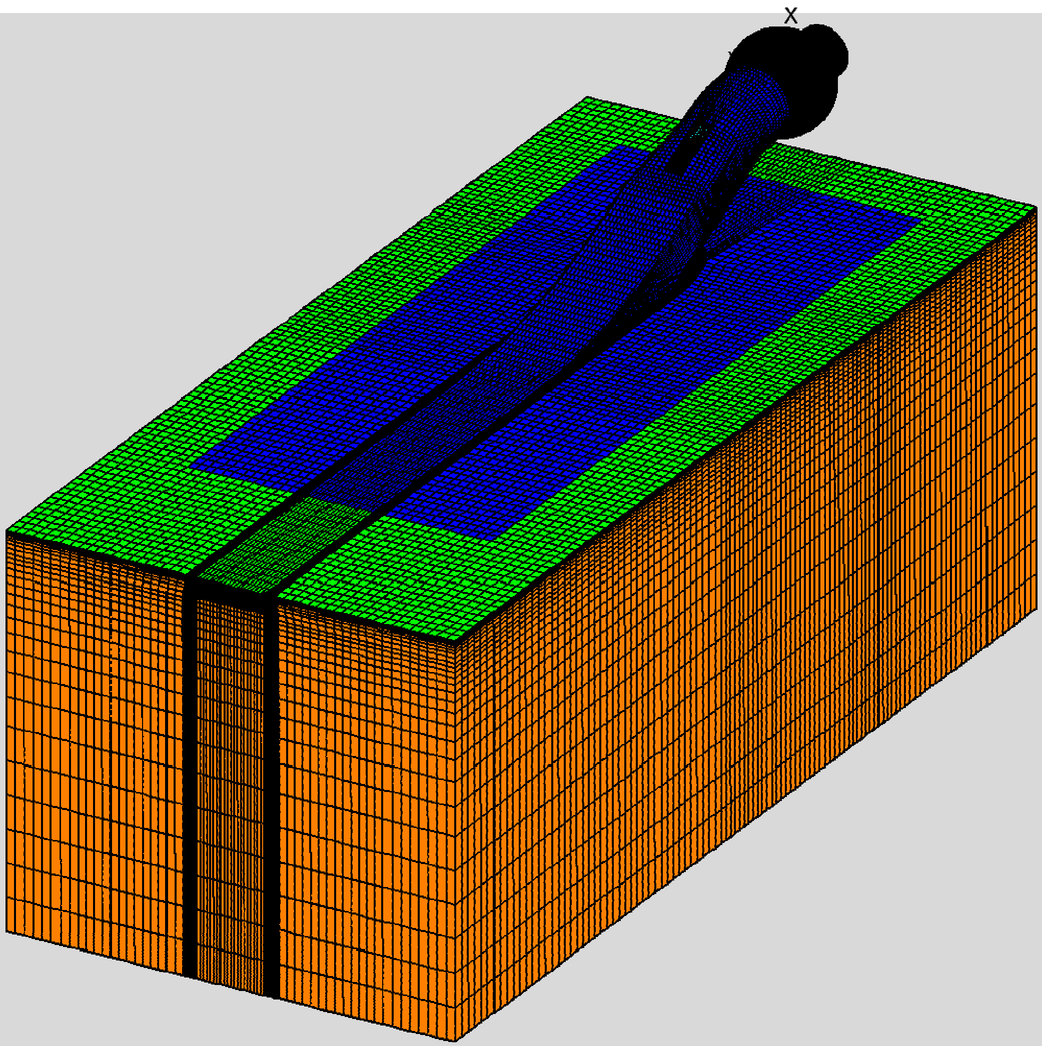

Numerical settings

- Fully hexahedral mesh
- Multiple-frame-of-reference method to include impeller rotation
- Inflow velocity based on drift-angle
- Input parameters:
  - Ship speed
  - Drift angle
  - Impeller RPM

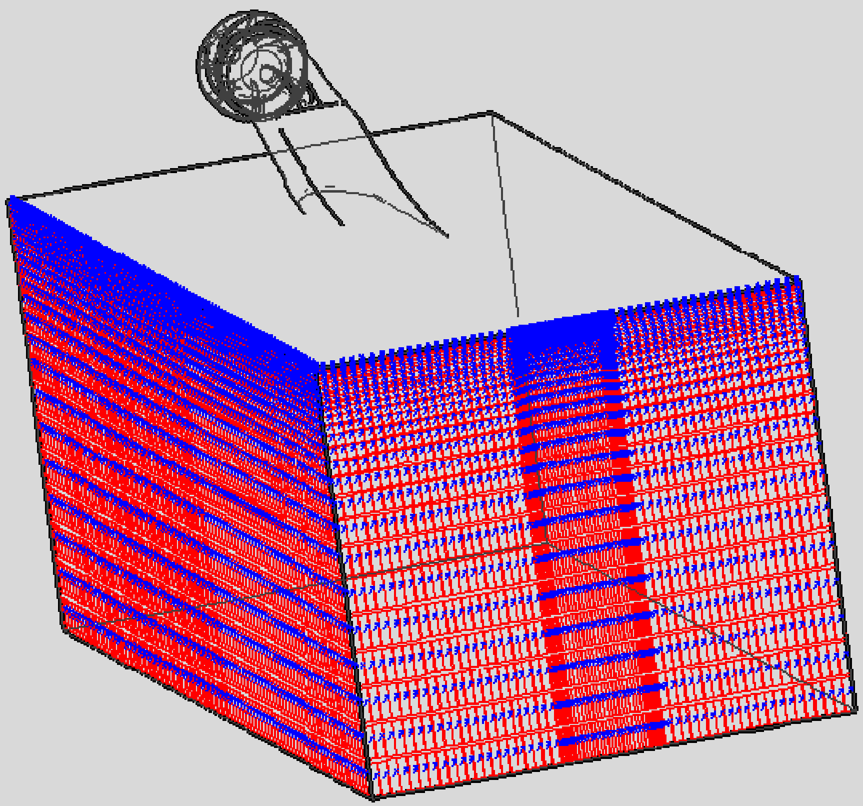

Results for low speed manoeuvring

- Calculations carried out for:
  - Ship speed of 3 and 6 knots
  - Drift angle varying from -60 to +60°
  - RPM represents about 30% power

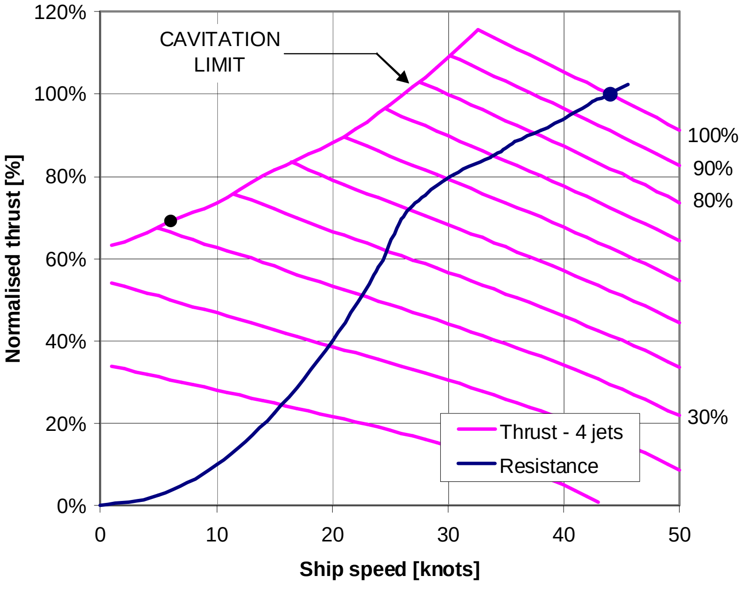

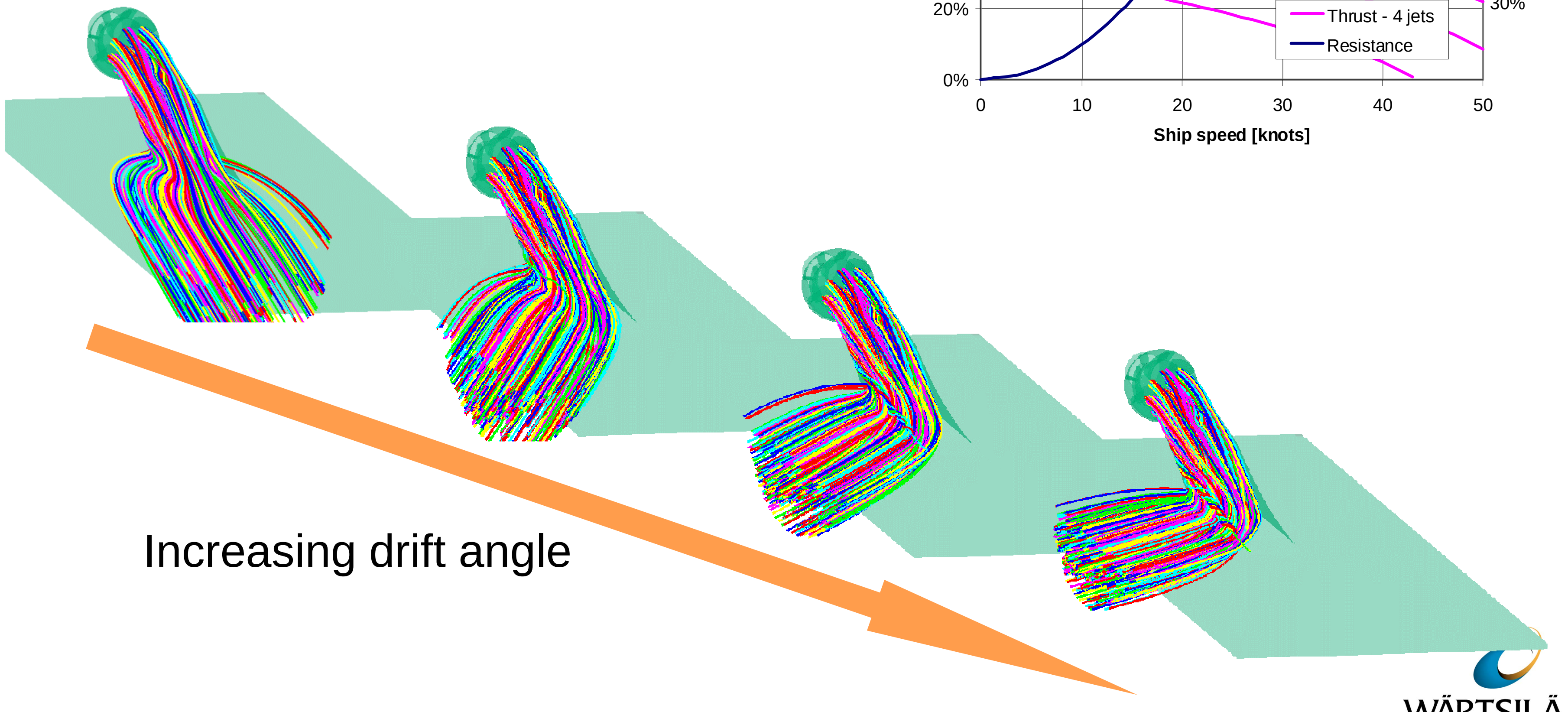

Results for low speed manoeuvring

- Effects on shaft power and NPSH

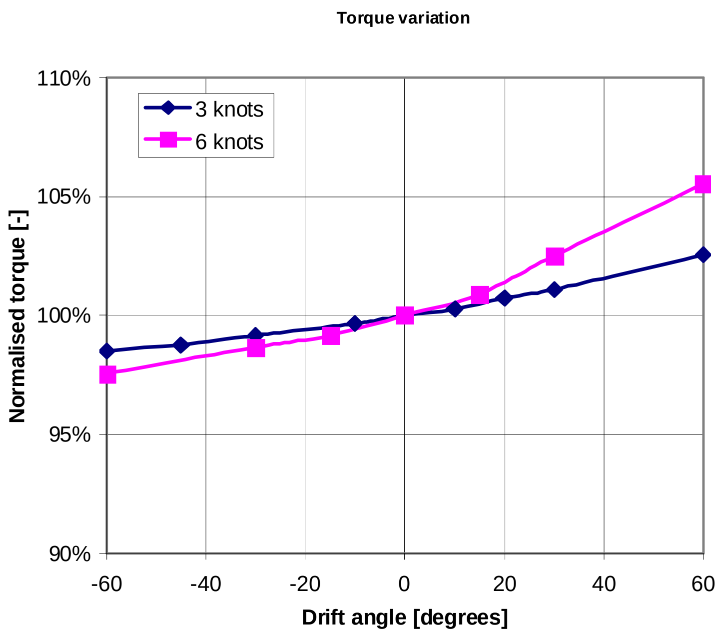

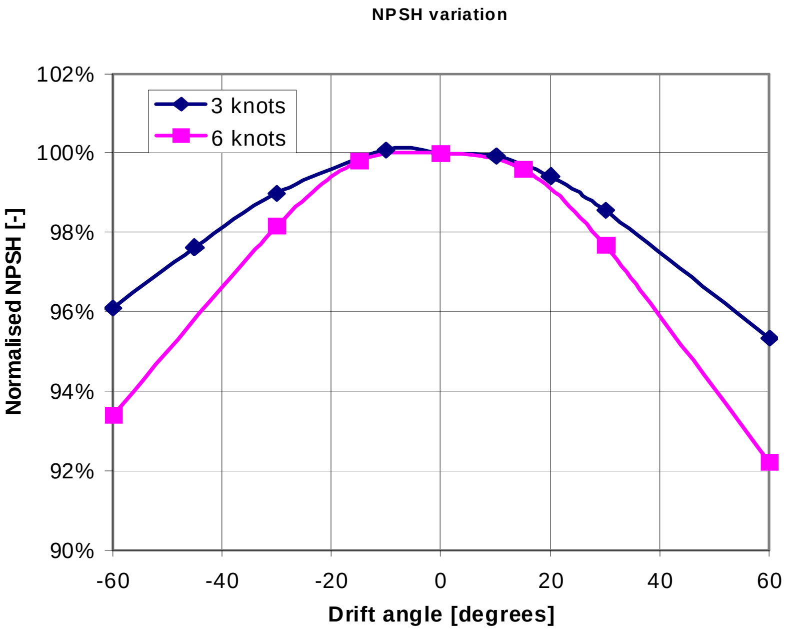

- 5% higher engine load at 60 degrees
- 8% less available NPSH at 60 degrees

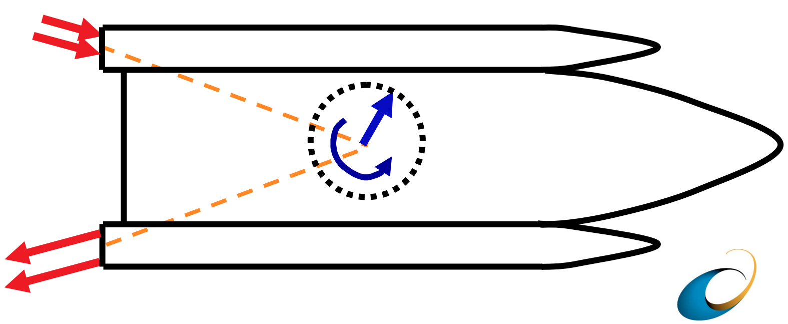

Results for high speed steering

- High speed turns at 30 and 35 knots
- Shaft power shows anti-symmetrical behaviour

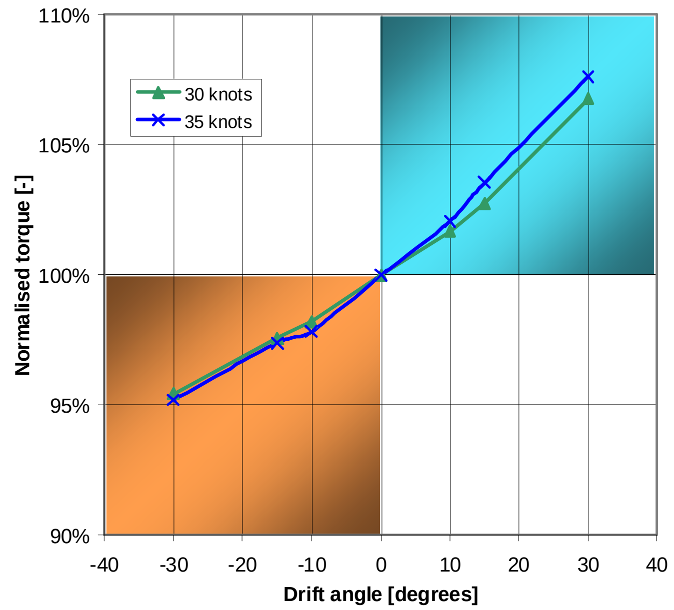

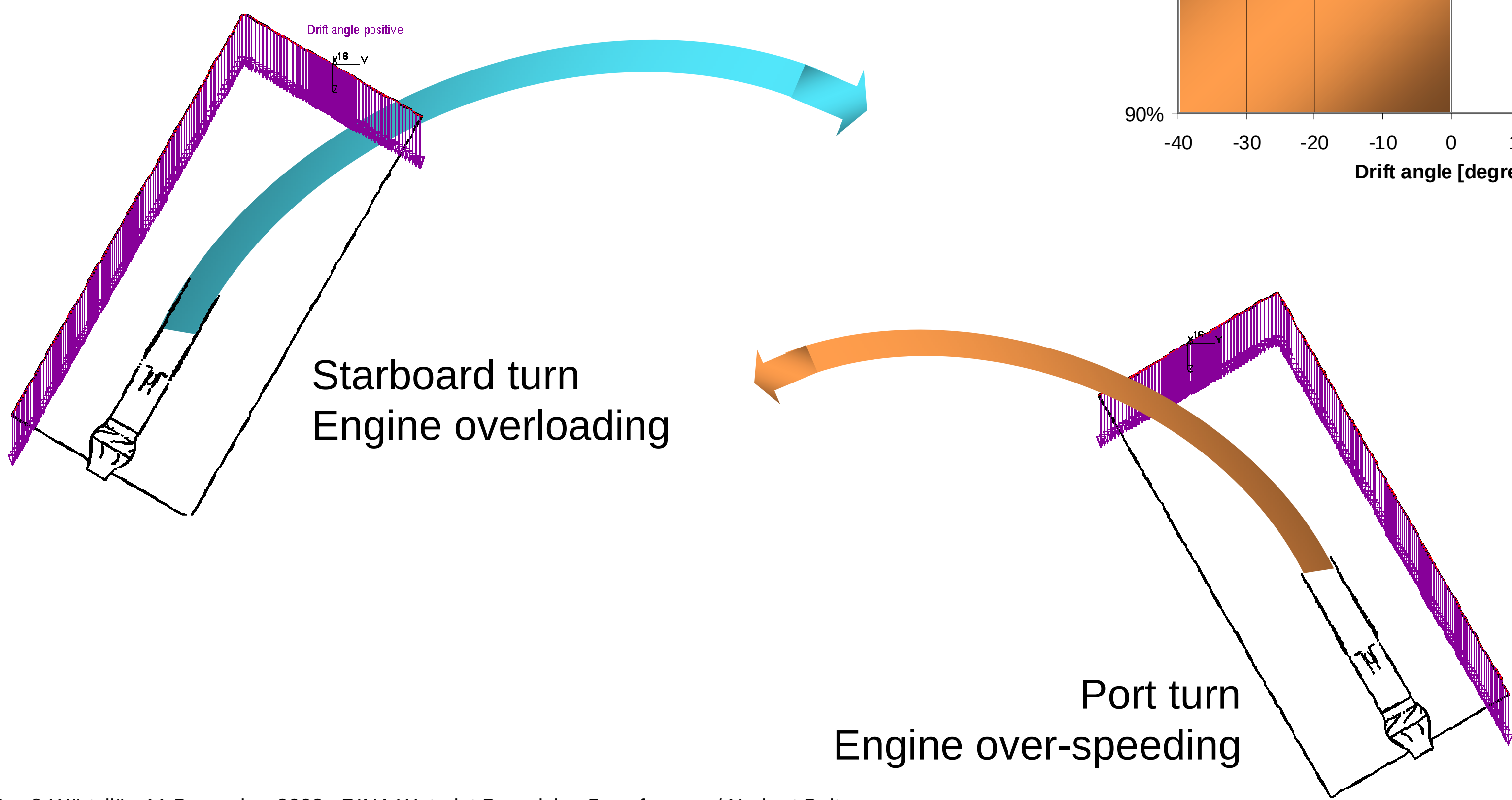

WÄRTSILÄ

Results for three-jet operation

- Three-jet operation means 75% available power

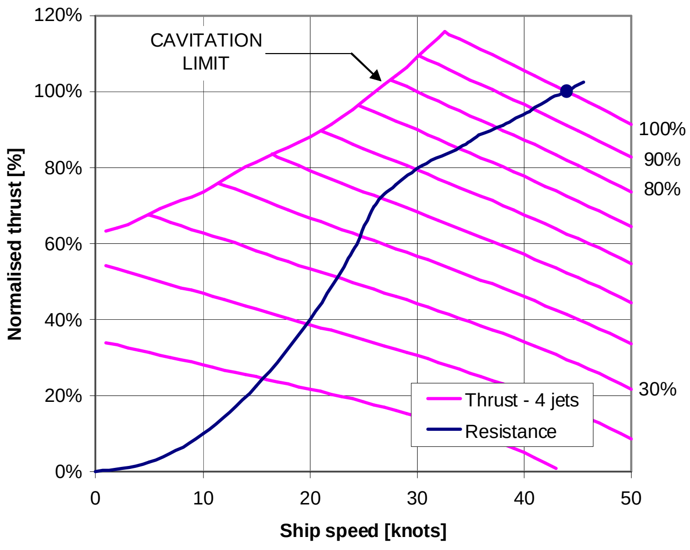

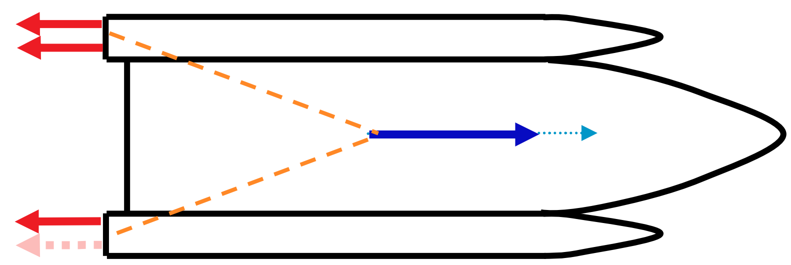

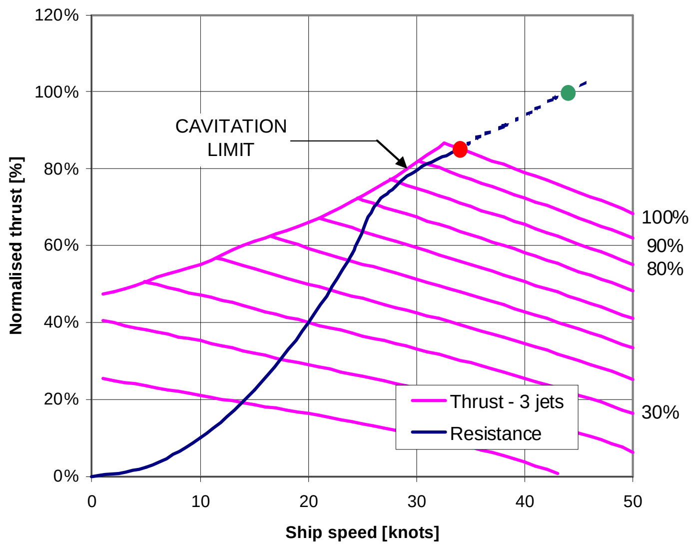

- Expected phenomena
  - Signification reduction of ship speed
  - Lower flow-rate through waterjet
  - Increased shaft torque
  - Decreased cavitation margins

WÄRTSILÄ

Results for three-jet operation

- Full power at reduced speed changes the cavitation behaviour
- Pressure distributions are shown for: 25, 30 and 45 knots at 100% power

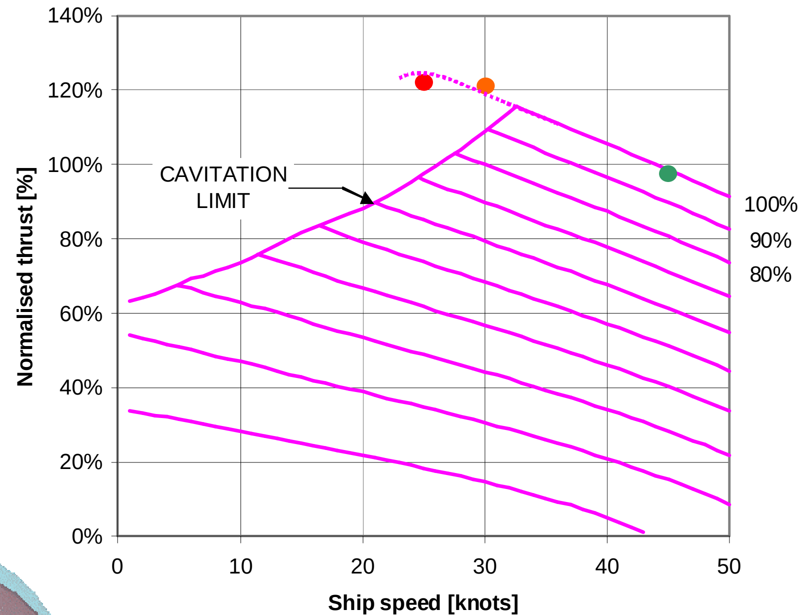

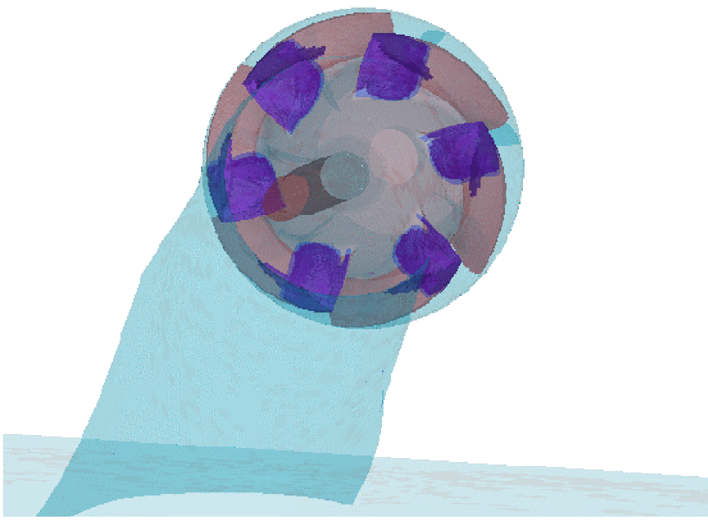

25 knots

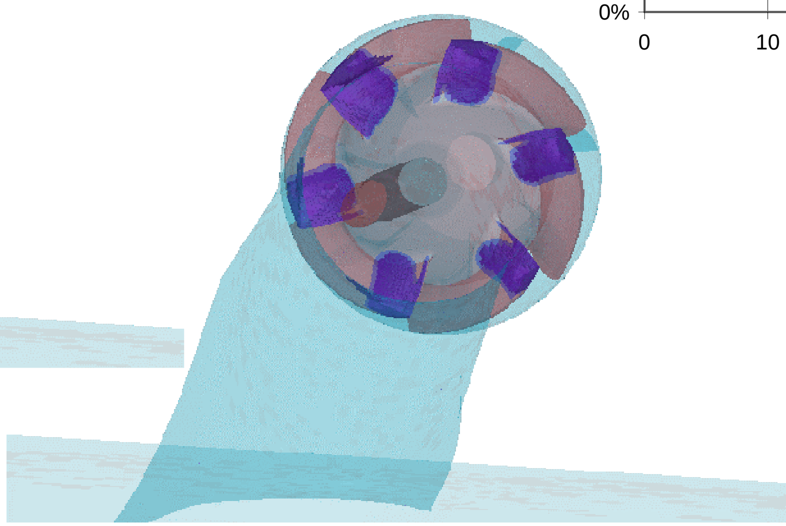

30 knots

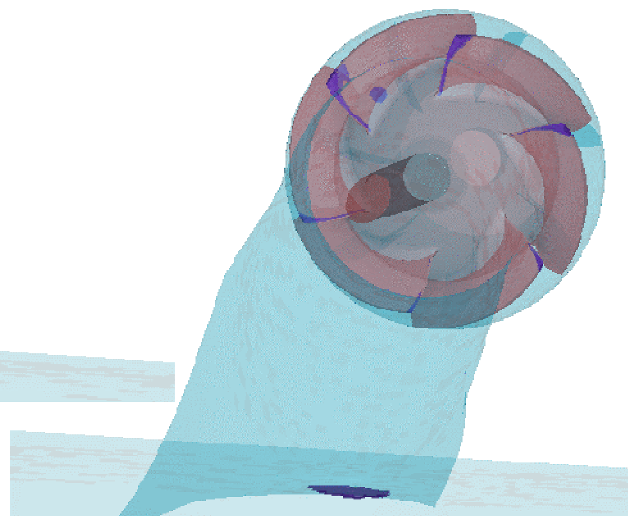

45 knots

WÄRTSILÄ

Summary

Off-design performance is causing no problems for normal operation:

- Manoeuvring
- Steering

What is the added value of further improvements of pump performance?

Evolution 112m	
Shipyard:	INCAT
Waterjet:	4 x LJX1500SRI
Power :	4 x 9.000 KW
Vs (full load):	41.9 knots

WÄRTSILÄ

Development of axial-flow pump

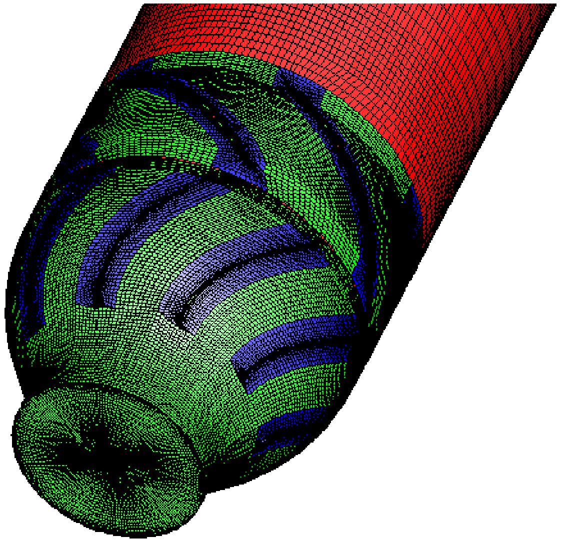

- Characteristics of new pump type:
  - Based on axial-flow geometry
  - Pump specific speed is similar to E-type pump
  - High pump efficiency is maintained
  - Cavitation margins have been increased

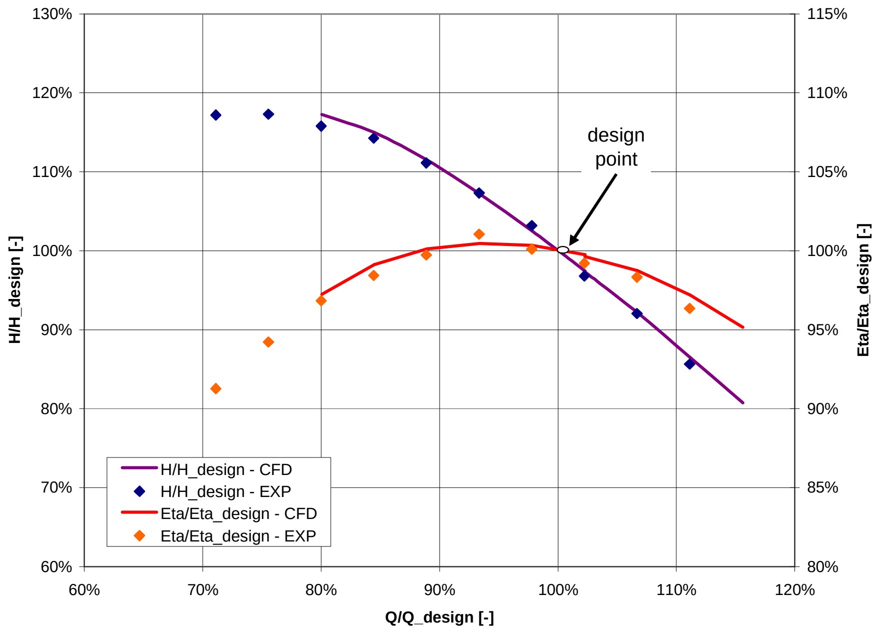

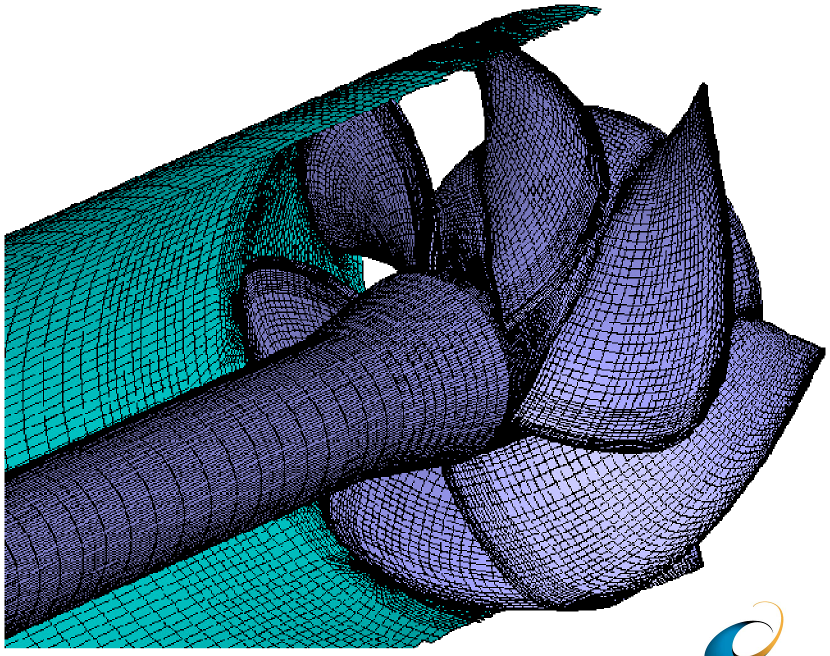

WÄRTSILÄ

Pump performance tests

- Performance measurements in different laboratories
  - Pump performance (head, efficiency)
  - Cavitation behaviour

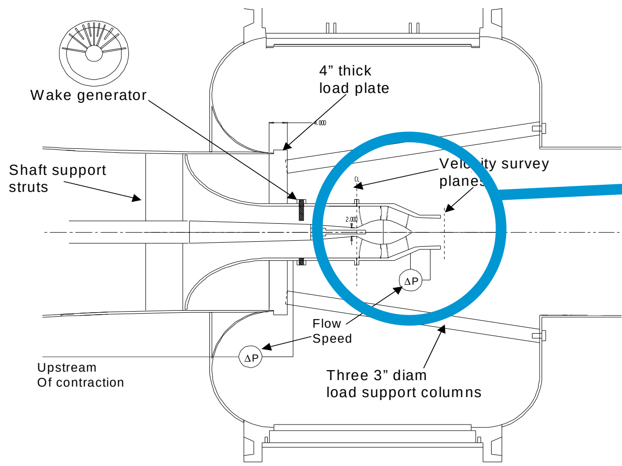

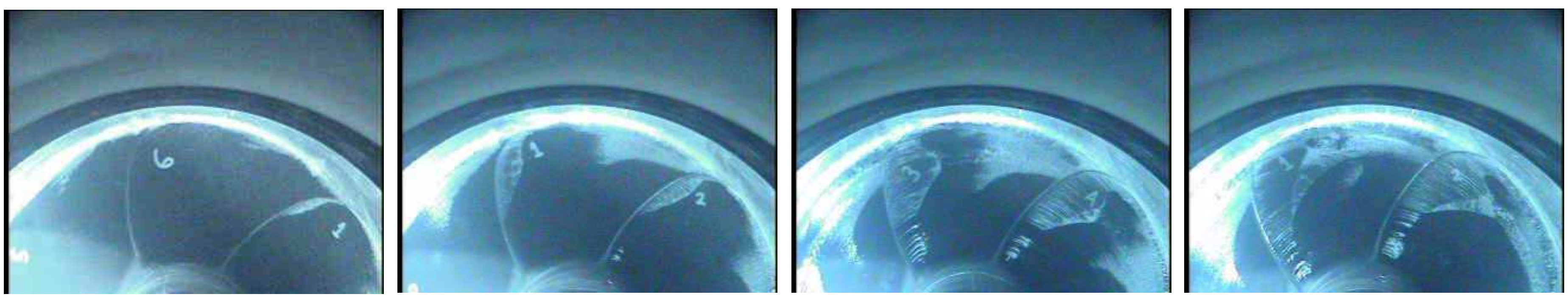

Decreasing inlet pressure

Features of new axial-flow pump design

- Flange diameter of axial-flow LJX-Type ≈ 25% smaller compared to similar size E-type

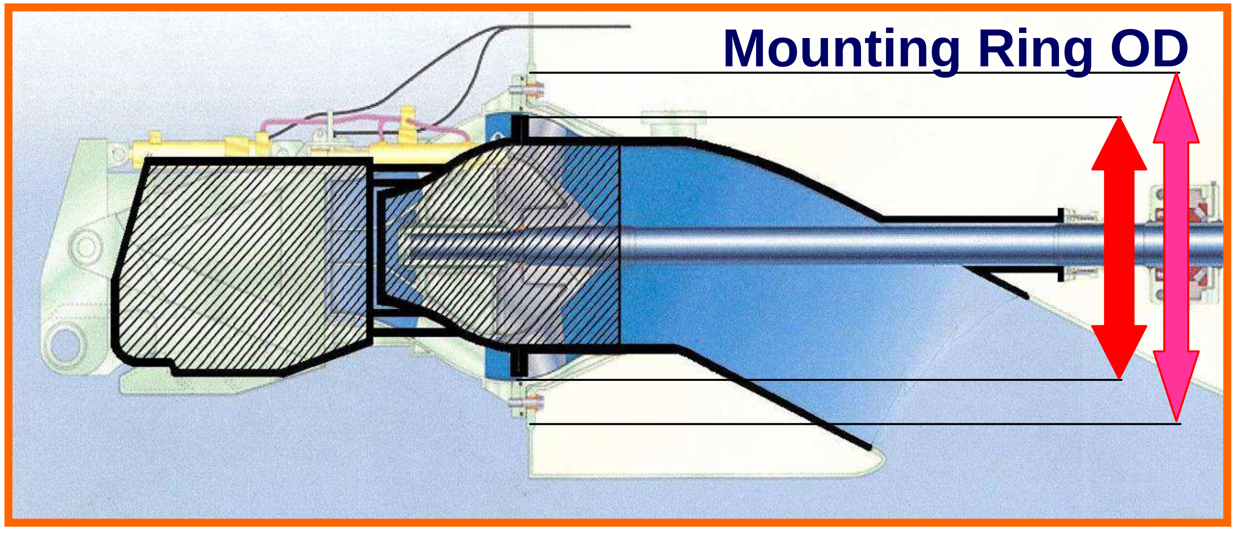

- Seatring-shape of axial pump ensures fixed tip clearance

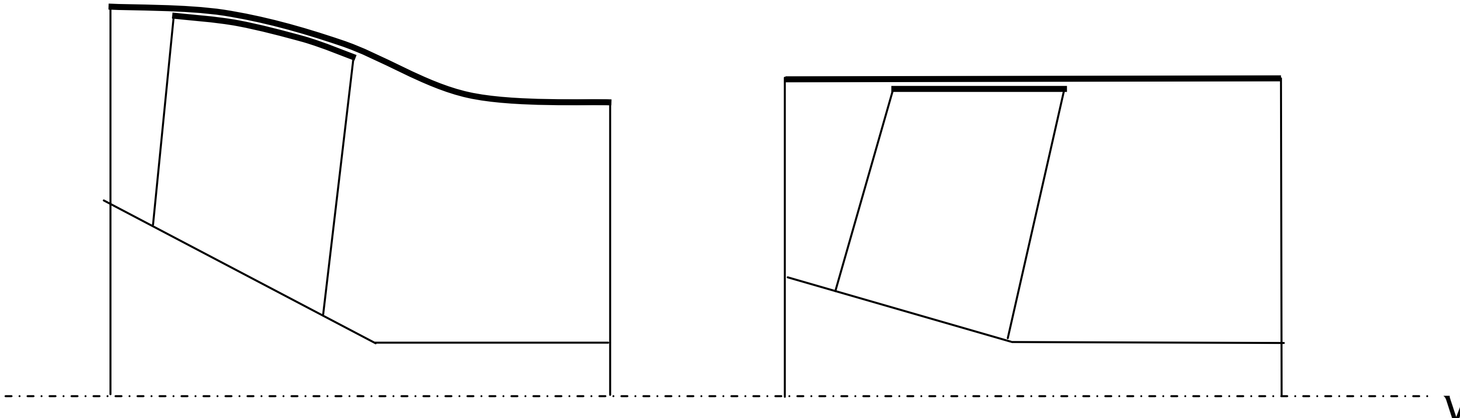

Performance of axial-flow pump

- Manoeuvring at 6 knots:
  - Maximum power increases from 32% to 41%
  - Thrust increases from 69% to 83% of design thrust at full speed

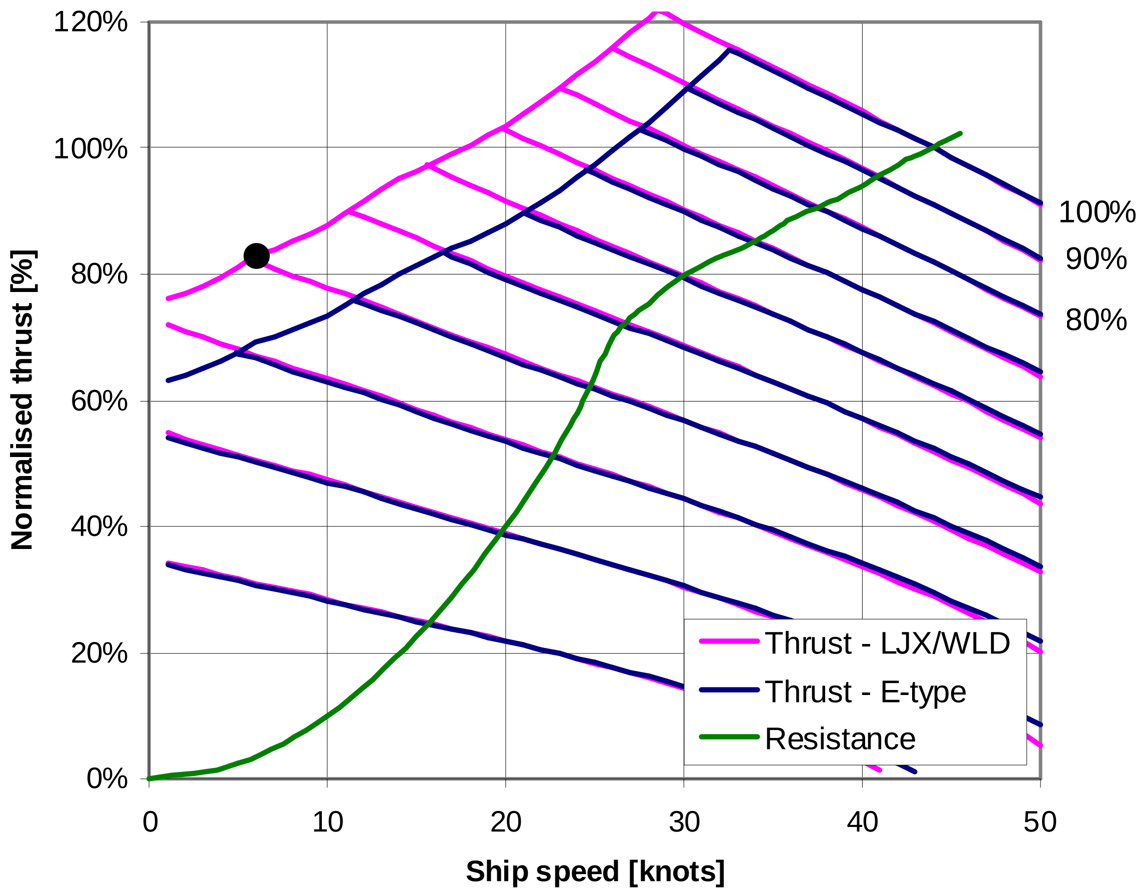

WÄRTSILÄ

Performance of axial-flow pump

- Three-jet operation
- Cavitation margins at full power increase to 6 knots
- Margins increases at critical hump speed as well

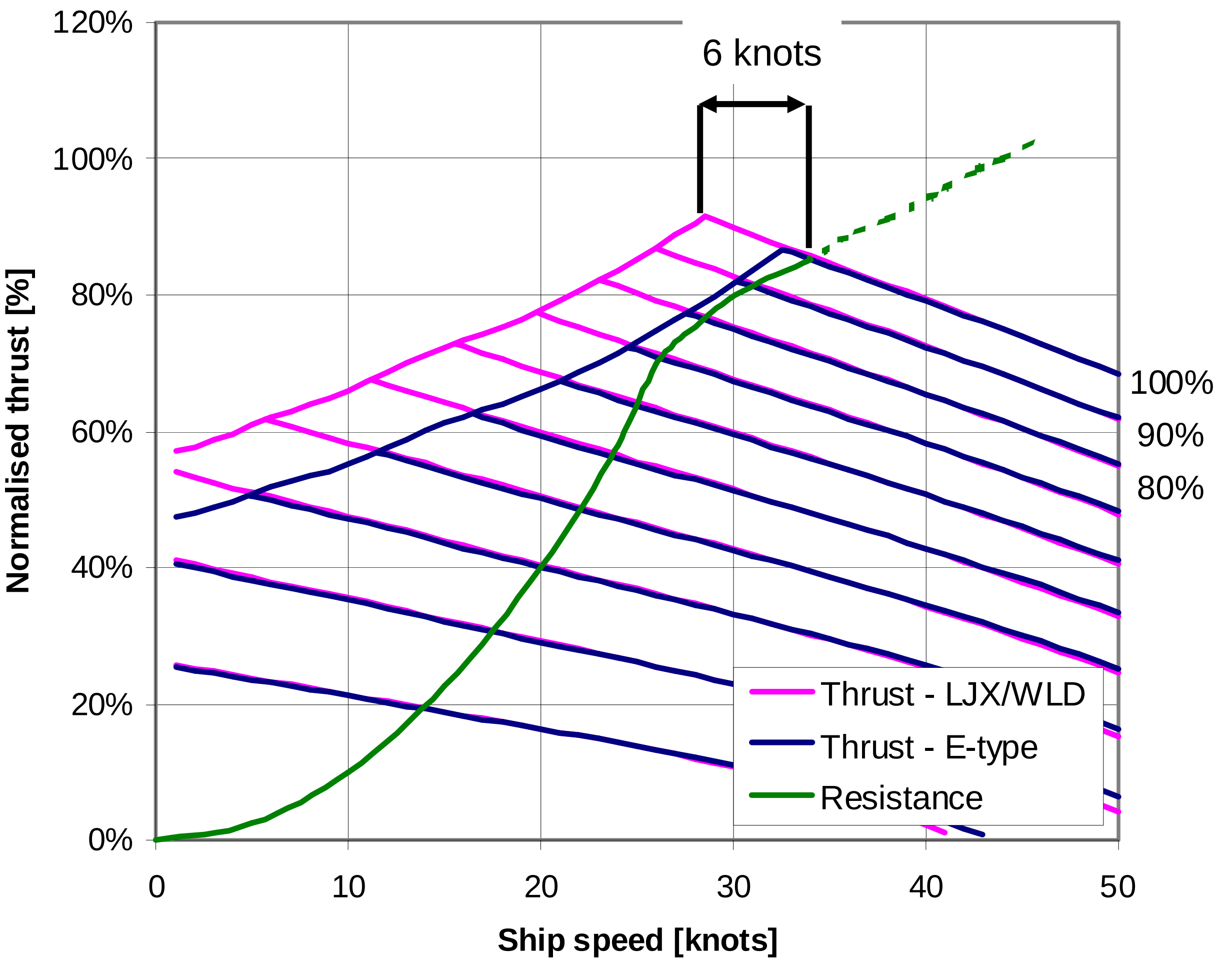

  11 December 2008 RINA Waterjet Propulsion 5 conference / Norbert Bulten

WÄRTSILÄ

Conclusions

- The shaft torque and the cavitation margins of a waterjet will be effected by steering and manoeuvring
- Starboard turns might lead to engine overload, whereas a port turn might result in over speeding of the engine
- Development of a new axial-flow pump type has resulted in increased cavitation margins for the waterjet installation
- For manoeuvring conditions 20% more thrust is available with axial-flow pump
- The free sailing cavitation performance has been increased to enable three-jet operation with sufficient margins

WÄRTSILÄ

Thank you for your attention

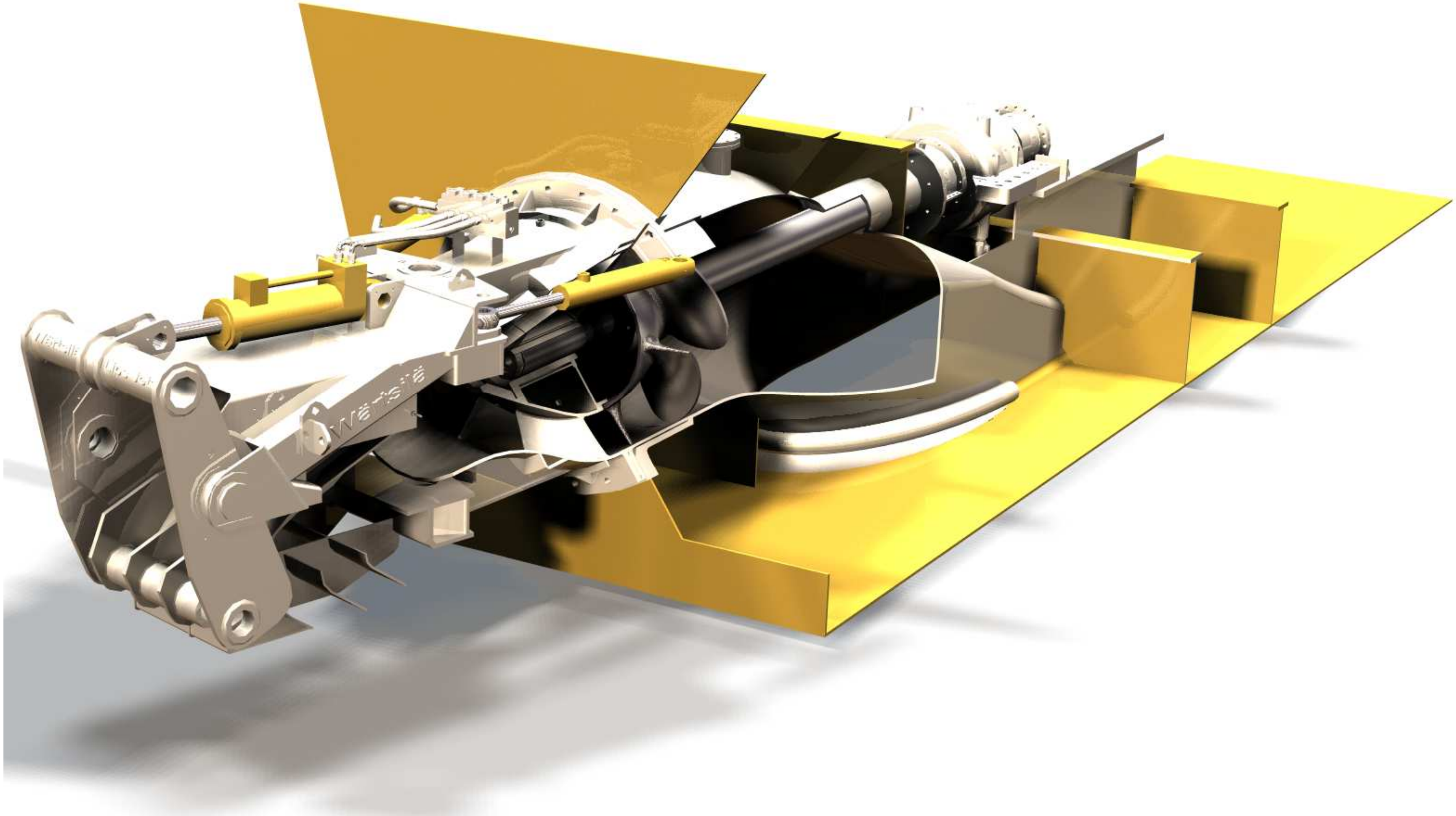

WÄRTSILÄ

RINA Waterjet Propulsion 5

Dec 11-12, London, UK

Overview of Recent Developments in Testing of Waterjets at NSWCCD

Martin Donnelly (presenting)

Scott Gowing

Naval Surface Warfare Center, Carderock Division

Code 5800 Resistance and Propulsion

Outline

- Introduction
- Model Test Arrangements
- Discussion of Results
  - Pump-loop facility
  - System test facility
  - Tow-tank self-propulsion
- Powering Predictions
- Acknowledgements

Introduction

- The use of waterjets to propel vessels > 40 knots without thrust breakdown limit of conventional open propellers
- Recent US Navy interest in waterjet propulsion
  - HSV-X1, HSV-2, modified ferry platforms
  - FSF-1 Sea Fighter, ONR funded high speed research vessel
  - LCS-1, LCS-2 – high speed Naval combatant
- NSWCCD has undertaken modifications to existing propeller test facilities to evaluate waterjets
- Evaluation of approaches developed by the ITTC for “Waterjet Test Procedures”

FSF-1 Sea Fighter

LCS-1 USS Freedom

HSV-2 Swift

Model Test Arrangements

- Pump-loop testing
  - Bypass setup
  - 7.5 in (19.05 cm) inlet diameter
  - Optical access for LDV measurements
  - Limited flowrate control
    - Water tunnel impeller limited impact
    - Use of different nozzle areas
  - Bellmouth flowmeter
    - Small area ratio difference

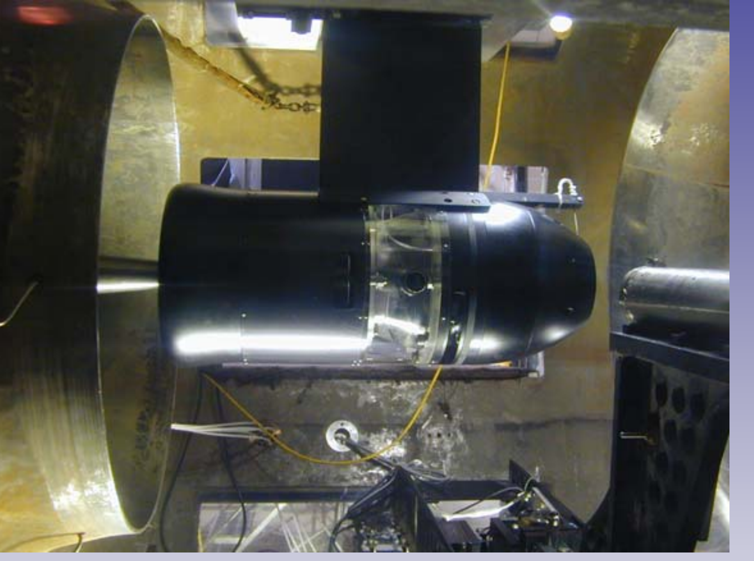

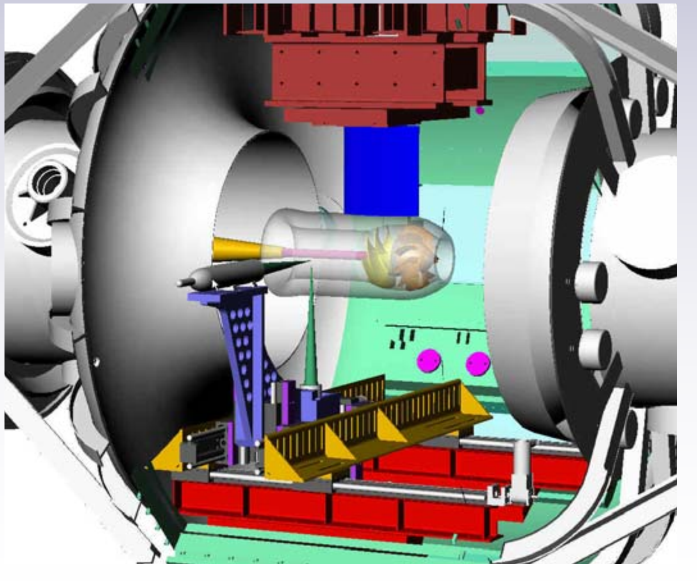

Model Test Arrangements through flow pump-loop

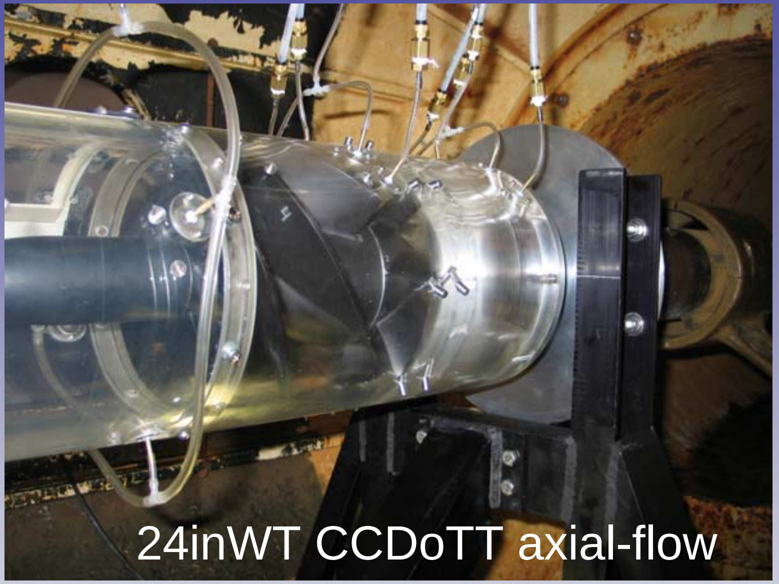

24inWT CCDoTT axial-flow

36inWT AWJ-21 mixed-flow

- Modifications to variable pressure water tunnel
- All flow through the tunnel goes through the waterjet
- 36inWT 12 in (30.5 cm) inlet diameter
- Uniform inflow confirmed with PIV
- Pressure measurements inflow plane, downstream of stator and nozzle exit
- LDV at inlet, mid-stage, nozzle exit

Model Test Arrangements through flow pump-loop

Bellmouth flowmeter

Flow control configurations

- Bellmouth flowmeter
  - Pressure drop calibrated against LDV and PIV
- Flow control
  - Combination of blockage plate, orifice plate, and tunnel impeller
  - ± 20% of design flow coefficient obtainable

Model Test Arrangements System Test - LCC

- Quantify impact on performance of non-uniform inflow
  - Ingested boundary layer
  - Rotating shaft wake
- Quantify inlet loss coefficient
- No calibrated flowrate measurements
  - Use of LDV at Stations 3 and 6 against pressure drop in nozzle
    - direct measurement of non-uniformity factors

AWJ-21 partial hull

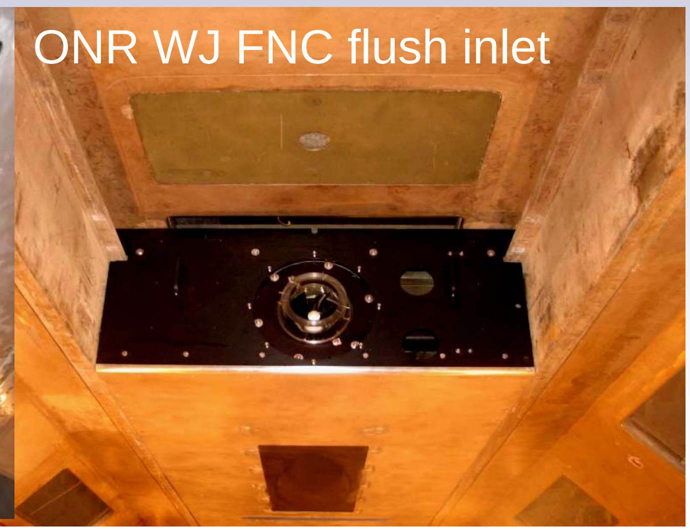

ONR WJ FNC flush inlet

Model Test Arrangements
System Test - LCC

- Thicken inflow boundary layer
  - Match ratio (δ_{bl} / D3)
  - Impacts non-uniformity factors
- Cavitation viewing
  - From top, leakage vortex
  - Suction side view along the shaft-line
  - Quantify blade coverage at breakdown

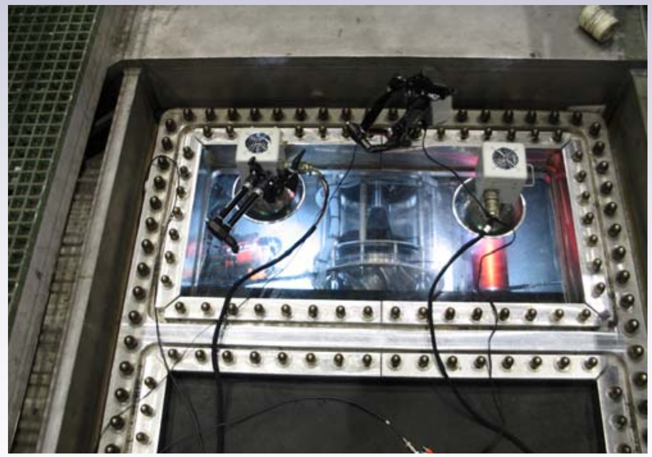
Impeller cavitation viewing

Pump Performance

- Good agreement between bypass and through flow facilities
  - Later testing attempted to locate peak efficiency
- Cavitation breakdown quantified as a 1% loss in torque
  - Used to define Zone 2 boundary in pump performance plot
  - No impact of non-uniformity on mean breakdown
- Impact of unsteady cavities on erosion not quantified

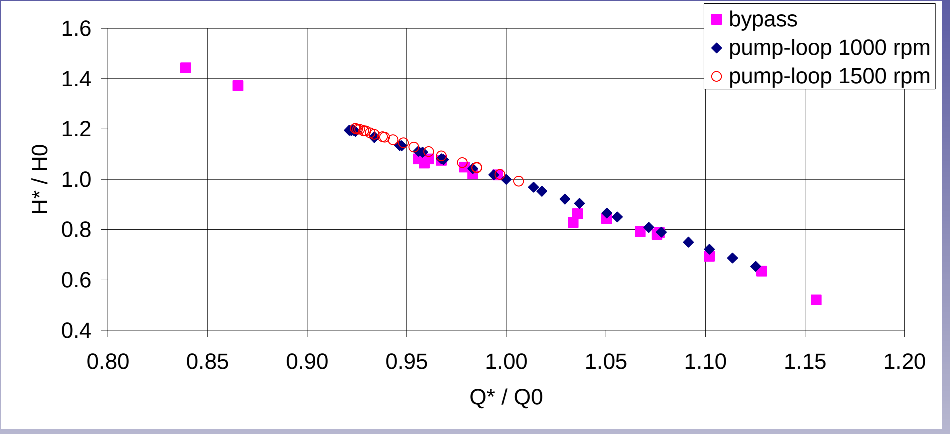

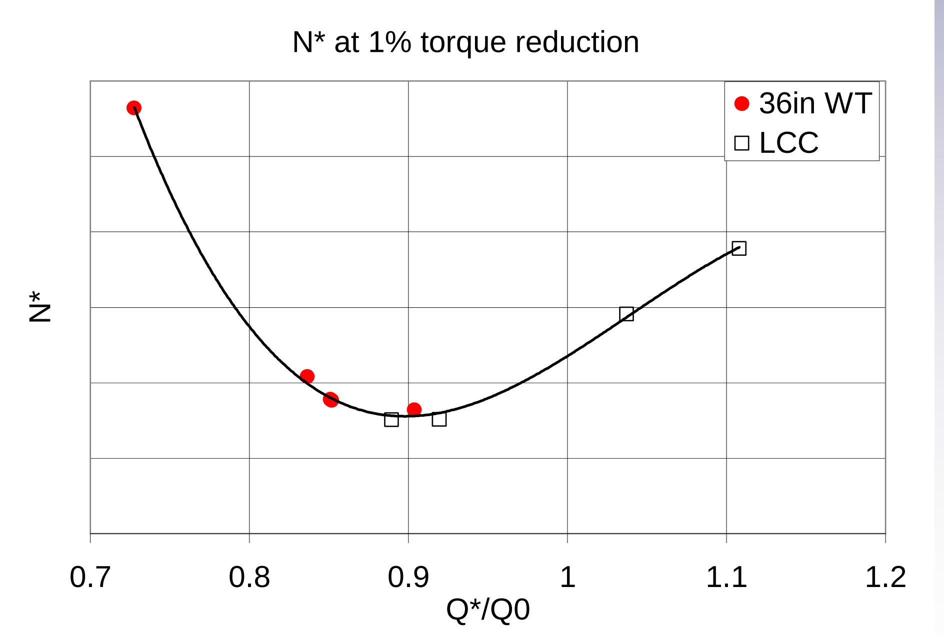

Laser flow measurements

- PIV and LDV measurements are used extensively in pump-loop and system tests
  - Flow-rate calibration
  - Quantify non-uniformity factors
  - Analysis of impeller and stator designs

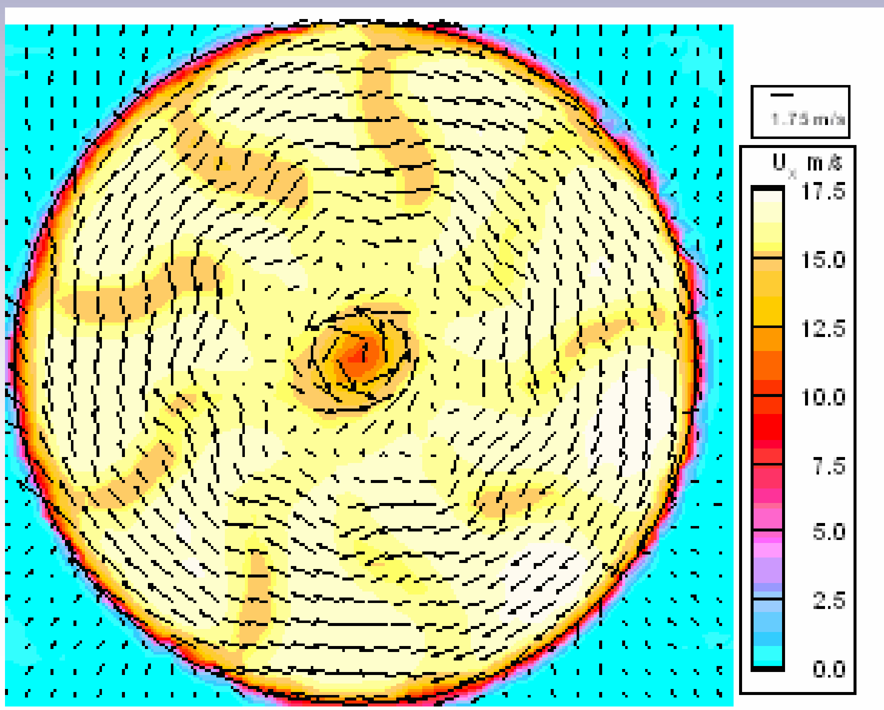

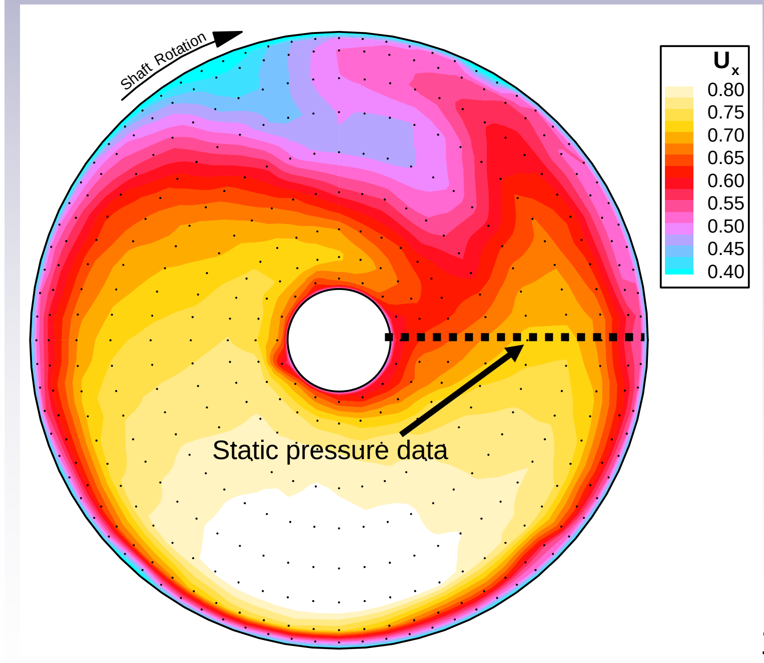

ITTC Station 3 – Static Pressure

- Kiel probe measurements at impeller inflow plane
  - Quantify error in assuming constant static pressure at Station 3
- CFD used to predict static pressures in tow-tank testing

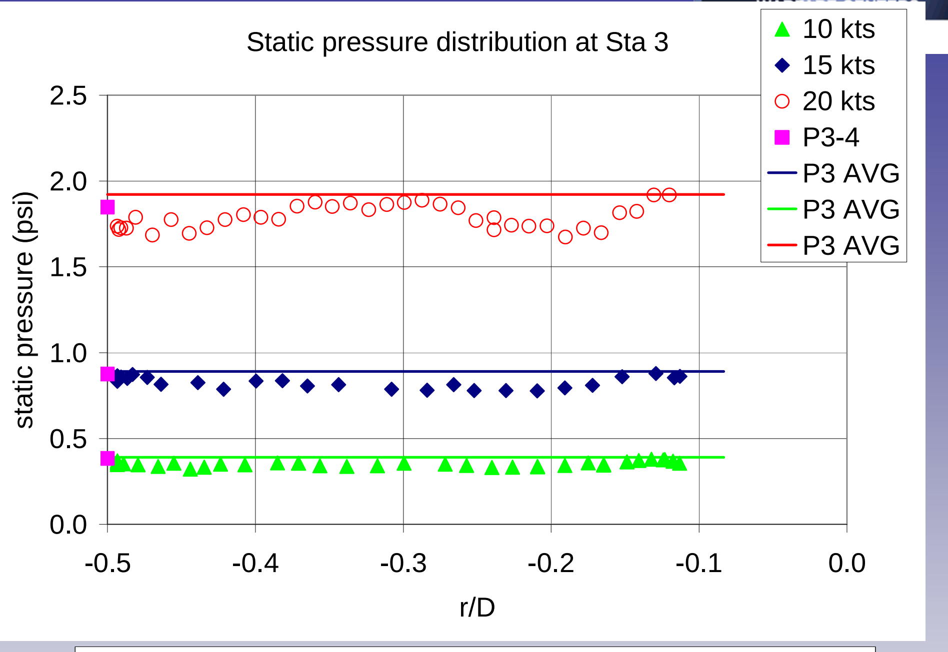

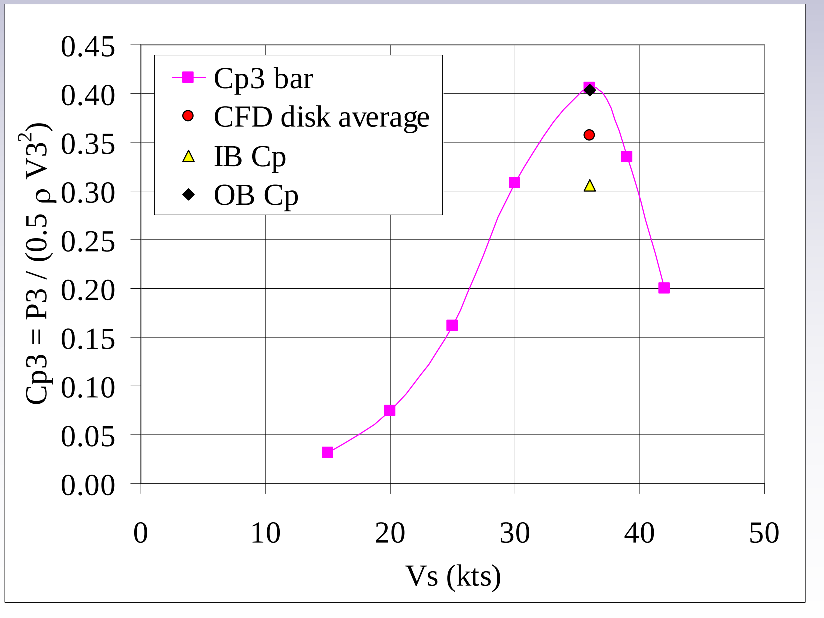

Tow-Tank Self Propulsion

- Objectives
  - quantify performance differences of a mixed vs. axial flow hullform
  - evaluate waterjet test procedures developed by 24th ITTC

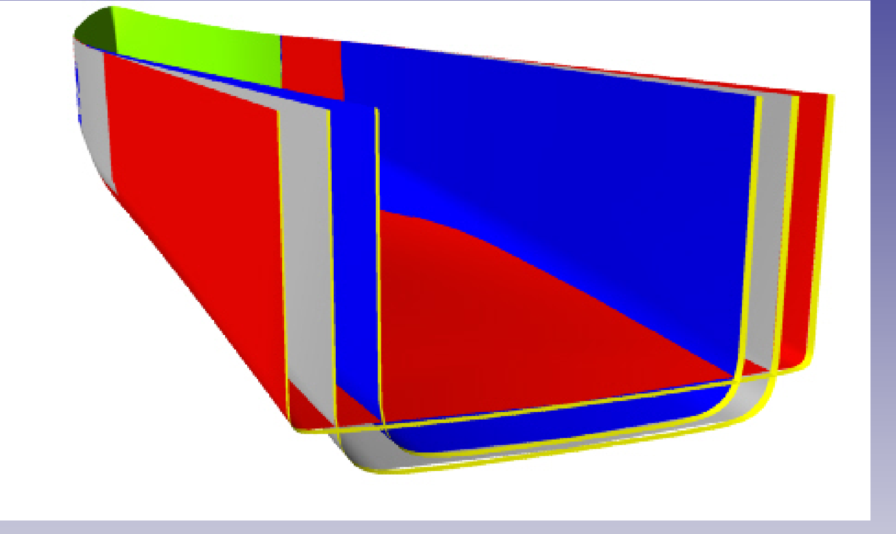

- Resistance gains of axial hull offset by thrust deduction
- Thrust deduction as measured in a tow-tank self propulsion test
- use of traditional tow force and inlet wake scaling procedure to account for Re# effects

Jet Nozzle flow rate tests using Collection Tank

- Dry dock height adjustment minimizes back pressure from collection plumbing
- LDV and pressure measurements taken simultaneously

Collection Tank on a scale in dry dock

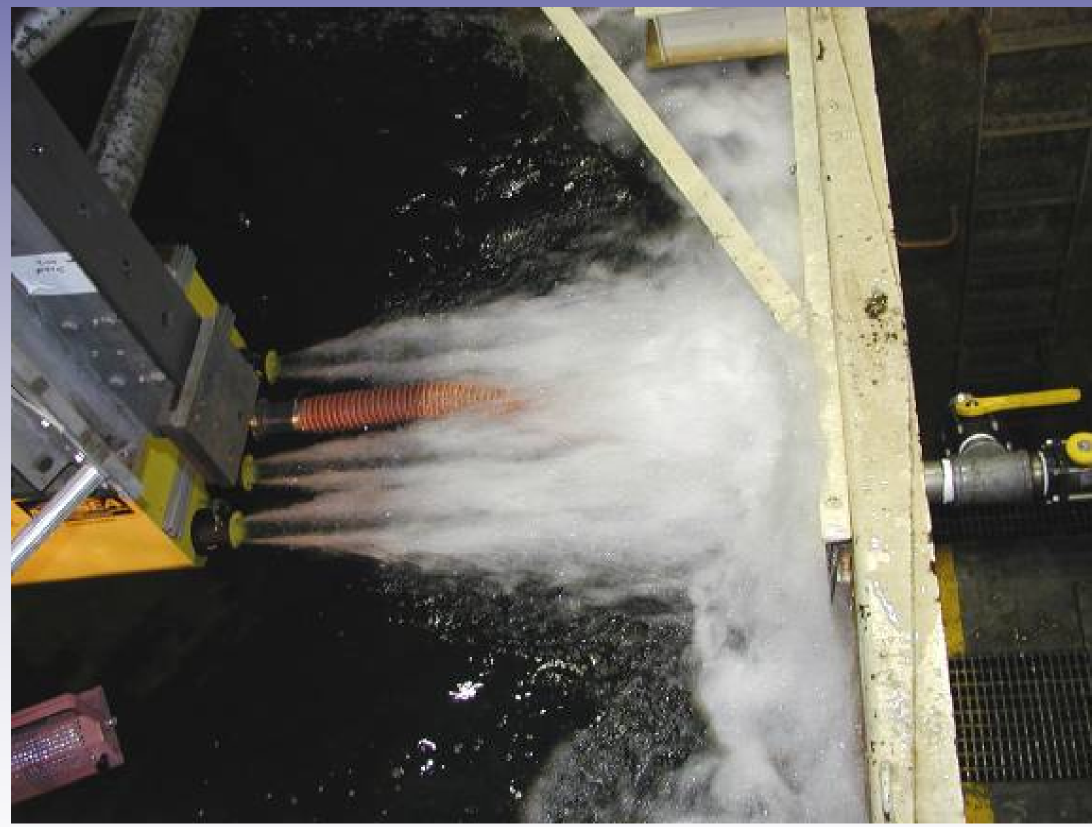

Flow rate measured, one nozzle at a time

Bollard Test Set-up

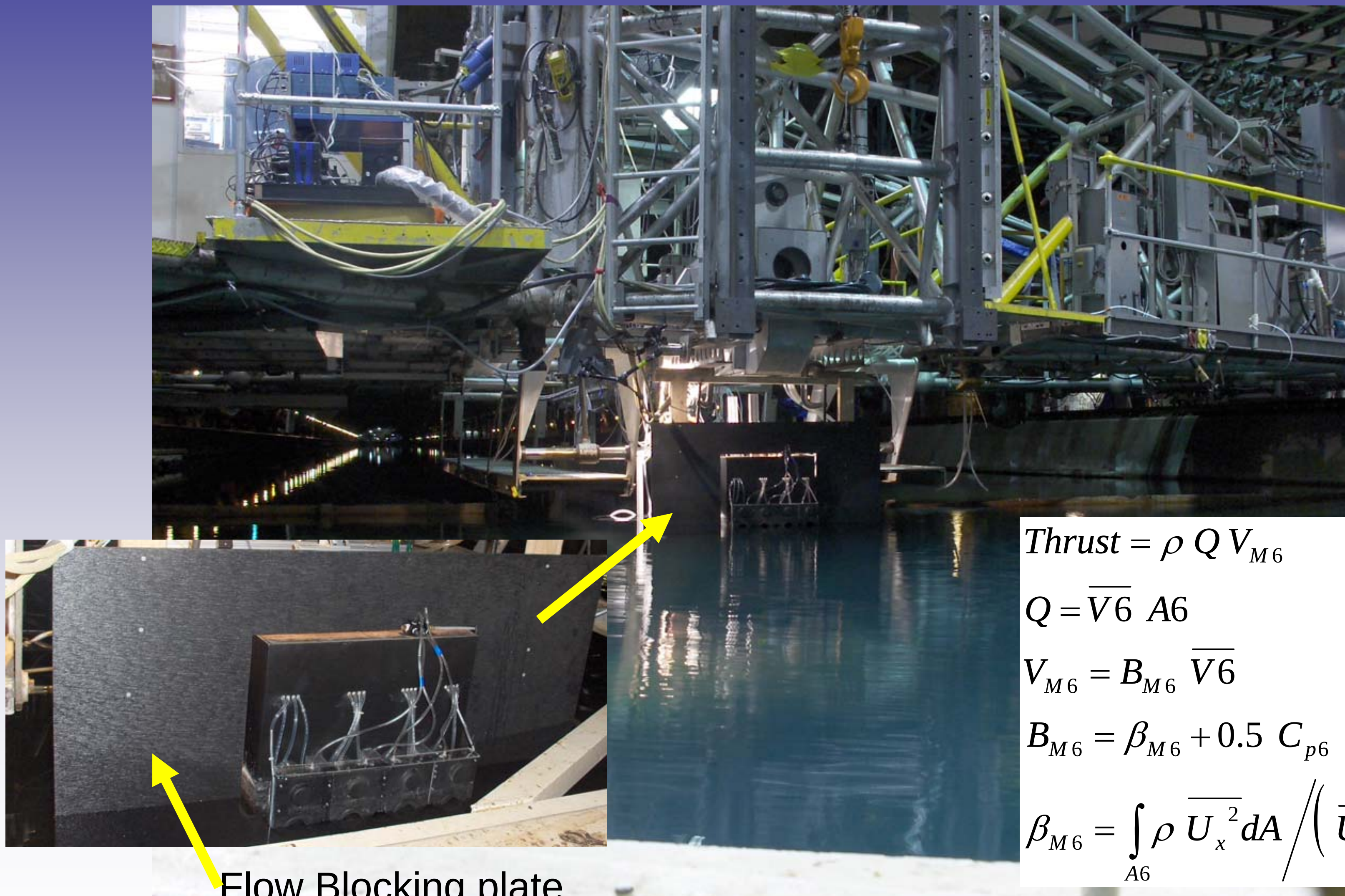

Flow Blocking plate

$$Thrust = \rho\, Q\, V_{M6}$$

$$Q = \overline{V6}\; A6$$

$$V_{M6} = B_{M6}\; \overline{V6}$$

$$B_{M6} = \beta_{M6} + 0.5\; C_{p6}$$

$$\beta_{M6} = \int_{A6} \rho\; \overline{U_x}^{2} dA \Big/ \left(\overline{U_x}^{2} A6 \right)$$

Accuracy of Methods

worst approach

Method	St 6 Sensor	Flux Calibration	St 6 Flux	Bias		95% Confidence Interval			
						1 Probe	2 Probes	3 Probes	4 Probes
A	Kiel Probes	Bollard Forces	Mass	-0.6%	+ / -	8.4%	4.3%	3.1%	3.0%
	$R = 0.8*R_{JET}$		Momentum	-1.0%	+ / -	16.6%	8.6%	6.3%	6.0%
			Energy	-1.5%	+ / -	24.6%	12.9%	9.5%	9.0%
B	Kiel Probes	Flow Rate Test	Mass	-0.4%	+ / -	9.0%	4.2%	3.0%	2.8%
	$R = 0.7*R_{JET}$		Momentum	-0.5%	+ / -	18.1%	8.3%	6.1%	5.7%
			Energy	-0.6%	+ / -	27.2%	12.4%	9.3%	8.5%
C-1	LDV Survey	None	Mass	-0.0%	+ / -	1.3%	1.3%		
	Single RPM		Momentum	-0.0%	+ / -	1.1%	1.1%		
			Energy	-0.0%	+ / -	1.8%	1.7%		
C-2	Kiel Probes	LDV Survey	Mass	0.1%	+ / -	2.6%	2.0%	1.8%	1.7%
	Other RPMs		Momentum	0.3%	+ / -	5.0%	3.7%	3.3%	3.1%
	$R = 0.7*R_{JET}$		Energy	0.4%	+ / -	7.7%	5.8%	5.2%	5.0%
D	LDV Survey	Bollard Force and Flow Rate Tests	Mass	NA	+ / -	1.2%	1.2%		
			Momentum	NA	+ / -	0.8%	0.8%		
			Energy	NA	+ / -	1.4%	1.2%		

best approach

Results

- As expected the narrower, shallower hull form has lower resistance throughout the speed range
- Between 30-36 knots this benefit is offset by a thrust deduction, 1-t, > 1
- Due to the larger inlet spacing of the axial hull the capture area is wider and narrower
  – Ingest more low momentum fluid from the boundary layer
  – This conclusion is a result of the use of CFD to define the inlet capture area
- Additional investigation into the role of sinkage and trim into thrust deduction factor is ongoing

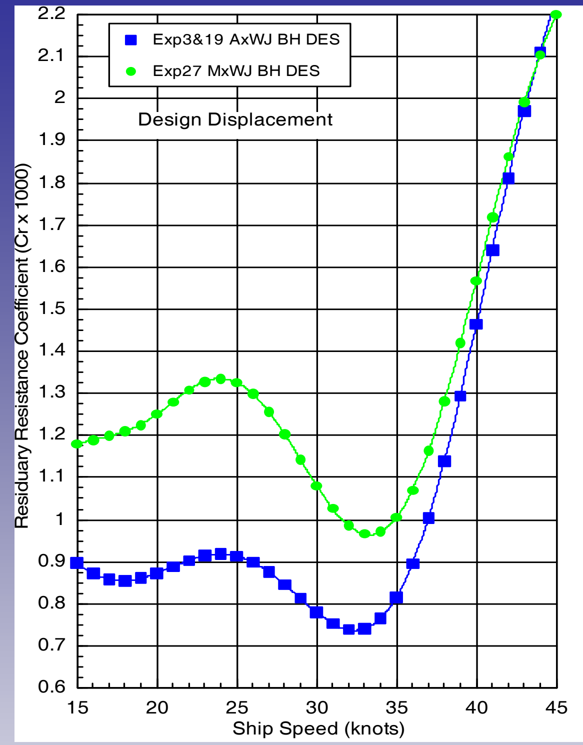

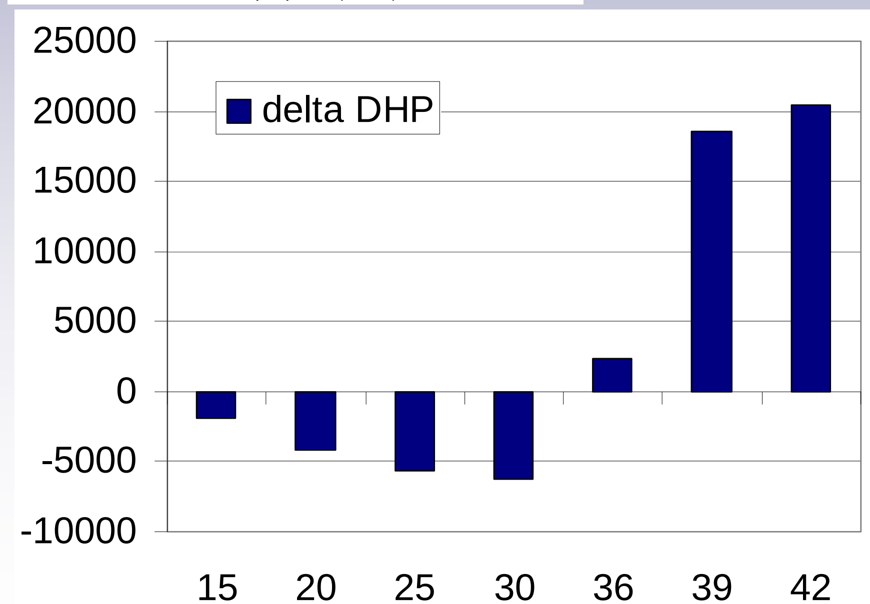

Role of tow-tank experiment

- Are tow-tank self-propulsion tests required and useful for waterjet propelled vessels?
  - YES, where full-scale experience is lacking, or novel waterjet arrangements are proposed
- What data do they provide?
  - Thrust deduction factor
  - Model-scale wake fraction
    - Definition of inlet capture area critical to these definitions
  - A direct scaling of energy rise across the pump (E5-E3) has shown good agreement (<5%) with alternative methods

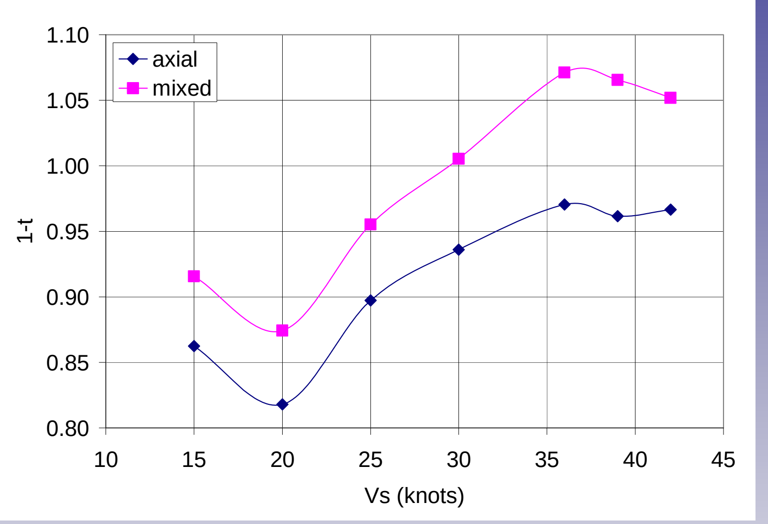

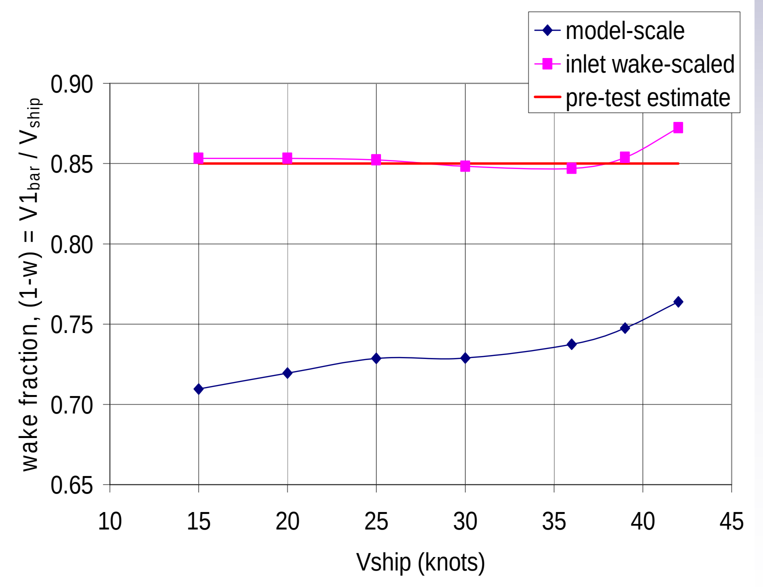

Inlet Capture Area

- Initial definition of a trapezoidal capture area refined with CFD
- Applying the CFD capture area to LDV measurements of ITTC Station 1 results in no significant change (<1% on power, system thrust)
- Using CFD capture area and computed boundary layer for the axial hull
  - 6.4% change in 1-t
  - 5.8% change in wake fraction, 1-w
- Current definition of trapezoidal capture area does not include inlet spacing

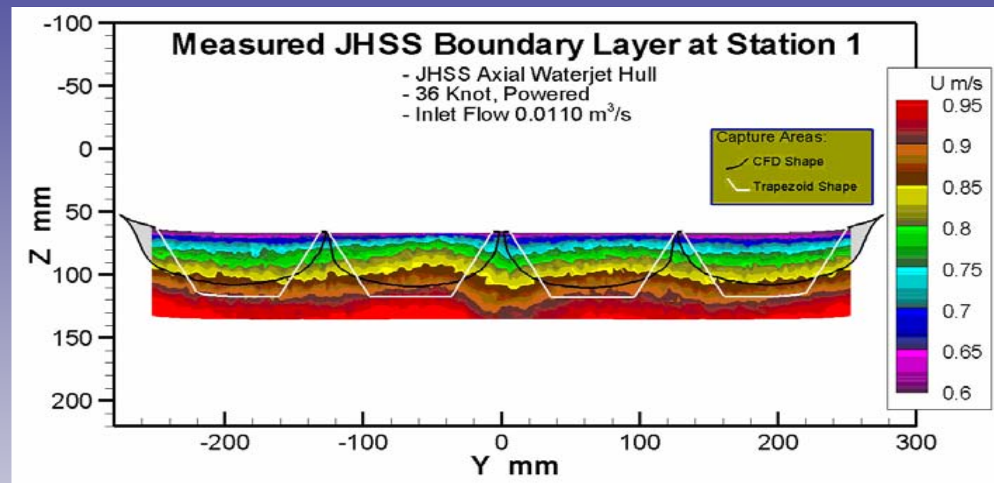

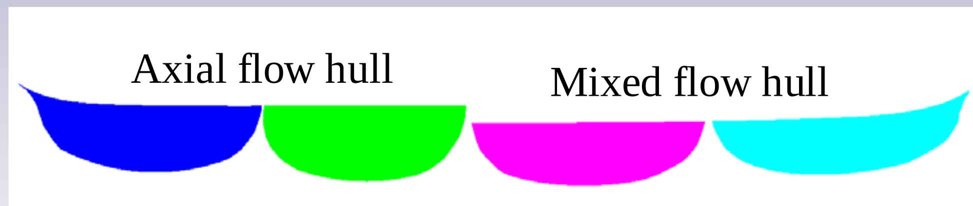

Additional details of this analysis will be published at the 1st Symposium on Marine Propulsors, Trondheim, Norway, June, 2009

Powering Predictions

- Options
  - Vendor approach
  - Direct scaling of tow-tank self propulsion data
- Accuracy of each approach
  - Vendor approach relies on the accuracy or source of predictions for 1-t, 1-w, ζ_{13} (inlet loss coefficient), hull resistance
  - Tow tank relies on measurement accuracy and Reynolds number scaling of ingested boundary layer
- Tow-tank uncertainty analyzed using a Monte Carlo approach
  - random variations on measurement channels within error bands determined by calibration and repeatability

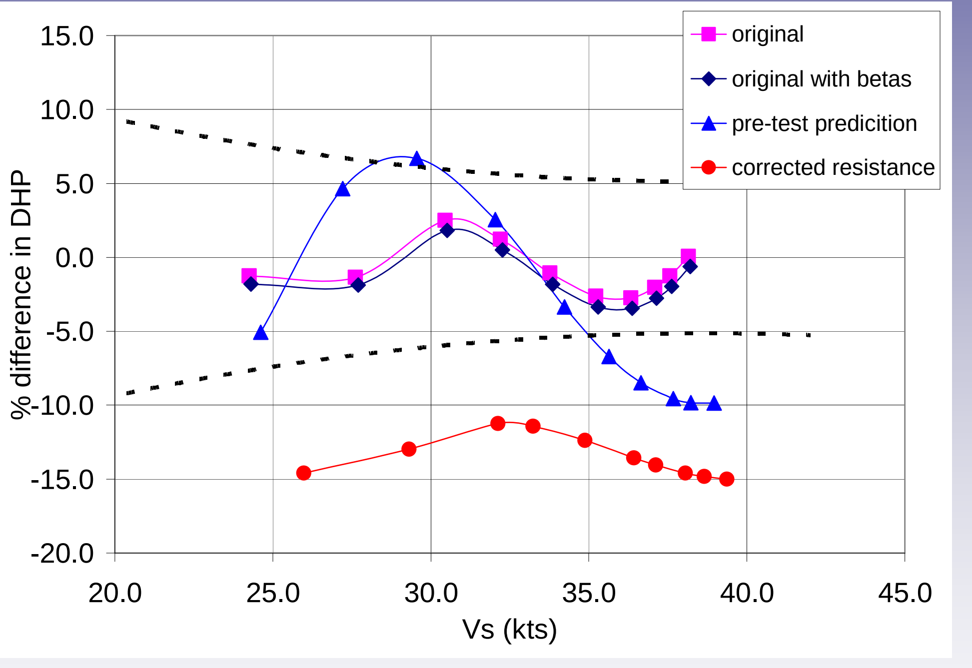

A full CFD solution is in the pipeline with NSWCCD and University of Iowa evaluating the use of CFDShip Iowa for WJ powering predictions

Conclusions

- NSWCCD has rapidly increased their waterjet testing capability
  - evaluate proposed vendor (COTS) propulsion solutions
  - evaluate waterjets as a propulsion option for high speed sealift vessels
- Introduced new experimental techniques, scanning LDV system, to push experimental uncertainty to lowest levels obtained with tow-tank self-propulsion testing
- Incorporating CFD into current measurement practices is essential for accurate powering predictions

Acknowledgements

This work has been sponsored by

- U.S. Office of Naval Research
  - Sponsor Dr. Ki-Han Kim
- NAVSEA PMS 325 JHSS Program Office
- Center for the Commercial Deployment of Transportation Technology (CCDoTT)

Commercial partners

- Wärtsilä Defense Inc
- Wärtsilä Propulsion Netherlands
- Rolls Royce Naval Marine Inc
- KaMeWa ABB
- CDI Marine Systems Development Division

- Numerous NSWCCD engineers, technicians, machinists, and interns who have contributed to the successful execution of these test programs

Questions?


No. 4
No. 3

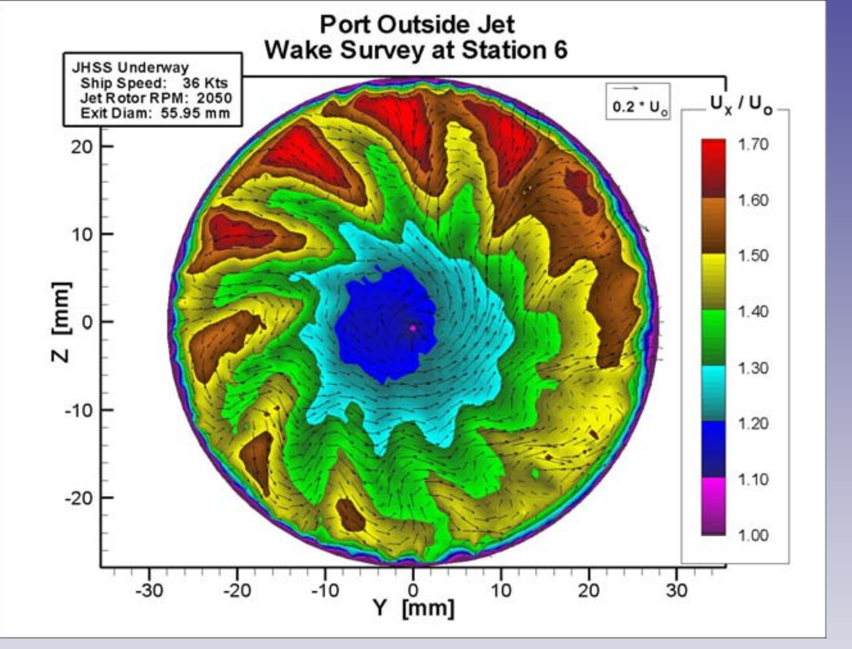
Port Outside Jet
Wake Survey at Station 6
JHSS Underway
Ship Speed: 36 Kts
Jet Rotor RPM: 2050
Exit Diam: 55.95 mm
0.2 * U_o
U_x / U_o
1.70
1.60
1.50
1.40
1.30
1.20
1.10
1.00
Z [mm]
Y [mm]
20
10
0
-10
-20
-30
-20
-10
0
10
20
30

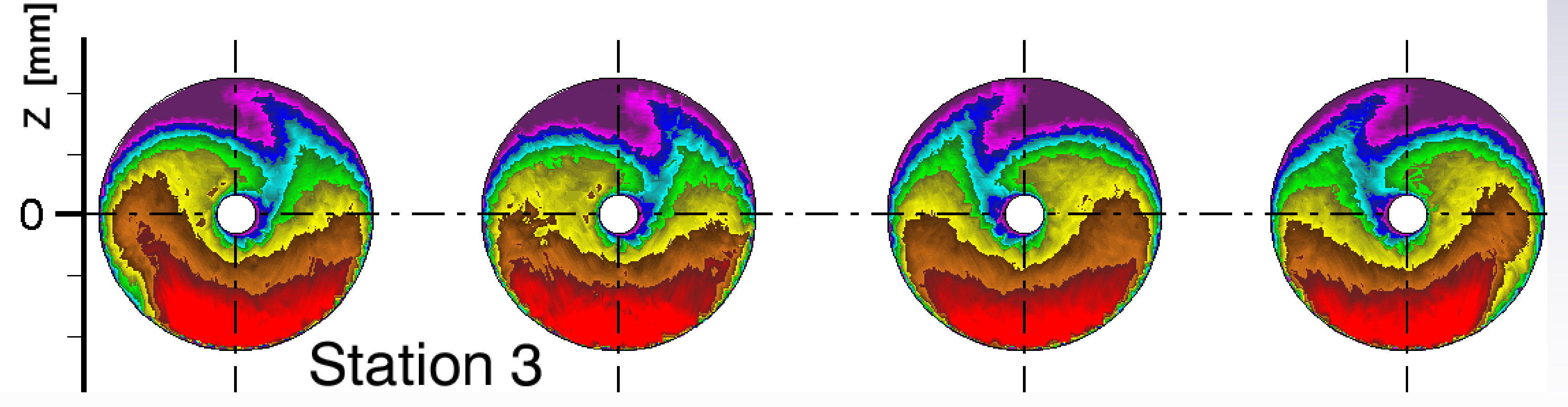
Z [mm]
0
Station 3

Waterjet Propulsion 5-International Conference

RINA-The Royal Institution of Naval Architects

Research on Hydrodynamic Performance of Hybrid Propulsion System

Cunlou Sun, Yongsheng Wang and Zhuying Li

University of Naval Engineering, China

Contents

1.Introduction

2.Concept design integration

3.Validation of CFD results

4. CFD analysis of hybrid propulsion system

4.1 flow characteristics of hybrid propulsion system

4.2 influence of the relative position of propellers and waterjet

4.3 influence of propeller shaft rotating direction

5. Theory analysis

6. Conclusion

1.Introduction

Advantages of hybrid propulsion systems of waterjet(s) and propeller(s):

a. Higher efficiency

b. More operation models

c. Both propeller/waterjet and diesel/gas turbine can work in an optimal way together

Model of MEKO A-200 SAN (courtesy of J.Wessel, Blohm+Voss GmbH)

Flow interaction of propellers and ducting inlet

Propellers and waterjet(s) arranged on hull aft together, There is an interaction between them.

2.Concept design integration

A hybrid propulsion system similar to MEKO A -200 was designed.

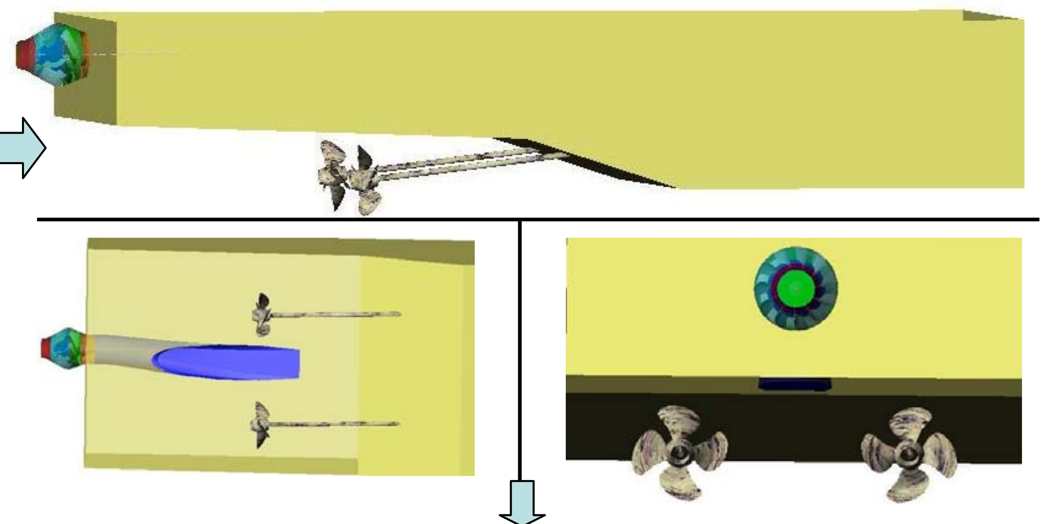

The main issue concerned is the interaction between waterjet and propellers so that only stern part of vessel is considered and no particular ship model is used. To further simplify the problem, the ship is truncated at the design waterline, eliminating the need to define the free surface.

Table 1 Selected Hybrid Propulsion System Data

Design speed	**30knot**
Waterjet intake duct diameter	**71cm**
Propeller diameter	**1.15m**
Power of propellers in mode III	**2*600kW**
Power of waterjet in mode III	**2000kW**
Propeller speed	**732rpm**
Waterjet speed	**850rpm**

3.Validation of CFD results

Mesh of isolated waterjet propulsion system

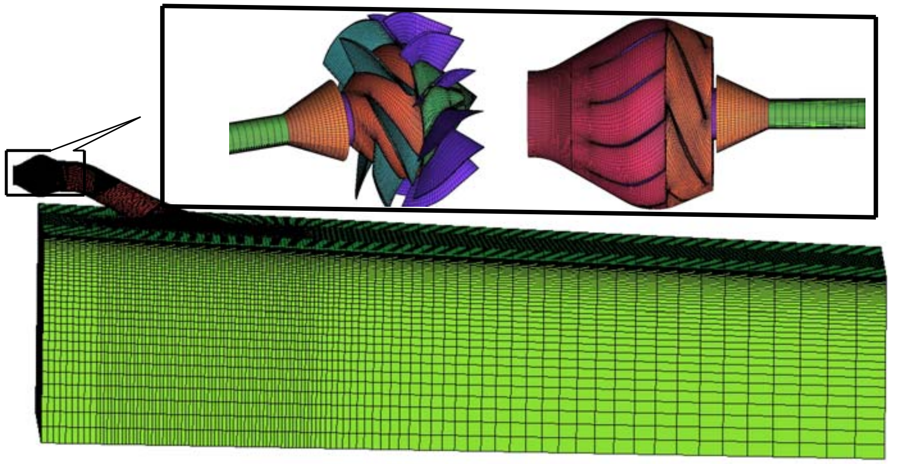

Maximum errors:

Thrust : 8.6%,

Torque:3.8%

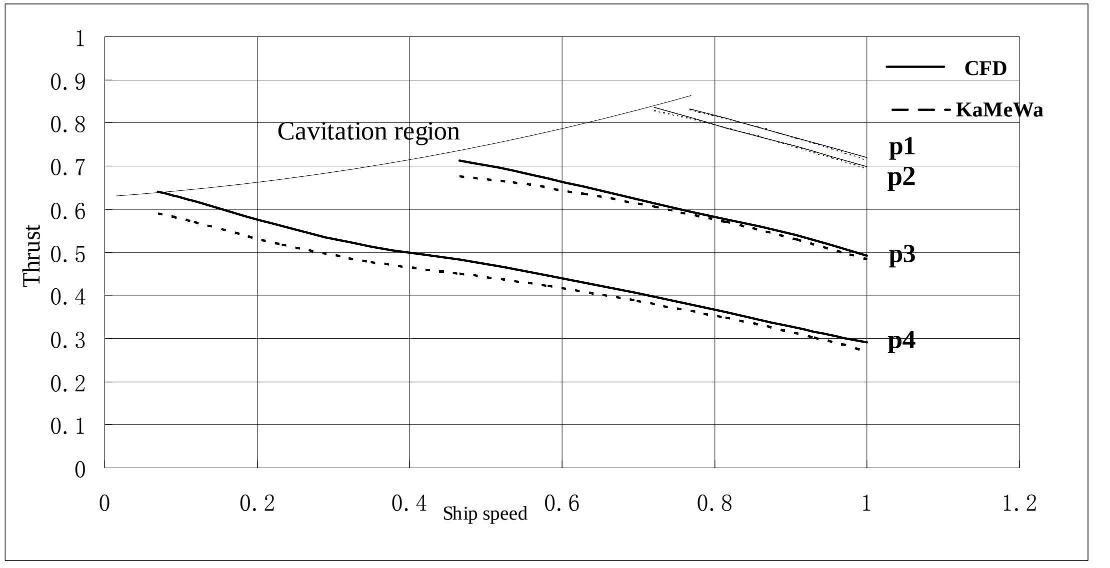

3.Validation of CFD results

Mesh of open water propeller.

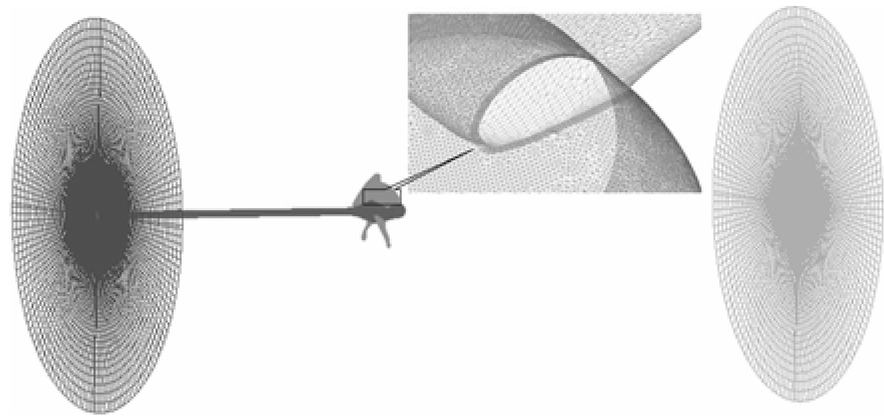

maximum errors of thrust and torque coefficients:8%

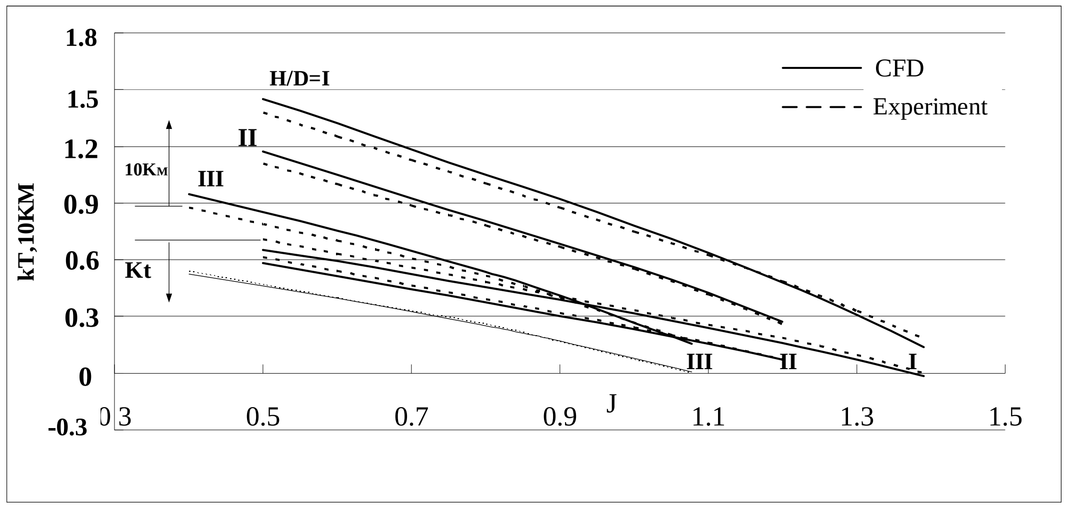

4. CFD analysis of hybrid propulsion system

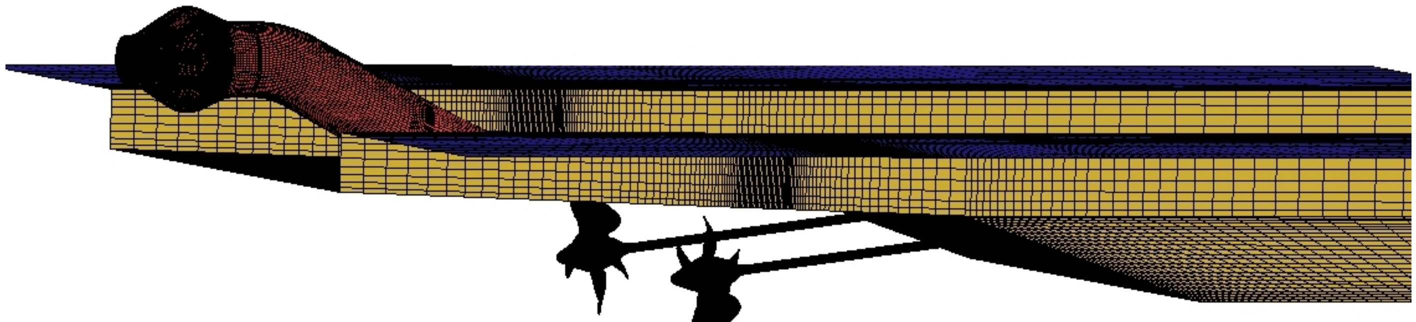

Surface mesh of hybrid propulsion system

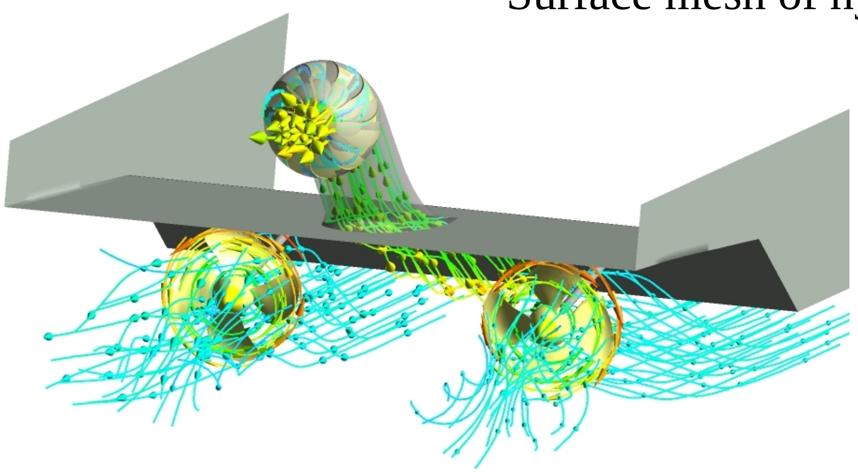

a. view from the afterbody of ship (inward)

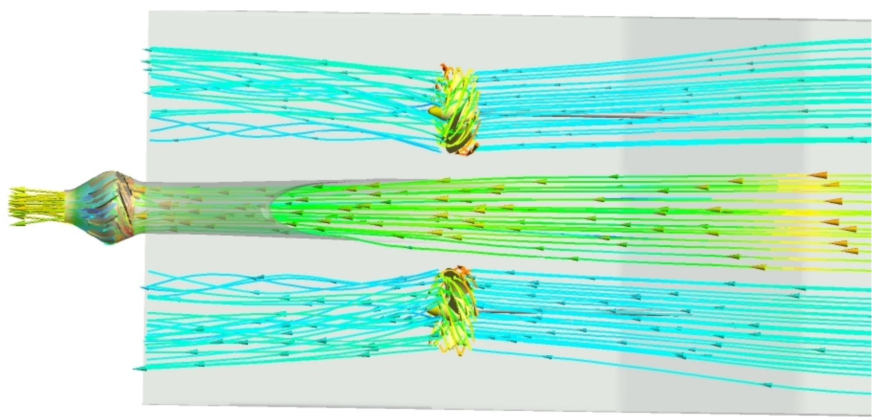

b. view from the bottom of ship (inward)

4. CFD analysis of hybrid propulsion system

4.1 Flow characteristics of hybrid propulsion system

Pressure distributions are different for different blades.

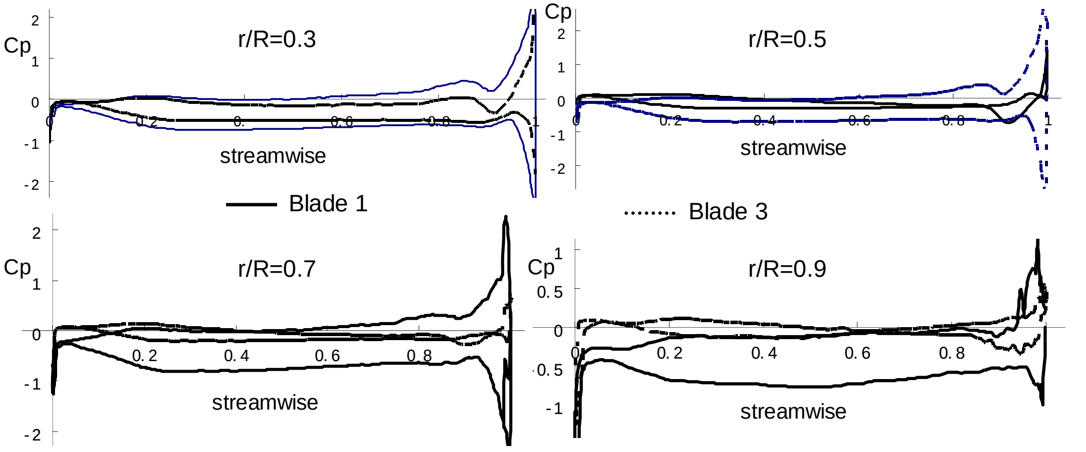

Blades near the ducting inlet are easy to occur cavitation.

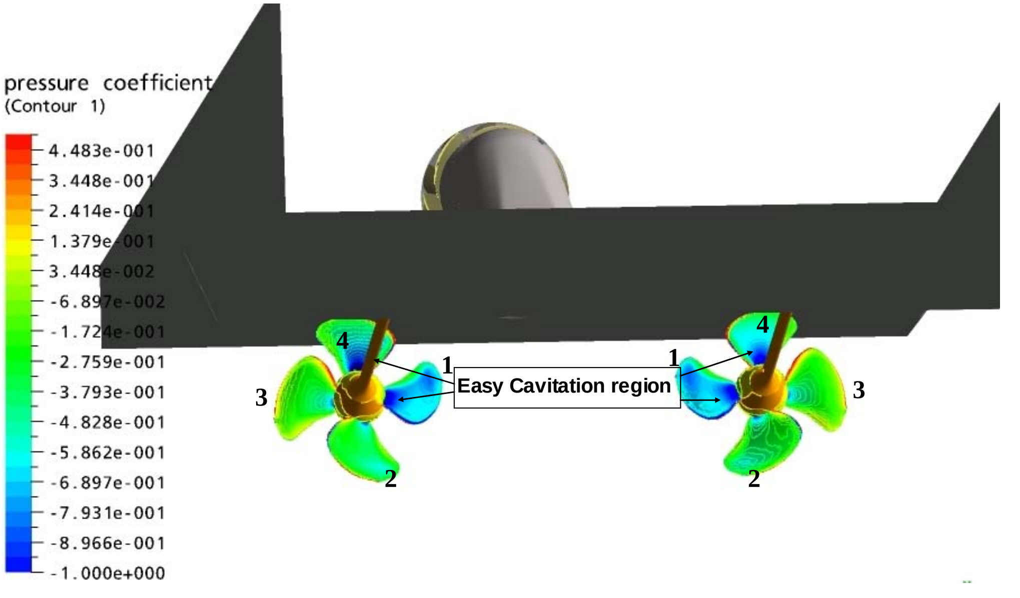

4. CFD analysis of hybrid propulsion system

4.2 Influence of the relative position of propellers and waterjet

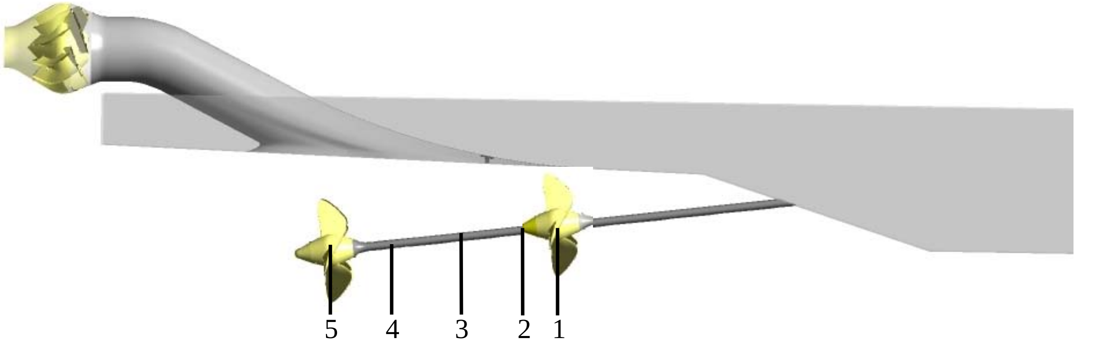

Five positions of propellers

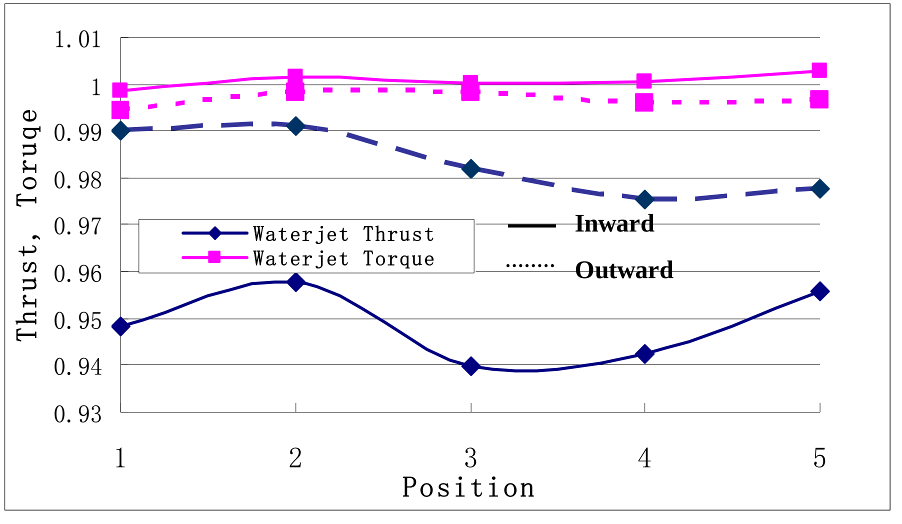

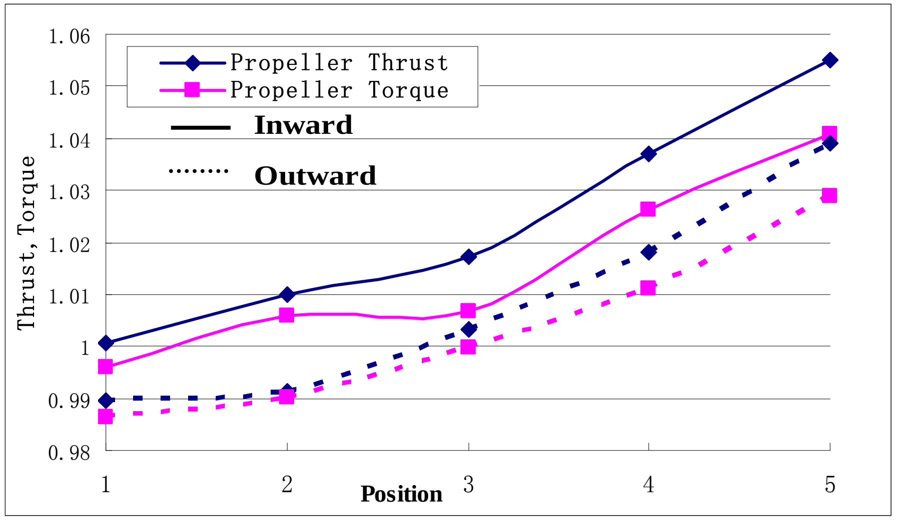

4. CFD analysis of hybrid propulsion system

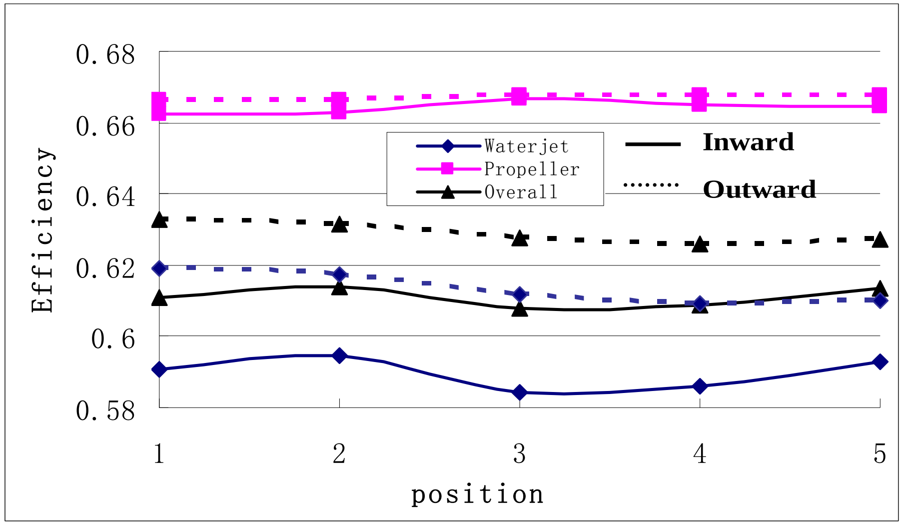

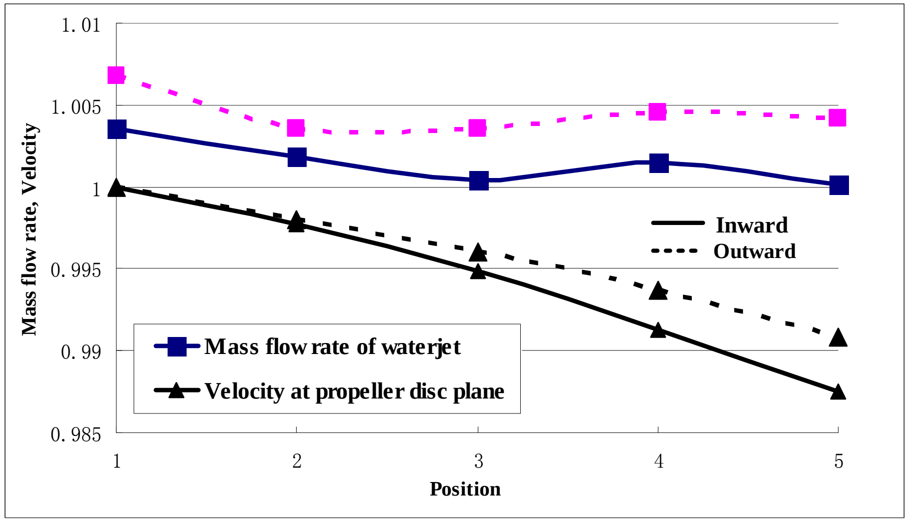

Waterjet's performance changed narrowly:2%

Propellers' Performances changed widely:6%

Propeller is more sensitive to the change of positions

4. CFD analysis of hybrid propulsion system

4.3 Influence of propeller shaft rotating direction

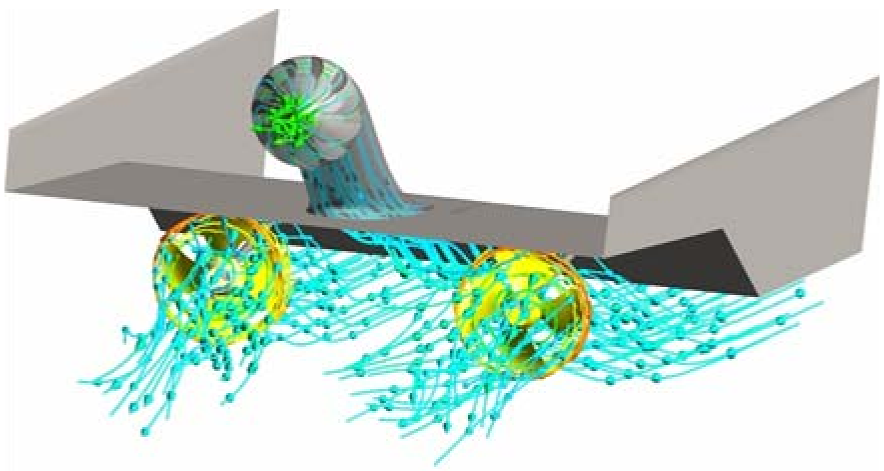

a. view from the afterbody of ship (outward)

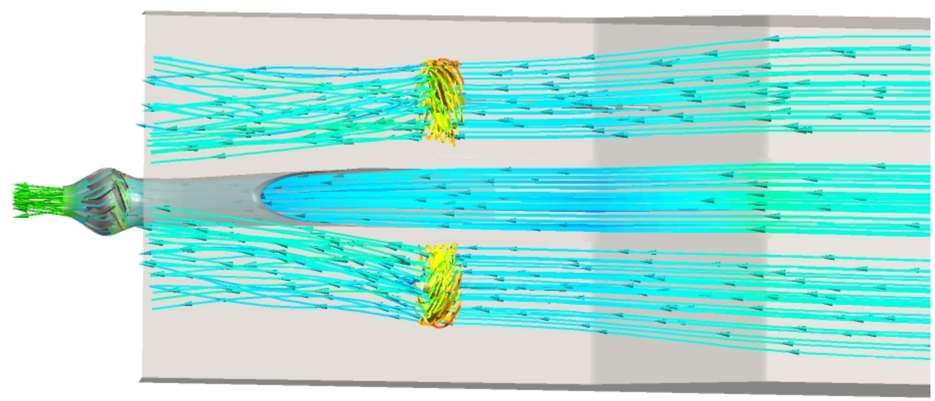

b. view from the bottom of ship (outward)

4. CFD analysis of hybrid propulsion system

4.3 Influence of propeller shaft rotating direction

non-uniformity of pump inflow is expressed as a single value ζ

$$\zeta = \frac{1}{Q}\int\sqrt{(v - v_{pump})^2}\,dA$$

non-uniformity of outward rotating propellers is smaller than inward rotating propellers. From this aspect, outward rotating propellers is better for hybrid propulsion system

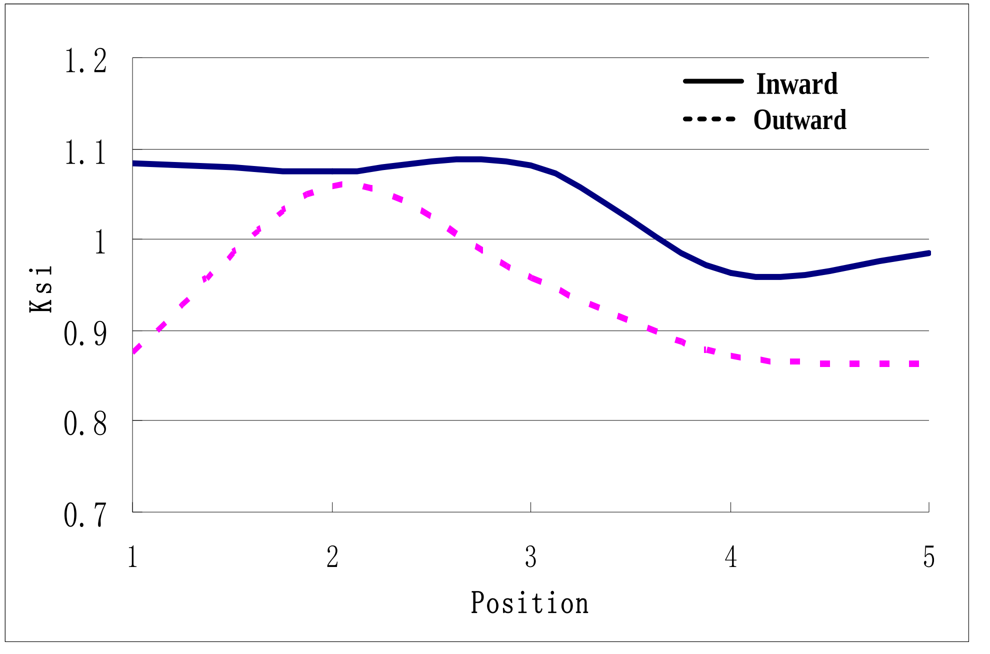

5. Theory analysis

Thrust of waterjet and propeller can be derived from the momentum balance for an incompressibility fluid.

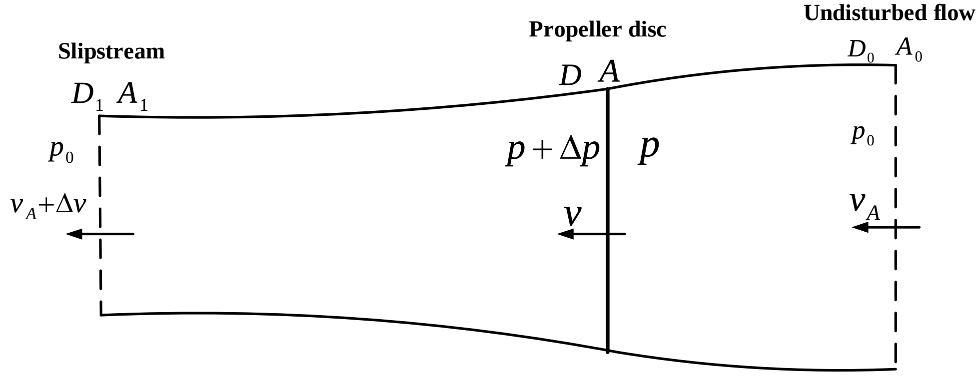

Define: $$\mu = \frac{v_{in}}{v_{out}}$$

For propellers: $$C_{Tprop} = \frac{T_{prop}}{1/2\rho v_A{}^2 A_{prop}} = \frac{(v_A+\Delta v)^2}{v_A{}^2} - 1 = \frac{1-\mu^2}{\mu^2}$$

For waterjets: $$C_{Tjet} = \frac{2(1-\mu)}{\mu^2}$$

For a waterjet the ratio between the inlet and nozzle area is fixed, whereas it is related to the thrust for an open propeller. For a hybrid propulsion system of waterjet(s) and propeller(s), propeller flow condition is greatly disturbed while waterjet flow condition only has small changes. This can be seen from the streamline of hybrid propulsion system. So propeller is weaker in hybrid propulsion system, more attention should be given to it.

6.Conclusion

a. Flow field of hybrid propulsion is different from isolated condition.

b. Performances of waterjet and propellers will be changed when the relative position of propellers and ducting inlet are changed and propellers' performances change more widely.

c. For hybrid propulsion system, propellers rotating outward is more better, non-uniformity of pump inflow is smaller and efficiency is higher.

d. Propellers are more sensitive to the change of flow field on hybrid propulsion system. More attention should be given to propellers when a hybrid propulsion system is designed.

The End

Thanks for your attention

Research on the Optimum Blades Number of Mixed Flow Pump based on CFD

Qiongfang Yang & Yongsheng Wang
Zhihong Zhang & Mingmin Zhang
Naval University of Engineering, China

Presented at the WATERJET PROPULSION 5 Nov. 2008 Meeting
London, UK
November 2008

Topics

- General introduction about waterjet
  - Down select to one shape
- Research method: CFD
  - Validation effort
  - Change rotor’s blades only
  - Change stator’s vanes only
  - Change rotor’s blades and stator’s vanes simultaneously
  - Comparison of pump incipient cavitation performances
  - Down select to nine shape
- Results of analyses
  - The optimum rotor-stator blades match
  - Down select to two shape
- Evaluate the flow noise level of the waterjet pump
  - The project forward
  - Down select to one shape

General waterjet introduction

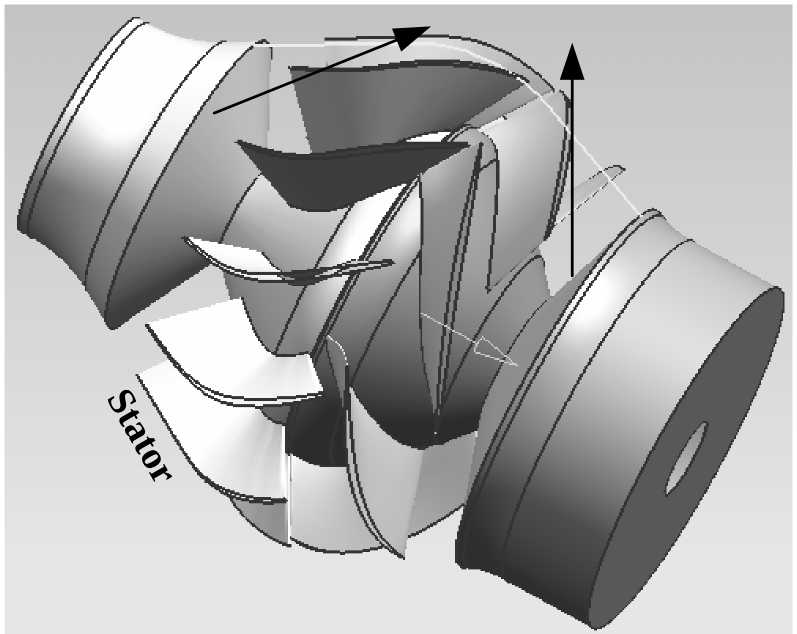

Mixed-flow Waterjet Pump Geometry

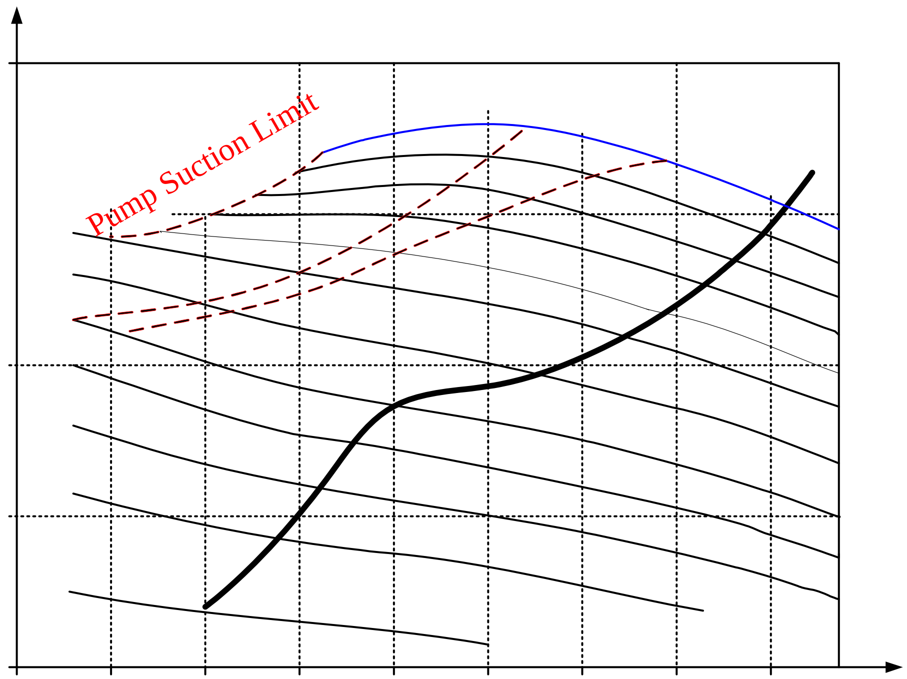

Waterjet Maps

Nozzle

Add

Computational Grid

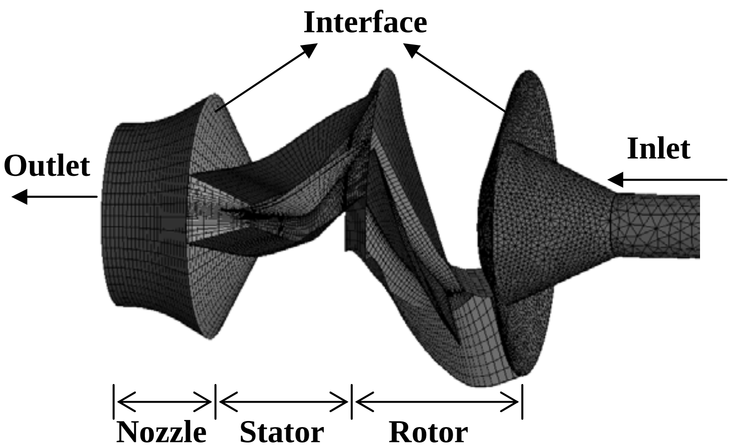

Single Passage

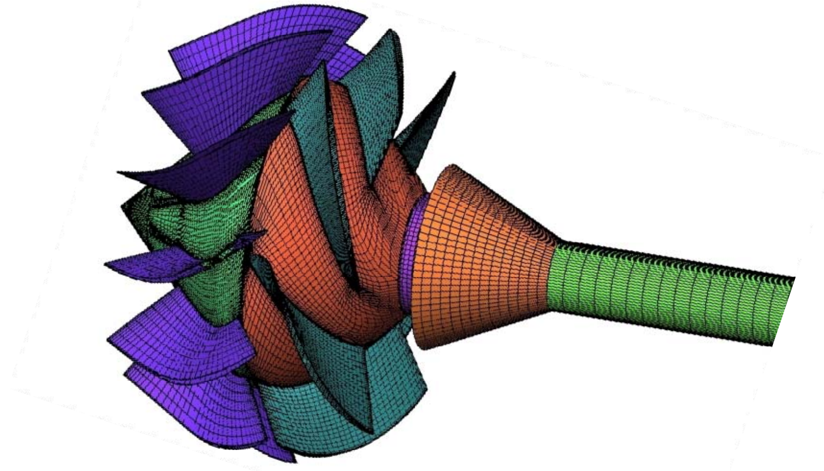

Surface Grids

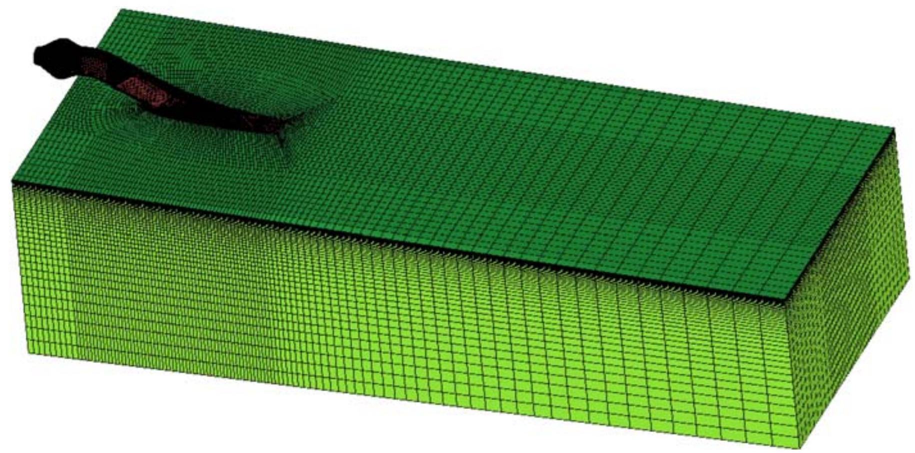

Whole Calculation Domain

Validation effort

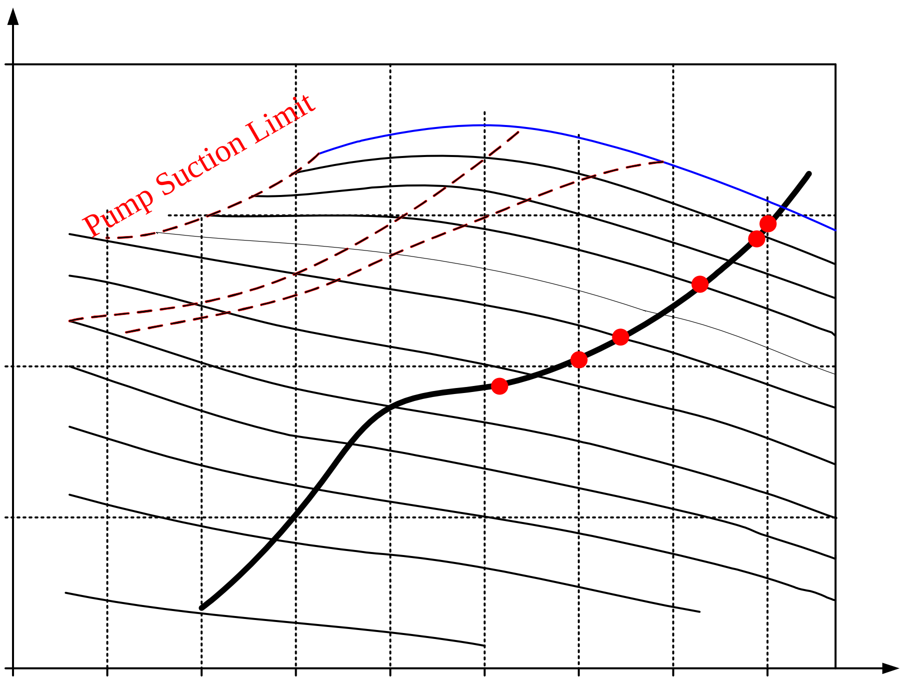

Calculated Conditions

T,R

- Half Load Intersections

N_5

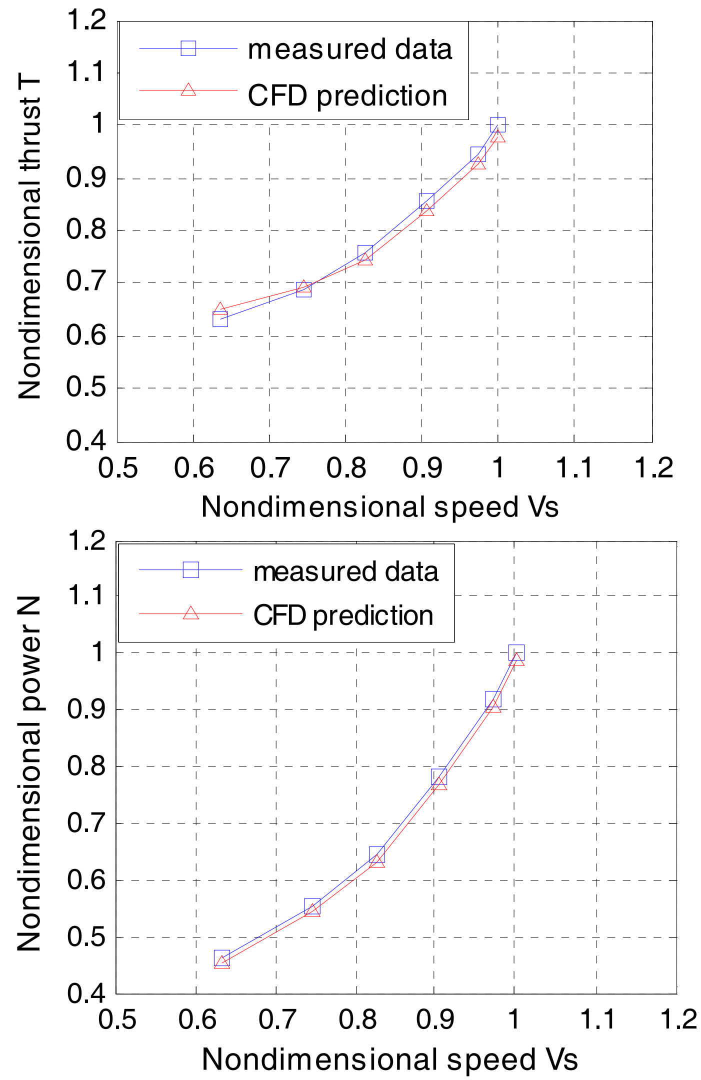

Results Comparison

En

⑤

Effects of variable number of blades

$$n_s = \frac{3.65 n \sqrt{Q}}{H^{3/4}}$$ (rpm, m^3/s, m)

- Specific speed

$$S_S = 1 - \frac{\pi \sin \beta_{b2}}{Z}$$

- Stodola slip factor

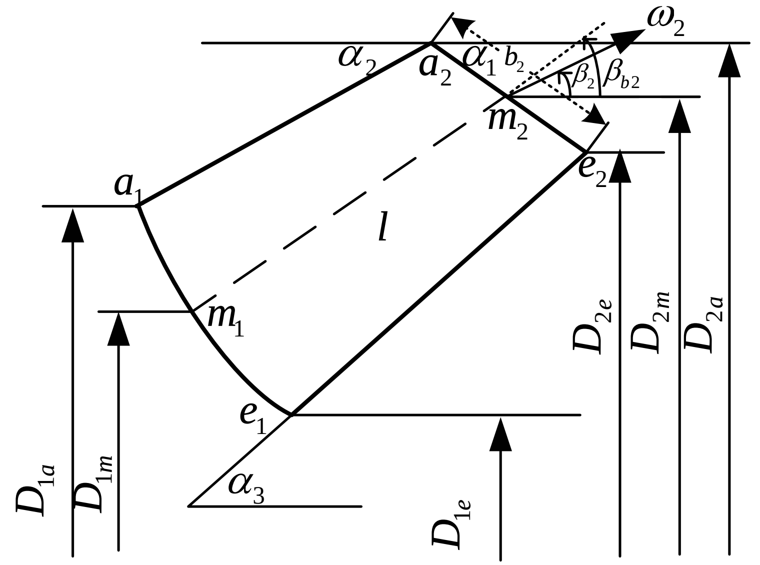

Rotor Meridional Surface

TABLE 1 Geometrical parameters of the rotor's blade

Number of blades	Specific speed	Width of outlet (m)	Average diameter at inlet (m)	Average diameter at outlet (m)	Velocity meridional at outlet (m/s)	Maximum diameter at outlet (m)	Minimum diameter at outlet (m)	Blade angle (°)	Stodoal slip factor
5	469.390	0.073	0.135	0.135	0.229	0.943	0.881	21.594	0.757
6	466.060	0.073	0.136	0.137	0.228	0.950	0.887	21.606	0.803
7	462.749	0.073	0.136	0.138	0.227	0.953	0.890	21.601	0.829

Change rotor’s blades only

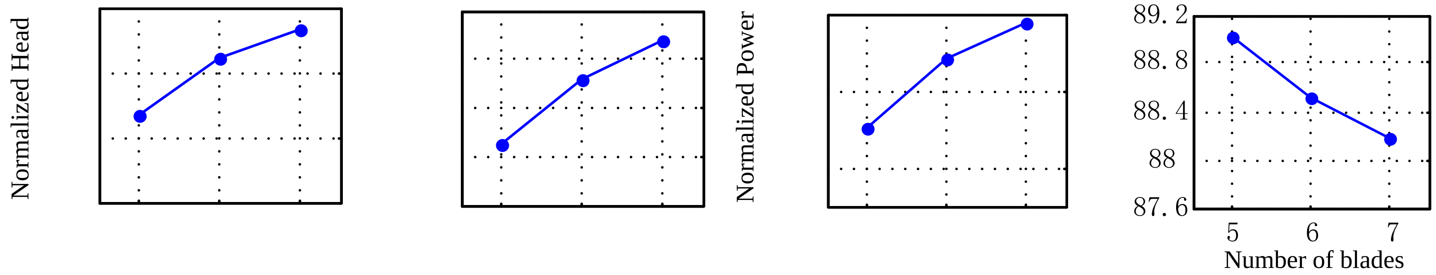

Waterjet Performances Comparison on Design Conditions

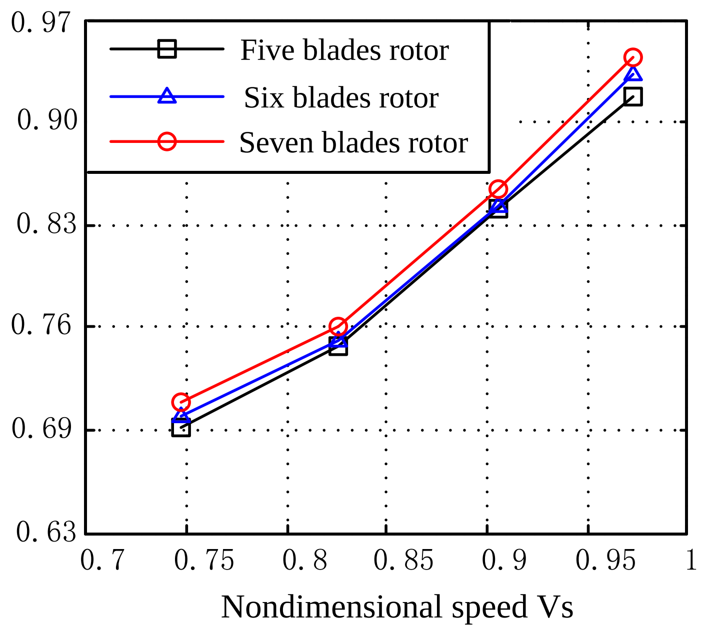

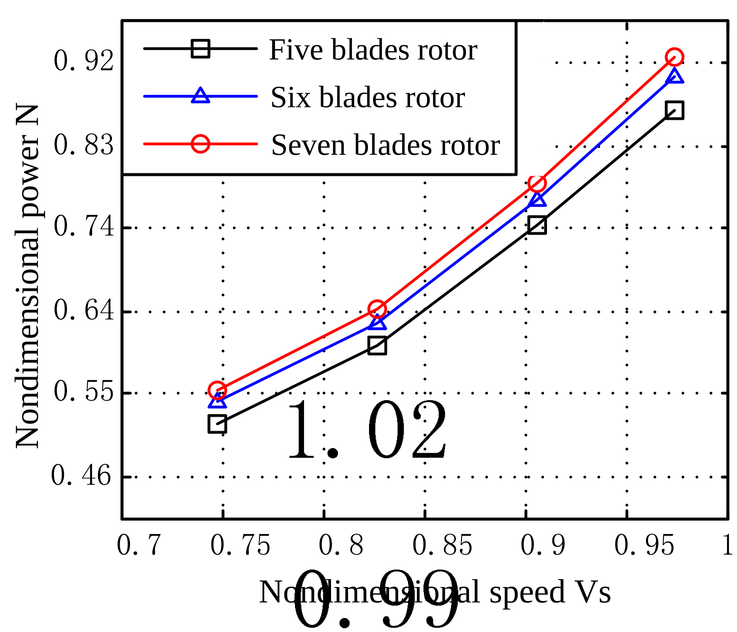

Off-design Conditions

Change stator's vanes only

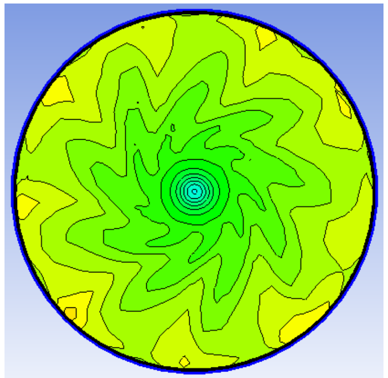

(a) 9

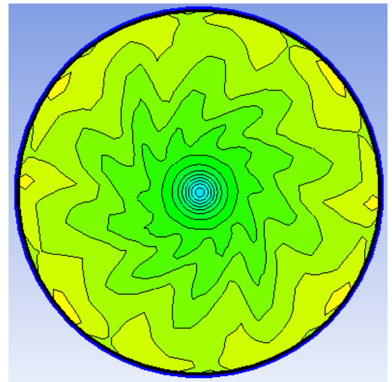

(b) 10

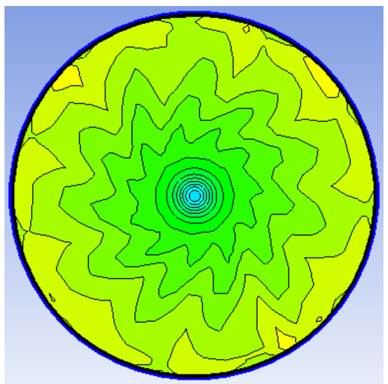

(c) 11

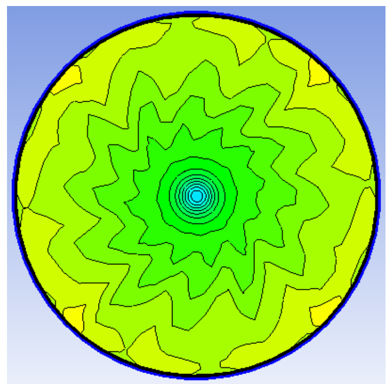

(d) 12

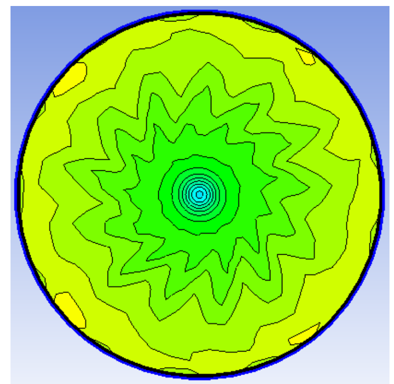

(e) 13

Iso-velocity Plot Distribution at the Exit of the Nozzle Discharge

Change both of the blades and vanes

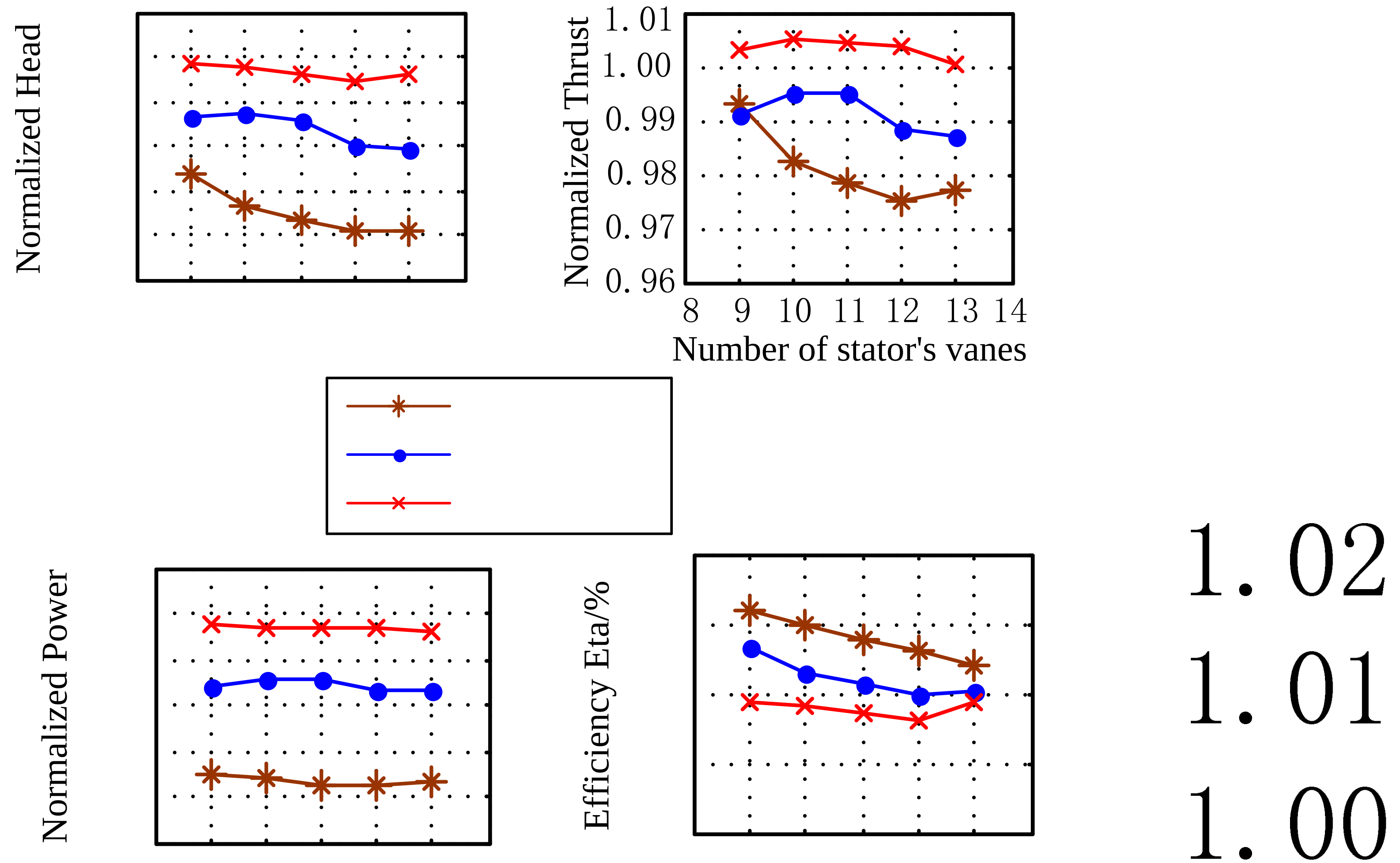

Waterjet Performances Comparison with Different Rotor-stator Blades Match

Pump incipient cavitation considering

$$\left.\begin{aligned} p_{01} &= p_1 + \frac{1}{2}\rho V^2 \\ NPSH_i &= \frac{p_{01,i} - p_v}{\rho g} \\ p_1 - p_{1,i} &= p_{\min} - p_v \end{aligned}\right\} \Longrightarrow$$

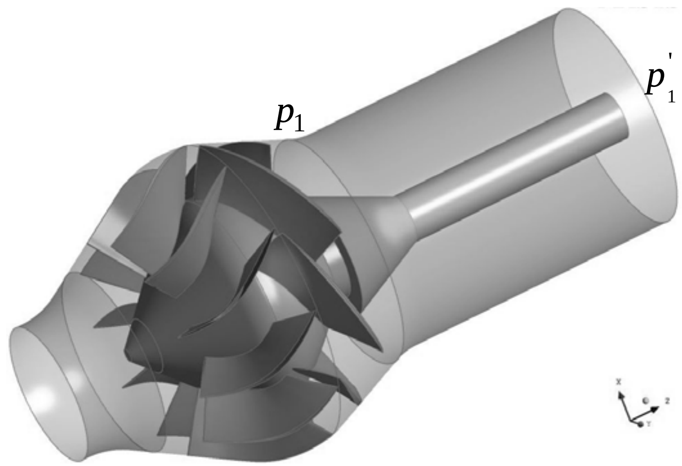

Waterjet Pump with Simplified Inlet

$$NPSH_i = \frac{p_{01} - p_{\min}}{\rho g}$$

- During the CFD calculation, without the effects of tensile strength, residence time, and dissolved gases, the prediction of inception level will be a straight forward matter of determining the local minimum pressure.
- A logical concept of NPSH
- For the six blades rotor pump, NPSHi is 114.0m.

Pump incipient cavitation consideration

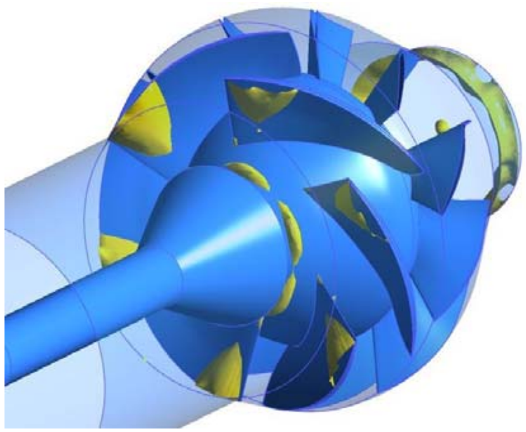

6 rotor-11 stator

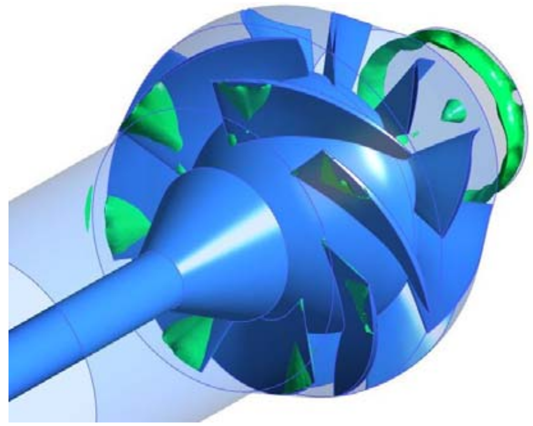

7 rotor-11 stator

Comparison of the Local $p < p_v$ Region between the Two Pump

- For both the pumps the local low pressure region starts a little distance after the blade leading edge, and has longest streamwise length near the rotor shroud .
- The pump with 6 blades rotor has the larger region for the bigger single blade load.

Pump incipient cavitation consideration

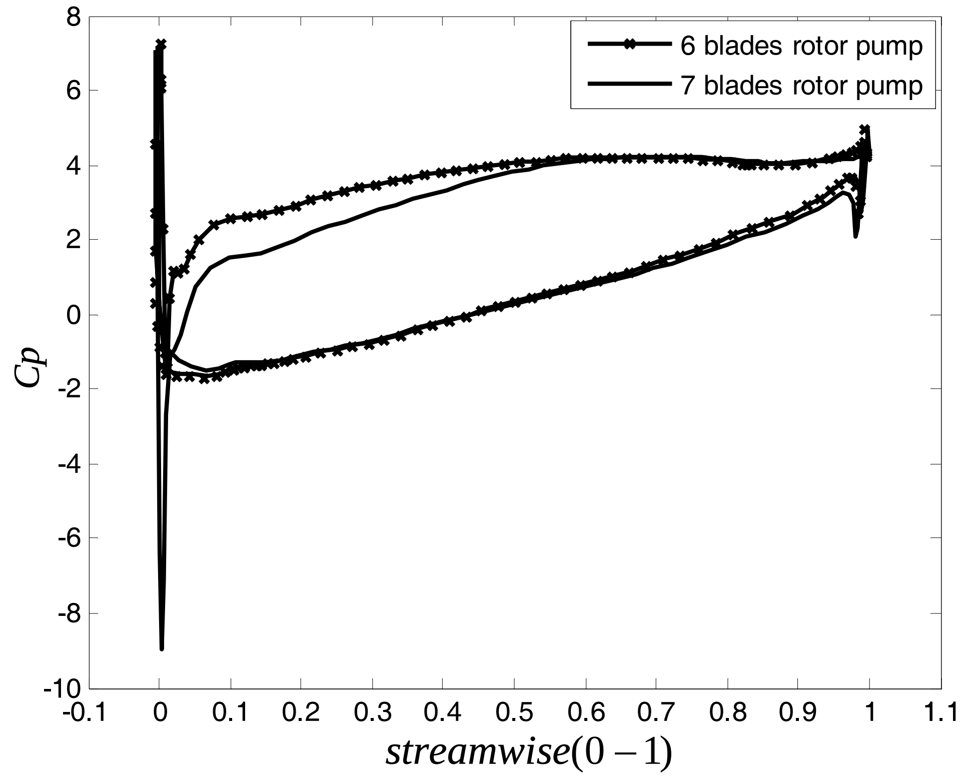

Comparison of the Pressure Coefficient at 0.7Span Location

- The pressure side of the rotor with the number of 6 is higher around the leading edge .

Generalized dimensionless performance curves

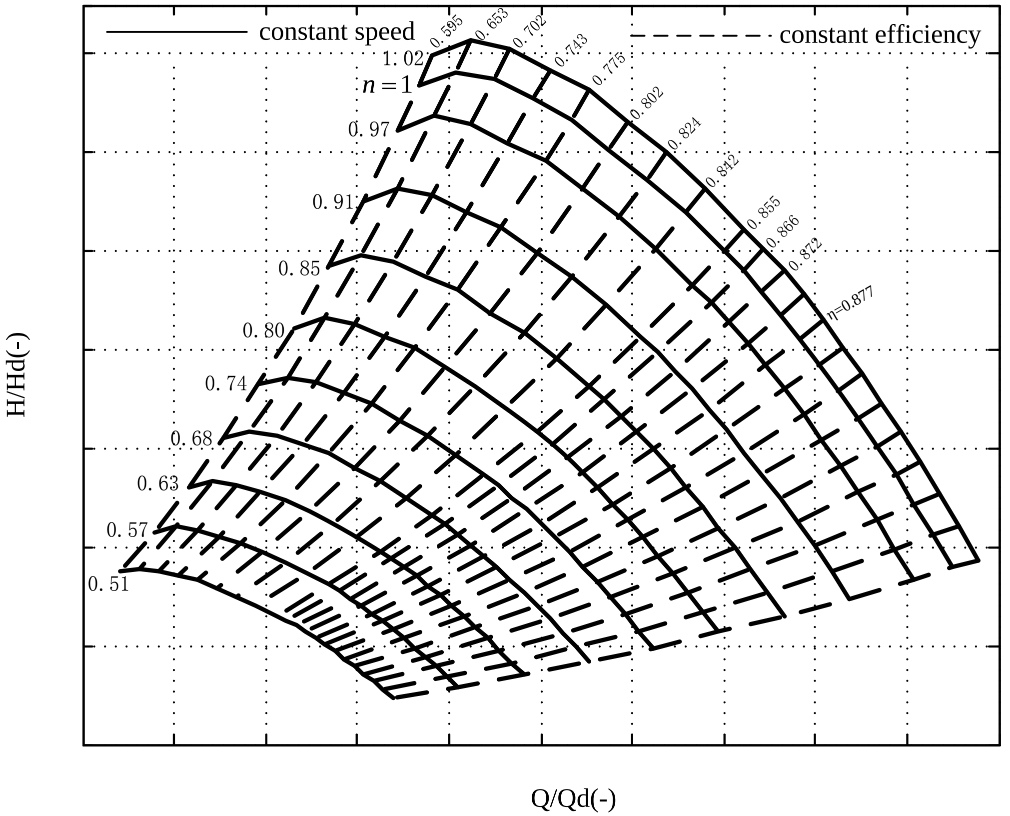

Generalized performance curves of the pump for propulsion prediction

1.5

1.4

1.2

Results

- CFD can be used to predict the waterjet propulsion performances accurately.
- As the increase of rotor's blades number, the Stodola slip factor gets larger, which weakens the rotational flow within the blade passage, hence results in the increase of the head. The propulsion efficiency reaches the highest with the five blades rotor configuration, but lowest with the seven blades rotor; while both the thrust and brake power are just on the contrast.
- The rotating discharge flow at the exit of the nozzle tends to uniformity as the vanes get larger, but the improvement is approximately unchangeable when the vanes comes to 11.

Results

- The characteristics for the series of six blades rotor lie intermediately compared to that of five-blade rotor and seven-blade rotor matching five different stator's vanes respectively.
- A five blades rotor combining a nine vanes stator can obtained the optimum propulsion performances, when the number of rotor's blades is six or seven, the optimum match is both the eleven-vane stator, while the 6 blades rotor pump's local low pressure region is bigger and so is easier to incipient cavitation.

Evaluate the Flow Noise Level of the Waterjet Pump

- The project forward
- A three step single-way coupling to predict the internal flow noise---predict the pressure fluctuations that take place on the water/casing interfaces by LES, then calculate the dynamic structural analysis of the casing based on FEM, do the acoustical propagation calculation based on BEM at last.
- Predict the turbulent jet noise by two step single-way flow-acoustic coupling.

This slide has been deliberately left blank

Diapositive intentionnellement blanche

Thanks !

RINA International Conference
Waterjet Propulsion V
11-12 December 2008

SCALING OF WATERJET PROPULSOR INLET WAKES

by
Michael B. Wilson

David Taylor Model Basin
NSWC, Carderock Division
West Bethesda, Maryland
USA

Scaling Inlet Wakes

BACKGROUND

- Continuing interest in the use of model testing for large sealift and LCS applications
  - Understanding propulsion interactions
  - Evaluation of designs
  - Prediction

- Progress toward more complementary use of computational and experimental investigations

- Develop experience and relevant database for
  - Validation
  - Correlation

Scaling Inlet Wakes

SCALE EFFECTS

- **Model hull boundary layers are relatively thicker than on full scale**
- **Full scale velocity distributions are fuller than on models (higher velocities closer to the hull)**
- **Influence of ingested propulsion flow on hull friction and viscous pressure drag**
- **Small, relatively less efficient model pumps are regarded as surrogates**
- **OBJECTIVE: Procedure for adjusting model scale flow rate for the estimation of full scale values based on an equal thrust-loading similarity condition**

Scaling Inlet Wakes

PRESENTATION

- **Outline of towing basin model waterjet testing**
- **Examples of wakes at the capture area plane for flush inlet arrangements**
- **Development of inlet wake scaling procedure**
- **Example case**
- **Summary**

Tow Basin Model Testing
For Waterjet System Thrust

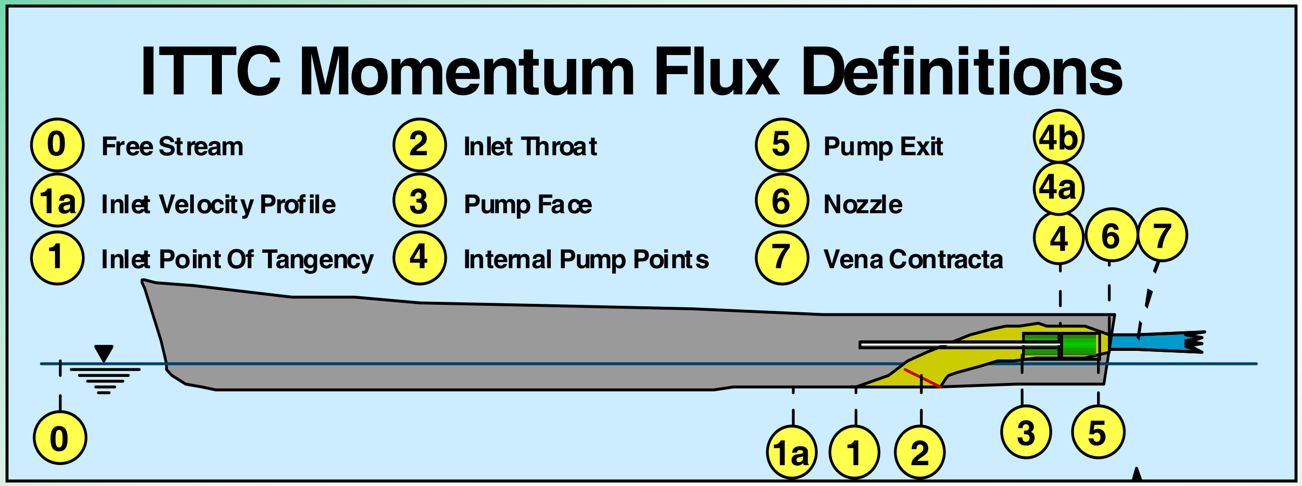

Waterjet Measurement Stations

- Hull resistance, heave , trim with inlets covered. Decision on target tow force, F_D. 0^{th} order Rn-corrected model drag is model total drag minus F_D

- Calibration of jet nozzle flow measurement at Station 6

Tow Basin Model
System Thrust Testing (Cont'd)

- **Over-and under-propelled testing. Match the model-measured tow force with target F_D . Measure static pressures and velocities at control planes Stations 1a, 5, and 6**

- **Determine flow factors at Station 6. Obtain $\overline{V}_6$ and (QJ) for self-propulsion.**

- **Determine flow factors at Station 1a. With velocity distributions measured, inferred, or computed estimate the capture area A_1 and $\overline{V}_1 = (1\text{-}w)_a$ and all other factors.**

- **Analysis: estimate $\overline{V}_7/V_0$ from $\overline{V}_6/V_0$ and data from Stations 5 and 6. Compute thrust equal to difference of momentum flux.**
  Apply wake scaling.

Example Model Wake at Station 1a

MONOHULL MODEL 5594

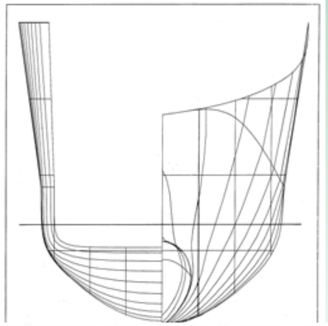

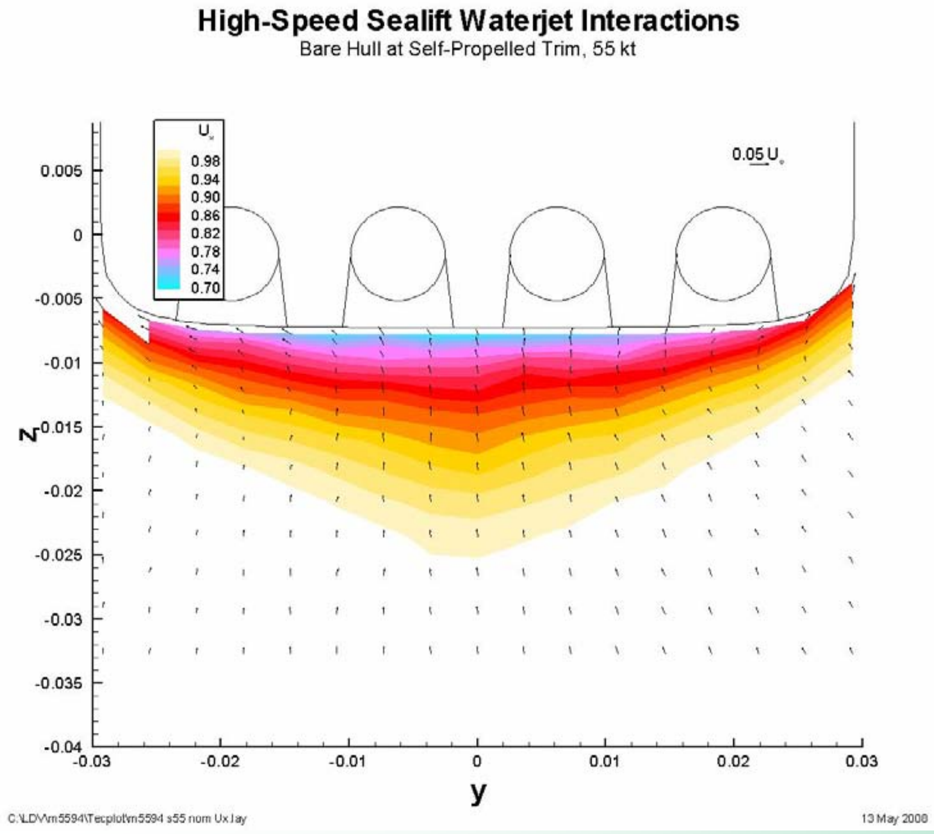

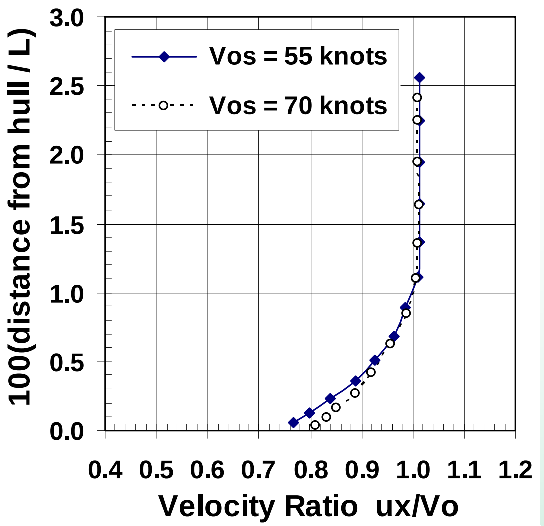

55 knots

Outboard Unit

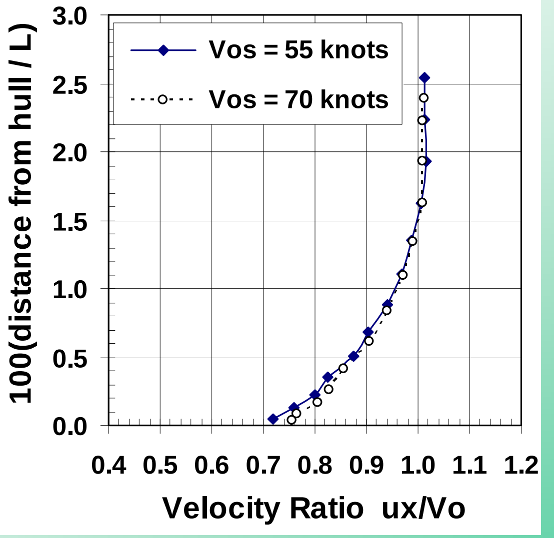

55 knots

Inboard Unit

Example Model Wake at Station 1a

JHSS MODEL 5662-1

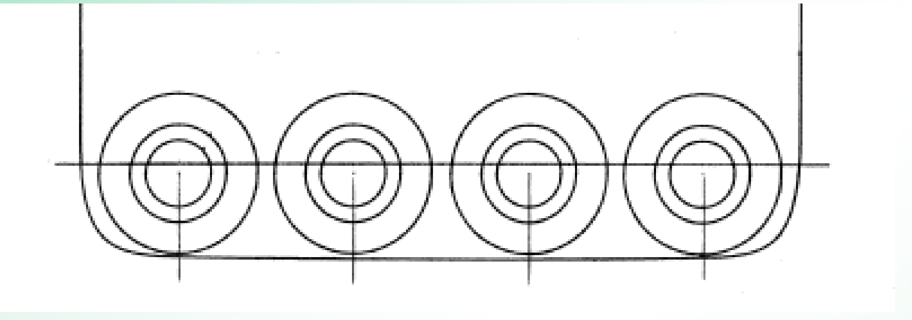

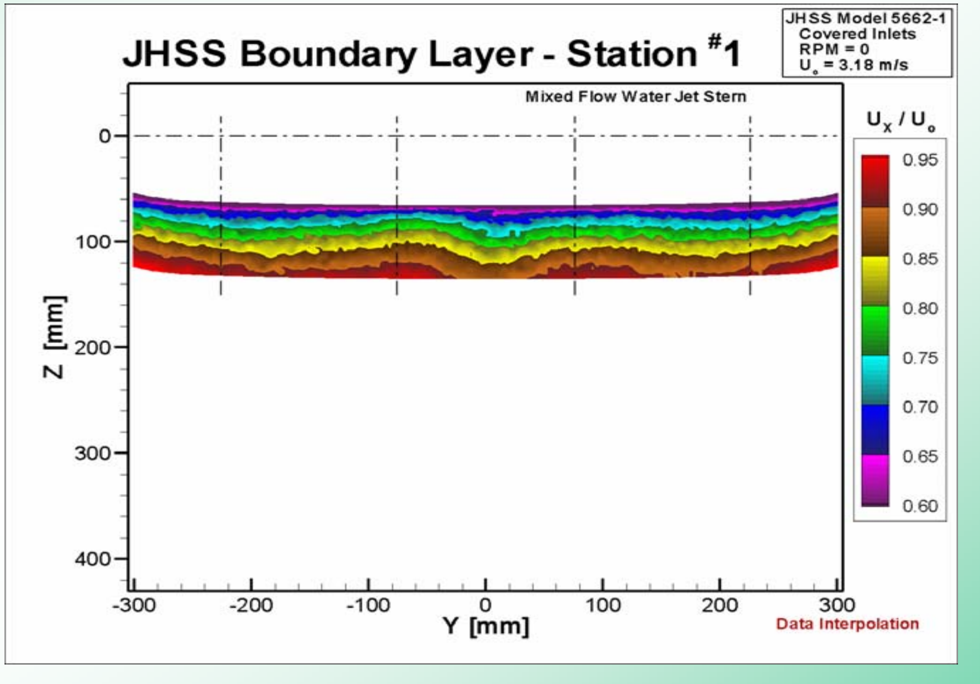

Development of
WAKE SCALING METHOD

Refined Jet System Thrust

$$T_{unit} = \rho(Q_J)\left(\overline{V}_{M7} - \overline{V}_{M1}\right)$$

Momentum Velocities:

$$\overline{V}_{M7} = (\beta_{M7} + \tfrac{1}{2}C_{p7})\overline{V}_7 = (B_{M7})\overline{V}_7$$
$$\overline{V}_{M1} = (\beta_{M1} + \tfrac{1}{2}C_{p1})\overline{V}_1 = (B_{M1})\overline{V}_1$$

Thrust Loading Coefficient

$$C_{Th} = \frac{T_{unit}}{\frac{1}{2}\rho V_0^2 A_7}$$
$$C_{Th} = 2\left(\frac{\overline{V}_7}{V_0}\right)\left\{\frac{\overline{V}_7}{V_0}(B_{M7}) - \frac{\overline{V}_1}{V_0}(B_{M1})\right\}$$

Equation for Full Scale Jet Velocity Ratio

Similarity Concept: Identical Thrust Loading Coefficient Model and Ship

- **Equate ship and model C_{Th}**
- **Assume full scale B_{M1} and B_{M7} are same as model values**
- **Obtain quadratic equation for ship** $(JVR_0)_s = (\frac{\overline{V}_7}{V_0})_s$

$$\left(\frac{\overline{V}_7}{V_0}\right)_s^2 = \left(\frac{\overline{V}_7}{V_0}\right)_s D_{M1} K \left(\frac{\overline{V}_1}{V_0}\right)_m - \left(\frac{\overline{V}_7}{V_0}\right)_m \left[\frac{\overline{V}_7}{V_0} - K\frac{\overline{V}_1}{V_0}\right]_m = 0 \qquad (1)$$

where the other unknown $(\overline{V}_1 / V_0)_s$ **is in factor**

$$D_{M1} = \frac{(\overline{V}_{M1}/V_0)_s}{(\overline{V}_{M1}/V_0)_m} \cong \frac{(\overline{V}_1/V_0)_s}{(\overline{V}_1/V_0)_m}, \qquad K = \frac{B_{M1}}{B_{M7}}$$

Reynolds Number Effect

Momentum Flux Deficit Between Stations 0 and 1a

$$M_0 - M_1 = \rho(A_7 \bar{V}_7)(V_0 - \bar{V}_{M1})$$

Made non-dimensional by $\frac{1}{2}\rho V_0^2 A_7$

$$C_{M0} - C_{M1} = 2\left(\frac{\bar{V}_7}{V_0}\right)\left(1 - \frac{\bar{V}_{M1}}{V_0}\right)$$

Ratio of ship-to-model momentum flux deficits set equal to ratio of flat plate friction coefficients

$$\frac{(C_F + C_A)_s}{C_{Fm}} = \frac{\left[\left(\frac{\bar{V}_7}{V_0}\right)(1 - \frac{\bar{V}_{M1}}{V_0})\right]_s}{\left[\left(\frac{\bar{V}_7}{V_0}\right)(1 - \frac{\bar{V}_{M1}}{V_0})\right]_m}$$

Reynolds Number Effect (Continued)

Solution of the ratio equation for D_{M1} is

$$D_{M1} = \frac{(\bar{V}_{M1}/V_0)_s}{(\bar{V}_{M1}/V_0)_m} = \frac{1}{(\bar{V}_{M1}/V_0)_m} + \left(\frac{(C_F + C_A)_s}{C_{Fm}}\right)\left[\frac{(\bar{V}_7/V_0)_m}{(\bar{V}_7/V_0)_s}\right]\left\{1 - \frac{1}{(\bar{V}_{M1}/V_0)_m}\right\} \qquad (2)$$

where $$\left(\frac{\bar{V}_{M1}}{V_0}\right)_m = B_{M1}\left(\frac{\bar{V}_1}{V_0}\right)_m$$

Then, the solution to Equation (1) and result of Equation (2) are solved simultaneously for the two unknowns

$$D_{M1} \cong \frac{(\bar{V}_1/V_0)_s}{(\bar{V}_1/V_0)_m}$$

$$\left(\frac{\bar{V}_7}{V_0}\right)_s = (JVR_0)_s$$

Outline of Application of Scaling Method

- **Model propulsion test provides thrust, wake velocity ratio $(\bar{V}_1/V_0)_m$; jet velocity ratio $(\bar{V}_7/V_0)_m$; and flow rate $Q_J = Q_6$.**

- **Obtain factors β_{M1}, $\beta_{M7} = \beta_{M6}$, C_{p1}, and C_{p6}. Calculate combined coefficients B_{M1}, B_{M7}. The value of C_{p7} is taken as zero**

- **Solve the two simultaneous equations for scaled $(\bar{V}_7/V_0)_s$ and scaled factor D_{M1}.**

- **Results for main performance factors are scaled $(\bar{V}_7/V_0)_s$; the scaled ratio $(\bar{V}_1/V_0)_s = (\bar{V}_1/V_0)_m \times D_{M1}$; and adjusted flow rate Q_J equal to $(\bar{V}_7) \times A_7$**

- **Scaled thrust deduction factor (1-t) determined at model scale remains the same as at full scale: $(1\text{-}t) = R_{Ts}/T_{tot,s}$, as assumed.**

Example Case

Large Sealift-Type Ship,

Design Speed 36 up to 39 knots

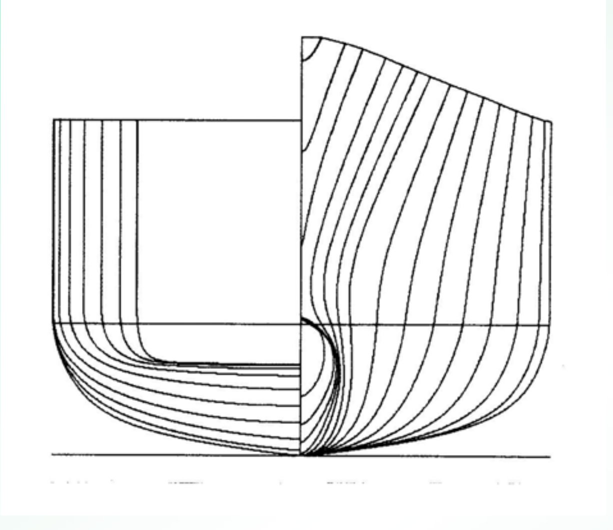

Principal Particulars – Model 5662-1 and Ship

	Model	Ship
Length WL, L	8.76 m	298.8 m
Beam, B_X	0.9364 m	31.95 m
Draft (even keel), T	0.253 m	8.62 m
Displaced Volume	0.9098 m^3	36140 m^3
Displacement	0.9333 mt	37075 mt
Wetted Surface Area	7.77 m^2	9046 m^2
Max Sect Area, A_X	0.1885 m^2	219.5 m^2
WJ Unit Inlet Diam., D_3	8.93 cm	3.047 m
WJ Unit Nozzle Diam., D_6	5.58 cm	1.904 m
Design Speed (Froude No)	6.16 knots (0.342)	36 knots (0.342)
Transom Area Ratio A_T/A_X	0.163	
Transom Draft Ratio T_T/T	0.247	
Trsm Beam Ratio B_T/B_X	0.540	
Scale Ratio, λ	34.121	

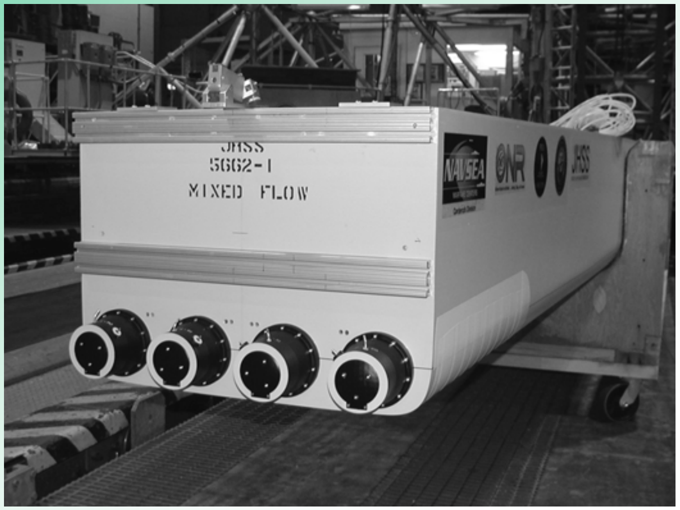

Wake-Scaled Values

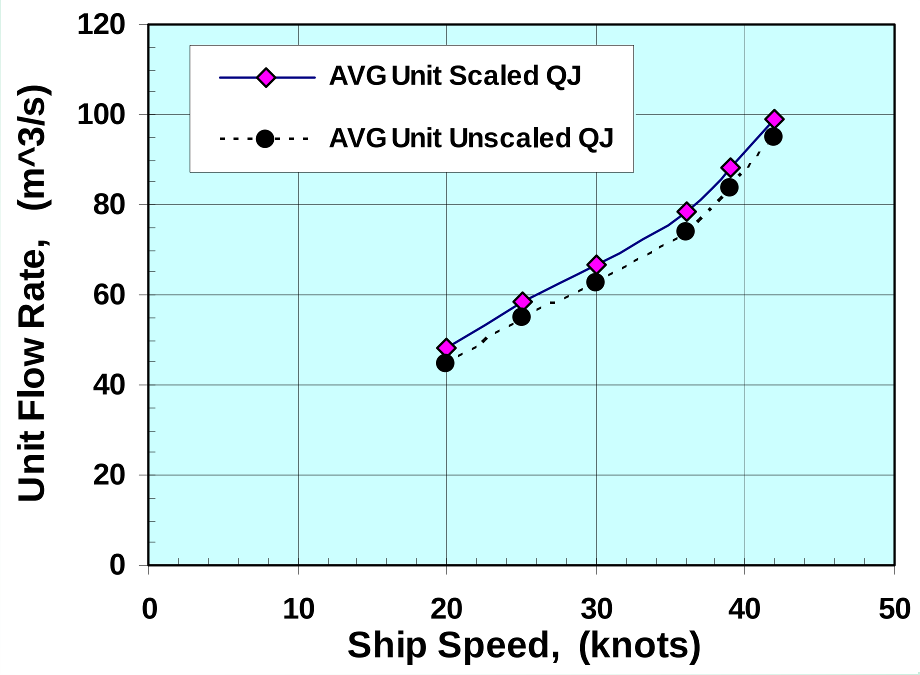

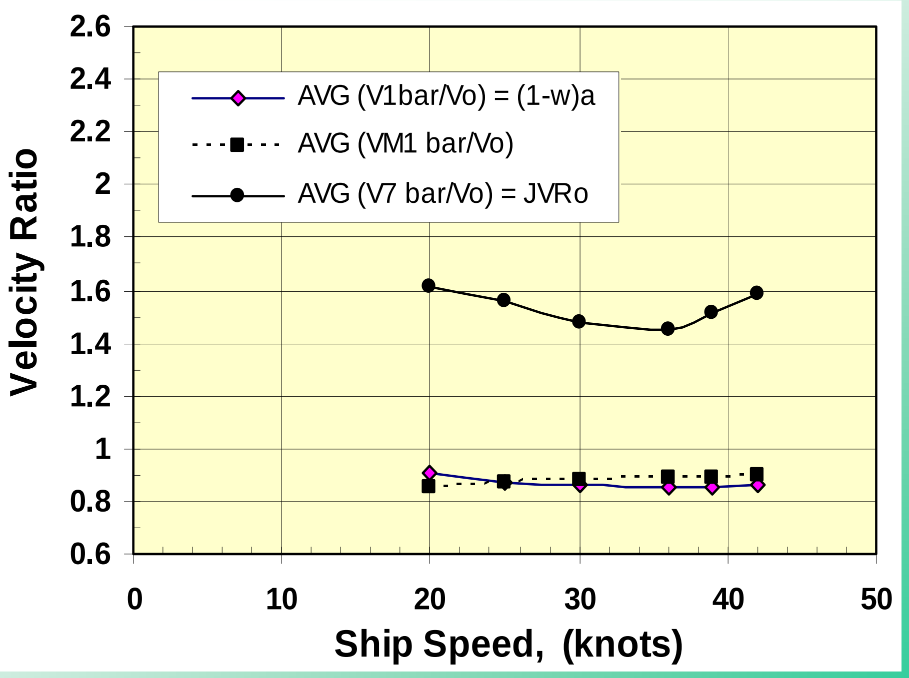

Scaling Inlet Wakes

Example Case – Interaction Factors

Pressure Coeffs at Stations 1a and 6

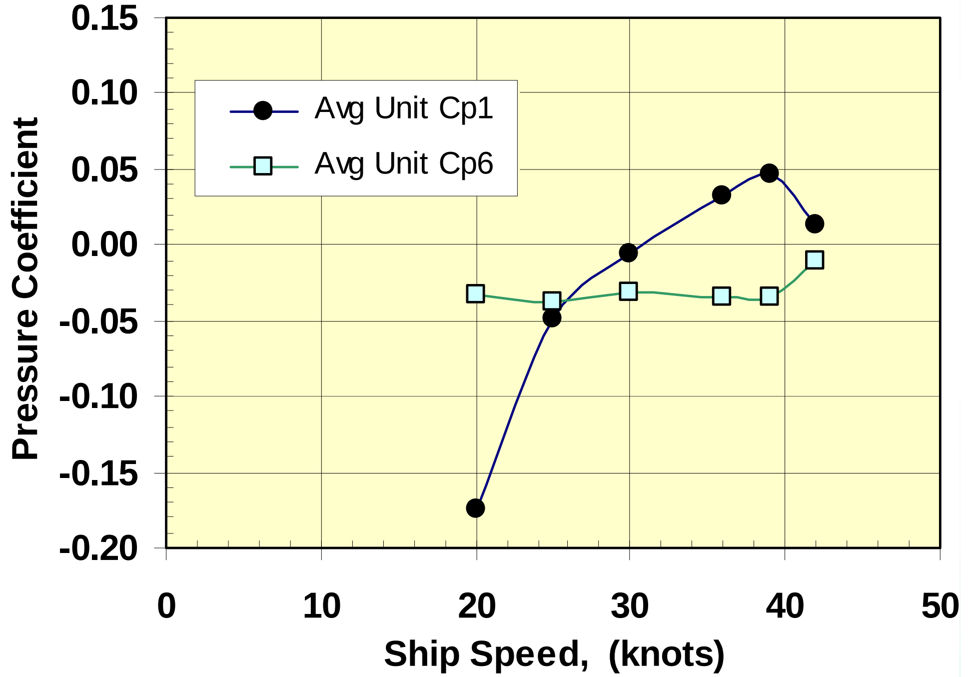

Non-Uniform Velocity Factors

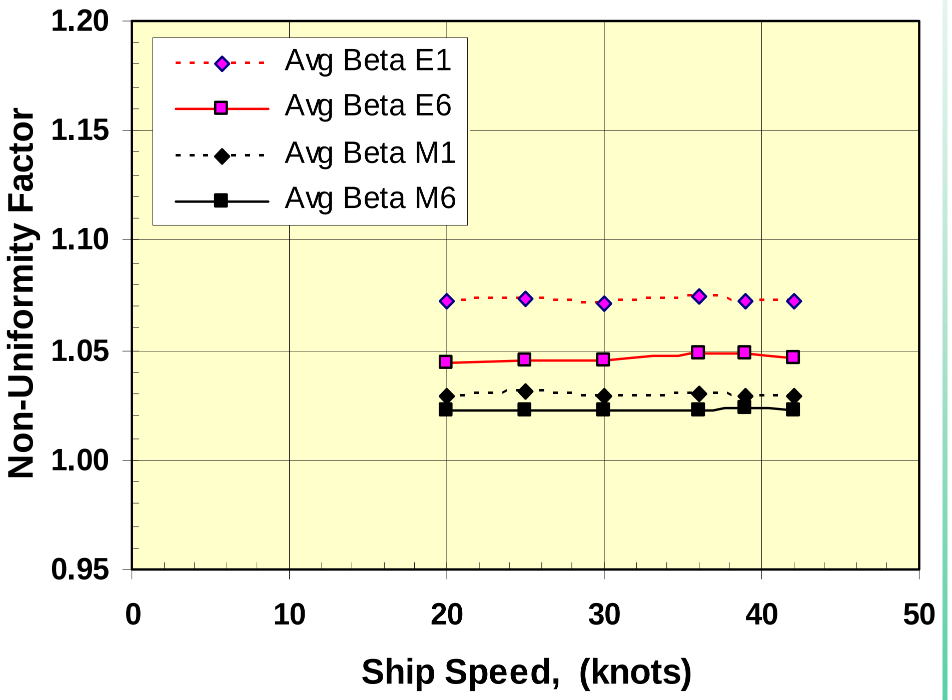

Scaling Inlet Wakes

Example Case - Thrust Deduction Fraction, t

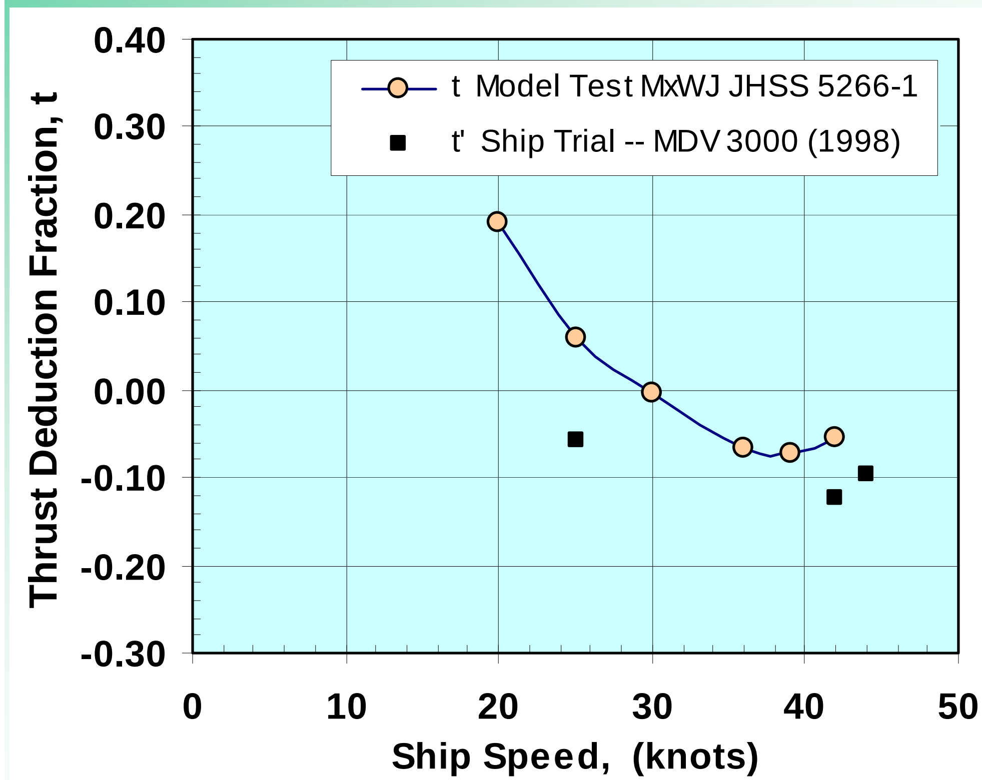

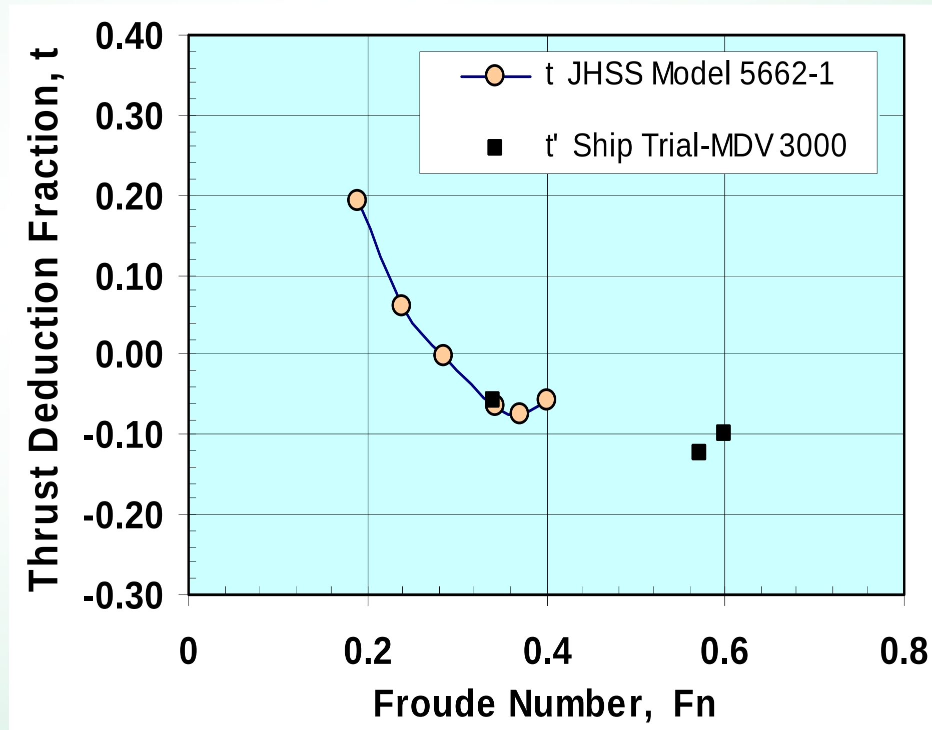

{ Reference for MDV 3000 Ship Trial Results: Svensson, et al. (1998) }

Example Results

Ship Speed = 25 knots	Model Un-ScaledWake	Model Scale for Ship Results Scaled Wake	Ship ScaledWake
Total Flow Rate, $(QJ)_{tot}$ [4 units] (m^3/s)	0.03225	0.03432	233.4
Avg Inlet Wake Vel. Ratio, $V_{1\ bar}/Vo = (1-w)a$	0.726	0.8687	0.8687
Avg Inlet Momentum Vel. Ratio, $V_{M1\ bar}/Vo$	0.731	0.875	0.875
Avg Jet Vel. Ratio, $V_{7\ bar}/Vo = JVRo$	1.46	1.556	1.556
Thrust Deduction Fraction, t	0.06	0.06	0.06

Ship Speed = 36 knots	Model Un-ScaledWake	Model Scale for Ship Results Scaled Wake	Ship ScaledWake
Total Flow Rate, $(QJ)_{tot}$ [4 units] (m^3/s)	0.04349	0.04607	313.4
Avg Inlet Wake Vel. Ratio, $V_{1\ bar}/Vo = (1-w)a$	0.733	0.8496	0.8496
Avg Inlet Momentum Vel. Ratio, $V_{M1\ bar}/Vo$	0.767	0.889	0.889
Avg Jet Vel. Ratio, $V_{7\ bar}/Vo = JVRo$	1.37	1.45	1.45
Thrust Deduction Fraction, t	-0.0677	-0.0666	-0.0666

SUMMARY

Item	Ship Speed 25 knots	Ship Speed 36 knots
Total Flow Rate	**+ 6.4 %**	**+ 5.9 %**
AVG Unit Jet Velocity Ratio JVR_0	**+ 6.6 %**	**+ 5.8 %**
AVG Unit Inlet Velocity Ratio	**+ 19.7 %**	**+ 15.9 %**
AVG Unit Momentum Inlet Velocity	**+ 19.7 %**	**+ 15.9 %**
Thrust Deduction Fraction, t	**0**	**≈ 0**

- **Paper provides description of the waterjet inlet wake scaling procedure**
- **The changes introduced by Reynolds number scaling are significant**
- **Table above summarizes the % changes of flow rate and velocity ratios**
- **Model and full scale loading and thrust deduction factor are equal**
- **Model test values for t for JHSS Model 5662-1 show similar general trends to the example full scale correlation values of t'**

Simulation of Dynamic Characteristics of Waterjet and Its Application on Troubleshooting

1. Yongsheng Wang， Jiangming Ding,
University of Naval Engineering, China
2. Zhirong Liu， Wenshan Xu,
Guangzhou Marine Engineering Corp. ,China

2008.12.11~12

A Case Study

Four sets of waterjet units are adapted in a fast boat, in which a main diesel engine drives a waterjet through a reduction gearbox in each set. In a maneuvering, four sets of waterjet units in sea trial were accelerated in step from idling to full speed with 15 seconds. Then a deceleration was done from the full speed to the idling with 8 seconds after the ship design speed was achieved. During the deceleration the rotary speeds of three sets of waterjet units were decreased in accordance with each other but the rotary speed of the remaining one was kept unchanged.

A Case Study (cont.)

Finding the unusual situation and wanting to correct it, an operator put the control lever back to the full speed position, ant then try a second deceleration. During the second deceleration the rotary speed of the remaining one still remained unchanged, and then an overspeed occurred. An emergent stop of the diesel engine was triggered off and at the same time a report came from engine room that white smoke came from the reduction gearbox in which the friction discs were destroyed after check.

A Case Study (cont.)

There were lots of opinions to the fault and what was a cause to the fault. The primary opinion among them to the fault analysis was that a load to the friction disks in the reduction gearbox is larger than the design load because the remaining one did not change the rotary speed due to malfunction of the control system, and bore much larger load when the three sets of waterjets decreased the rotary speed.

A Case Study (cont.)

- Towards the primary opinion this whole operating process are simulated by the dynamic simulation model based on the four sets of waterjet propulsion units, and analysis of simulation results are done in order to find out the cause of this fault.
- The first layer of the dynamic simulation model is demonstrated in Figure 5.

Fig. 5 First Layer of Waterjet Propulsion Model

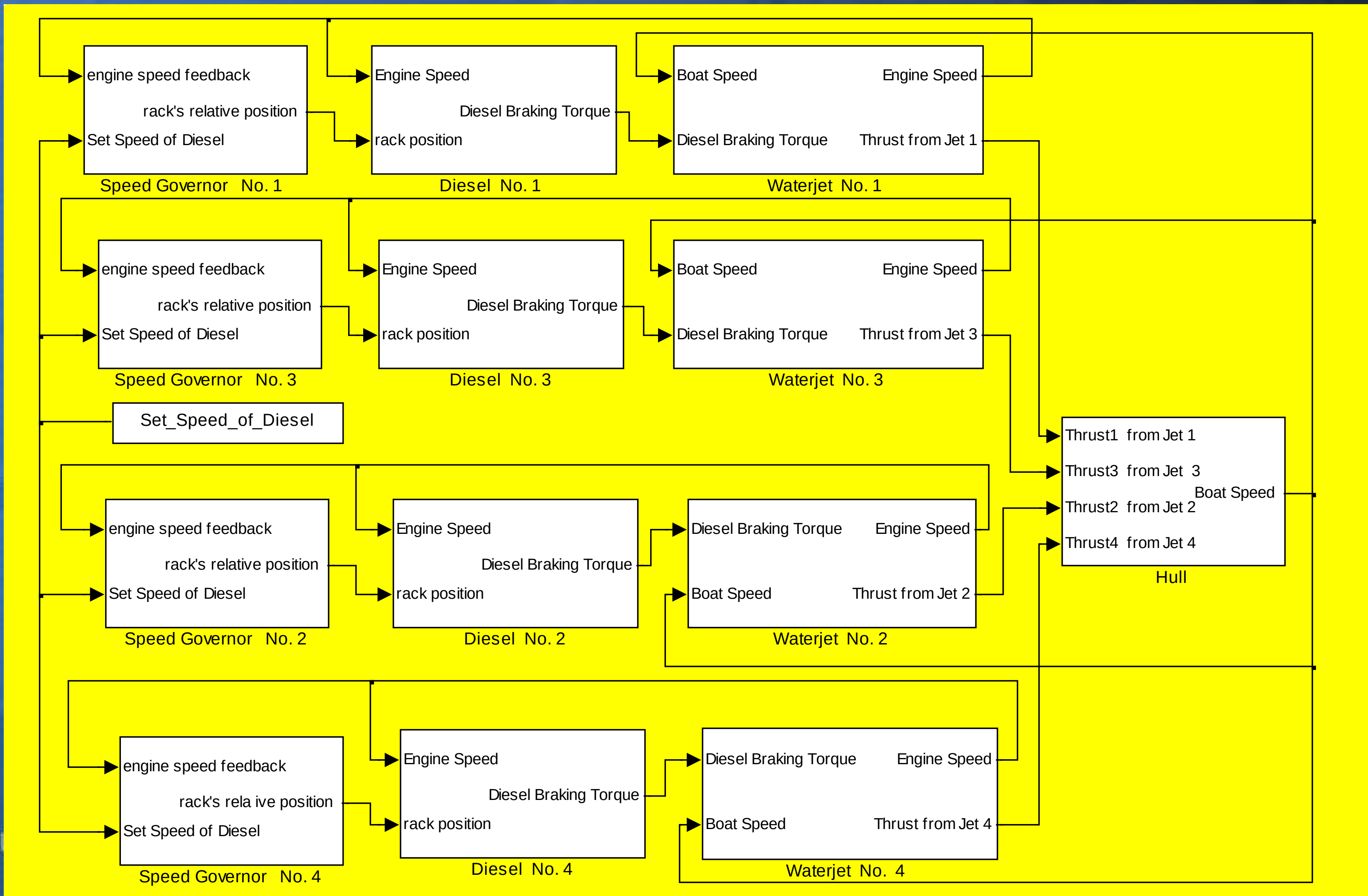

Two Subsystems

- a subsystem in a rotating movement of "main engine—waterjet "

$$iM_e - M_f - M_p = J\frac{d\omega}{dt} \qquad (1)$$

- a subsystem in a translation movement of "waterjet—hull"

$$nT - R - \Delta R = m\frac{dV_s}{dt} \qquad (2)$$

Methodology of Modeling

- （1）and（2）are two basic governing equations in simulation of the dynamic characteristics of waterjet propulsion. In order to describe the dynamic characteristics with accuracy it is a key that all parameters and coefficients and their relations in the two basic governing equations should be determined with accuracy. In arriving at this goal a first step is to well and truly develop components’ models of the waterjet propulsion system, i.e. the models of speed governor, diesel engine, reduction gearbox and shaft, waterjet, hull resistance. Then these models are integrated into the whole model of the waterjet propulsion system.

Characteristics of Waterjet by Manufacturer

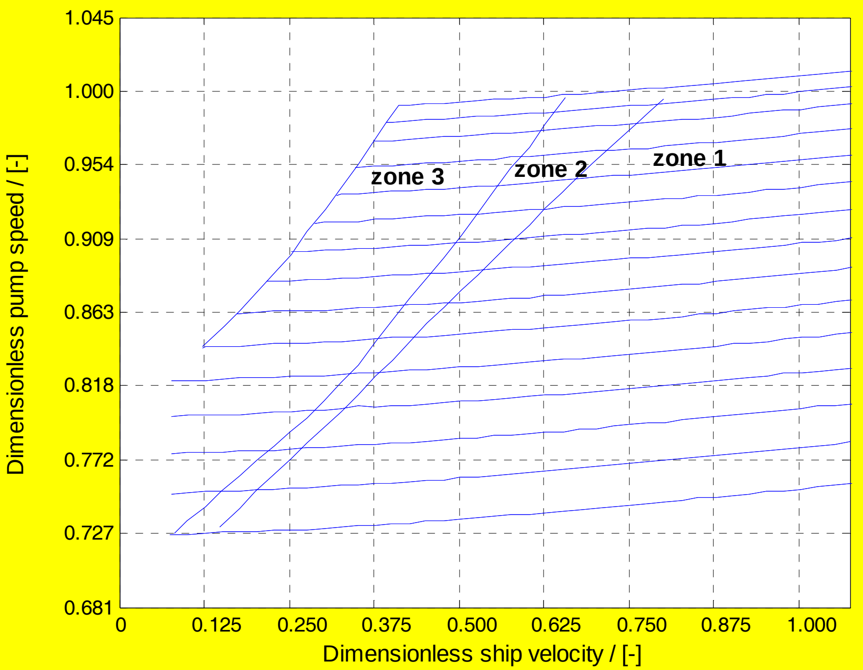

the rev. speed curve

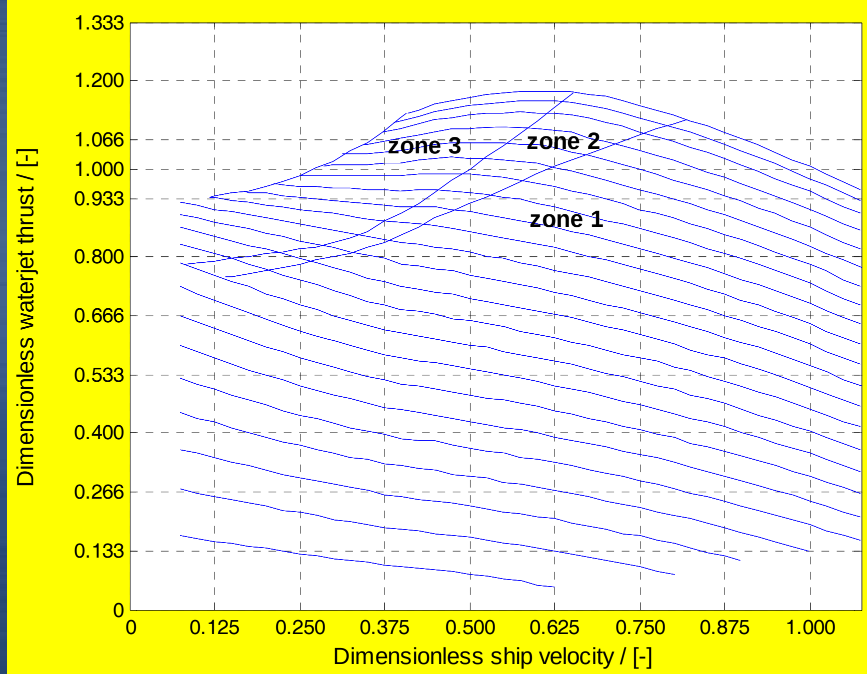

the thrust curve

Simulation Model of Waterjet

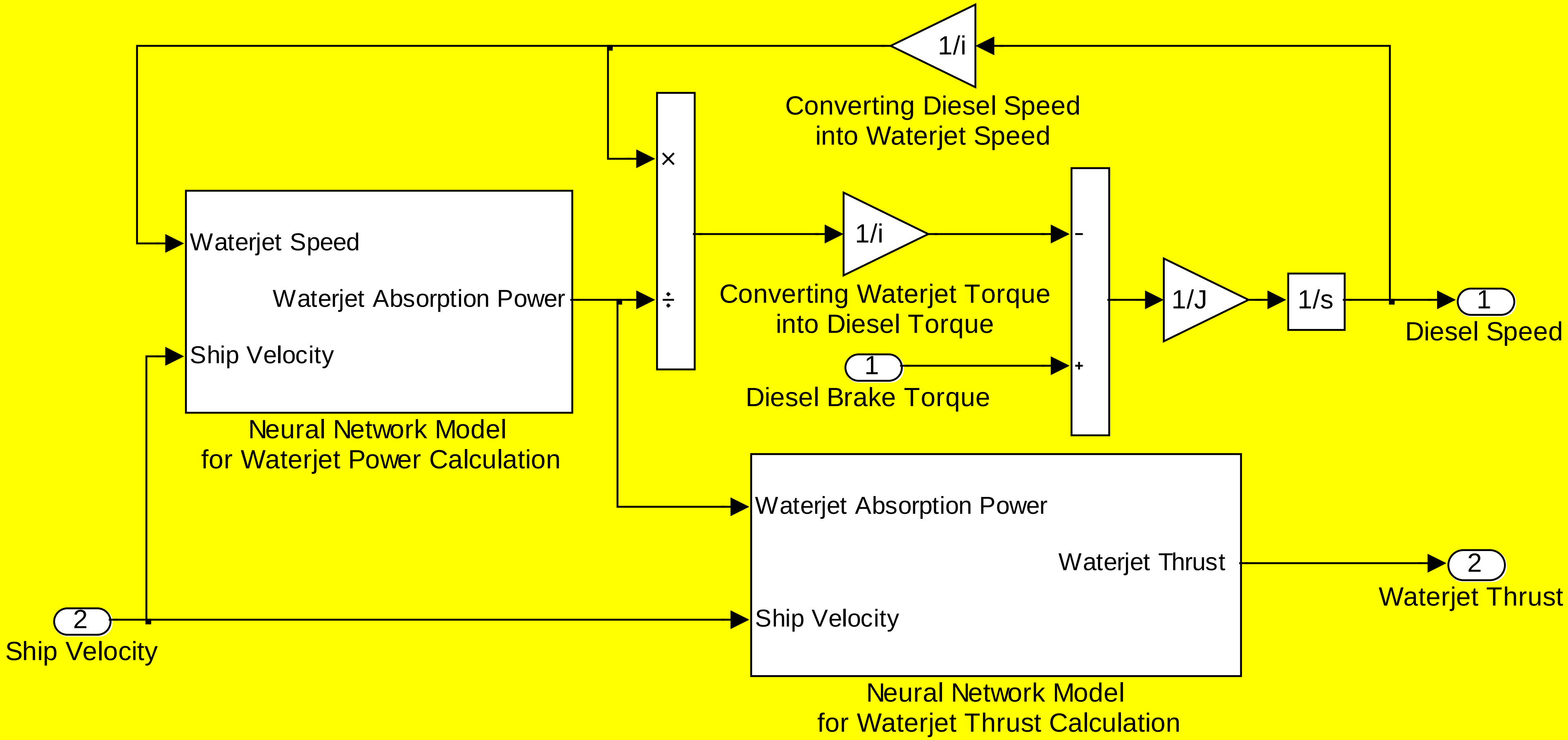

Waterjet Control Diagram

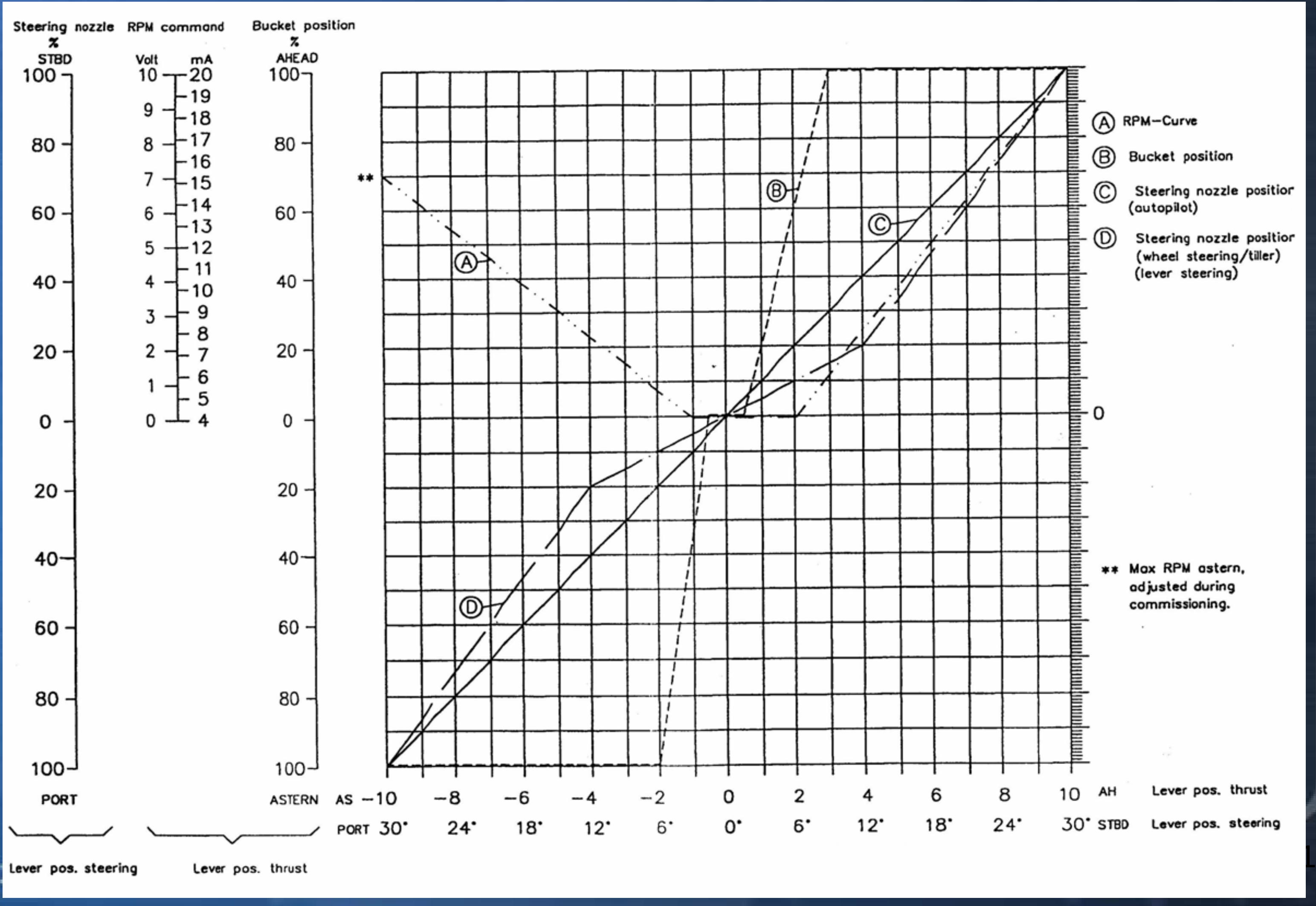

Is a load to the friction disks in the gearbox much larger than the design Value?

- The whole operating process are simulated by the dynamic simulation model based on the four sets of waterjet propulsion units, and analysis of simulation results are done in order to find out the cause of this fault.

THE NAVY UNIVERSITY OF ENGINEERING

Decelerated First and then Accelerated during Normal Maneuver

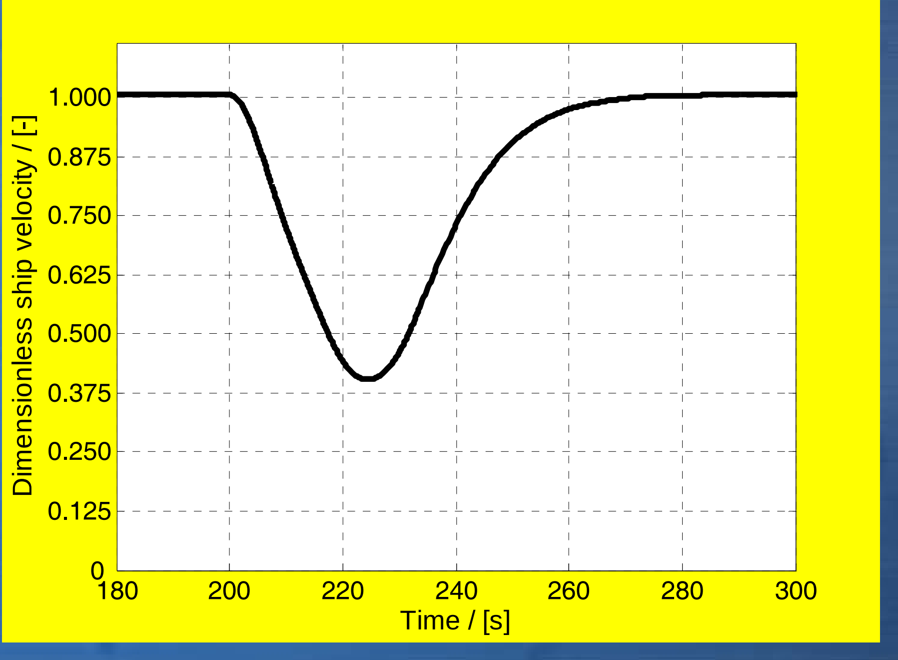

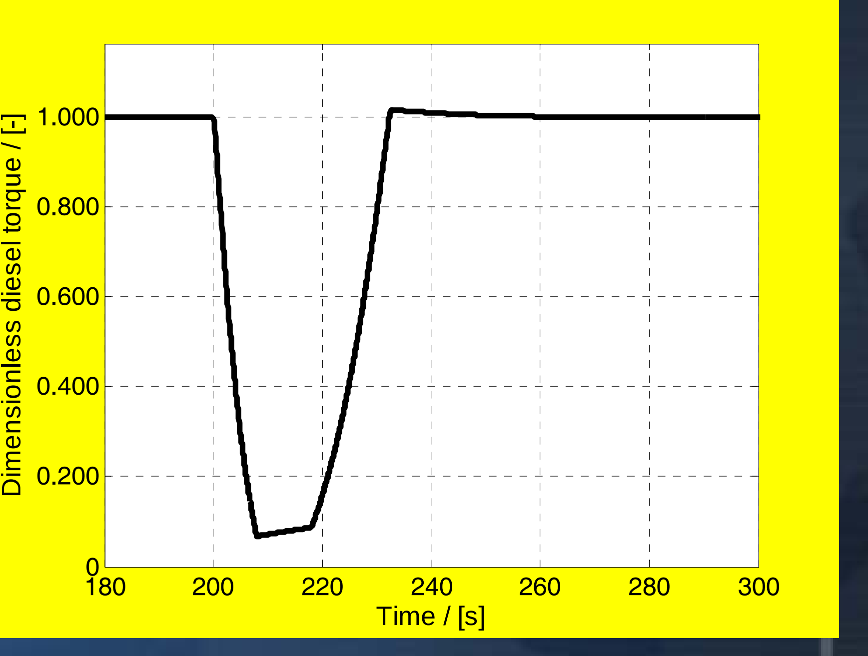

Ship Speed during Normal Maneuver **Engine Torque during Normal Maneuver**

In Malfunction Process

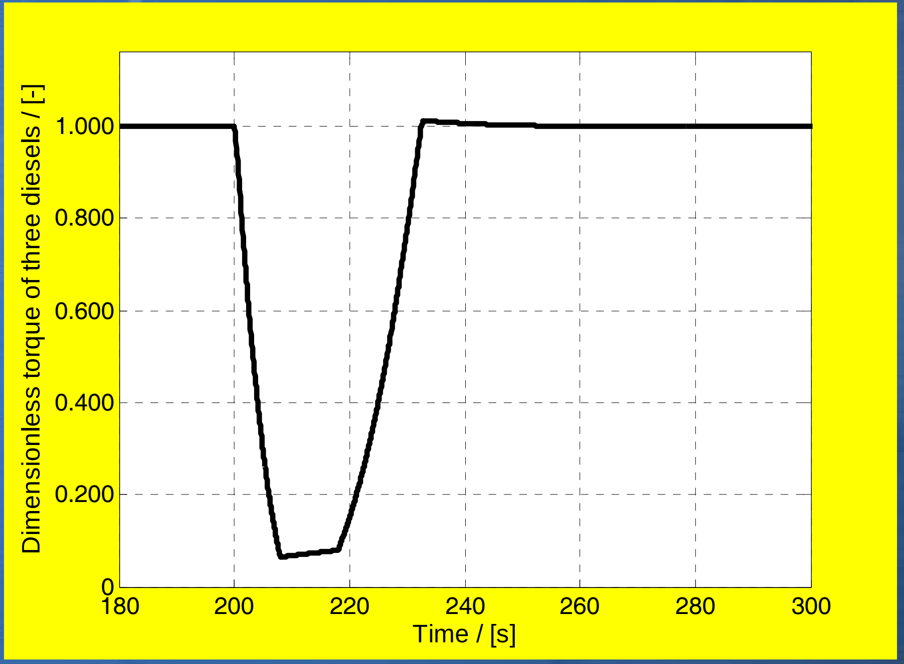

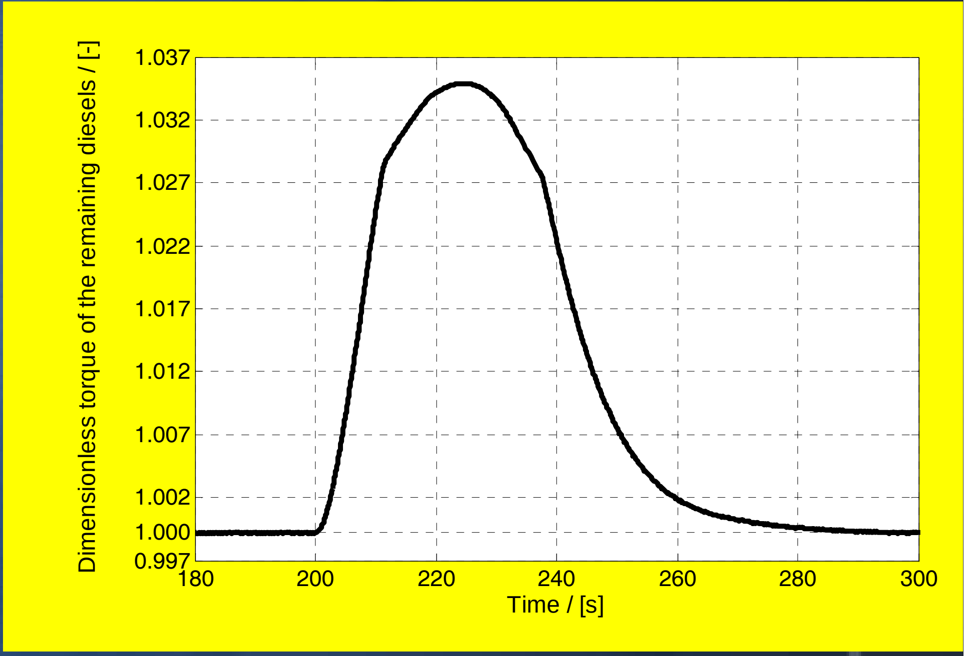

Engine Torque during Abnormal Maneuver

The Remaining Engine Torque during Abnormal Maneuver

Why Does Propeller Load Change Much When Ship Speed Varies Much?

- waterjet is a propulsor with internal flow and propeller with external flow.
- Ship speed mainly decides advance velocity of propeller which and the circumferential speed determine an angle of attack and a relative water velocity approaching to propeller blade. The advance velocity is a main factor to affect propeller's load i.e. torque. This is why ship speed will remarkably affect propeller torque.

Why Does Waterjet Load Change a Little When Ship Speed Varies Much?

- In waterjet the flow enter impeller after water-flow is reformed or reshaped through inlet duct. Thus an influence of ship speed to an angle of attack and a relative water velocity approaching to impeller blade become weak. This is why ship speed will weakly affect waterjet torque. Now we can understand why the torque of waterjet changes a little when ship speed changes a lot as waterjet speed maintains constant.

- The scope for searching through the reason triggered the fault is narrowed after the waterjet torque is excluded the possibility of troublemaker.

CONCLUSIONS

1. Characteristics of waterjet are much different from propeller. Steady-state and dynamic properties of waterjet during maneuvers can be studied by modeling and simulation. This kind of simulation can be applied in design, optimization and troubleshooting of waterjet propulsion. A case study in the paper is one application of them.

CONCLUSIONS

2. The only difference between the waterjet propulsion and propeller propulsion is propulsor, and so waterjet modeling is a key component in modeling of whole waterjet propulsion system. Manufacture's maps or external characteristics of thrust curves and rotary speed curves can be utilized to waterjet's modeling by quasi-steady-state method.

The End

Thank You for Your Attention!

Testing Air-Augmented Waterjet Propulsion

Alon Gany, Arik Shemer, Aviad Gofer and Doron Har-Lev
Faculty of Aerospace Engineering
Technion - Israel Institute of Technology
Haifa, Israel
gany@tx.technion.ac.il

Waterjet Propulsion 5, RINA HQ, London, Dec 11-12, 2008

Background and Past Accomplishments:

Marine Two-Phase Jet Propulsion

Thrust Equation
(Adapted Nozzle)

$$F = \dot{m}\left(U_e - U\right)$$

In two-phase jet propulsion we would like to convert the expansion work of air or gas bubbles into kinetic energy of the exhaust jet:

Gas expansion work: $$W = \int p\,dV$$

In isothermal conditions: $$w = RT \ln r$$

Where r is the pressure ratio.

Past accomplishment:

Analysis and testing of novel marine two-phase ramjet propulsion

Air or gas bubbles are injected into the water within a ramjet-type propulsion unit. The expanding bubbles accelerate the flow, generating thrust without moving parts in contact with the water

Bubbly Water Ramjet

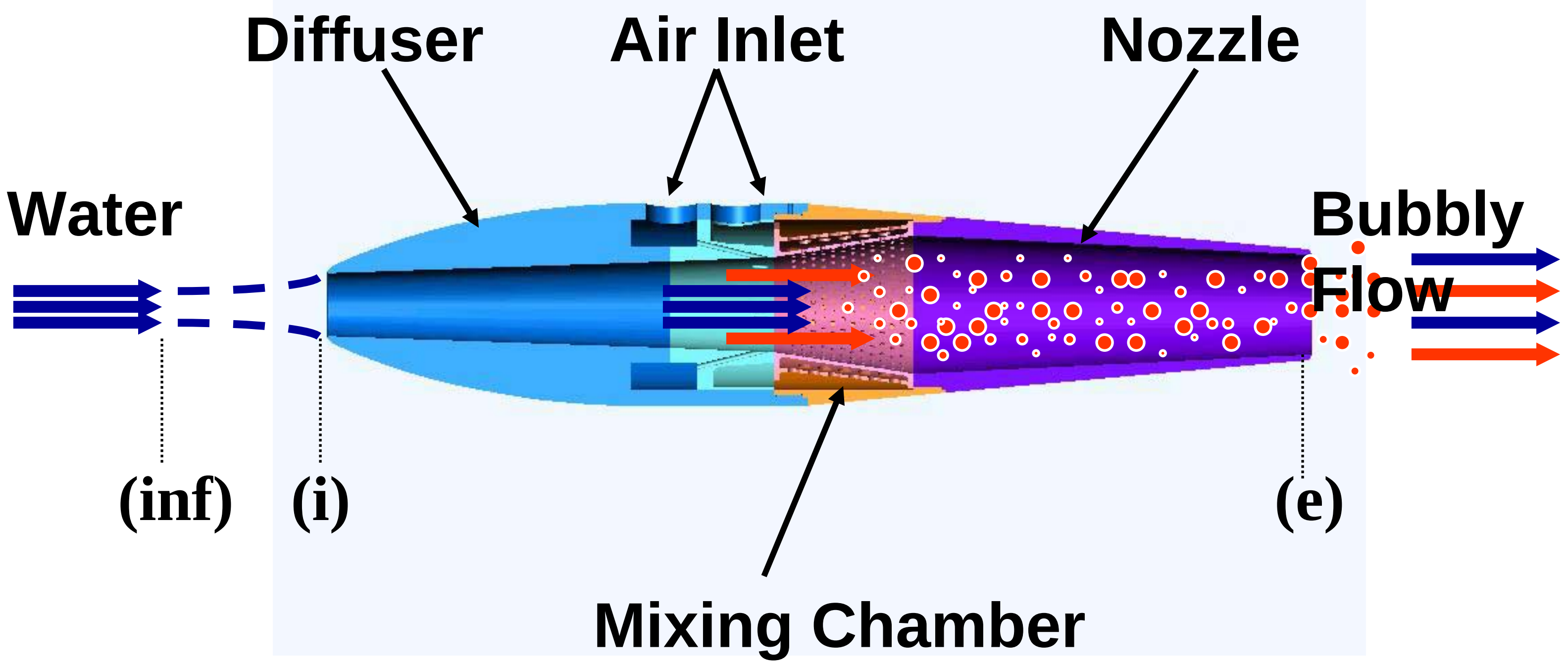

Sea Trials: Experimental Boat

Sea Trials: Experimental vs. Theoretical Results

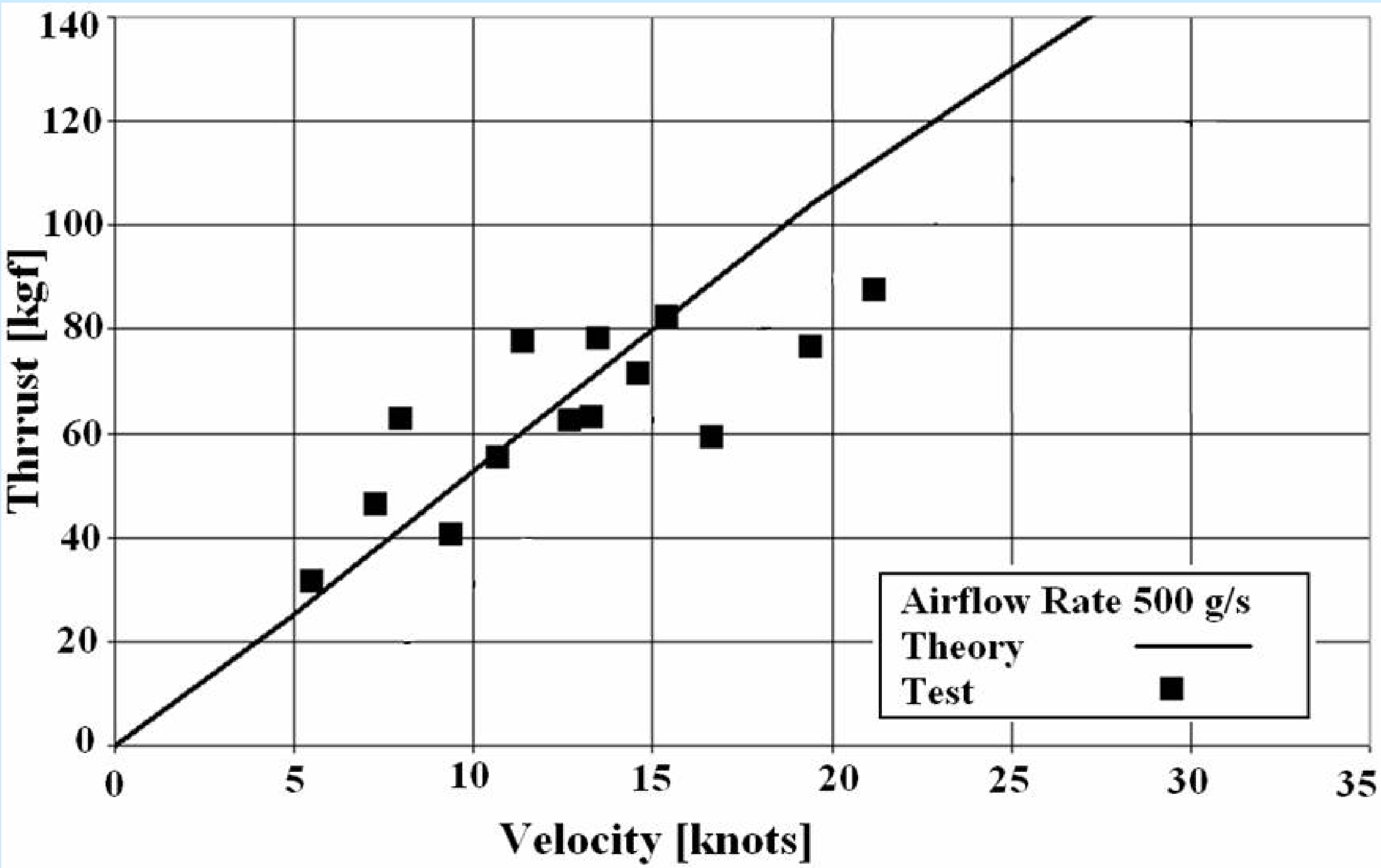

The marine ramjet is an elegant propulsion solution for high speed cruise regime.
However, it cannot start from rest and has relatively low boost capability.

Air-Augmented Waterjet Propulsion

Waterjet Thrust Enhancement by Air Injection

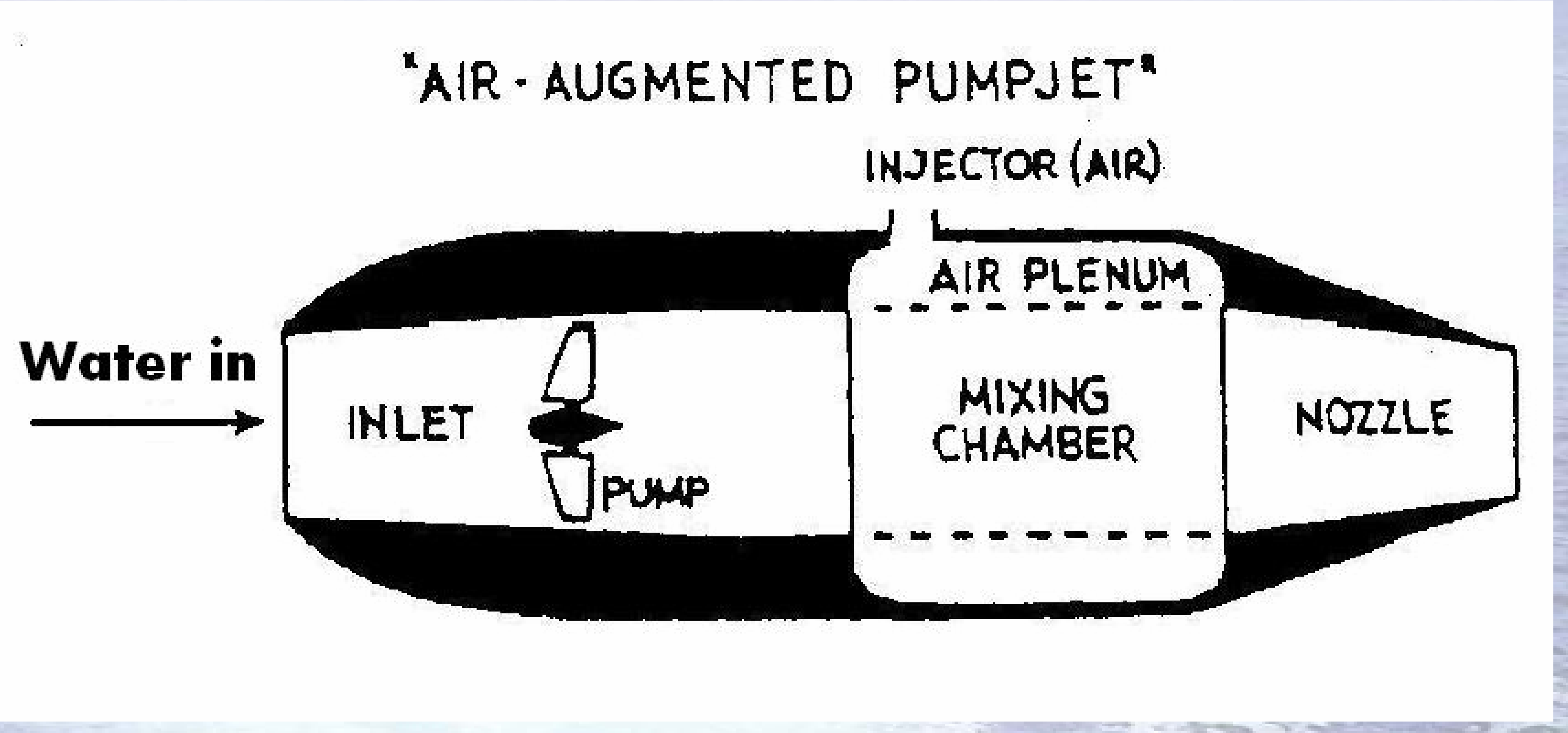

Revolutionary Concept and Pioneering Research in Marine Propulsion

The concept is to enable thrust increase of an existing waterjet unit by injection of air bubbles into the nozzle section without affecting the pump operation.

This concept is parallel to an after-burner in an aeronautical jet engine.

Unique Advantages

* Higher thrust capability when necessary without changing the operation of the main waterjet thrust unit.
* Higher boost capability when required without getting into cavitation problems.
* Overcoming resistance hump.
* Higher maximum velocity from the same basic unit.
* Masking acoustic signature.

Waterjet Thrust Enhancement by Air Injection – Avoiding Cavitation: an Example

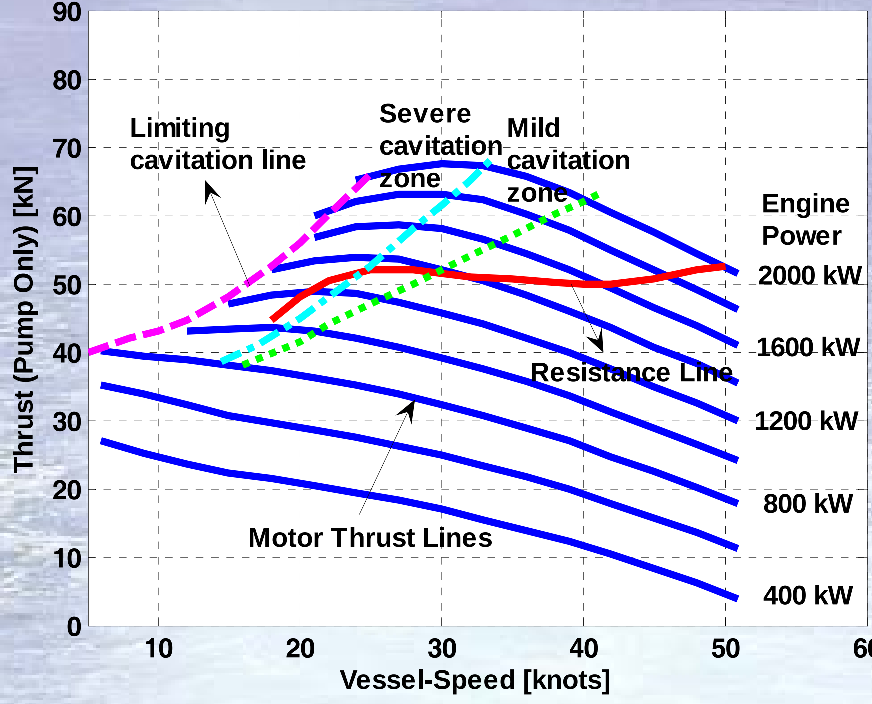

No Air

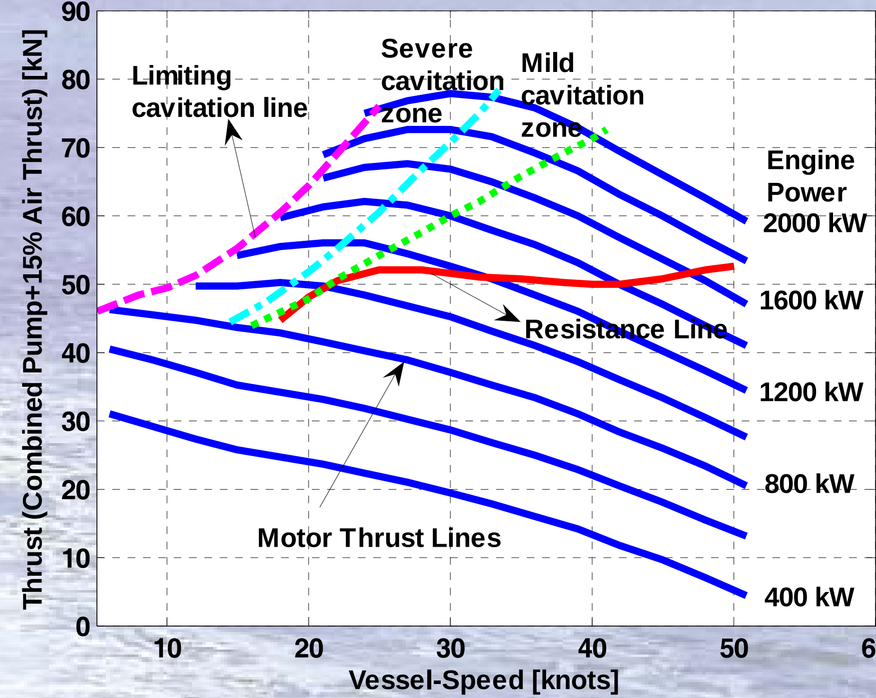

With Air

Special Engineering and Performance Advantages:

Upgrading an existing waterjet system.

Does not require modification of the vessel or the overall waterjet system. Only attachment of a mixing chamber and air supply after the pump and adjustment of the exit nozzle.

Experimental

Static Tests Using Yamaha Waterjet

Schematic of the Test System

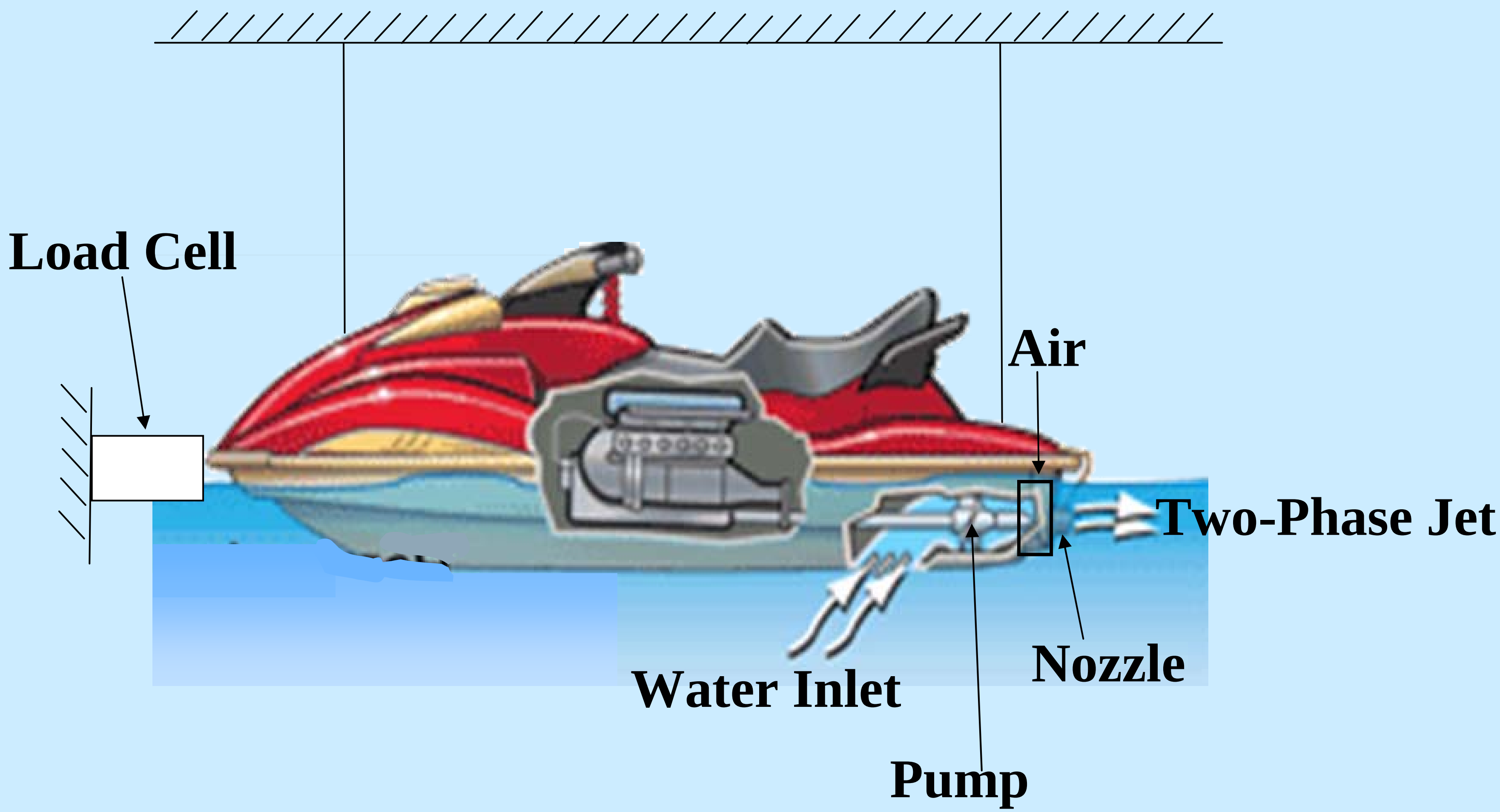

Thrust vs. RPM with and without Mixing Chamber. No Air

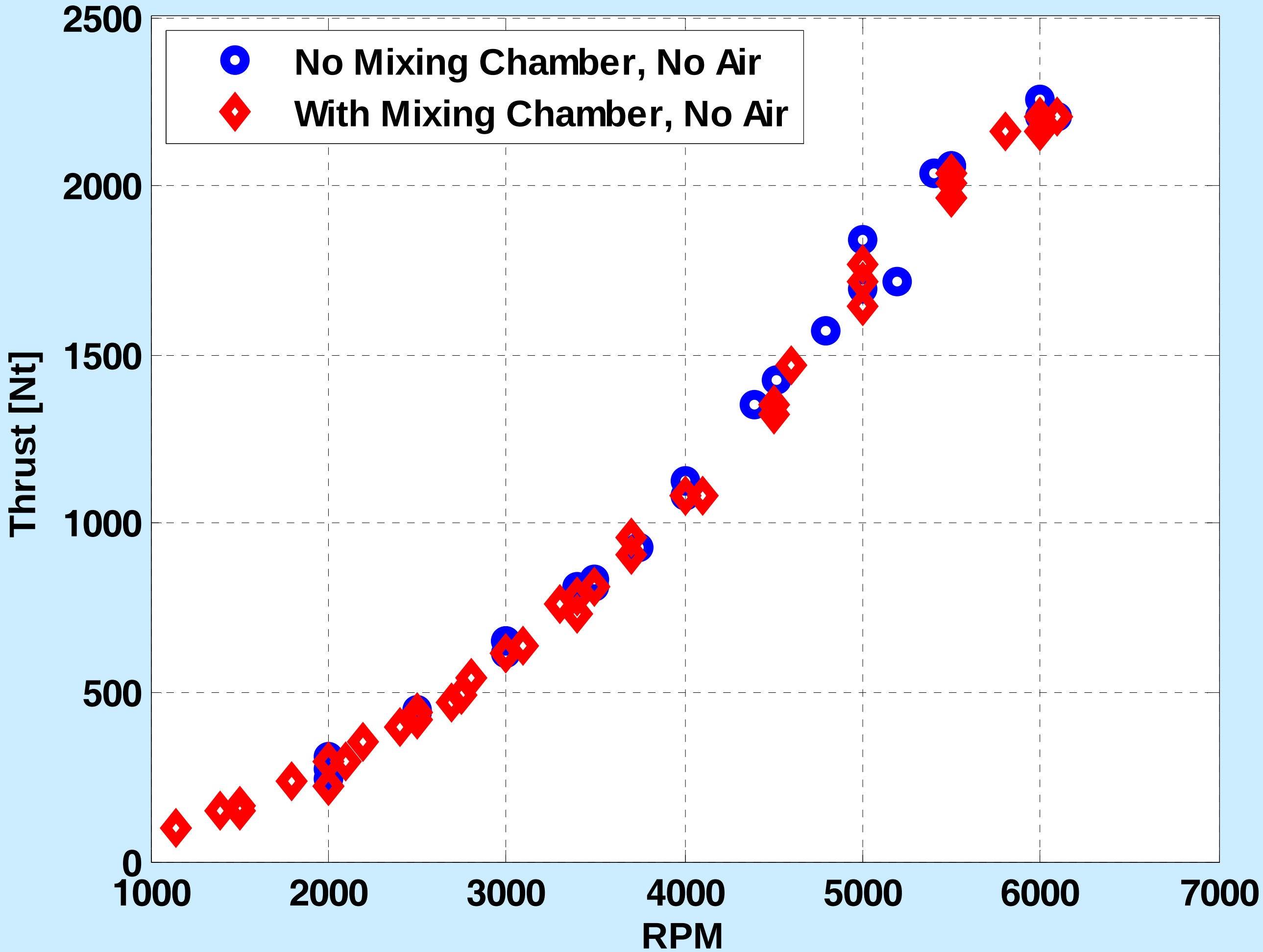

Thrust Enhancement by Air Injection

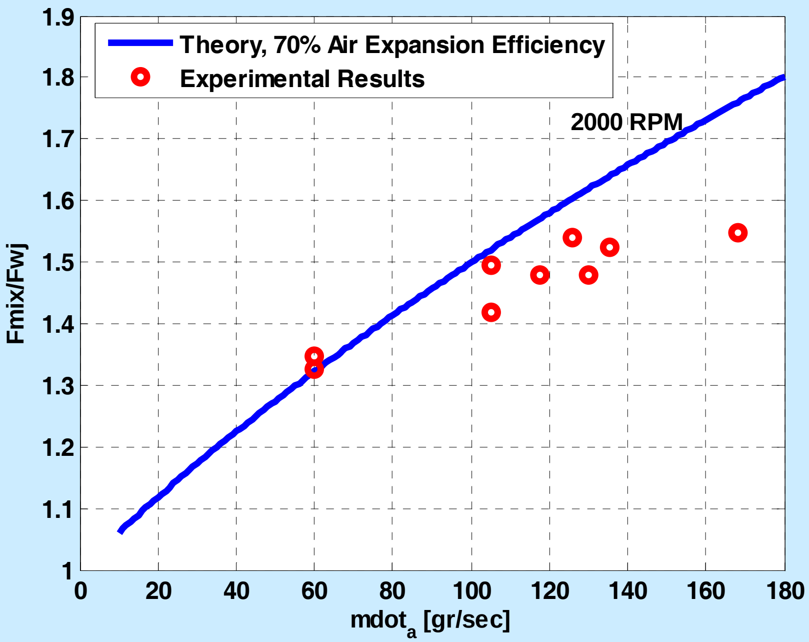

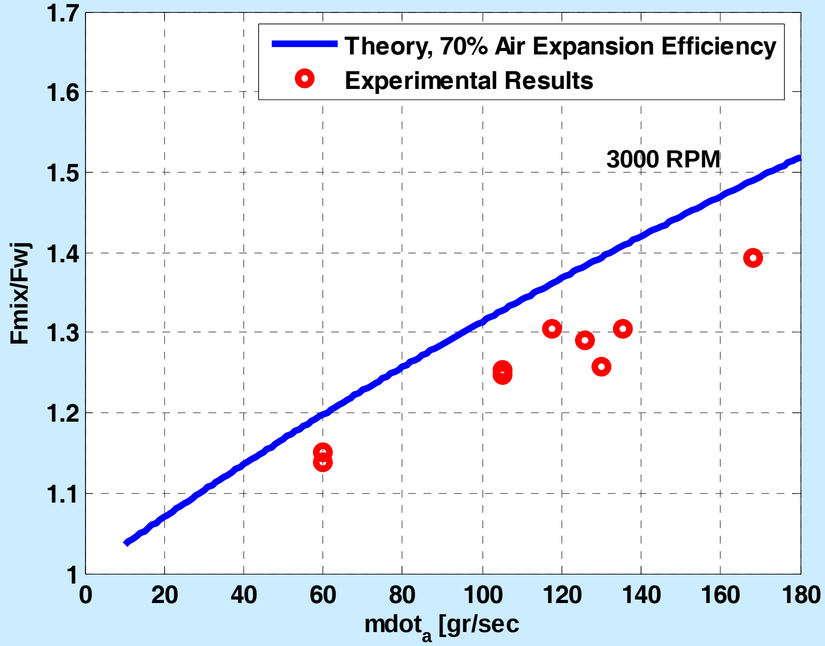

Thrust Enhancement by Air Injection

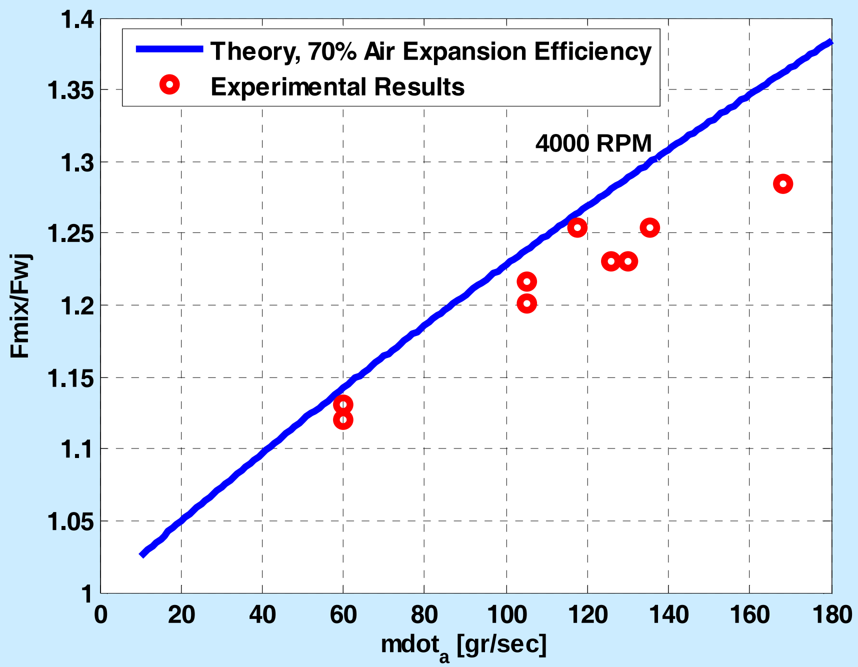

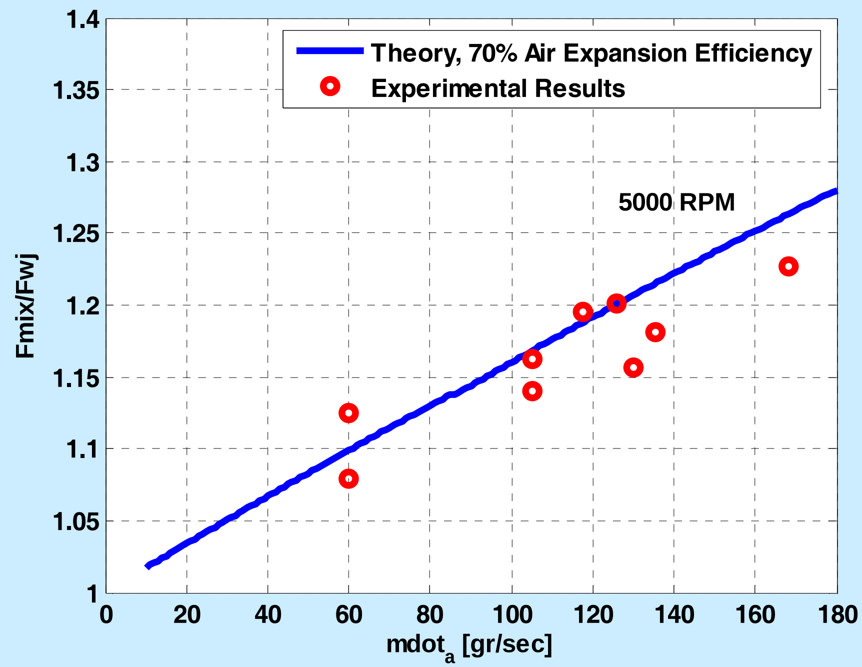

Summary

- A concept of thrust augmentation of a waterjet engine via air injection has been presented.
- This thrust increase concept is parallel to an after-burner in a turbojet engine.
- The concept enables increase of vessel’s acceleration and speed as well as overcoming resistance hump, avoiding cavitation and influence on the pump operation.
- An existing waterjet system can be upgraded with no modification of the vessel and overall propulsion system except for inclusion of air supply and adjustment of the exit nozzle.

Waterjet Applications in Vessels that Operate in Multiple Modes

Dick Borrett and Philip Rae

Hamilton Jet

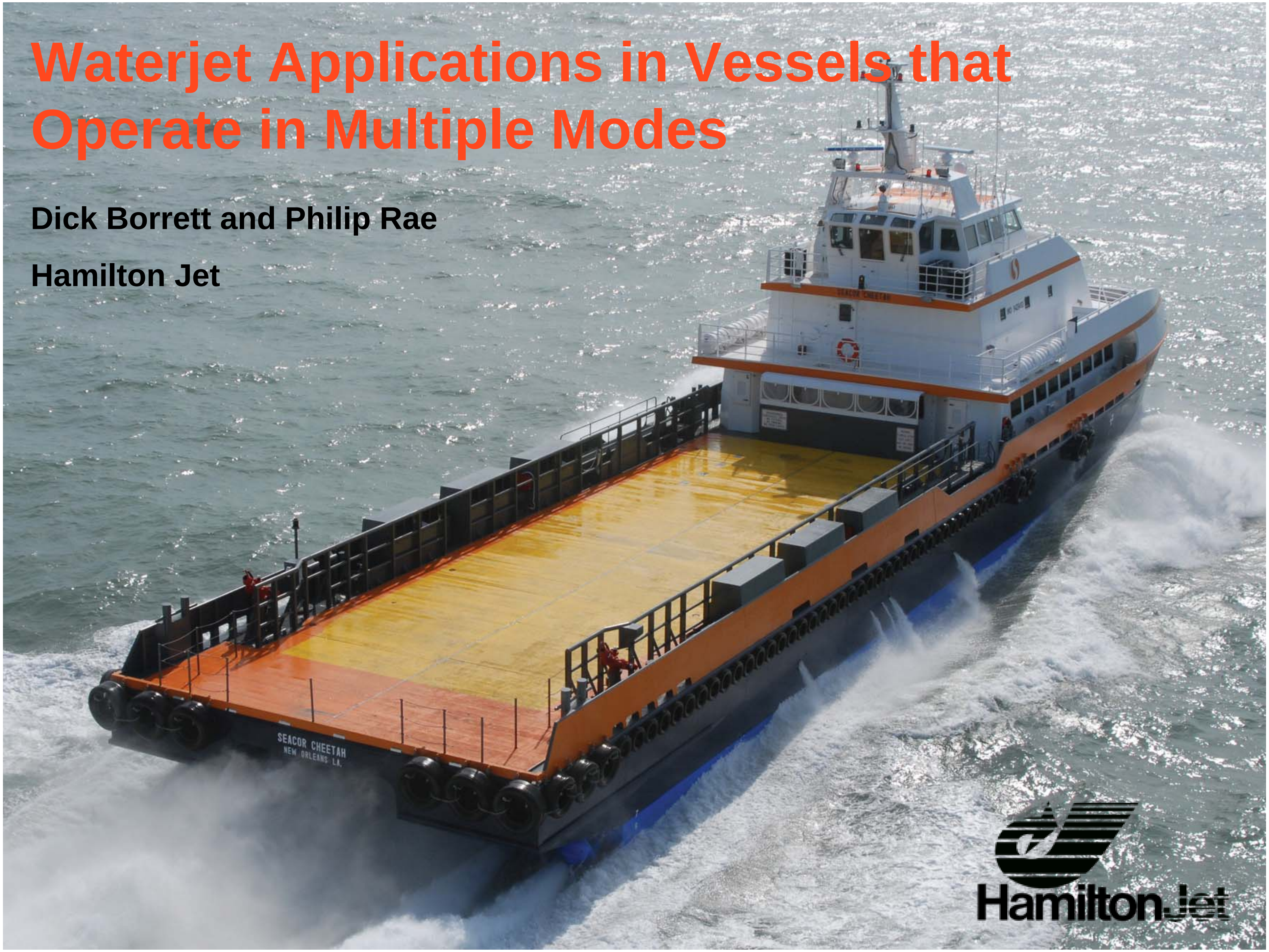

Overview

- Definition of multi-mode vessels
- Typical multi-mode vessels and their operational requirements
- Waterjet design considerations for multi-mode vessels :-
  - Hydrodynamic design
  - Thrust control
- Case study – offshore crew boat application

What is a Multi-Mode Vessel?

- In the simplest case all vessels need to :-
  - Transit at cruise speed
  - Transit at low speed in harbour
  - Manoeuvre for docking

- Many special purpose vessels have a high speed requirement but also need to operate at lower speeds for significant time

- Definition: "*A vessel required to operate for significant durations within a number of different speed regimes*"

Pilot Boats

- Transfer speed 8-10 knots
- Interaction effects
- High thrust levels
- Rapid thrust response

Patrol Boats

- High speed intercept
- Efficient transit and loiter
- Rapid acceleration
- Aggressive manoeuvring

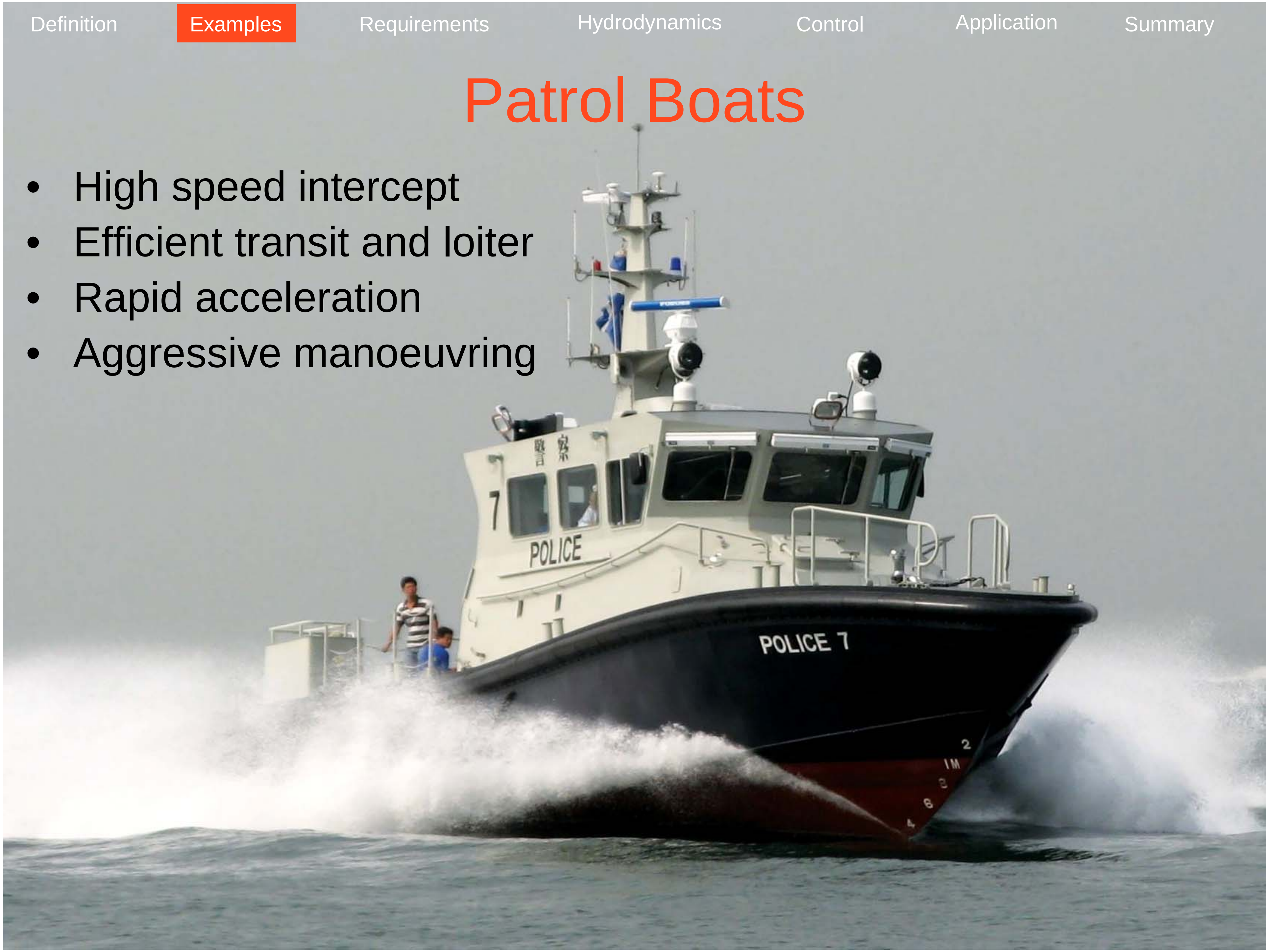

Crew Boats

- Optimal use of engine power - light and loaded
- High static thrust
- 360 degree vectoring
- Fast thrust response

Requirements Summary

- Hydrodynamic Performance
  - Thrust characteristics to give optimum overall operational efficiency of the vessel
  - Cavitation performance for high operational hours at lower speeds
- Control Performance
  - 360 degree thrust vectoring
  - Fast and accurate steering, reverse response

Hydrodynamic Design Objectives

Desired characteristics :-

- Minimise cavitation zone ‘A’
- Maximise static thrust
- Maximise efficiency over zone ‘B’

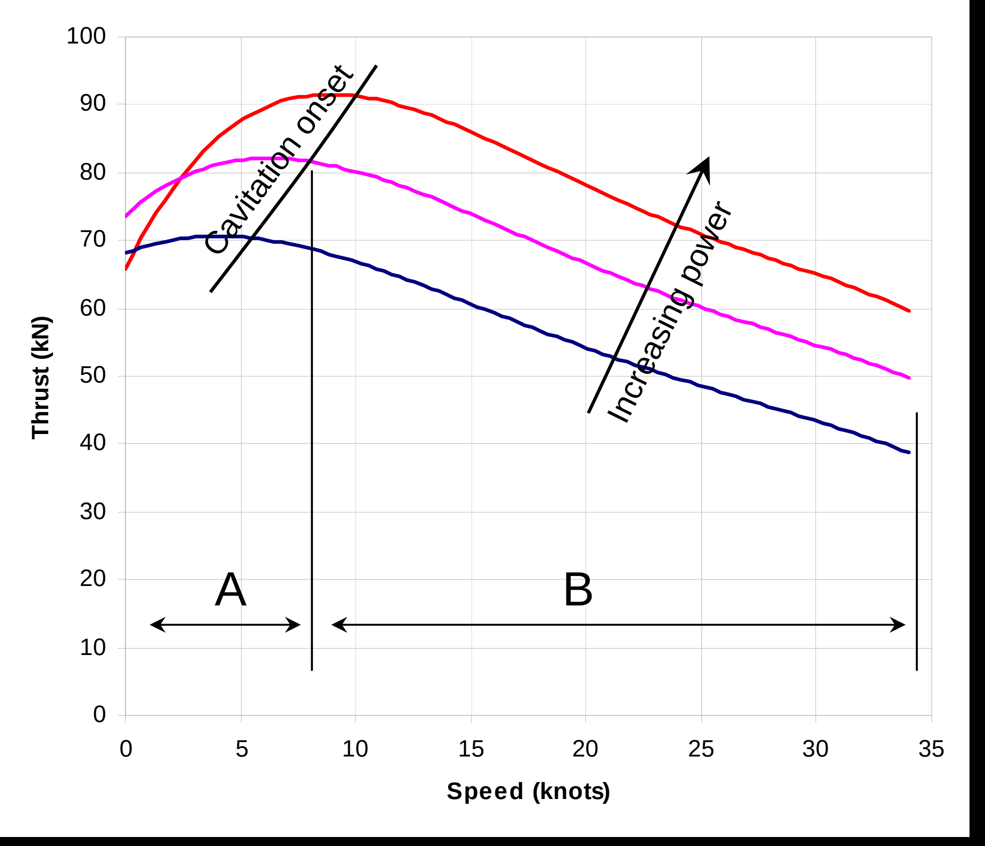

Aspects to consider include…

Jet Sizing

Over-sizing provides :-

- Higher cavitation margins
- Higher static thrust
- Improved efficiency

But with higher :-

- Cost
- Weight
- Entrained water mass
- Physical envelope

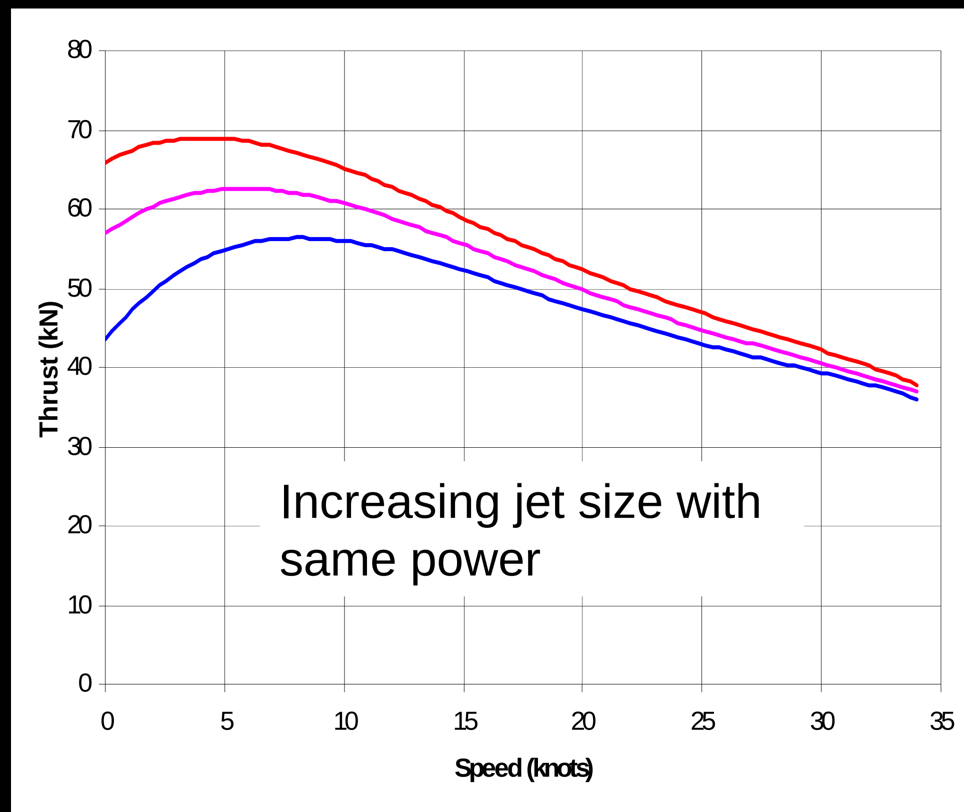

Pump Configuration

- Pumps with large nozzle/inlet ratio (NIR) have :-
  - High efficiency at high speed, lower static thrust and cavitation margin
- For multi-mode vessels, axial flow pumps with relatively small NIR have the following benefits :-
  - More compact – potential for over-sizing
  - 15-20% higher static thrust*
  - 5 to 6 knots lower vessel speed for continuous application of full power*
- In multi-mode vessels we must achieve the best *overall operational efficiency*

*Based on published data for axial and mixed flow pumps (same nozzle size) from two manufacturers

Thrust Vectoring

Required : -

- 360 degree thrust vectoring

Solution : -

- Split duct reverse
- 'JT' steering nozzle

Features : -

- Side thrust 30-40%
- Reverse thrust ~ 60%
- Envelope scaled with RPM
- Low actuation loads

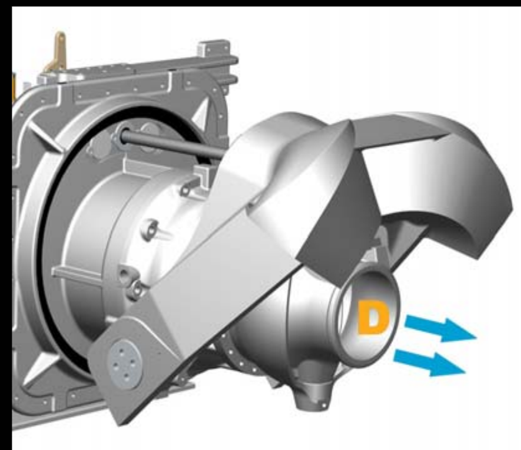

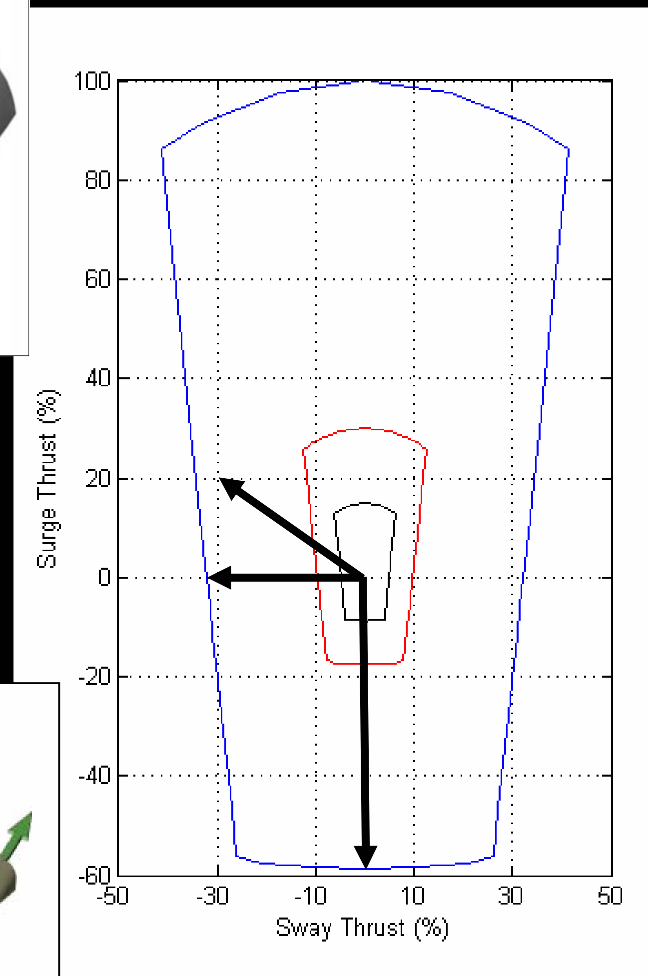

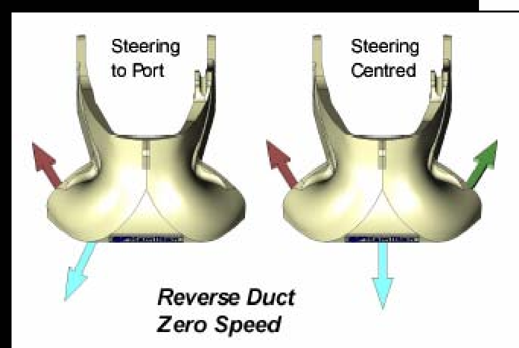

Thrust Response

- Rapid response needed for :-
  - manual control
  - automatic station keeping

- Considering the station keeping requirement :-
  - Position error increases exponentially with reverse time constant
  - Fast response reduces position error & uses less energy

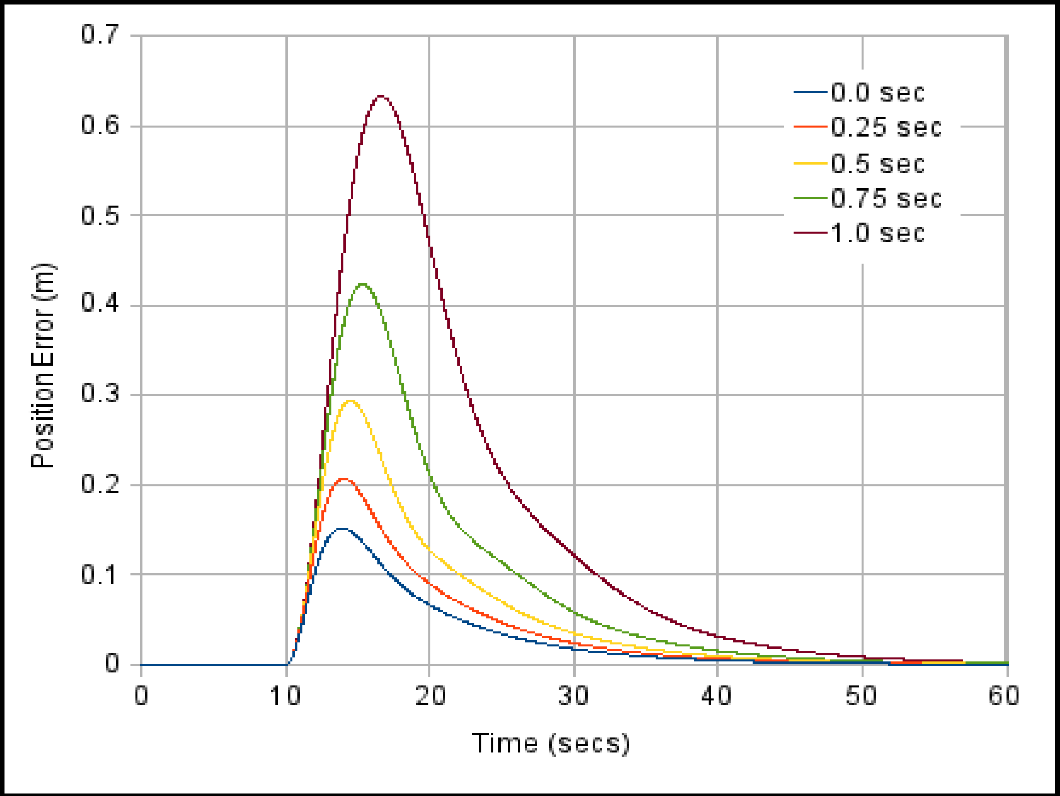

Station-Keeping Test

Station-keeping over 5 minute period

- ~12 knot wind
- Max error 0.35m

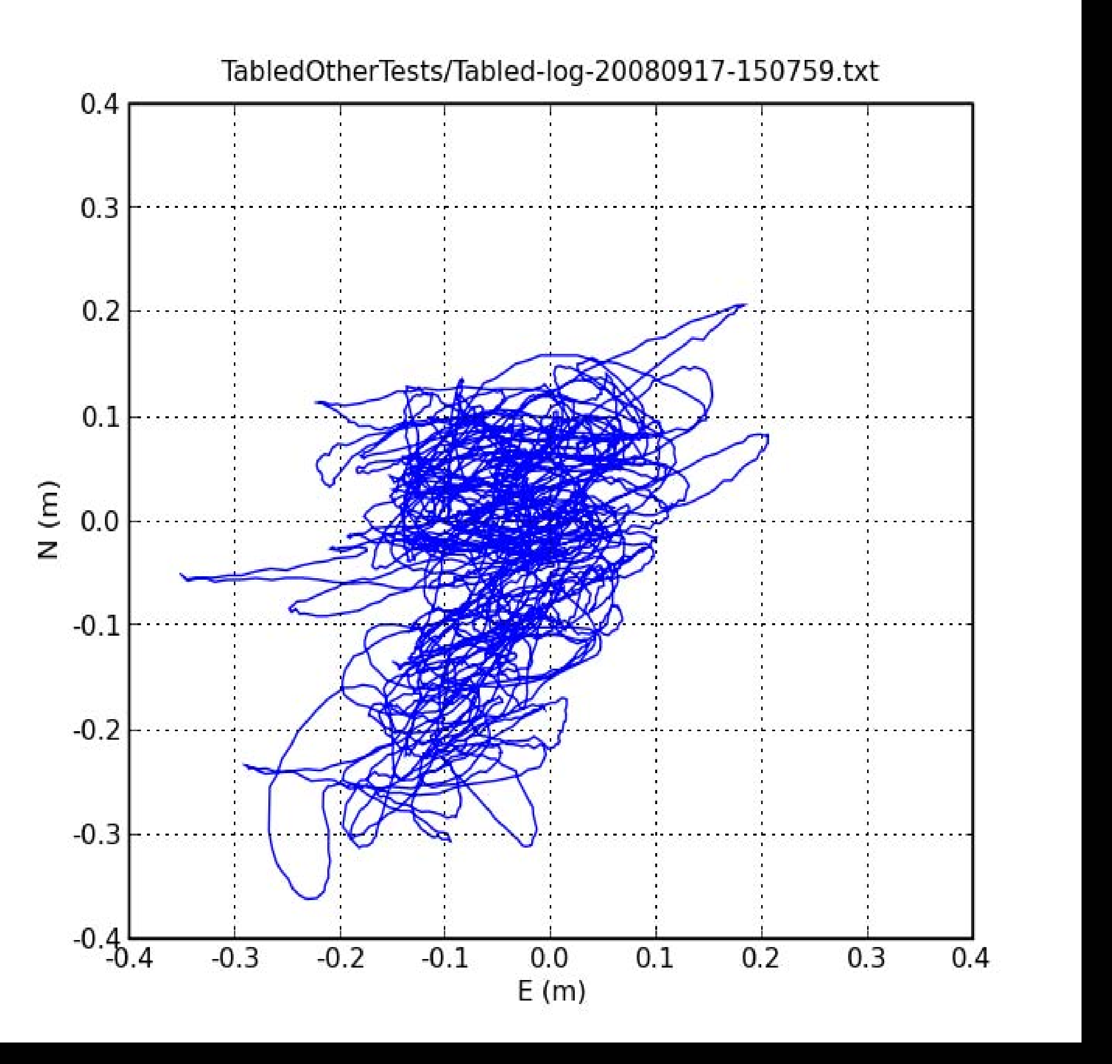

Crew Boat Application

LOA: 54 m

Light: 205MT ~31 kts

Loaded: 500MT ~18 kts

Power - 4 x 1340 kW

150 kW Bow Thruster

4 x HM811 Waterjets

4 x 7.1T Static Thrust

‘Over-size’ jets

Axial flow

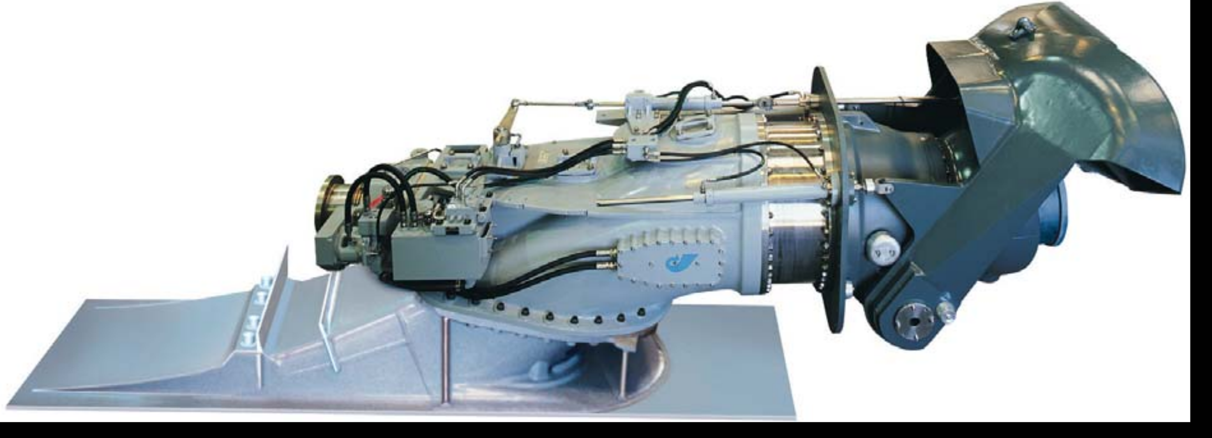

Crew Boat – Static Thrust

- Thrust levels off as cavitation increases
- Engine power matched to maximum thrust
- Cavitation limited by engine power
- DP system can limit power level

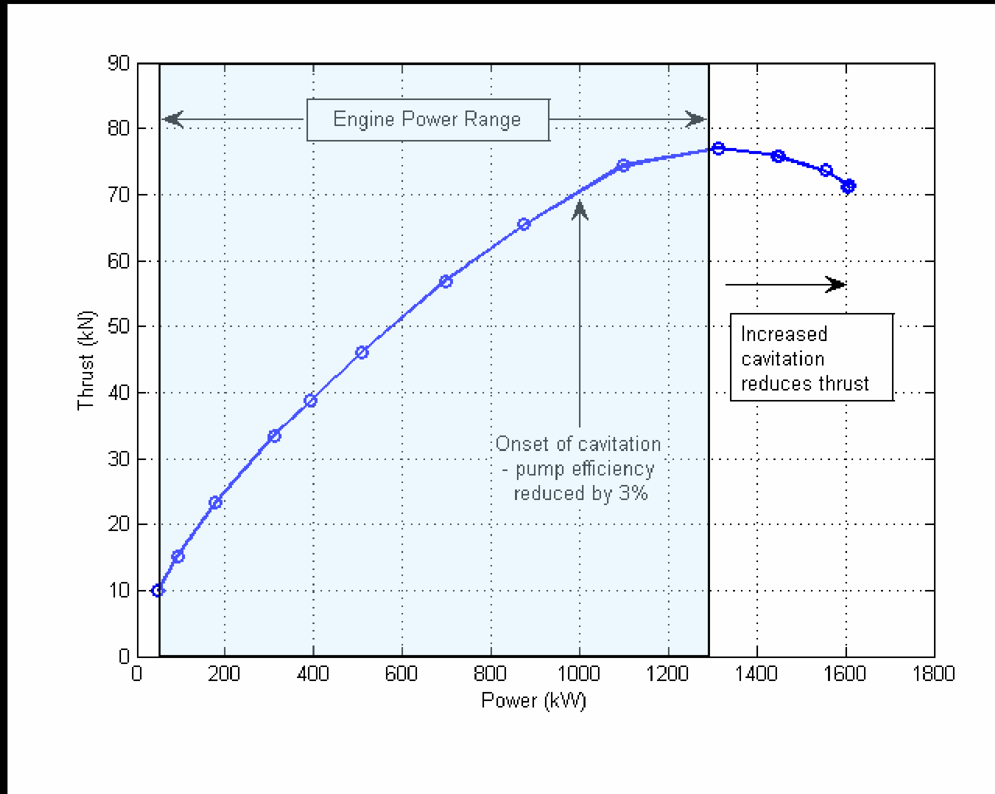

Crew Boat - Transit

- Resistance increases 3x between light and loaded
- Full engine power at all states of loading
- High cavitation margin
- Faster round trips

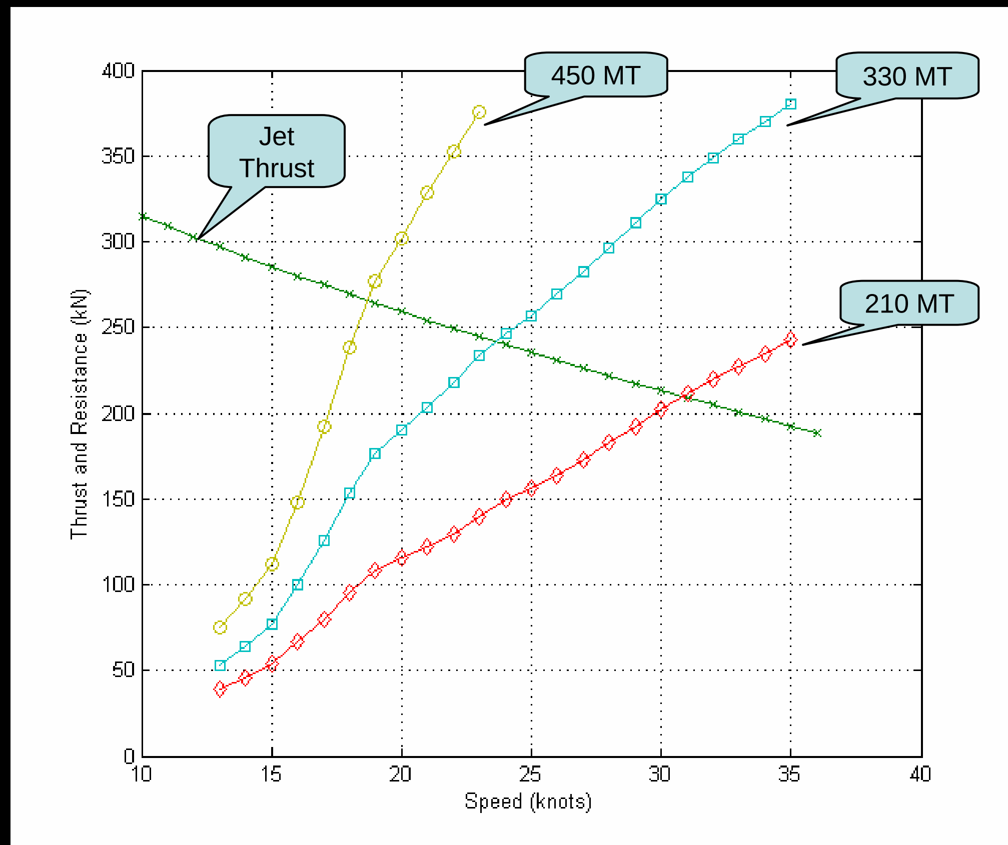

Summary

- Waterjets are an excellent solution for multi-mode vessels
- Primary requirement are : -
  - Wide operating thrust range
  - 360 degree thrust vectoring
  - Fast response
- Achieved through :-
  - Oversizing of jet
  - Optimum hydrodynamic configuration
  - High efficiency, independent steering nozzle and split duct reverse
  - Low actuation loads
- Crew boat application example


HamiltonJet

Waterjet pump development for high performance and power density

Mats Heder, Ph. D., M. Sc.
R & D, Kamewa Waterjets, Rolls-Royce AB, Kristinehamn, Sweden

Summary

- A new WJ pump with higher power density has been developed
- CFD, model tests and structural analysis were integrated
- Dynamic stress was found to be crucial

Result

- The new S3NP WJ range developed
- Improved cavitation performance
- Increased efficiency
- Reduced WJ size for given ship speed and power
- Lower weight of propulsion system

The design process adopted

- Pump design code
- CFD
- Model scale testing
- FE analysis
- Fatigue
- Full scale test

Design process (1)

- **Pump design code**
  - **Obtain pump geometry**

Design process (2)

- CFD
  - Predict performance
  - Obtain pressure distribution for FE analysis

CFD model of pump

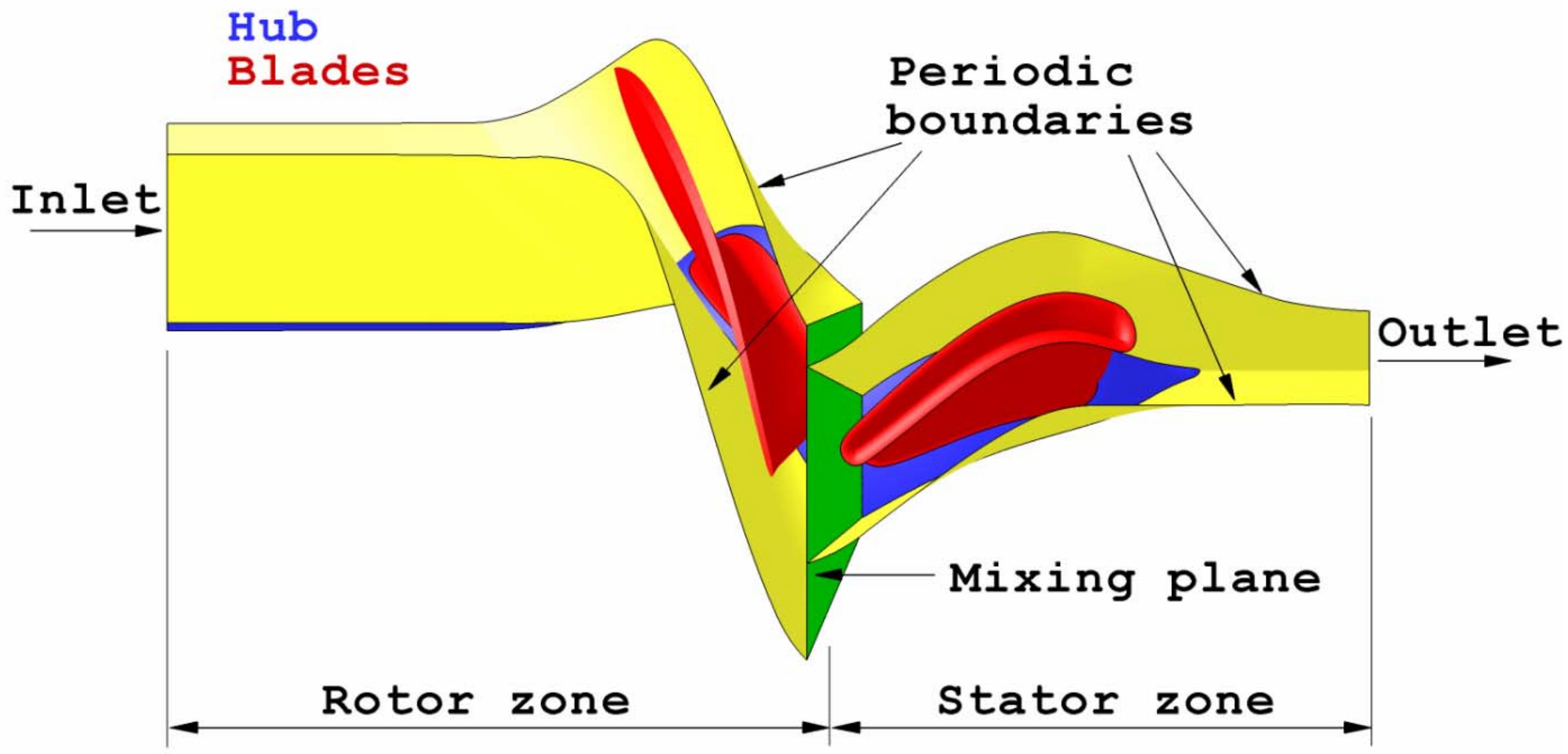

Contour plot of pressure on blade

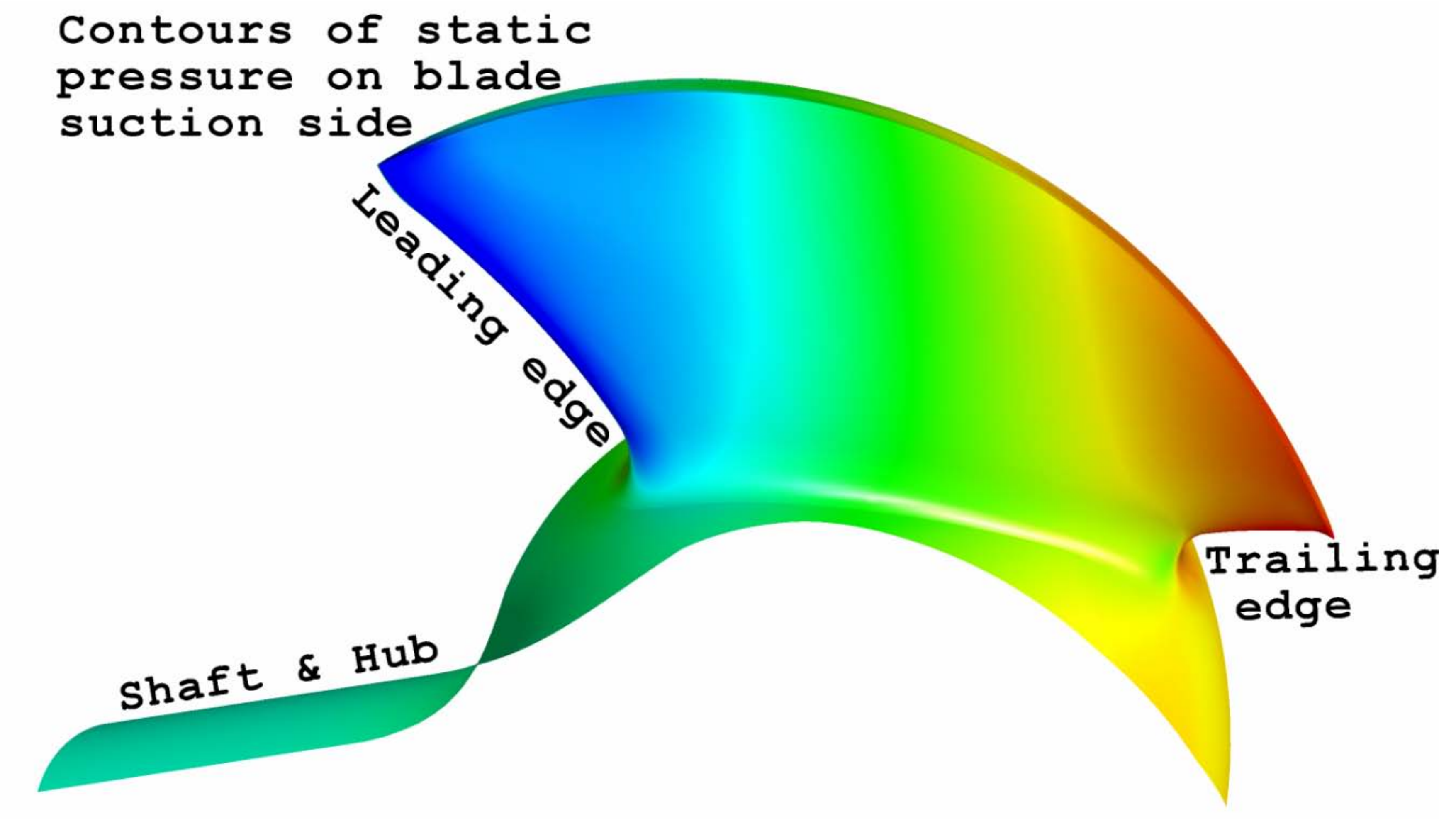

Design process (3)

- **Model test**
  - **Verify performance data**
  - **Pump loop tests**
  - **System tests**
  - **Obtain impeller loads**
  - **Obtain static and dynamic blade stress**

Rolls-Royce Hydrodynamic Research Centre, Kristinehamn, Sweden

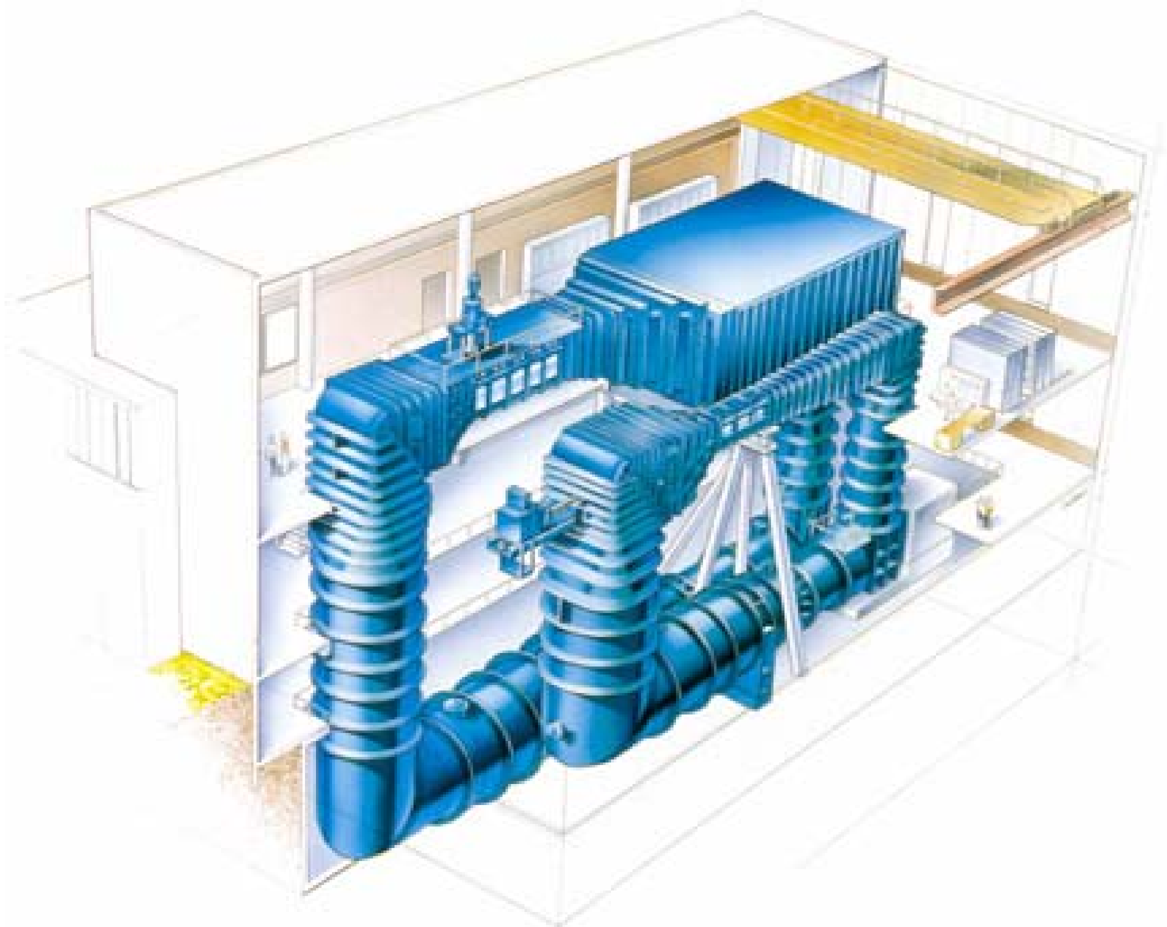

Set up for pump loop test at RRHRC

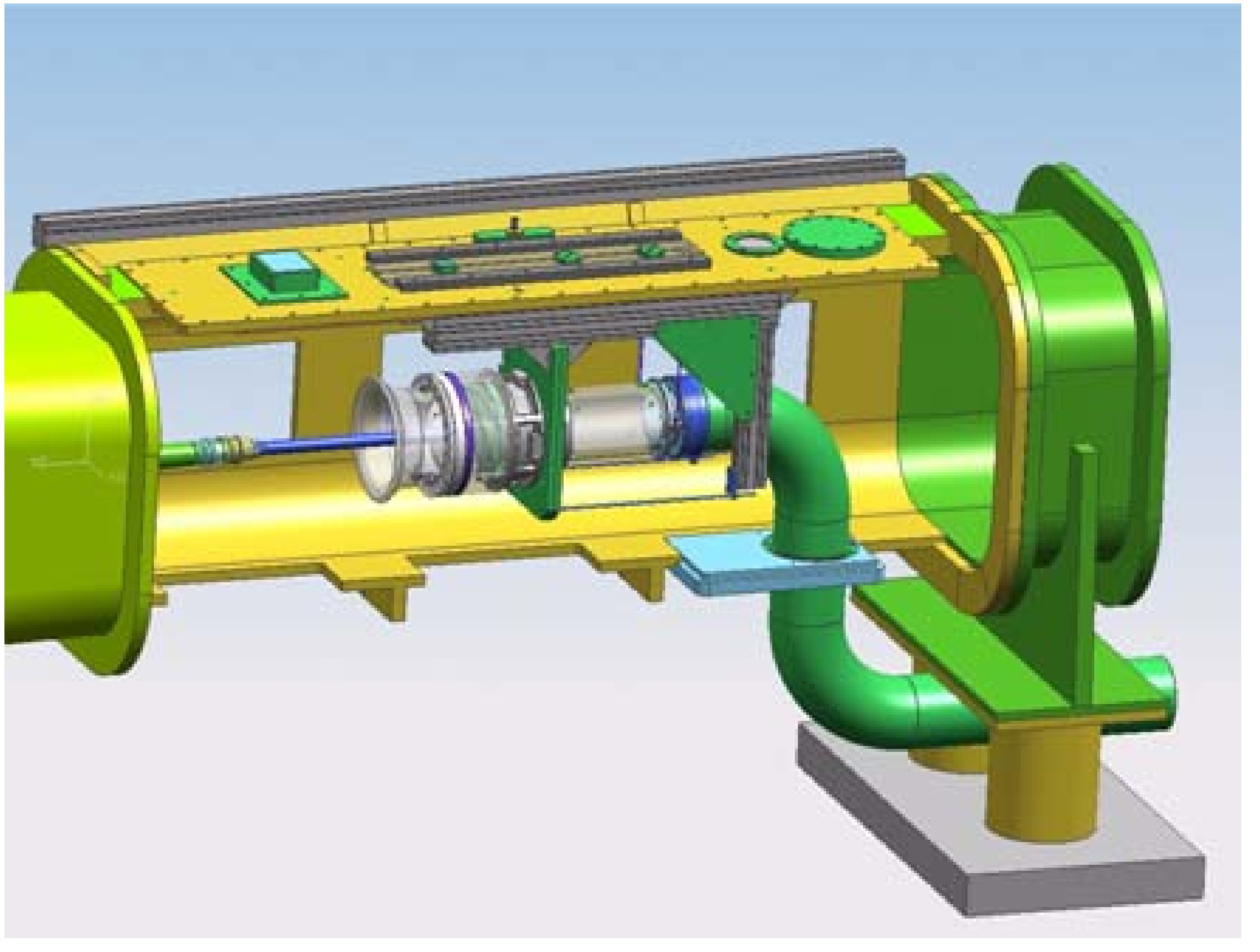

Set up for waterjet system tests at RRHRC

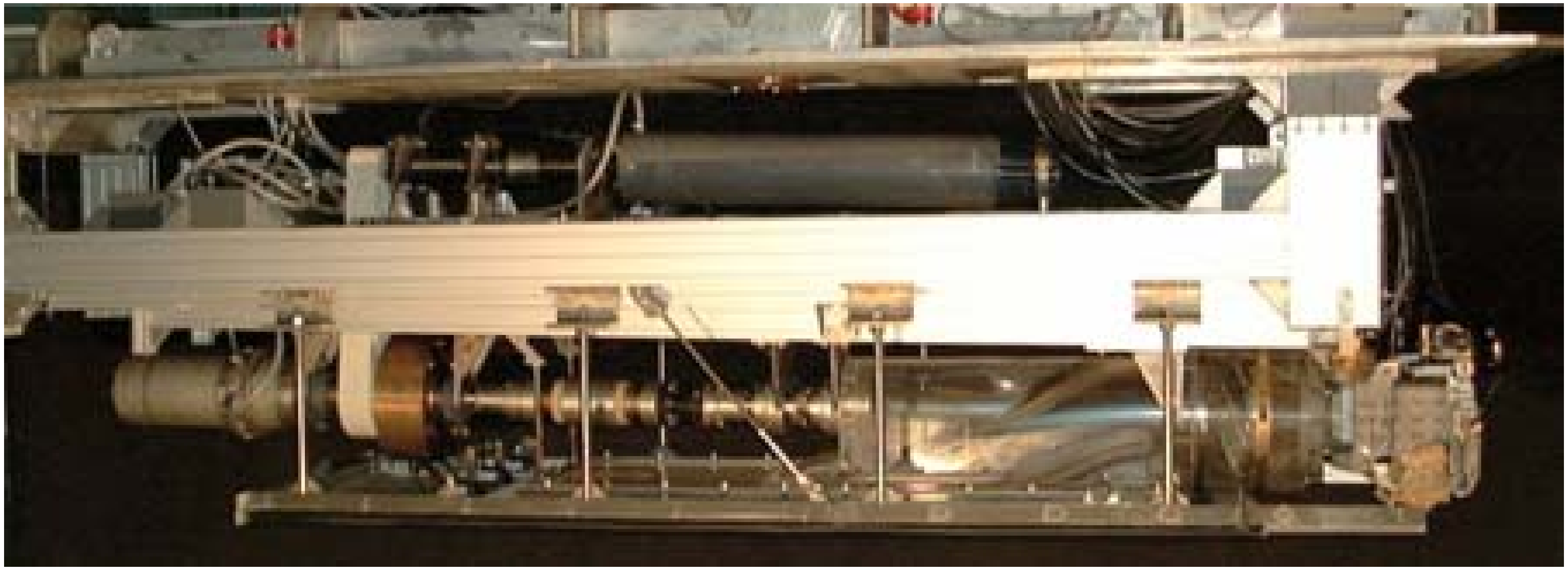

Strain gauges on impeller pressure side

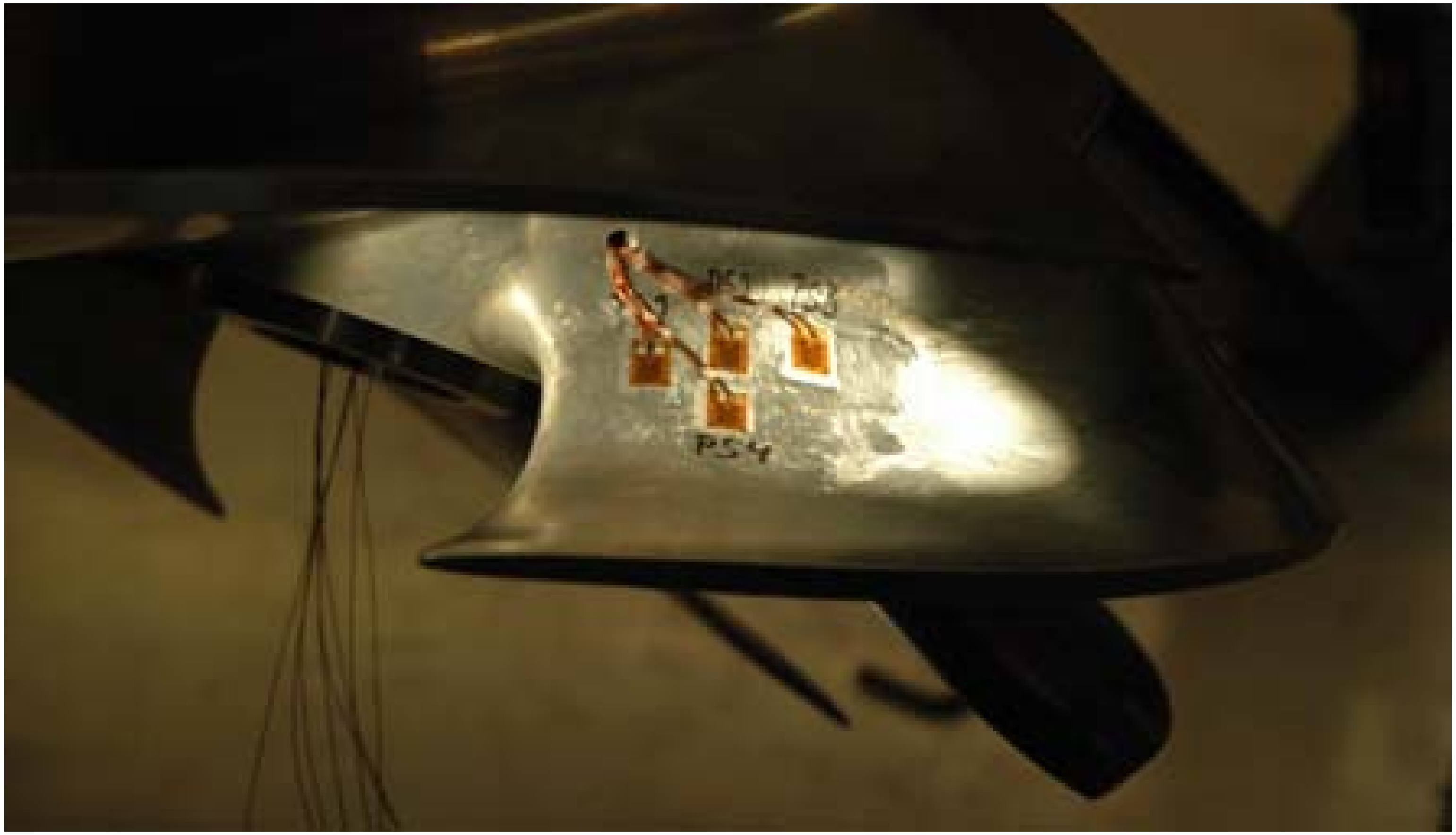

Example of signal from 4 strain gauges

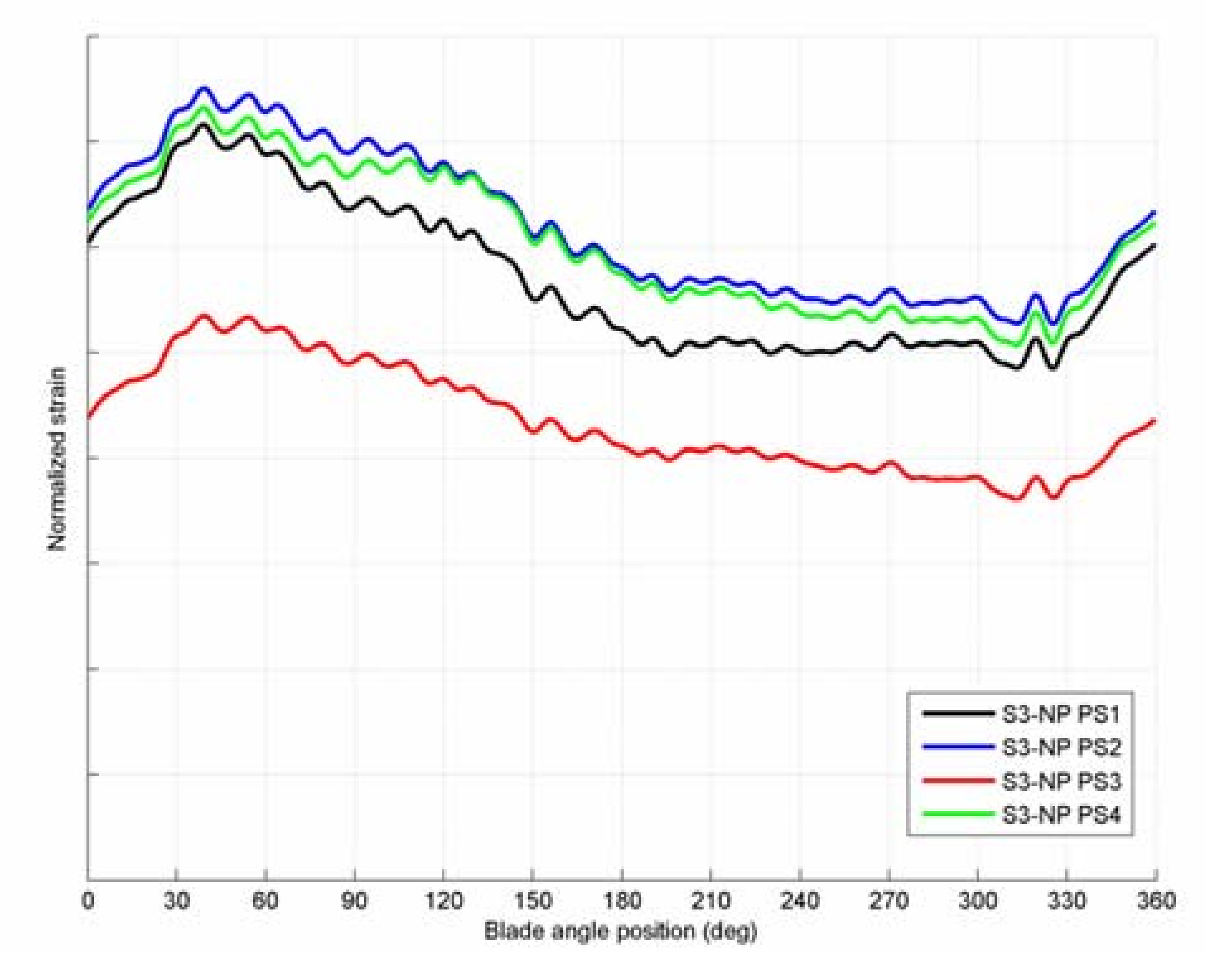

Design process (4)

- FE analysis
  - Obtain static stress
  - Obtain stress distribution of blades

FE analysis of impeller

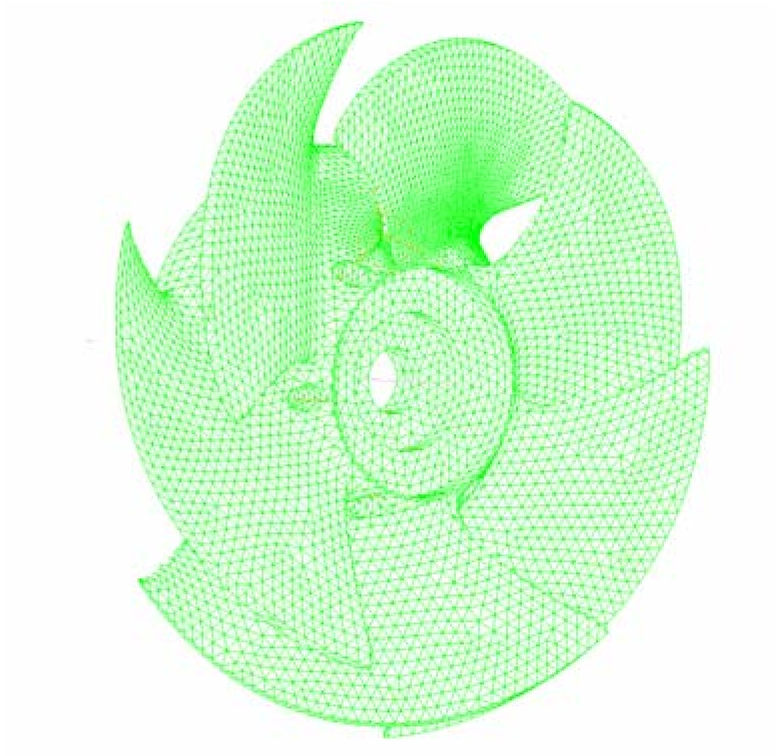

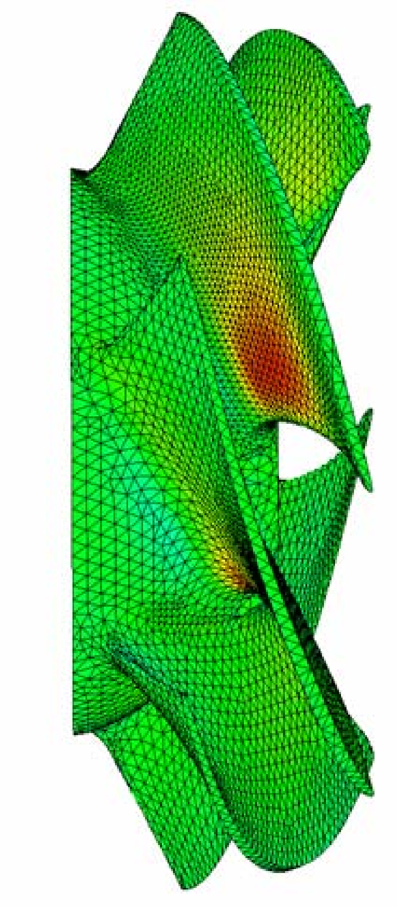

Design process (5)

- **Comparision**
  - **Static stress obtained by FE and model test show good agreement**

Non-dimensional strain obtained in model scale test and by FE analysis

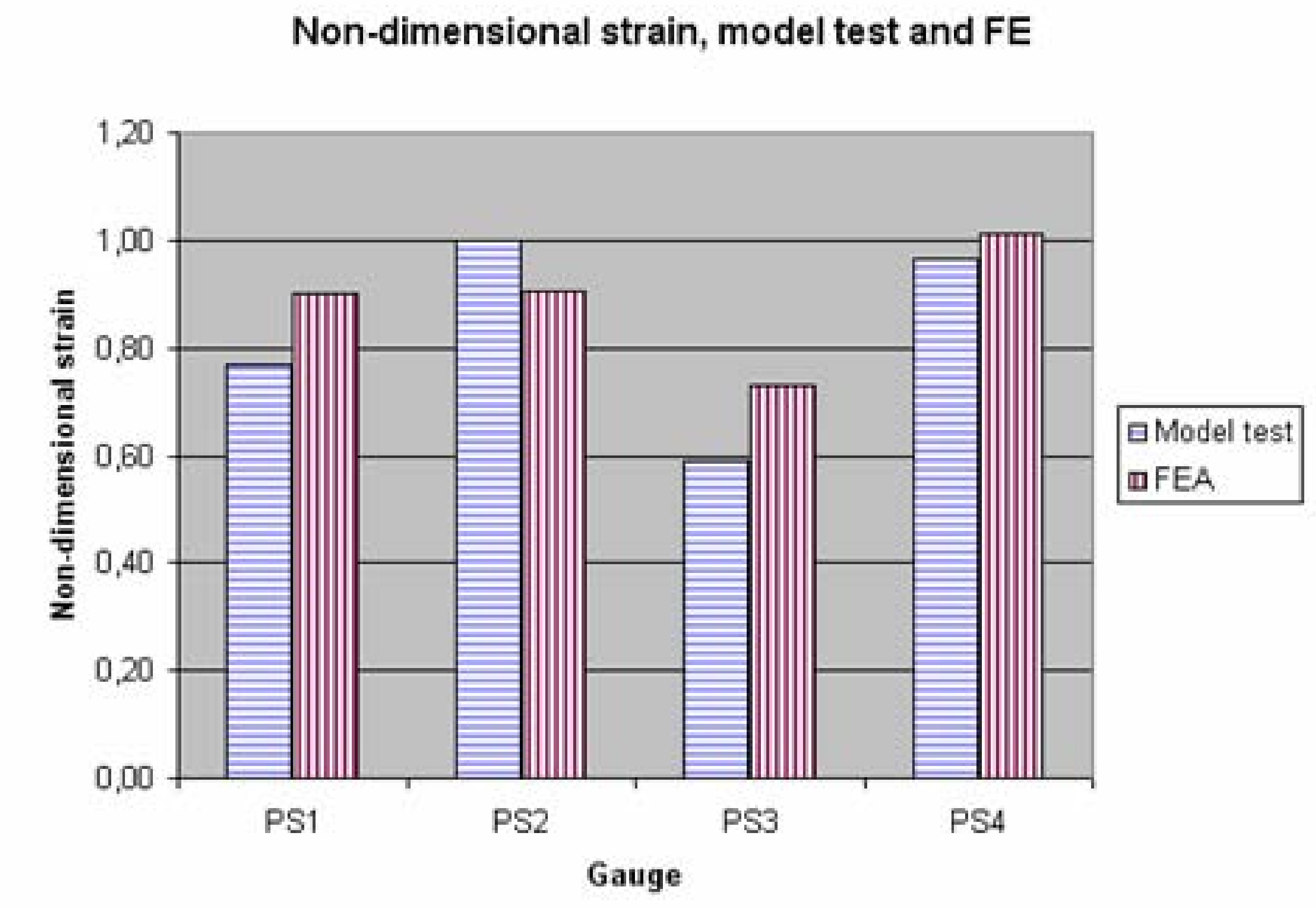

Design process (6)

- **Dynamic strain**
  - **Obtained by model testing**
  - **Gauges applied to a number of locations**

Non-dimensional stress amplitude in gauges

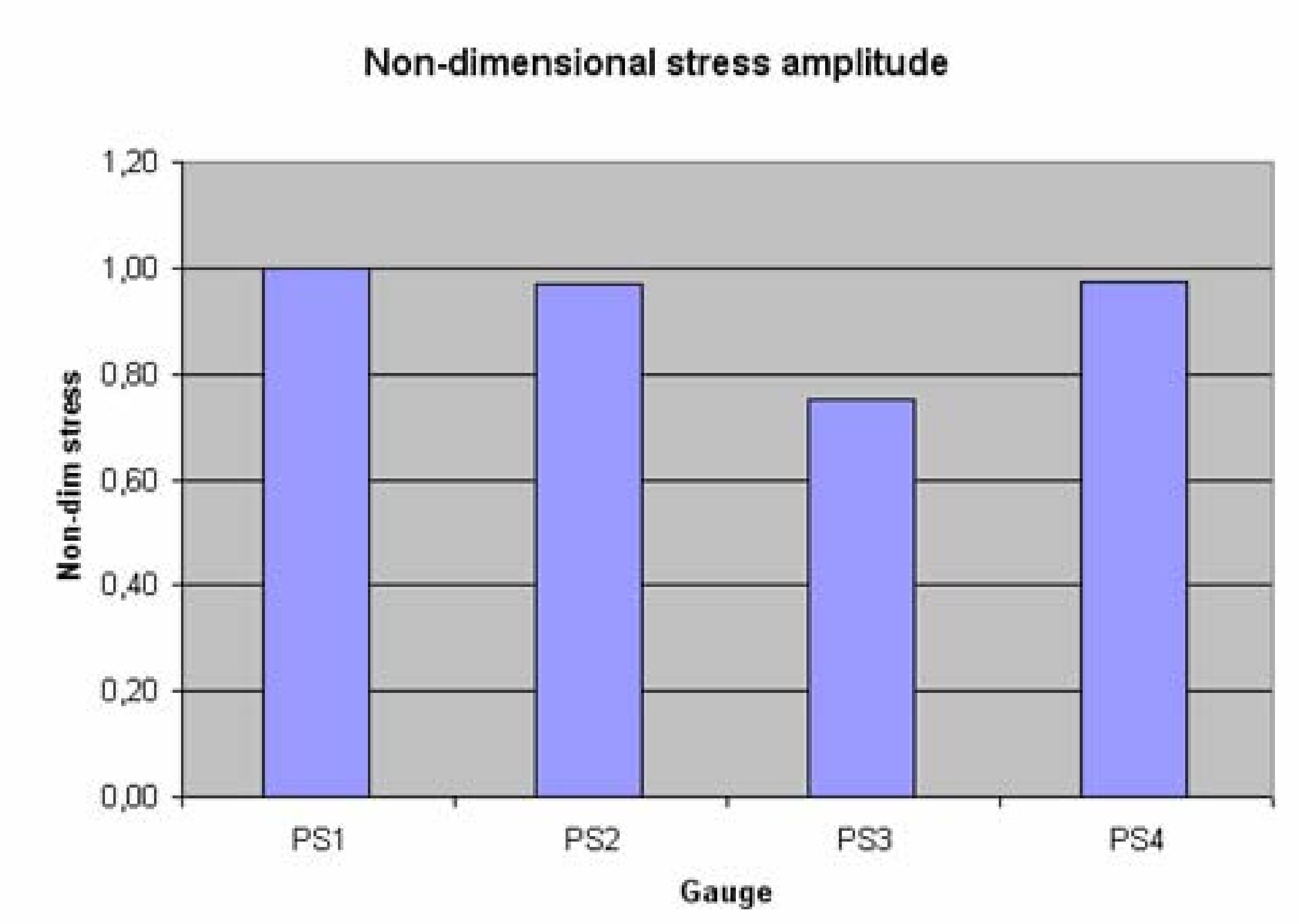

Fatigue of blades

- Cumulative damage computed
  - Palmgren-Miner cumulative damage rule employed
  - SN curve based on testing and full scale experience
  - Effect of operating profile

Design process (7)

- **Full scale test**
  - **Verify performance**
  - **Scheduled for early 2009**

First Kamewa S3NP WJ installed on vessel

Conclusions

- A new high power density WJ mixed flow pump has been developed
- Structural analysis has been an integral part of the process
- Static stress has been obtained with good accuracy by CFD/FEM
- Model tests are essential in order to obtain dynamic stress